Quantum Chaos in Conformal Field Theories

by

Wyatt Austin Reeves

A THESIS SUBMITTED IN PARTIAL FULFILLMENT OF
THE REQUIREMENTS FOR THE DEGREE OF

DOCTOR OF PHILOSOPHY

in

The Faculty of Graduate and Postdoctoral Studies

(Physics)

THE UNIVERSITY OF BRITISH COLUMBIA

(Vancouver)

December 2023

The following individuals certify that they have read, and recommend to the Faculty of Graduate and Postdoctoral Studies for acceptance, the thesis entitled:

Quantum Chaos in Conformal Field Theories

submitted by Wyatt Austin Reeves in partial fulfillment of the requirements for

the degree of Doctor of Philosophy

in Physics

Examining Committee:

Moshe Rozali, Professor, Physics, UBC
Supervisor

Mark van Raamsdonk, Professor, Physics, UBC
Supervisory Committee Member

Joanna Karczmarek, Professor, Physics, UBC
University Examiner

Sven Bachmann, Associate Professor, Mathematics, UBC
University Examiner

Jan de Boer, Professor, Physics, University of Amsterdam
External Examiner

Additional Supervisory Committee Members:

Gordon Semenoff, Professor, Physics, UBC
Supervisory Committee Member

Joshua Folk, Associate Professor, Physics, UBC
Supervisory Committee Member

Abstract

Understanding quantum chaos in conformal field theories is extremely important. Chaotic dynamics can explain why so many systems can be studied with statistical mechanics, and why systems reach "typical" states so quickly. Outside of the simplest, highly symmetric systems, all systems are expected to be described by chaotic dynamics; whether and how these dynamics can appear in theories with conformal symmetry is thus essential to further our understanding of most CFTs. Moreover, the AdS/CFT correspondence suggests that chaotic CFTs are important for understanding black holes, which themselves are chaotic systems.

However, the highly symmetric structure of these systems can tend to hide the underlying chaotic behaviour; this unique structure requires us to find the right language and diagnostics for discussing chaotic phenomena. In this thesis we make significant progress to this end: we demonstrate the part of the energy spectrum that is unconstrained by symmetry and displays chaotic behaviour; we study the link between quantum chaos and the strange properties of "arithmetic chaos"; we create an effective field theory for analyzing chaotic behaviour and its link to standard CFT technology; and we analyze CFTs with a boundary and their AdS/CFT dual, which have been used to model chaotic black holes.

Lay Summary

The laws of nature are often sensitive to small changes, as stated by the butterfly effect: a tiny change in a system ("a butterfly flapping its wings in Brazil…") can lead to massive changes given enough time ("…can cause a tornado in Canada"). In this thesis, we further our understanding of such chaotic phenomena for special types of systems called conformal field theories (CFTs). These systems obey the same quantum laws that govern the tiniest systems, but are so symmetric they "look the same" no matter how much you zoom in or out. These systems are interesting as models of complicated systems of interacting particles, and can also describe black holes through a "dictionary" called AdS/CFT that relates CFTs with gravitational systems. We will show how a CFT can be chaotic and the consequences of chaos on the structure of a CFT, and deepen our understanding of the AdS/CFT dictionary.

Preface

Chapter 1 contains introductory material based on the references therein, written by myself.

Chapter 2 is a version of a paper published in [1] with Felix Haehl, Charles Marteau, and Moshe Rozali. All authors were involved equally in conceptual and theoretical considerations. Felix Haehl, Charles Marteau, and myself were all equally involved in technical calculations. Moshe Rozali conceived of the initial version of the project, while I helped guide further developments of the project and formulate the exact quantities we would need to calculate. I wrote the first draft for approximately 60 per cent of the paper, and thoroughly proofread and made edits for all versions.

Chapter 3 is a version of a paper with Felix Haehl and Moshe Rozali, which has been submitted for publication and is available at [2]. All authors were involved equally in conceptual and theoretical considerations. Felix Haehl and myself were equally involved in technical calculations. The project was conceived by all authors. I wrote the first draft for approximately 50 per cent of the paper, and thoroughly proofread and made edits for all versions.

Chapter 4 is a version of a paper published in [3] with Felix Haehl and Moshe Rozali. All authors were involved equally in conceptual and theoretical considerations. Felix Haehl and myself were equally involved in technical calculations. Felix Haehl and Moshe Rozali conceived of the project. Felix Haehl wrote the first draft, while I thoroughly proofread and made edits for all versions.

Chapter 5 is a version of a paper published in [4] with Moshe Rozali, Petar Simidzija, James Sully, Christopher Waddell, and David Wakeham. All authors were involved in conceptual and theoretical considerations, except for section 5.6 which was independent work done by Chris Waddell and James Sully. My particular contribution was analyzing large c holographic CFTs with a boundary to find whether the spectrum of boundary operator dimensions we found in AdS with an "end-of-the-world brane" can be found in a BCFT without any additional assumptions. The project was conceived by James Sully and Moshe Rozali. Petar Simidzija derived the spectrum of boundary operators in AdS. David Wakeham analyzed the singularities in the BCFT and AdS. Chris Waddell performed a top-down analysis of a holographic model matching the bottom-up description. I proofread and made edits to the manuscript.

Table of Contents

Appendices

List of Tables

List of Figures

List of Key Terms

Collected here are the italicized, key terms from the introduction. Each is a hyperlink bringing to where the term is introduced.

Holographic CFT
Hydrodynamics
Linear ramp
Local conformal transformations
Lyapunov exponent λ
Maximally chaotic
Microcanonical averaging
Modular invariance
Near-extremal spectrum
OPE block $\mathfrak{B}_{\mathcal{O}}$
OPE coefficient
Operator product expansion (OPE)
Operator-state correspondence
Out-of-time-ordered correlator $\langle V(t)W(0)V(t)W(0)\rangle$
Partition function $Z(\beta)$
Path integral Z
Plateau
Pole skipping
Primary operators
Quantum chaos
Quasi-primary operators
Random matrix statistics
Random matrix theory
Random matrix universality
Scaling dimension Δ
Scrambling
Semi-classical approximation
Shadow operator formalism
Spectral correlations

Spectral form factor

Spectral statistics

Ward identities

Acknowledgements

I would like to thank my supervisor Moshe Rozali, for all the guidance in developing as a physicist, and his unmatched understanding and aid throughout my whole program. I would also like to thank my frequent collaborator Felix Haehl; without both of these physicists' expertise, intuition, insight, and many discussions, this thesis would not exist.

I would like to give my heartfelt thanks to Sean Cooper and Eric Lees, for their overwhelming help as roommates, friends, and scientists; and David Wakeham and Chris Waddell, for their friendship, intelligence, and camaraderie in going through the full process of graduate school together. I would also like to thank all the other graduate students of Hennings 418; Dominik Neuenfeld, Alex May, Petar Simidzija, Jonah Berean-Dutcher, Shovon Biswas, Abhisek Sahu, Pompey Leung, and Rana Zibakhsh, for their friendship and conversations.

I would like to thank all the post-doctoral researchers at UBC throughout my program, in particular James Sully and Charles Marteau. Finally, I would like to thank the many friends I made at UBC and in Vancouver, who helped keep me motivated.

Dedication

To my parents and siblings, for their unbelievable support throughout my decade of university.

Chapter 1

Introduction

The primary goal of this thesis is investigating quantum chaotic phenomena in conformal field theories.

We begin by providing a conceptual overview and motivations, situating the thesis in the broader field of high energy theory. We then provide a technical overview for the theories underlying this thesis; chaos, conformal field theory, and holography. First, we define quantum chaos using the standard language of quantum mechanics; this section is comparatively less mathematically technical, focused primarily on physical phenomena and their mathematical expression. Next we introduce conformal field theories, focusing on their properties that are relevant for quantum chaos. This section is mathematically technical, with some results of conformal field theories being "derived" to familiarize the reader with the technical analysis of conformal field theories. Finally we introduce holography and the AdS/CFT correspondence, since it is both a motivation for studying quantum chaos as well as the topic of one of the projects in this thesis. This section is also less mathematically technical. The introduction is concluded by providing summaries of each chapter.

1.1 Motivation and background

Chaotic dynamics are incredibly important for physical systems of all scales, from black holes to atomic nuclei. Whenever a system is no longer the simple and symmetric kind found in undergraduate courses, classical and quantum systems alike begin displaying extremely complicated behaviour. Yet despite this complexity, we can still categorize these systems in a way that patterns and predictable phenomena can still be found; chaos is the framework that allows this. It can explain the approach of systems to thermodynamic equilibrium or "typical" states, justify the use of statistical mechanics, and explain various transport phenomena [6–8].

In classical physics, chaos is often defined via "the butterfly effect"; small differences in initial conditions (e.g. the position and velocities of particles) lead to exponentially diverging trajectories as time goes on. Videos of double

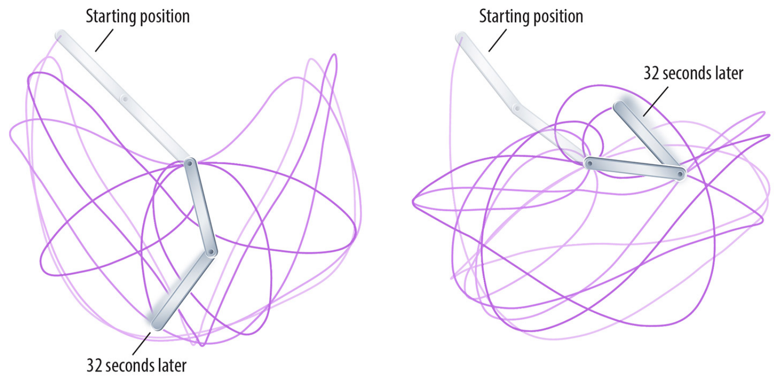

Figure 1.1: An image showing the effect of small changes in a chaotic system, a double-pendulum. The two pendulums start with almost exactly the same position, but end up at wildly different positions as time goes on. This image was taken from [5].

pendulums or billiards bouncing in oddly shaped cavities can show this beautifully; even if they start nearly at the same point, the objects start following wildly different trajectories, as if there was no connection between their starting points.

When we try to apply this logic to quantum mechanics, the story gets trickier. We can quantize any classical system, so the existence of chaos in the classical system should impact some part of the quantized system. But the entire concept of "trajectories" loses meaning in quantum mechanics, where we only have probability amplitudes to work with. There are also quantum mechanical systems with no simple classical analog; an intrinsically quantum definition of chaos is thus needed for these systems.

Moreover, classical chaos is usually a consequence of non-linearities in the equations of motion; the superposition of two chaotic trajectories need not be a valid trajectory itself. But the Schrodinger equation is, by definition, a linear equation of motion, so where can quantum chaos come in?

One way it can come in is random matrix universality. By looking at the allowed energies of a quantum chaotic system, nearby energy levels look like they just come from a random matrix[8–11]. This matches the intuition that chaos means "random" dynamics; the Hamiltonian of a system determines both how a system evolves in time and its energies, so "random" dynamics should come with "random" energy levels. Random matrix universality was first put forward to explain the energies of heavy atomic nuclei [12], and has been found in many classically chaotic systems after being quantized [13–15]. Importantly, it is a feature of the *coarse-grained* statistics of the energy levels, not their fine-grained features; one needs to do some kind of averaging, for example over small energy windows, to see random matrix universality.

Another way quantum chaos comes in for systems with many degrees of freedom (e.g. a system with many particles) brings back exponential growth, but in a new context. This is the idea of scrambling; if one makes a small perturbation that affects only a few degrees of freedom in a chaotic system, that perturbation will grow exponentially quickly until all the degrees of freedom are affected [16–18]. For example, one could add some energy to a few particles in a system, and chaotic dynamics will spread this change, affecting every particle in the system. Scrambling has been demonstrated in many systems [19–23], most famously in black holes and (as we will soon see, their related) systems with enormous amounts of symmetry called conformal field theories (CFTs).

CFTs arise naturally as limits of systems containing many interacting particles, the Ising model being one of the most famous [24, 25]. They are systems with an enormous amount of symmetry, such that they "look the same" when zooming in or out on the system. In other words, the dynamics are the same at any length scale. Thanks to this symmetry, CFTs come with a unique structure that makes them much simpler to analyze compared to other quantum field theories.

In the last 25 years, CFTs have become even more interesting thanks to the fascinating discovery that certain CFTs in d spacetime dimensions can actually describe systems of quantum gravity in one spacetime dimension higher[26–28]. This is the famous AdS/CFT correspondence, a type of "holography" where two systems in different numbers of dimensions describe each other. It has become one of the most active fields in the quest to understand (and define!) quantum gravity.

Holography is one of the major reasons understanding chaos in CFTs is so timely. The fact that scrambling occurs when the spacetime is a black hole background, together with the AdS/CFT correspondence, tells us that CFTs should also contain scrambling. Moreover, the calculations one does in gravity seem to inherently probe only the coarse-grained information of the CFT [29, 30], and this coarse-grained information shows that certain high energy states in gravity obey random matrix universality [31–35]; thus holographic CFTs must also contain random matrix universality. Understanding chaos in CFTs, both in the sense of random matrix universality and scrambling, is essential.

However, chaos can be difficult to see in symmetric systems. The symmetries tend to "wash away" any consequences of chaos, as they cause the theory to acquire a unique structure that cannot come from a random matrix [36]. For example, in a system with conserved angular momentum, states with different angular momentum are completely unrelated, and the symmetry can be exploited to generate new states from old ones. If chaos exists in these systems, it needs to be understood in terms of their unique structure, and the parts of the theory that are unrelated by symmetry and can have chaos in them need to be identified.

Many results on the relationship between chaos and the general structure of CFTs have been discovered in the last several years, including: scrambling in two-dimensional CFTs [21, 37], the coefficients of three-point functions [38–41], the eigenstate-thermalization hypothesis [42, 43], and defining ensembles of CFTs [44–46].

In this thesis, we make several contributions to the understanding of chaos in conformal field theories. We demonstrate how random matrix universality can appear in two-dimensional conformal field theories, and its connection to their rich structure of symmetry. We show how "arithmetic chaos" and proper quantum chaos are connected, and discover that the gravity result that predicts random matrix universality in CFTs can be re-discovered from simple assumptions. We analyze scrambling in higher-dimensional CFTs, creating an effective theory to capture it and find a deep connection to CFT structure. Finally, we improve our understanding of the AdS/CFT correspondence by looking at CFTs with boundaries, which can be models for black holes.

We now review the technical details that will allow the reader to understand the results of this thesis. We work in natural units, with $c = \hbar = k_B = 1$. The technical overview is based largely off [8, 11, 25, 47–52]. We assume the reader is familiar with quantum mechanics and special relativity, and has seen some basics about quantum field theory and general relativity (although we will review the most relevant parts of them). Definitions of key terms are denoted by *italics* and can be found in the glossary beginning on page xx, while important facts and key takeaways are denoted by **bolded statements**. Footnotes are used primarily for clarifications and non-essential information. At the end of each subsection, we provide summaries.

1.2 Chaos in quantum systems

Whenever we want to explain some physical phenomenon or general characteristic in a physical system governed by quantum mechanics, we have to do so using the theoretical building blocks of quantum mechanics:

- States that are vectors in a Hilbert space $|\psi\rangle \in \mathcal{H}$, which gives us the physical state of the system at a given time. These are usually defined with respect to a specific basis of states. These states come with an inner product or "overlap", $\langle\psi_1|\psi_2\rangle \in \mathbb{C}$.

- The Hamiltonian operator H that evolves these states forward in time according to the Schrodinger equation $H|\psi(t)\rangle = i\partial_t|\psi(t)\rangle \Leftrightarrow |\psi(t_2)\rangle = e^{iH(t_2-t_1)}|\psi(t_1)\rangle$. We can often think of the Hamiltonian as a matrix. The Hamiltonian also tells us the energy levels E_n or spectrum of our system via its eigenvalues, $H|E_n\rangle = E_n|E_n\rangle$. Energy eigenstates are a common basis of states.

- The other operators $\mathcal{O}_i$ that correspond to measurements, along with their expectation values $\langle\psi|\mathcal{O}|\psi\rangle$, and correlation functions/correlators $\langle\psi|\mathcal{O}_1\cdots\mathcal{O}_n|\psi\rangle$. If we work in the Heisenberg picture, where operators evolve in time instead of states, then $\mathcal{O}(t) = e^{-iHt}\mathcal{O}(0)e^{iHt}$.

With these building blocks, we can say what state our system is in, how it will evolve in time, the allowed energies, what the results of any measurement could be in that state, and how different measurements are statistically correlated; in other words, any question we could ever want to answer.

What does it mean, in terms of these building blocks, for a quantum system to be chaotic? In classical mechanics, the standard definition of chaos for a particle (similar definitions exist for a more general classical system) is that under a small change in initial position, the change in the particle's path $\mathbf{x}(t)$ grows exponentially in time:

$$\text{Classical chaos: } \mathbf{x}_2(0) = \mathbf{x}_1(0) + \delta\mathbf{x} \implies |\mathbf{x}_2(t) - \mathbf{x}_1(t)| \approx \delta\mathbf{x}e^{\lambda t}. \quad (1.2.1)$$

However, this definition cannot work for *quantum chaos*. Because of the probabilistic nature of quantum mechanics, the "particle's path" is not a well-defined observable. The "difference" (overlap) between two states $\langle\psi_1(t)|\psi_2(t)\rangle$ also can't be used, since this overlap is actually constant in time.

Two primary approaches exist to defining what is meant by quantum chaos. The first focuses on the Hamiltonian and energies of a system, and is called random matrix universality. The second focuses on operators and correlation functions, and is called scrambling. Both are deeply linked to classical notions of chaos, and have been discovered analytically and numerically in a variety of systems.

1.2.1 Random matrix universality

The idea that quantum chaotic systems should be related to random matrices goes back to Wigner and Dyson [9, 10] trying to understand the energy levels in complex systems such as heavy atomic nuclei. Their first insight was that instead of trying to precisely model and predict the exact spectrum of these systems theoretically, you could "smooth out" the spectrum, looking only at its approximate and average, or *coarse-grained*, behaviour of the spectrum. For example, one could ask about the probability that two energy levels are close together, or the average number of energy levels close to a given level. Thus, one should focus on *spectral statistics*, rather than the exact, discrete spectrum. This can be achieved explicitly by doing a *microcanoncial average*, where one averages energy-dependent quantities over a small window of energies, then replacing any erratic, non-continuous behaviour with approximate smooth behaviour.[1] However, any method of coarse-graining is expected to be equivalent (e.g. averaging over coupling constants).

The second insight was that many of these statistics could be understood by assuming that, in a narrow enough energy window and away from the smallest and largest energies in the spectrum, the Hamiltonian was essentially a random matrix. By this we mean that if we only examine states that lie in some energy window $[E-\Delta E, E+\Delta E]$, which we achieve by multiplying the Hamiltonian with a projection operator $\mathcal{P}_{[E-\Delta E,E+\Delta E]}$, we expect

$$H\,\mathcal{P}_{[E-\Delta E,E+\Delta E]} \approx \text{a random matrix.} \tag{1.2.3}$$

The intuition is that these Hamiltonians are so complex, and any structure they have is only visible for the most precise questions, that one could

[1] Explicitly, we can write an energy-dependent function $f(E)$ as

$$\begin{gathered} f(E) = \langle f(E)\rangle + \widetilde{f}(E)\,, \\ \langle f(E)\rangle \approx \frac{1}{\Delta E}\int_{E-\Delta E/2}^{E+\Delta E/2} dE'\, f(E)\,, \quad \frac{1}{\Delta E}\int_{E-\Delta E/2}^{E+\Delta E/2} dE'\, \widetilde{f}(E) \approx 0 \end{gathered} \tag{1.2.2}$$

where $\langle f(E)\rangle$ is a smooth function called the coarse-grained or averaged $f(E)$, while $\widetilde{f}(E)$ are the erratic fluctuations. We will often use angle brackets to refer to this (or similar) types of averaging procedures.

possibly model them by a random matrix.[2] The upshot would be their coarse-grained, average statistics could be discovered by doing an average over an appropriate ensemble of random matrices. In other words, the spectral statistics in quantum chaotic systems should be the same as in *random matrix theory*. This statement is called *random matrix universality*.

Random matrix theory is described by defining a probability distribution over the space of $D \times D$ Hermitian matrices and performing averages with it. We focus on the most basic example, the Gaussian Unitary Ensemble (GUE):

$$\begin{aligned} P(H) &\propto \exp\left\{-\frac{D}{2}\operatorname{Tr}\left(H^2\right)\right\}, \; H = H^\dagger\,, \\ \langle\cdots\rangle_P &\equiv \int dH P(H)\cdots\,, \end{aligned} \tag{1.2.4}$$

i.e. we calculate averages by integrating over all Hermitian matrices weighted with the probability distribution $P(H)$. Each matrix can be thought of as a Hamiltonian for a system in a $D \equiv \dim \mathcal{H}$ dimensional Hilbert space. There are two other Gaussian ensembles, which differ by the discrete symmetries they possess: the Gaussian Orthogonal Ensemble (GOE), which models systems with time-reversal symmetry; and the Gaussian Symplectic Ensemble (GSE), which models systems with time-reversal but not rotational symmetry. We will take the large D limit $D \gg 1$.

Note that here the angle brackets indicate an ensemble average, not a quantum correlation function; the meaning of the angle brackets will usually be clear from context, and we will often drop the P subscript.

For any system, we primarily characterize the statistics of energy levels via the *density of states* (a function of energy) and its Legendre transform, the *partition function* (a function of temperature)

$$\rho(E) = \sum_n \delta(E - E_n) = \operatorname{Tr}\delta(E - H)\,, \tag{1.2.5}$$

$$Z(\beta) = \sum_n e^{-\beta E_n} = \int dE \rho(E) e^{-\beta E} = \operatorname{Tr} e^{-\beta H}\,. \tag{1.2.6}$$

$\delta(x)$ is the Dirac delta function. Both are fully determined by the energy levels of the system. The partition function from statistical mechanics is used to calculate expectation values and correlators for systems at a fixed

[2] Note that (1.2.3) is a basis-dependent statement; we could always diagonalize any Hamiltonian with its energy basis $|E_n\rangle$, making it just a diagonal list of energies. The claim is that the Hamiltonian looks like a random matrix in a non "fine-tuned" basis, i.e. a basis that doesn't depend on the energies of the system.

inverse-temperature $\beta > 0$ i.e. systems in a thermal state or in the canonical ensemble. For example, for regular quantum operators we can calculate their correlation function in a thermal state as

$$\langle \mathcal{O}_i \mathcal{O}_j \rangle_\beta = \frac{1}{Z(\beta)} \mathrm{Tr}\Big\{ e^{-\beta H} \mathcal{O}_i \mathcal{O}_j \Big\} . \tag{1.2.7}$$

The statistical quantity we are most interested in is the "connected two-point function of the density of states", i.e. the *spectral correlations*,

$$\langle \rho(E_1)\rho(E_2) \rangle_{P,\mathrm{conn.}} \equiv \langle \rho(E_1)\rho(E_2) \rangle_P - \langle \rho(E_1) \rangle_P \langle \rho(E_2) \rangle_P . \tag{1.2.8}$$

where we are averaging over the ensemble of random matrices. This measures the correlation of energy levels; if the presence of an energy level at E_1 had no effect on whether there was an energy level at $E_2 \neq E_1$, the connected correlator would be zero. In the GUE, the connected correlator for small energy differences $\omega \equiv E_1 - E_2$ is

$$\left\langle \rho\left(E_{\mathrm{av}} + \frac{\omega}{2}\right) \rho\left(E_{\mathrm{av}} - \frac{\omega}{2}\right) \right\rangle_{\mathrm{conn.}} \approx \langle \rho\left(E_{\mathrm{av}}\right) \rangle \, \delta(\omega) - \frac{\sin^2\Big(\pi\omega \, \langle \rho\left(E_{\mathrm{av}}\right) \rangle \Big)}{(\pi\omega)^2} . \tag{1.2.9}$$

This form of the spectral correlations is called *random matrix* statistics. The first term is just the auto-correlation of an energy level with itself, and is not unique to random matrix theory. It is present for any system under some coarse-graining and any ensemble. The second term, known as the "sine kernel", is responsible for *eigenvalue repulsion*; it is negative and gets larger as ω gets smaller (until $\omega \sim \langle \rho\left(E_{\mathrm{av}}\right) \rangle^{-1}$). Indeed, for $\omega \gg \langle \rho\left(E_{\mathrm{av}}\right) \rangle^{-1}$, the $\sin^2(\cdots)$ in the numerator oscillates sufficiently rapidly that we can replace it with its average value of $\frac{1}{2}$ in integrals that the spectral correlations appear in. In this situation, the correlator actually takes a nearly universal form for any Gaussian ensemble,

$$\left\langle \rho\left(E_{\mathrm{av}} + \frac{\omega}{2}\right) \rho\left(E_{\mathrm{av}} - \frac{\omega}{2}\right) \right\rangle_{\mathrm{conn.}} \approx -\frac{1}{\beta \pi^2 \omega^2} , \quad \beta = \begin{cases} 1 & \mathrm{GOE} \\ 2 & \mathrm{GUE} \\ 4 & \mathrm{GSE} \end{cases} . \tag{1.2.10}$$

The interpretation is that the probability of finding two energy levels close to each other decreases the closer they get.

The statement of random matrix universality is that, under some method of coarse-graining and in certain energy ranges, **the spectral correlations**

in any chaotic system exactly matches that of random matrix theory (using the correct ensemble for the symmetries of the system). In other words, the statistical properties of certain pairs of energies are the same in quantum chaotic systems and random matrix theory. For example, if a system has no discrete symmetries, its connected correlator should contain eigenvalue repulsion (1.2.10) for appropriate energy differences.

Any method of coarse-graining is believed to be equivalent; *microcanonical averaging* is the most standard, but one could also average over some parameters that appear in the theory (e.g. coupling constants) or over a true ensemble if one is defined.

We can also express random matrix universality in terms of the partition function, through what is called the *spectral form factor*. This is defined by taking the product of two partition functions with different inverse-temperatures and coarse-graining:

$$\langle Z(\beta_1)Z(\beta_2)\rangle = \int dE\, d\omega \left\langle \rho\left(E+\frac{\omega}{2}\right)\rho\left(E-\frac{\omega}{2}\right)\right\rangle e^{-(\beta_1+\beta_2)E+\frac{\beta_1-\beta_2}{2}\omega}\,. \tag{1.2.11}$$

This is most commonly presented by analytically continuing the inverse-temperatures, $\beta_{1,2}\to\beta\pm iT$,[3] with T being thought of as time (which is unfortunately the standard notation in chaos literature, despite T meaning temperature in almost all other contexts). Then plugging in (1.2.9) gives the connected part of the spectral form factor,

$$\begin{aligned}
&\langle Z(\beta+iT)Z(\beta-iT)\rangle_{\text{conn.}}\\
&\quad=\int dE\, d\omega \left\langle \rho\left(E+\frac{\omega}{2}\right)\rho\left(E-\frac{\omega}{2}\right)\right\rangle_{\text{conn.}} e^{-2\beta E+iT\omega}\\
&\quad=\min\left(\frac{T}{4\pi\beta}e^{-2\beta E_0}, Z(2\beta)\right)\,.
\end{aligned} \tag{1.2.12}$$

[3]The reason for this continuation is that under this analytic continuation, the spectral form factor looks like a thermal two-point function (1.2.7) with the matrix elements stripped off,

$$\frac{1}{Z}\operatorname{Tr}\left\{e^{-\beta H}\mathcal{O}(t)\mathcal{O}(0)\right\} = \frac{1}{Z}\sum_{m,n} e^{-\beta E_m+it(E_m-E_n)}|\langle m|\mathcal{O}|n\rangle|^2\,,$$

where we've inserted two complete sets of energy eigenstates. If we split the Boltzmann factor up (which is a common method of regularizing the thermal two-point function in quantum field theories), we get

$$\frac{1}{Z}\operatorname{Tr}\left\{e^{-\frac{\beta}{2}H}\mathcal{O}(t)e^{-\frac{\beta}{2}H}\mathcal{O}(0)\right\} = \frac{1}{Z}\sum_{m,n} e^{-\frac{\beta}{2}(E_m+E_n)+it(E_m-E_n)}|\langle m|\mathcal{O}|n\rangle|^2\,.$$

Relabelling $\beta\to 2\beta$ and $t\to T$, and using the density of states, we get (1.2.12) after removing the matrix elements $|\langle m|\mathcal{O}|n\rangle|^2$ and normalization $\frac{1}{Z}$.

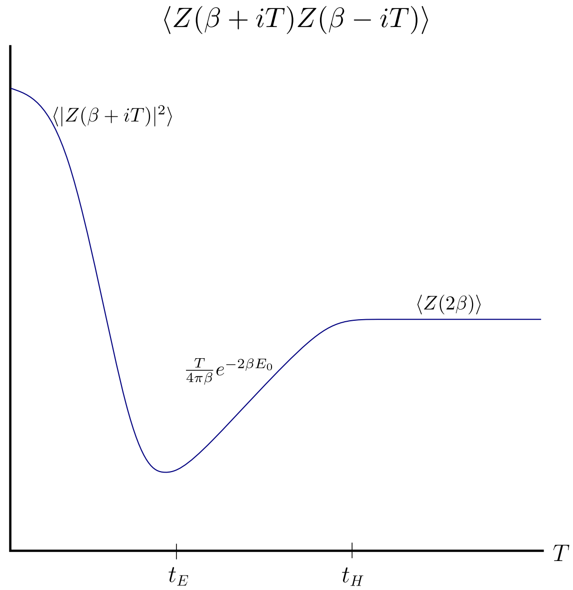

Figure 1.2: A plot showing the general form of the spectral form factor for some fixed β. We see the transition between the dip, ramp, and plateau.

where E_0 is the ground state energy. The first term comes from eigenvalue repulsion (1.2.10), and is known as the *linear ramp* (the other Gaussian ensembles have the appropriate factor of 2). The second term comes from the auto-correlation term, and is known as the *plateau*. The time where the ramp transitions into the plateau is called the Heisenberg time $t_H \sim \langle \rho(E) \rangle$, when the spectral form factor begins probing neighboring energy levels.

Note that (1.2.12) is just the connected part of the spectral form factor; in the full spectral form factor for a real physical system (1.2.11), the disconnected part $|\langle Z(\beta+iT)\rangle|^2$ dominates at early times, but begins decaying until being overtaken by the ramp. This initial behaviour is called the "dip"; the time the dip transitions into the ramp is called the ergodic or Thouless time t_E, and is theory-dependent. We show the general dip-ramp-plateau behaviour in Figure 1.2

The fact that the connected part of the spectral form factor is not zero is a consequence of the fact that we are coarse-graining the product of partition functions (for example, by taking an ensemble average or averaging over windows of time T). If we weren't, and we just had $Z(\beta+iT)Z(\beta-iT)$ with no averaging, then obviously this is disconnected by definition; it is just the product of two functions.

Random matrix universality and symmetry: An important note is that thus far, the Hamiltonians we have considered (e.g. (1.2.4)) do not have any additional symmetry. **If a Hamiltonian has symmetry, only the symmetry-unconstrained part of the spectrum can exhibit random matrix statistics.** In other words, all the consequences of this symmetry on the spectrum must be discovered and fixed, and whatever part of the spectrum of energies that remains can have correlations in the energy levels that look like random matrix theory.

As an example, consider $SU(2)$ symmetry: the Hamiltonian has conserved angular momentum with the conserved charges $[H, J_i] = 0$, $i = x, y, z$, and we analyze the spectrum of energies/states. We categorize states by their energy E, their (total) angular momentum $j^2 \equiv l(l+1)$, $l = 0, 1/2, 1, \ldots$, and the eigenvalue of J_z $m = -l, -l+1, \ldots l$. In summary, the spectrum is given by the states $|E, l, m\rangle$. We can have multiple states with the same value of l and m but different energies, however the Hamiltonian will never evolve a state from one value of l or m into a different value. Thus, right away we know that energies/states with different l and m are unrelated by the Hamiltonian.

This categorization of states also shows how symmetry constrains the spectrum of energies. For any state $|E, l, m\rangle$, there must exist states with the same energy and total angular momentum but with m raised or lowered by one,

$$(J_x \pm iJ_y)|E, l, m\rangle \propto |E, l, m \pm 1\rangle \, , \; m \neq \pm l \, . \tag{1.2.13}$$

where once $m = \pm l$, we cannot raise or lower the state anymore. Thus, starting with the "highest weight state" $m = l$ generates $2l$ additional states in the spectrum with the same energy, which clearly cannot be a spectrum coming from a random matrix. This also tells us that the structure of the Hamiltonian in a basis other than the energy basis[4] is

$$\langle i, l, m|H|j, l', m'\rangle = \delta_{l,l'}\delta_{m,m'}H^{(l)}_{i,j} \tag{1.2.14}$$

($\delta_{i,j}$ is the Kronecker delta), where the matrix on the right hand side does not depend on m.

However, this structure tells us nothing about what specific energies the highest-weight states have, i.e. it tells us nothing about the matrix $H^{(l)}_{i,j}$. Thus the energies of the highest weight states in a given angular momentum sector (i.e. all states with a given l) are the symmetry unconstrained part of the spectrum and can exhibit random matrix statistics.

[4] $|i, l, m\rangle = \sum_n a_n |E_n, l, m\rangle$ is a linear combination of energy eigenstates with the same l and m.

Random matrix universality has been demonstrated in many systems, particularly those whose classical analog is also chaotic e.g. a particle moving in a two-dimensional stadium with non-circular walls. However, many of these systems have a low number of degrees of freedom. Chaos in systems with many degrees of freedom is a new field; while random matrix universality still applies, such systems can come with additional structure that makes chaos more rich, as we discuss next.

Summary: Quantum chaotic systems are often defined as systems where the statistical correlation between energy levels matches that of random matrix theory. These correlations cause the spectral correlations to contain eigenvalue repulsion (1.2.10), and cause the spectral form factor to contain a linear ramp (1.2.12). Symmetry tends to wash away the presence of chaos in the spectrum unless we focus on the energy levels that symmetry does not constrain.

1.2.2 Scrambling

The random matrix theory approach to chaos focuses on the Hamiltonian and energy levels of the system. In the *scrambling* approach to quantum chaos, we focus instead on the other building blocks of a quantum theory: operators and their correlation functions. The idea is to look at systems with many degrees of freedom, e.g. many particles on a lattice interacting, and examine what happens if just a few of those particles are perturbed. In any system where the particles interact the perturbation will spread to the other particles, but in a chaotic system this spread is exponentially fast!

We motivate this using the standard classical definition of chaos, (1.2.1). We can recast this in terms of the Poisson bracket,

$$\text{Classical chaos: } \{x(t), p(0)\} \equiv \frac{\delta x(t)}{\delta x(0)} = e^{\lambda t} \,. \tag{1.2.15}$$

When we quantize a classical system, Poisson brackets become commutators $i\{\cdot,\cdot\} \to [\cdot,\cdot]$, and classical variables become operators. This suggests that we could look for exponential growth in quantities like operator commutators.

A candidate that works well for this purpose in systems with many degrees of freedom N[5] is the commutator squared for a system at finite

[5]Note that the number of degrees of freedom N and the dimension of the Hilbert space D are not the same. For example, a one-dimensional Harmonic oscillator is considered to have a single degree of freedom $N = 1$, as it only comes with a single position operator

temperature β,

$$\begin{aligned}-\langle [V(t), W(0)]^2\rangle_\beta = &\langle V(t)W(0)W(0)V(t)\rangle + \langle W(0)V(t)V(t)W(0)\rangle \\ &- \langle V(t)W(0)V(t)W(0)\rangle - \langle W(0)V(t)W(0)V(t)\rangle\,,\end{aligned} \tag{1.2.16}$$

where on the left hand side we stress that we are taking a thermal correlation function (1.2.7), i.e. calculating the expectation value of the commutator in a system at inverse-temperature β. $V(0)$ and $W(0)$ are operators involving only a few different degrees of freedom each (e.g. if we had a system of 100 particles, $V(0)$ and $W(0)$ would excite particles 1 through 4 and 85 through 87 respectively). For simplicity, we assume their $t = 0$ two-point function is equal to 1, $\langle V(0)V(0)\rangle = \langle W(0)W(0)\rangle = 1$.

The physical intuition is that the commutator measures how much perturbing the system with $W(0)$ affects a later measurement of $V(t)$. Since they involve different degrees of freedom at time $t = 0$, we expect that they shouldn't impact each other significantly up until the so-called relaxation time t_r;[6] the commutator should be small compared to the number of degrees of freedom. However, for chaotic systems the dynamics are expected to cause all degrees of freedom to be "intermixed" with each other exponentially quickly as time goes on, and so $V(t)$ will start to involve $W(0)$'s degrees of freedom. Thus for chaotic systems, we expect that heuristically

$$-\langle [V(t), W(0)]^2\rangle \sim \begin{cases} \frac{1}{N} & t \lesssim t_r \\ \frac{1}{N}e^{\lambda t} & t_r \ll t \ll t_s \end{cases}. \tag{1.2.17}$$

This behaviour is what we call *scrambling*. The operator $V(t)$ grows exponentially with *Lyapunov exponent* λ in the space of degrees of freedom, up until the scrambling time $t_s \equiv \lambda^{-1}\log N$. At the scrambling time, the operator is "scrambled" among all the degrees of freedom in the system, as shown in Figure 1.3. In other words, small perturbations of chaotic systems with many degrees of freedom grow exponentially fast, until all the degrees of freedom are affected.

When operators are local, i.e. associated with a particular position in space, scrambling still occurs. The spatial spread of the correlator can take

x and its conjugate momentum p. However, the harmonic oscillator has infinitely many energy eigenstates, so $D = \infty$. Meanwhile, the prototypical many-body system, a chain of N spin-$\frac{1}{2}$ particles at fixed positions has N degrees of freedom (one for each spin), and the basis states are fully specified by saying whether each spin is up or down, so $D = 2^N$.

[6] t_r is the time scale associated with the exponential decay of the thermal two-point function $\langle V(t)V(0)\rangle$.

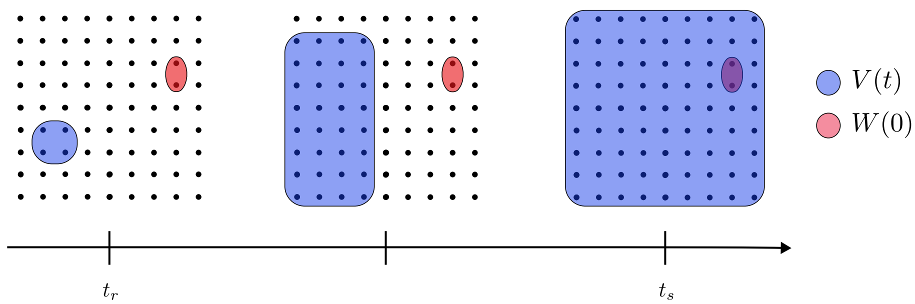

Figure 1.3: A cartoon of scrambling. The dots represent the degrees of freedom (e.g. a lattice of particles that interact with each other). The blue region represents the degrees of freedom that the operator $V(t)$ involves, while the red region represents the degrees of freedom for $W(0)$. We see that the blue region grows in time until it includes all degrees of freedom at the scrambling time t_s.

different forms, but we focus on so-called "ballistic spreading",

$$-\langle [V(x,t), W(0,0)]^2 \rangle \approx \frac{1}{N} e^{\lambda\left(t - \frac{x}{v_B}\right)}\,,\; t_r \ll t \ll t_s\,. \tag{1.2.18}$$

v_B is the *butterfly velocity*, and describes the speed at which scrambling spreads throughout the spatial system.

The exponential growth of the correlator is a consequence of the decay of the third and fourth terms in (1.2.16), called *out-of-time-ordered correlators* (OTOCs),

$$\langle V(t)W(0)V(t)W(0) \rangle \approx \left(1 - \frac{1}{N} e^{\lambda t}\right)\,, \quad t_r \ll t \ll t_s\,. \tag{1.2.19}$$

This correlator is often what is explicitly calculated to show scrambling, however the commutator is more physically motivated.

It's important to note that the scrambling time is always less than the ergodic time t_E, when random matrix statistics begins to take over. Thus, scrambling is often called early time chaos, while random matrix statistics is called late time chaos.

One can show that, unlike in classical chaos, there is a limit to how fast operators can scramble:

$$\text{Chaos bound: } \lambda \leq \frac{2\pi}{\beta}\,. \tag{1.2.20}$$

Maximal chaos and hydrodynamics

Physical systems that saturate the bound (1.2.20) are called *maximally chaotic*. Black holes are one example of a maximally chaotic system; the commutator squared for operators that create a few particles in a black hole background grows exponentially [16]. In [53], **it was proposed that the presence of scrambling in maximally chaotic systems is due to *hydrodynamics*.**

Hydrodynamics is the effective theory for conserved quantities, such as energy and momentum. That is, it describes the dynamics of conserved quantities (e.g. the transport of energy and momentum throughout the system) on length and time scales where the only relevant degrees of freedom are those that are directly related to these conserved quantities. These dynamics appear in any theory with no other long-lived, low-energy (i.e. gapless) degrees of freedom, and thus hydrodynamics is extremely general and important for many physical phenomena.

[53] showed that a hydrodynamic effective field theory can easily contain scrambling, matching perfectly with many known maximally chaotic systems (including black holes). This suggests that maximal chaos is hydrodynamic in nature. One of the main predictions of this link is that the two-point correlation function of the energy density $T^{00}(t,x)$ contains a unique structure called *pole skipping*. In general hydrodynamic theories, the Fourier transform of the energy density two-point function can be written as

$$\langle T^{00}(\omega,k)T^{00}(-\omega,-k)\rangle \approx \frac{f(\omega,k)}{g(\omega,k)}\,, \tag{1.2.21}$$

and generally has a line of poles for imaginary frequencies $\omega = i\tilde{\omega}(k)$ due to zeroes in the denominator, $g(i\tilde{\omega}(k),k) = 0$. But for a hydrodynamic theory that contains maximal chaos, there is a single point on this line where the singularity is "skipped" due to a simultaneous zero in the numerator $f(\omega_s,k_s) = 0$. The location of this point is explicitly related to scrambling; the pole is skipped at $\omega_s = i\lambda$, $k_s = i\frac{\lambda}{v_B}$, where λ is the Lyapunov exponent and v_B is the butterfly velocity from (1.2.18).

In summary, if scrambling in a maximally chaotic theory is explained by hydrodynamics, the energy density correlator should behave as

$$\langle T^{00}(\omega,k)T^{00}(-\omega,-k)\rangle \approx \frac{f(\omega,k)}{g(\omega,k)}\,,\; f\left(i\lambda, i\frac{\lambda}{v_B}\right) = g\left(i\lambda, i\frac{\lambda}{v_B}\right) = 0\,. \tag{1.2.22}$$

Summary: Quantum chaotic systems are sometimes defined as those where perturbations of a few degrees of freedom grow exponentially quickly in time. We can measure this by the exponential growth of certain thermal correlation functions, i.e. the commutator squared (1.2.17) and the OTOC (1.2.19). This growth is bounded, and systems that saturate this bound are proposed to be connected to hydrodynamics.

1.3 Conformal Field Theories

Common to many areas of physics is the focus on symmetries; systems with a large number of symmetries are often much simpler to describe, and can often be fully determined from those symmetries alone. The hydrogen atom remains one of the only quantum systems we can describe analytically thanks to its spherical symmetry. And as we saw in section 1.2.1, symmetric systems can still exhibit chaos.

For quantum field theories, one of the most powerful symmetries is *conformal symmetry*. Roughly speaking, conformal symmetry means that the system looks the same no matter how far you "zoom in" on the system. Such a symmetry can arise in various condensed matter systems, and has gained further importance due to the link to gravity, which we will discuss in section 1.4. This symmetry provides an overwhelming amount of structure to physical systems, allowing us to categorize them in a unique and powerful way. As our goal is to understand how chaotic phenomena appear within this structure, here we lay out its fundamentals. To understand these, we must first review some of the basics of standard quantum field theory.

This section is quite technical and pedagogical, with the goal of introducing and justifying enough conformal field theory to understand the calculations in the rest of the thesis. The bold statements and their clarification around (1.3.37), (1.3.42), (1.3.48), (1.3.74), (1.3.82), and (1.3.84) are the key takeaways, i.e. the relationship between operators and states, how states can be categorized as (quasi-)primaries or descendants, the existence of the OPE, the relationship between the thermal partition function and the Euclidean time circle, and modular invariance.

1.3.1 Review of quantum field theory

Quantum field theories are systems where the fundamental objects are fields that can create and annihilate particles, rather than the particles themselves. One motivation for considering fields instead of particles is that in a relativistic system, where the Einstein relation tells us $E = mc^2$, the creation of particle-antiparticle pairs becomes expected if the energy is high enough. Moreover, a relativistic single-particle quantum mechanics ends up violating causality. By utilizing quantum fields (the quantum equivalent of classical fields e.g. the electric and magnetic fields), these issues are avoided.

These theories have a very unique mathematical structure, quite different from the standard quantum mechanical systems in section 1.2.[7] Thankfully, conformal field theories recover some of that familiar structure, but because they are a specific example of quantum field theories, we very briefly mention some of their basic theoretical framework.

We consider a theory in d dimensions with coordinates x^μ, $\mu = 0, 1, \cdots, d-1$. Throughout this thesis, we will often work in Euclidean coordinates, i.e. all of our dimensions will be spacelike. This is a standard trick for quantum field theories in general, as it makes the convergence of various quantities much easier to deal with. We can always go back to Minkowski spacetime by analytic continuation of the time coordinate $\tau \equiv x^0 \to -it \equiv -ix^0$; τ is Euclidean or imaginary "time", and t is Minkowski or regular time. The remaining coordinates will often be specified by $\vec{x}$, i.e. $x^\mu = (x^0, \vec{x})$.

Theories will live in a geometry given by the metric $g_{\mu\nu}(x)$, which determines lengths via

$$ds^2 = g_{\mu\nu}(x) dx^\mu dx^\nu \,, \; \mu, \nu = 0, 1, \cdots, d-1 \,. \tag{1.3.1}$$

We can change coordinates $x'^\mu(x)$, which also changes the metric via

$$g'_{\mu\nu}(x') = g_{\sigma\rho}(x) \frac{\partial x^\rho}{\partial x'^\mu} \frac{\partial x^\sigma}{\partial x'^\nu} \,. \tag{1.3.2}$$

Flat Euclidean space $\mathbb{R}^d$ in Cartesian coordinates is given by the simplest non-trivial metric, $g_{\mu\nu} = \delta_{\mu\nu} = \text{diag}(1, \cdots, 1)$. Unless otherwise specified, this is the geometry and coordinates we always use.

Correlation functions and the path integral: The primary quantities we are interested in for quantum field theories are correlation functions of

[7] A comment on terminology; in most of high energy physics, the word "theory" is often synonymous with the word "system". This is in contrast to the more general use of the word in e.g. the theory of general relativity (or even worse, the use of theory in the phrase quantum field theory itself!), where it means the more general scientific and mathematical framework that describes a whole class of physical systems. Thus when we refer to e.g. "a conformal field theory", we mean a particular physical system with some specified dynamics and observables, described by conformal field theory. We apologize for this confusion, and hope that context will always make the meaning clear.

local operators $\mathcal{O}_i(x_i)$, primarily in the vacuum i.e. ground state:

$$\langle \mathcal{O}_1(x_1)\cdots\mathcal{O}_n(x_n)\rangle \equiv \langle 0|\mathcal{O}_1(x_1)\cdots\mathcal{O}_n(x_n)|0\rangle\,. \tag{1.3.3}$$

We can generalize to states other than the vacuum $|0\rangle$, or to correlation functions at a finite temperature as in (1.2.7). The fact that we are using local operators in a continuous geometry is one of the primary distinctions between a quantum field theory and standard quantum mechanics. Examples of such operators are the creation of a particle or the energy density at some position.

To calculate these correlation functions, we introduce the Euclidean *path integral*

$$Z \equiv \int [d\Phi]\, e^{-S[\Phi]}\,. \tag{1.3.4}$$

$\Phi(x)$ refers to the collection of fundamental fields in our quantum field theory (e.g. those that create and annihilate particles), which are all functions of position. The action

$$S[\Phi] \equiv \int d^d x\, \mathcal{L}(\Phi(x), \partial_\mu \Phi(x)) \tag{1.3.5}$$

is a functional of these fields (i.e. it takes the functions $\Phi(x)$ and spits out a number), where $\mathcal{L}(\Phi(x), \partial_\mu\Phi(x))$ is the Lagrangian density. The meaning of $\int [d\Phi]$ is that we are integrating over all possible field configurations, i.e. all possible functions $\Phi(x)$. The fields can be simple functions or have multiple components (e.g. they can be scalars, vectors, spinors, tensors, etc).

If we are quantizing a classical field theory, then both $\Phi(x)$ and $S[\Phi(x)]$ are just their classical counterparts. The classical equations of motion are given by the principle of least action, i.e. $\delta S = 0$ for any variation of the fields $\Phi(x) \to \Phi(x) + \delta\Phi(x)$.

The simplest example of a quantum field theory is the free scalar field in flat space with mass m:

$$S[\phi] = \int d^d x\, \frac{1}{2}\phi(-\Box_\delta + m^2)\phi\,,\; \Box_\delta \equiv \delta^{\mu\nu}\partial_\mu\partial_\nu\,. \tag{1.3.6}$$

Because it will be relevant for Lorentz invariance and gravity calculations, we also give the action for a scalar field in an arbitrary curved space,

$$S[g_{\mu\nu}, \phi] = \int d^d x\, \sqrt{-g}\frac{1}{2}\phi(-\Box_g + m^2)\phi\,,\; \Box_g \equiv \frac{1}{\sqrt{-g}}\partial_\mu\left(g^{\mu\nu}\sqrt{-g}\,\partial_\nu\right)\,, \tag{1.3.7}$$

where $g \equiv \det g_{\mu\nu}$.

We can use the path integral to calculate time-ordered correlators,

$$\begin{gathered}\langle T\{\mathcal{O}_1(x_1)\cdots\mathcal{O}_n(x_n)\}\rangle = \frac{\int[d\Phi]\,e^{-S[\Phi]}\mathcal{O}_1(x_1)\cdots\mathcal{O}_n(x_n)}{\int[d\Phi]\,e^{-S[\Phi]}}\,,\\ T\{\mathcal{O}_1(x_1)\cdots\mathcal{O}_n(x_n)\} \equiv \mathcal{O}_{i_1}(x_{i_1})\mathcal{O}_{i_2}(x_{i_2})\cdots\mathcal{O}_{i_n}(x_{i_n}) \text{ where}\\ x^0_{i_1} > x^0_{i_2} > \cdots > x^0_{i_n}\,.\end{gathered} \tag{1.3.8}$$

Using the path integral automatically time-orders the operators. In the following we will usually drop the time-ordering symbol, and implicitly have $x^0_1 > x^0_2 > \cdots > x^0_n$, with alternate orderings as in e.g. (1.2.19) indicated appropriately.

The operators must be expressed in terms of the fundamental fields in order to calculate them via the path integral. In conformal field theories we won't need to use the path integral to find our correlators, but keeping the path integral definition in mind will be useful for certain aspects, and it will reappear in other situations as well. (1.3.8) shows that the path integral is actually the zero temperature partition function, hence why it is labelled as Z.

A common way of obtaining correlation functions is by adding "sources" $J_i(x)$ for each operator to the path integral, creating the *generating functional*,

$$Z[J_i(x)] \equiv \int [d\Phi]\, e^{-S[\Phi]+\sum_i \int d^dx J_i(x)\mathcal{O}_i(x)}\,. \tag{1.3.9}$$

Here J_i denotes a collection of sources; as many can be non-zero ("turned on") as we like. The standard path integral in (1.3.4) is just $Z[0]$. We can obtain correlation functions by taking functional derivatives of the generating function, then setting the sources to zero, [8]

$$\langle T\{\mathcal{O}_1(x_1)\cdots\mathcal{O}_n(x_n)\}\rangle = \frac{1}{Z}\frac{\delta^n Z[J_i]}{\delta J_1(x_1)\cdots\delta J_n(x_n)}\bigg|_{J_i=0}\,. \tag{1.3.11}$$

[8] The functional derivative $\frac{\delta Z[J]}{\delta J(x)}$ is defined analogously to a regular derivative, as the linear term after infinitesimally shifting the function J:

$$Z[J+\delta J] = Z[J] + \int d^dx \left(\frac{\delta Z[J]}{\delta J(x)}\right)\delta J(x) + \cdots\,. \tag{1.3.10}$$

Mechanically, the functional derivative can be found by using the fundamental relation $\frac{\delta J(x)}{\delta J(y)} = \delta(x-y)$ and integration by parts. The Euler-Lagrange equations from the principle of least action is just $\frac{\delta S}{\delta\Phi(x)} = 0$ in this language.

We can also define the *connected generating functional* $W[J_i]$ by taking the logarithm of Z, which gives the connected correlation functions,

$$e^{-W[J_i]} = Z[J_i]\,,$$
$$\left.\frac{\delta^2 W[J_i]}{\delta J_1(x_1)\delta J_2(x_2)}\right|_{J_i=0} = -\Big(\langle\mathcal{O}_1(x_1)\mathcal{O}_2(x_2)\rangle - \langle\mathcal{O}_1(x_1)\rangle\langle\mathcal{O}_2(x_2)\rangle\Big)\,, \tag{1.3.12}$$

(similar for correlators with more operators).

Another use of the path integral is that by putting boundary conditions on the fields, we can evolve states in time. As mentioned in section 1.2, the time evolution operator in any quantum theory is given by e^{itH}; in Euclidean time this becomes

$$U(t) = e^{-\tau H}\,. \tag{1.3.13}$$

As with any operator, we can equivalently consider the matrix elements. For example, for energy eigenstates $\langle n|e^{-\tau H}|m\rangle = e^{-E_n\tau}\delta_{nm}$. In quantum field theories, a good set of states are states with a specified field configuration at a specific time τ, $|\Phi(\tau,\vec{x})\rangle$ i.e. on a time slice.[9] In this basis, the time evolution operator is

$$\langle\Phi_f(\tau_f,\vec{x})|e^{-(\tau_f-\tau_i)H}|\Phi_i(\tau_i,\vec{x})\rangle = \int_{\Phi(\tau_i,\vec{x})=\Phi_i(\tau_i,\vec{x})}^{\Phi(\tau_f,\vec{x})=\Phi_f(\tau_f,\vec{x})}[d\Phi]\,e^{-S[\Phi]}\,. \tag{1.3.14}$$

That is, we integrate over all functions $\Phi(x)$, but where the functions at $\tau_{i,f}$ have boundary conditions given by $\Phi_{i,f}(\tau_{i,f},\vec{x})$.

Lorentz symmetry, conserved quantities and Ward identities: Since conformal symmetry is essentially a simple generalization of Lorentz symmetry, we review Lorentz symmetry and its conserved quantities. Consider d dimensional flat Euclidean space. Lorentz symmetry refers to coordinate transformations, $x'^\mu(x)$, that leave the metric $\delta_{\mu\nu}$ unchanged:

$$ds^2 = \delta_{\mu\nu}dx^\mu dx^\nu = \delta_{\mu\nu}dx'^\mu dx'^\nu \longleftrightarrow \delta_{\mu\nu} = \delta_{\rho\sigma}\frac{\partial x^\rho}{\partial x'^\mu}\frac{\partial x^\sigma}{\partial x'^\nu}\,. \tag{1.3.15}$$

(In Minkowski spacetime $\mathbb{R}^{1,d-1}$, the equations are all the same with $\delta_{\mu\nu}$ replaced with $\eta_{\mu\nu}\equiv\mathrm{diag}(-1,1,\cdots,1)$.) The transformations that accomplish this form the Poincare group, consisting of translations and Lorentz

[9]Note that here, τ is a single value while $\vec{x}$ runs over all values.

transformations/rotations. These transformations, along with the *generators for infinitesimal coordinate transformations*, are

$$\begin{array}{llll} \text{Translation:} & x'^{\mu} = x^{\mu} + a^{\mu} & p_{\mu} = -i\partial_{\mu}\,, \\ \text{Rotation:} & x'^{\mu} = \Lambda^{\mu}{}_{\nu} x^{\nu}\,, \Lambda \in \mathrm{SO}(d) & l_{\mu\nu} = i(x_{\mu}\partial_{\nu} - x_{\nu}\partial_{\mu})\,. \end{array} \tag{1.3.16}$$

The generators act via $\delta x^{\mu} \equiv i\omega^{a} g_{a} x^{\mu}$, where a is some collection of (spacetime) indices and ω^{a} are infinitesimal constants. For example, under translation $\delta x^{\mu} = i\omega^{\nu} p_{\nu} x^{\mu} = \omega^{\nu}\partial_{\nu} x^{\mu} = \omega^{\mu}$, i.e. the momentum generator p_{μ} creates an infinitesimal translation. The generators satisfy commutation relations that define the Poincare albegra,

$$\begin{aligned} [p_{\rho}, l_{\mu\nu}] &= i(\delta_{\rho\mu} p_{\nu} - \delta_{\rho\nu} p_{\mu})\,, \\ [l_{\mu\nu}, l_{\rho\sigma}] &= i(\delta_{\nu\rho} l_{\mu\sigma} + \delta_{\mu\sigma} l_{\nu\rho} - \delta_{\mu\rho} l_{\nu\sigma} - \delta_{\nu\sigma} l_{\mu\rho})\,. \end{aligned} \tag{1.3.17}$$

The algebra of the $l_{\mu\nu}$ by themselves is called the "Lorentz algebra".

We also have to consider how these transformations act on the fields $\Phi(x)$ and operators $\mathcal{O}(x)$ of our theory, $\Phi'(x') = \mathcal{F}(\Phi(x))$ (similar for operators). This is the "active" perspective on coordinate transformations; both the coordinates change, and the functional form of the fields change. For infinitesimal transformations on fields, the generators are defined via just the change in the functional form of the field, $\Phi'(x) - \Phi(x) \equiv -i\omega^{a} G_{a}$.[10]

For Lorentz invariant theories, the fields are in representations of the Lorentz group; the transformation of the fields and their infinitesimal generators are

$$\begin{array}{lll} \text{Translation:} & \Phi'(x+a) = \Phi(x) & P_{\mu} = -i\partial_{\mu}\,, \\ \text{Rotation:} & \Phi'(\Lambda x) = L_{\Lambda}\Phi(x) & L_{\mu\nu} = i(x_{\mu}\partial_{\nu} - x_{\nu}\partial_{\mu}) + S_{\mu\nu}\,. \end{array} \tag{1.3.18}$$

L_{Λ} is a representation of the Lorentz group, and $S_{\mu\nu}$ is the corresponding spin generator that satisfies the Lorentz albegra (i.e. it has the same commutation relations as $l_{\mu\nu}$ from (1.3.16)). The value of the spin m of the field, which is a (half) integer, determines L_{Λ} and $S_{\mu\nu}$.[11] We also require that our operators $\mathcal{O}(x)$ live in representations of the Lorentz group.

[10] Note the minus sign, which is different from the coordinate generators.

[11] The simplest examples are when $\Phi(x)$ is a scalar $\phi(x)$ with $m = 0$, or vector $A_{\mu}(x)$ with $m = 1$, in which case

$$\begin{array}{ll} \phi'(\Lambda x) = \phi(x) & S^{\mu\nu}_{\text{scalar}} = 0\,, \\ A_{\mu}(\Lambda x) = \Lambda_{\mu}{}^{\nu} A_{\nu}(x) & S^{\mu\nu}_{\text{vector}} \in \mathfrak{so}(d) \end{array} \tag{1.3.19}$$

i.e. the trivial and defining representations of the Lorentz group and Lorentz algebra.

A field theory (quantum or classical) is then Lorentz symmetric if the action is invariant under $x \to x'$, $\Phi(x) \to \Phi'(x')$; in the quantum case, we also require that the measure $[d\Phi]$ is invariant. This implies a symmetry for correlation functions:

$$\langle \mathcal{O}_1(x_1') \cdots \mathcal{O}_n(x_n') \rangle = \langle \mathcal{F}(\mathcal{O}(x_1)) \cdots \mathcal{F}(\mathcal{O}_n(x_n)) \rangle \,, \tag{1.3.20}$$

i.e. the effect of a coordinate transformation on a correlation function is entirely captured by the transformation of the operators themselves.

As is well known from Noether's theorem, in a classical theory every symmetry implies a conserved quantity. A standard way of deriving Noether's theorem is to allow the infinitesimal parameters for the transformation ω^a to depend on position $\omega^a(x) \equiv \epsilon(x)\omega^a$; the variation of the action under the transformation becomes

$$\delta S = \int d^d x \, \partial_\mu j^\mu_a \omega^a(x) \,. \tag{1.3.21}$$

If the fields obey the equations of motion, then $\delta S = 0$ for any variation of the field, and so $j^\mu_a = -\frac{\delta S}{\delta \partial_\mu \omega^a(x)}$ is conserved, $\partial_\mu j^\mu_a = 0$.

The conserved quantity for Lorentz symmetry is expressed via the stress tensor or energy-momentum tensor $T^{\mu\nu}(x)$. One way of defining the stress tensor that is extremely useful for correlation functions is to put the theory in a curved geometry, where the metric is some arbitrary $g_{\mu\nu}(x)$ as in (1.3.1), rather than the flat Eucliden metric $\delta_{\mu\nu}$. For example, in a free scalar theory we replace the action (1.3.6) with (1.3.7). We can then use a similar logic as in (1.3.21); we consider an arbitrary infinitesimal coordinate transformation $\delta x^\mu = \omega^\mu(x)$, which creates an infinitesimal variation of the metric $\delta g_{\mu\nu} = -(\partial_\mu \omega_\nu + \partial_\nu \omega_\mu)$. The stress tensor is then the change of the action in response to this metric fluctuation,

$$\delta S[g_{\mu\nu}] = -\frac{1}{2} \int d^d x \, \sqrt{-g} T^{\mu\nu}_{(g)} \delta g_{\mu\nu} \,. \tag{1.3.22}$$

This gives us the stress tensor for any metric $g_{\mu\nu}$:

$$T^{\mu\nu}_{(g)}(x) \equiv -2 \frac{1}{\sqrt{-g}} \frac{\delta S[g_{\mu\nu}]}{\delta g_{\mu\nu}(x)} \,, \tag{1.3.23}$$

The subscript (g) stresses that this is for any metric; we will here-on ignore this notation, and the stress tensor will always be defined relative to the geometry we are considering. By setting the metric back to flat space

$g_{\mu\nu} = \delta_{\mu\nu}$, we get the flat space stress tensor $T^{\mu\nu} \equiv T^{\mu\nu}_{(g=\delta)}$. It encodes the symmetries of Lorentz invariance:

$$\begin{aligned} &\text{Translation invariance} && \Longrightarrow \partial_\mu T^{\mu\nu} = 0\,, \\ &\text{Rotation invariance} && \Longrightarrow \partial_\mu (T^{\mu\nu} x^\sigma - T^{\mu\sigma} x^\nu) = 0 \Leftrightarrow T^{\mu\nu} - T^{\nu\mu} = 0\,. \end{aligned} \tag{1.3.24}$$

The first is the conservation of energy and momentum, the second is the conservation of angular momentum.

In a quantum field theory, conserved quantities are operators that are conserved in correlation functions *only* if there are no other operators nearby. When another operator is close to the insertion of the conserved quantity, we instead get the *Ward identities*. We discover these by using the path integral to find correlation functions, (1.3.8), and doing a change of integration variables, i.e. $\Phi(x) \to \Phi'(x)$. Then we find

$$\begin{aligned} \partial_\mu \langle T^{\mu\nu} \mathcal{O}_1(x_1) \cdots \mathcal{O}_n(x_n) \rangle &= -\sum_{i=1}^n \delta(x - x_i) \partial^\nu_{(x_i)} \langle \mathcal{O}_1(x_1) \cdots \mathcal{O}_n(x_n) \rangle\,, \\ \partial_\mu \langle (T^{\mu\nu} x^\rho - T^{\mu\rho} x^\nu) \mathcal{O}_1(x_1) \cdots \mathcal{O}_n(x_n) \rangle &= \sum_{i=1}^n \delta(x - x_i)(x_i^\nu \partial^\rho_{(x_i)} - x_i^\rho \partial^\nu_{(x_i)} - i S_i^{\nu\rho}) \\ &\qquad \times \langle \mathcal{O}_1(x_1) \cdots \mathcal{O}_n(x_n) \rangle\,, \\ \Leftrightarrow \langle (T^{\mu\nu} - T^{\nu\mu}) \mathcal{O}_1(x_1) \cdots \mathcal{O}_n(x_n) \rangle &= -\sum_{i=1}^n \delta(x - x_i) i S_i^{\mu\nu} \langle \mathcal{O}_1(x_1) \cdots \mathcal{O}_n(x_n) \rangle\,, \end{aligned} \tag{1.3.25}$$

where $S_i^{\nu\rho}$ is the spin generator for the i-th operator and $\partial^\mu_{(x_i)} \equiv \frac{\partial}{\partial x_{i\mu}}$. We recognize on the right hand side the effect of the generators in (1.3.18). The meaning of these Ward identities is essentially that the conserved quantity, the stress tensor, provides the generator of infinitesimal Lorentz transformations on correlation functions. For example, the momentum generator (with the time x^0 dependence explicit here) is

$$P_\mu(x^0) = \int dx^1 \cdots dx^d \, T^0_\mu(x)\,, \tag{1.3.26}$$

The momentum generator then acts on operators via a commutator, generating the infinitesimal transformation,

$$\begin{aligned} [P_\mu(x_i^0), \mathcal{O}_i(x_i)] &\equiv \lim_{\epsilon \to 0} P_\mu(x_i^0 + \epsilon) \mathcal{O}_i(x_i) - \mathcal{O}_i(x_i) P_\mu(x_i^0 - \epsilon) \\ &= -\partial_\mu \mathcal{O}_i(x_i) \equiv \delta \mathcal{O}_i \\ \Leftrightarrow \langle \mathcal{O}_1(x_1) \cdots [P_\mu(x_i^0), \mathcal{O}_i(x_i)] \cdots \mathcal{O}_n(x_n) \rangle &= \langle \mathcal{O}_1(x_1) \cdots (-\partial_\mu O_i(x_i)) \cdots \mathcal{O}_n(x_n) \rangle\,, \end{aligned} \tag{1.3.27}$$

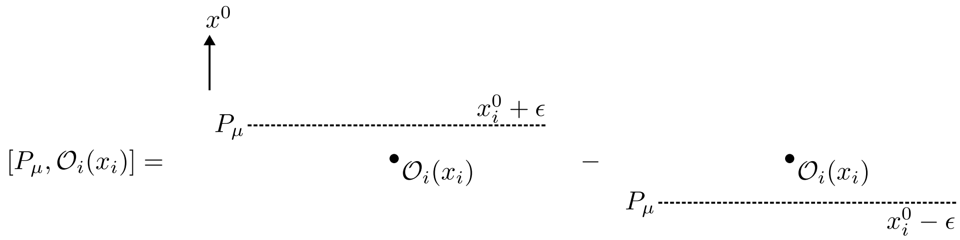

Figure 1.4: A graphical representation of the commutator between the momentum generator and some operator. The operator lives at a single point, while the momentum generator is defined on a full time slice.

where in the last line, we show that the commutator should be interpreted as an operator equation, i.e. it holds in correlation functions. See figure 1.4

We could also integrate (1.3.25) over a ball containing some of the operators, generating transformations of just those operators. If we integrate over a ball containing all the operators, we get the *total* variation of the correlation function under an infinitesimal coordinate transformation. Using Stokes theorem, this becomes the surface integral of the current on a large ball, but by sending the radius to infinity one can show this integral vanishes. Hence the total variation of any correlation function under a Lorentz transformation is *zero*,

$$\delta\langle\mathcal{O}_1(x_1)\cdots\mathcal{O}_n(x_n)\rangle = 0\,. \tag{1.3.28}$$

This is just a restatement of (1.3.20), in infinitesimal form.

Finally, we note the quantum interpretation of (1.3.22). The fact that the stress tensor is just the response of the action to an arbitrary metric fluctuation means that we can actually use (1.3.22) to define the generating functional for stress tensor correlators via an arbitrary metric fluctuation:

$$Z[\delta g_{\mu\nu}] = \int [d\Phi] e^{-S[\delta_{\mu\nu},\Phi] - \frac{1}{2}\int d^dx\, T^{\mu\nu}\delta g_{\mu\nu}} \tag{1.3.29}$$

where we are focusing on the flat space stress tensor. Then we can find stress tensor correlators via functional derivatives, just like (1.3.11). In other words, we source the stress tensor by putting our theory in a curved space time.

1.3.2 Conformal field theories in d dimensions

We now analyze CFTs. We show how they can be described solely in terms of certain types of local operators that generate the states of our theory and whose correlation functions are fixed by conformal symmetry.

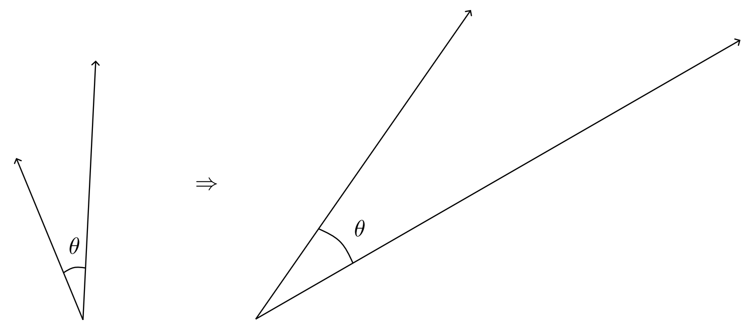

Figure 1.5: The effect of a conformal transformation on two vectors at the same point. Their lengths and orientations change, but the angle between them is fixed.

Conformal symmetry is an extension of Lorentz symmetry (1.3.15), allowing a position-dependent factor $\Omega(x')$ to sit in front of the metric after changing coordinates:

$$ds^2 = \delta_{\mu\nu} dx^\mu dx^\nu = \Omega(x') \delta_{\mu\nu} dx'^\mu dx'^\nu \,, \tag{1.3.30}$$

i.e. $\delta_{\mu\nu} \to \Omega(x)\delta_{\mu\nu}$ is a symmetry. A theory invariant under these transformations is conformally invariant; a quantum field theory that is conformally invariant is called a *conformal field theory* (CFT). These transformations include the Poincare group and two additional ones; scale transformations/dilations, and special conformal transformations. The full conformal group, along with the generators for infinitesimal coordinate transformations, consists of

$$\begin{array}{lll} \text{Translation:} & x'^\mu = x^\mu + a^\mu & p_\mu = -i\partial_\mu \,, \\ \text{Rotation:} & x'^\mu = \Lambda^\mu{}_\nu x^\nu & l_{\mu\nu} = i(x_\mu \partial_\nu - x_\nu \partial_\mu) \,, \\ \text{Dilation:} & x'^\mu = \lambda x^\mu & d = -i x^\mu \partial_\mu \,, \\ \text{Special:} & x'^\mu = \frac{x^\mu - b^\mu x^2}{1 - 2b^\mu x_\mu + b^2 x^2} & k_\mu = -i(2x_\mu x^\nu \partial_\nu - x^2 \partial_\mu) \,. \end{array} \tag{1.3.31}$$

These transformations leave the *angle* between two vectors unchanged, while their *length* changes, as in Figure 1.5. The fact that these theories don't care about lengths means that our theory can't have any inherent length scale in it; in particular, these theories are massless.

These generators satisfy a set of commutation relations called the "conformal algebra". This can be seen most easily written down by defining a new set of generators: let $A, B = I, II, 0, 1, \cdots, d-1 = I, II, \mu$ be a $d+2$

dimensional index in $\mathbb{R}^{1,d+1}$. Then we define L_{AB} via

$$\begin{aligned} L_{\mu\nu} &= l_{\mu\nu}\,, \quad L_{I\mu} = \tfrac{1}{2}(p_\mu - k_\mu)\,, \\ L_{I,II} &= D\,, \quad L_{II\mu} = \tfrac{1}{2}(p_\mu - k_\mu)\,. \end{aligned} \tag{1.3.32}$$

The generators L_{AB} then satisfy the same algebra as the Lorentz algebra from (1.3.17), just in $d+2$ dimension Minkowski spacetime. Thus the conformal group in d dimensions is the same as the Lorentz group in $d+2$ dimensions, $\mathrm{SO}(1, d+1)$. This motivates the so called "embedding space" picture, which we will discuss in chapter 4.

We also write explicitly the most important commutators for us,

$$\begin{aligned} [d, p_\mu] &= i p_\mu\,, \\ [d, k_\mu] &= -i k_\mu\,. \end{aligned} \tag{1.3.33}$$

More broadly, we could consider a theory in any geometry and metric $g_{\mu\nu}(x)$, not just flat space; a theory in such a geometry is conformally invariant if it is invariant under rescalings $g_{\mu\nu}(x) \to \Omega(x) g_{\mu\nu}(x)$.

We also note that in the theories we consider, invariance under the Poincare group and scale transformations alone implies full conformal invariance. We will thus only mention special conformal transformation when necessary.

By demanding that our operators live in representations of the full conformal group, we find the generators for infinitesimal conformal transformations acting on an operator $\mathcal{O}(x)$:

$$\begin{array}{lll} \text{Translation:} & \mathcal{O}'(x+a) = \mathcal{O}(x) & P_\mu = -i\partial_\mu\,, \\ \text{Rotation:} & \mathcal{O}'(\Lambda x) = L_\Lambda \mathcal{O}(x) & L_{\mu\nu} = i(x_\mu\partial_\nu - x_\nu\partial_\mu) + S_{\mu\nu}\,, \\ \text{Dilation:} & \mathcal{O}'(\lambda x) = \lambda^{-\Delta}\mathcal{O}(x) & D = -ix^\mu\partial_\mu - i\Delta\,, \\ \text{Special:} & \ldots^{12} & K_\mu = -i(2x_\mu x^\nu \partial_\nu - x^2\partial_\mu) \\ & & \qquad -2ix_\mu\Delta - x^\nu S_{\mu\nu}\,. \end{array} \tag{1.3.34}$$

Δ is called the *scaling dimension* of the operator.

We also obtain a new conserved current and Ward identity, the full set of which are

$$\begin{array}{llll} \text{Translation invariance} & \Longrightarrow \partial_\mu T^{\mu\nu} = 0\,, & \\ \text{Rotation invariance} & \Longrightarrow \partial_\mu(T^{\mu\nu}x^\sigma - T^{\mu\sigma}x^\nu) = 0 & \Leftrightarrow T^{\mu\nu} = T^{\nu\mu}\,, \\ \text{Scale invariance} & \Longrightarrow \partial_\mu(T^\mu_\nu x^\nu) = 0 & \Leftrightarrow T^\mu_\mu = 0\,, \end{array} \tag{1.3.35}$$

[12]The transformation of a general operator under a special conformal transformations is rather complicated, hence we neglect it here. Later we will discover a certain class of operator with simple transformation rules for any conformal transformation.

$$\begin{aligned}
\partial_\mu \langle T^{\mu\nu} \mathcal{O}_1(x_1) \cdots \mathcal{O}_n(x_n) \rangle &= - \sum_{i=1}^{n} \delta(x - x_i) \partial^\nu_{(x_i)} \langle \mathcal{O}_1(x_1) \cdots \mathcal{O}_n(x_n) \rangle \,, \\
\langle (T^{\mu\nu} - T^{\nu\mu}) \mathcal{O}_1(x_1) \cdots \mathcal{O}_n(x_n) \rangle &= - \sum_{i=1}^{n} \delta(x - x_i) i S_i^{\mu\nu} \langle \mathcal{O}_1(x_1) \cdots \mathcal{O}_n(x_n) \rangle \,, \\
\langle T^\mu_\mu \mathcal{O}_1(x_1) \cdots \mathcal{O}_n(x_n) \rangle &= - \sum_{i=1}^{n} \delta(x - x_i) \Delta_i \langle \mathcal{O}_1(x_1) \cdots \mathcal{O}_n(x_n) \rangle \,.
\end{aligned} \tag{1.3.36}$$

We note that these expressions are valid for flat space only. In fact, in other geometries and in even spatial dimensions, quantizing a classical conformal field theory produces the "conformal anomaly" which breaks conformal symmetry: because the path integral measure $[d\Phi]$ isn't invariant under conformal transformations, the trace of the stress tensor is no longer zero, $\langle T^\mu_\mu \rangle \neq 0$, and depends on the curvature of the space. The conformal anomaly also produces anomalous terms when one of the operators $\mathcal{O}_i$ above is the stress tensor itself.

Operators and states in CFTs: The power of conformal symmetry allows us to characterize our theories without explicit reference to an explicit action or path integral, thanks to an extremely powerful relationship called the *operator-state correspondence*; **any state in a CFT can be written as an operator acting on the vacuum, and every operator can be obtained via its corresponding state**

$$\text{Operator-state correspondence: } \mathcal{O}(x) \Leftrightarrow |\mathcal{O}\rangle \equiv \mathcal{O}(0)|0\rangle \,. \tag{1.3.37}$$

Thus we can fully understand the spectrum of states in our theory and all correlation functions just by analyzing the operators in a CFT. To do so, we will analyze the effect of the generators from (1.3.34).

Our operators $\mathcal{O}(x)$ with scaling dimension Δ are eigenfunctions of the dilation operator at the origin:

$$[D, \mathcal{O}(0)] = -i\Delta \mathcal{O}(0) \,, \tag{1.3.38}$$

By using the commutation relations (1.3.33), we see that K_μ acts as a lowering operator and P_μ acts as a raising operator:

$$[D, [K_\mu, \mathcal{O}(0)]] = -i(\Delta - 1)\mathcal{O}(0) \,, \tag{1.3.39}$$

$$[D, [P_\mu, \mathcal{O}(0)]] = -i(\Delta + 1)\mathcal{O}(0) \,, \tag{1.3.40}$$

i.e. the operators $[K_\mu, \mathcal{O}(x)]$, $[P_\mu, \mathcal{O}(x)]$ are also eigenfunctions of the dilation operator with scaling dimension $\Delta \pm 1$. Similar to the harmonic oscillator in quantum mechanics then,[13] there must be some operators that can't be lowered anymore, which we call *quasi-primary*:

$$\text{quasi-primary: } [K_\mu, \mathcal{O}(0)] = 0\,. \tag{1.3.41}$$

All operators are then either quasi-primary, *descendants* of a quasi-primary operator generated by repeated commutation with P_{μ_i}, or a linear combination of any number of these (this last point can be seen from the operator-state correspondence, as we need to have linear combinations of distinct states). In terms of states, the basis of states in our theory are

$$\begin{aligned} \text{Quasi-primary states: } & |\mathcal{O}\rangle \equiv \mathcal{O}(0)|0\rangle\,, \text{ dimension } \Delta \\ \text{Descendant states: } & P_{\mu_1}\cdots P_{\mu_n}|\mathcal{O}\rangle^{14}\,, \text{ dimension } \Delta + n\,. \end{aligned} \tag{1.3.42}$$

The spectrum of quasi-primary operators determines the entire spectrum of states for a conformal field theory. In other words, in a CFT we have a collection of simple operators with known properties, characterized by their transformation under scaling $x^\mu \to \lambda x^\mu$ and by their spin. These operators determine all the other operators in the theory. Through the operator-state correspondence, these simple operators also determine all the states in our theory.

There is an equivalent condition to being quasi-primary that is very simple for scalar operators: under any finite conformal transformation,

$$\text{quasi-primary scalar: } \phi'(x') = \left|\frac{\partial x'}{\partial x}\right|^{-\Delta/d} \phi(x)\,, \tag{1.3.43}$$

where $\left|\frac{\partial x'}{\partial x}\right|$ is the Jacobian of the coordinate transformation. This is similar to how any operator transforms under dilations (1.3.34), but it includes special conformal transformations. This definition will be important for two-dimensional CFTs in section 1.3.3. We also note that the stress tensor $T^{\mu\nu}(x)$ is a quasi-primary operator with scaling dimension d and spin 2.

Correlation functions: Conformal symmetry also fixes the two- and three-point correlation functions of operators, using the Ward identity for

[13] This is also similar to the raising and lowering operators in (1.2.13), however as we will see in section 1.3.4, the scaling dimension plays the role of energy in CFTs.

[14] We could also contract the indices in the momentum generators, e.g. have $P^2 = P_\mu P^\mu$.

the total variation of the correlator (1.3.28). For quasi-primary scalars,

$$\langle \phi_1(x_1)\phi_2(x_2)\rangle = \begin{cases} \frac{C}{x_{12}^{2\Delta_1}} \text{ if } \Delta_1 = \Delta_2 \\ 0 \text{ otherwise} \end{cases} , \tag{1.3.44}$$

$$\langle \phi_1(x_1)\phi_2(x_2)\phi_3(x_3)\rangle = \frac{C_{123}}{x_{12}^{\Delta_1+\Delta_2-\Delta_3} x_{23}^{\Delta_2+\Delta_3-\Delta_1} x_{31}^{\Delta_3+\Delta_1-\Delta_2}} , \tag{1.3.45}$$

where $x_{ij} \equiv x_i - x_j$. We generally normalize our operators so two-point functions have $C = 1$, although we will not do so with e.g. the stress tensor. Operators with spin have similar expressions; for examples the two-point function has the $\frac{1}{x_{12}^{2\Delta_1}}$ factor multiplied by a known, scaling-invariant function of x_{12} with the appropriate indices.

The four-point function, however is not fixed. With four different points, we can form the "conformal cross-ratios", which are invariant under conformal symmetry:

$$u = \frac{x_{12}^2 x_{34}^2}{x_{13}^2 x_{24}^2} , \; v = \frac{x_{23}^2 x_{14}^2}{x_{13}^2 x_{24}^2} . \tag{1.3.46}$$

Then for e.g. identical scalar operators, conformal invariance only requires

$$\langle \phi_1(x_1)\phi_1(x_2)\phi_1(x_3)\phi_1(x_4)\rangle = \frac{g(u,v)}{x_{12}^{2\Delta_1} x_{34}^{2\Delta_1}} , \tag{1.3.47}$$

for some function $g(u, v)$.

We can push conformal symmetry even further. As we said, any operator is just a linear combination of quasi-primaries and descendants. We can apply this to a product of two different operators at different points, performing the *operator product expansion* (OPE):

$$\phi_i(x_1)\phi_j(x_2) = \sum_{\mathcal{O}} C_{ij\mathcal{O}} \mathfrak{C}(x_{12}, \partial_{x_2}, \Delta_{i,j,\mathcal{O}})\mathcal{O}(x_2) , \tag{1.3.48}$$

where $\mathfrak{C}(x_{12}, \partial_{x_2}, \Delta_{i,j,\mathcal{O}})$ is a differential operator and $\mathcal{O}$ are quasi-primaries with dimension $\Delta_{\mathcal{O}}$ (the descendants are taken care of by the differential operator). The OPE shows how two external probe operators fuse into a sum of individual quasi-primary operators and their descendants (the "conformal families" of quasi-primary operators). This statement holds inside correlation functions, so long as there are no other operator insertions closer to x_1 or x_2.

The important thing is that the differential operator can be explicitly derived via conformal symmetry, and that the coefficient $C_{ij\mathcal{O}}$ is the same coefficient that appears in the three-point function (1.3.45), called the *OPE* *coefficient*. This means that for any correlation function of any number of operators, we can apply the OPE repeatedly to write down the correlation function in terms of the scaling dimensions and OPE coefficients. Thus, since the scaling dimensions also determine the states of the theory, **all the dynamical data of a CFT is determined by the scaling dimension and OPE coefficients of quasi-primary operators**. In other words, if we know how the simple quasi-primary operators transform under scaling the coordinates, and all the constants that sit in front of their three-point correlation functions, we can calculate any quantity in the theory.

For example, the four-point function in (1.3.47) can be written as

$$\langle \phi_1(x_1)\phi_1(x_2)\phi_1(x_3)\phi_1(x_4)\rangle = \frac{1}{x_{12}^{2\Delta_1}x_{34}^{2\Delta_1}}\sum_{\mathcal{O}}(C_{11\mathcal{O}})^2 G_{\Delta_{\mathcal{O}}}^{(l_{\mathcal{O}})}(u,v)\,, \quad (1.3.49)$$

where $l_{\mathcal{O}}$ is the spin of the operator $\mathcal{O}$. $G_{\Delta_{\mathcal{O}}}^{(l_{\mathcal{O}})}(u,v)$ is a function fixed by conformal symmetry called a *global conformal block*. In any number of even spacetime dimensions, these functions are known exactly.[15] For example, doing a change of variables where $u = z\bar{z}$, $v = (1-z)(1-\bar{z})$, the stress tensor conformal block in 4 dimensions is

$$G_4^{(2)} = 10\left(-\frac{\bar{z}}{z}\frac{z^2-6z+6}{z-\bar{z}}\log(1-z)+3\right) + (z \leftrightarrow \bar{z})\,. \quad (1.3.50)$$

A crucial fact about the OPE is the way it constrains CFT data. The reason is that the OPE is associative; operators can be paired up however one wants. For example, in a generic four-point function, we represent the operators we choose to take the OPE of by connecting then with a line. Then

$$\langle \overbracket{\mathcal{O}_1\mathcal{O}_2}\,\overbracket{\mathcal{O}_3\mathcal{O}_4}\rangle = \langle \overbracket{\mathcal{O}_1\overbracket{\mathcal{O}_2\mathcal{O}_3}\mathcal{O}_4}\rangle = \langle \mathcal{O}_1\mathcal{O}_2\mathcal{O}_3\mathcal{O}_4\rangle \quad (1.3.51)$$

This is referred to as *crossing symmetry*. The fact that all of these must be equal imposes strong constraints on the operator dimensions and OPE coefficients; in particular not every set of this data defines a consistent CFT. The method of using crossing symmetry and other fundamental features of CFTs to find consistent CFT data is called the "conformal bootstrap".

Finally, an important note about these correlators is that even though our theory is living in flat Euclidean space, we can find the correlators for theories living in different geometries. Of course, the geometry our theory

[15]In four-point functions where the operators are not pair-wise equal, the conformal block depends on the dimension of those operators, not just $\mathcal{O}$.

lives in shouldn't depend on the coordinates we use to describe it; while we have been using Cartesian coordinates with $g_{\mu\nu} = \delta_{\mu\nu}$, we can use any coordinates we want. For example, we could go to polar coordinates,

$$ds^2 = dr^2 + r^2 d\Omega_{d-1}^2 \tag{1.3.52}$$

where $d\Omega_{d-1}^2$ is the metric on a $d-1$ dimensional sphere with radius 1.

But thanks to conformal invariance, we can do a change of coordinates and a subsequent conformal transformation, putting ourselves in a legitimately different geometry. For example, setting $r = e^\tau$ in (1.3.52) gives

$$ds^2 = e^{2\tau}\left(d\tau^2 + d\Omega_{d-1}^2\right) \tag{1.3.53}$$

The metric inside the brackets is the metric of a d dimensional cylinder, $\mathbb{R}\times S^{d-1}$. Thus, flat Euclidean space is *conformally equivalent* to the cylinder, and we can find correlation functions on a cylinder via a change of coordinates followed by a conformal transformation. This will be important in section 1.3.4.

Introduction to shadow operators: Here, we sketch out the *shadow operator formalism* approach to the OPE and conformal blocks, as it is one of the main focuses of chapter 4. The details will be left to that chapter.

One way of deriving the conformal blocks is to exploit the fact that they have specific short distance behaviour, and are eigenfunctions of the "conformal Casimir", $\mathcal{C} \equiv L_{AB}L^{AB}$ where L_{AB} are the conformal generators from (1.3.32). The conformal Casimir is the operator that commutes with all the other generators, similar to total angular momentum. It can be written as a second order differential operator of the cross ratios u, v; the conformal blocks have eigenvalue and short distance behaviour

$$\begin{aligned}\mathcal{C}\, G_\Delta^{(l)}(u,v) &= \big(\Delta(d-\Delta) - l(l+d-2)\big)G_\Delta^{(l)}(u,v)\,,\\ G_\Delta^{(l)}(u,v) &\overset{u\to 0, v\to 1}{\approx} u^{\frac{\Delta-l}{2}}(1-v)^l\,.\end{aligned} \tag{1.3.54}$$

Notably, the eigenvalue is symmetric under $\Delta \leftrightarrow d-\Delta$; this is sign that there is another eigenfunction of the Casimir, the "shadow block" $G_{d-\Delta}^{(l)}(u,v)$, with the same eigenvalue but different short distance behaviour.

This suggests the introduction of the "shadow operator" $\widetilde{\mathcal{O}}$, a fictitious operator with dimension $d-\Delta$ and spin l, given by integrating the original operator $\mathcal{O}$: schematically,

$$\widetilde{\mathcal{O}}(x) = \int d^dy\, I(x,y)\mathcal{O}(y)\,, \tag{1.3.55}$$

where the integral kernel is chosen to contract properly with any indices in $\mathcal{O}$ and to give the proper scaling behaviour. The shadow operator isn't a true operator in the theory; it is simply a calculational tool.

The shadow operator really comes into play when we consider the OPE. A useful representation of the OPE (1.3.48) that holds for pairwise-equal scalar operators $V(x)$ is

$$\begin{aligned} V(x)V(y) &= \frac{1}{|x-y|^{2\Delta_V}} \sum_{\mathcal{O}} C_{VV\mathcal{O}} \mathfrak{B}_{\mathcal{O}}(x,y)\,, \\ \mathfrak{B}_{\mathcal{O}}(x,y) &\equiv |x-y|^{\Delta_{\mathcal{O}}} \left[\mathcal{O}(y) + \text{conformal descendants}\right]. \end{aligned} \tag{1.3.56}$$

We call $\mathfrak{B}_{\mathcal{O}}$ the OPE block; it represents the fusion of the two V's into the primary operator $\mathcal{O}$ and its descendants. Since there are infinitely many descendants of any operator, the OPE block contains infinitely many derivatives of $\mathcal{O}$ and thus depends on the operator far away from the point y. This can actually be captured by instead writing the OPE block as an integral using the shadow operator:

$$\mathfrak{B}_{\mathcal{O}}(x,y) = \text{const.} \times \int d^d\xi \, \frac{1}{C_{VV\mathcal{O}}} \frac{\langle V(x)V(y)\widetilde{\mathcal{O}}(\xi)\rangle}{\langle V(x)V(y)\rangle} \mathcal{O}(\xi) \tag{1.3.57}$$

While it isn't clear from the way its defined, the integral kernel is actually completely independent of the operator V! Since three-point functions are fixed by conformal symmetry, the kernel can be written down explicitly; we thus have a concise way of calculating OPE blocks (and thus conformal blocks) using a series of conformal integrals; first to define the shadow operator, then to define the OPE/conformal blocks.

Summary: By using the structure of conformal symmetry, CFTs can be characterized entirely in terms of the scaling dimensions and OPE coefficients of the quasi-primary operators in the theory. With this data we can determine any state and calculate any correlation function we could ever want. We can also calculate correlation functions in many different geometries, and introduced some of the technology for calculating them.

1.3.3 Conformal symmetry in two dimensions

Two dimensional CFTs have even more structure than generic CFTs, as conformal invariance actually becomes infinite dimensional in two dimensions. This leads to a refinement of the notion of primary and descendant operators, as well as an extremely powerful symmetry called modular invariance.

First we define complex coordinates and put our theory on the complex plane:

$$ds^2 = dx_0^2 + dx_1^2 = dz d\bar{z}\,,\; z = x^1 + ix^0, \bar{z} = x^1 - ix^0. \tag{1.3.58}$$

This form of the metric reveals how extensive conformal symmetry becomes in 2D: any "holomorphic" change of coordinates becomes a conformal transformation, as

$$z' = z'(z)\,,\; \bar{z}' = \bar{z}'(\bar{z}) \implies ds^2 = \left|\frac{dz}{dz'}\right|^2 dz' d\bar{z}'\,, \tag{1.3.59}$$

$z'(z)$ is any arbitrary function of z alone (i.e. it does not depend on $\bar{z}$), and $\bar{z}'(\bar{z})$ is its complex conjugate. By doing this transformation, we just get the Jacobian sitting out front, which shows it is indeed a conformal transformation.

We can allow $\bar{z}$ to be an independent complex coordinate, such that independent transformations of z and $\bar{z}$ are symmetries (i.e. we extend our theory from $\mathbb{C}$ to $\mathbb{C}^2$). We can always go back to the actual 2D Euclidean plane by re-imposing that $\bar{z} = z^*$, the complex conjugate of z.

The generators of this symmetry group and their algebra are

$$\begin{array}{lll}
\text{Holomorphic:} & z' = z + a z^{n+1} & l_n = -z^{n+1}\partial_z\,, \\
\text{Anti-holomorphic:} & \bar{z}' = \bar{z} + \bar{a}\bar{z}^{n+1} & \bar{l}_n = -\bar{z}^{n+1}\partial_{\bar{z}}\,, \\
 & [l_n, l_m] \;= (n-m) l_{n+m}\,, & \\
\text{Algebra:} & [\bar{l}_n, \bar{l}_m] \;= (n-m)\bar{l}_{n+m}\,, & \\
 & [l_n, \bar{l}_m] \;= 0\,. &
\end{array} \tag{1.3.60}$$

Note that so far, our discussion has only been local; a well defined, global conformal transformation must be defined everywhere (i.e. map the complex plane into itself) and be invertible. This is accomplished by a subset of the transformations and generators considered thus far, the generators l_{-1}, l_0, l_1. They form a closed subalgebra, and in fact are the generators of translations, scale transformations plus rotations, and special conformal transformations. They thus correspond to the conformal transformations from section 1.3.2, and are called *global conformal transformations*. The remaining transformations are *local conformal transformations*, which still have significant consequences for 2D CFTs.

In complex coordinates, conservation of the stress tensor and its tracelessness becomes

$$\begin{gathered}
\text{Traceless: } T_{z\bar{z}} = 0\,, \\
\text{Conservation: } \cancelto{0}{\partial_z T_{z\bar{z}}} + \partial_{\bar{z}} T_{zz} = 0\,,\; \partial_z T_{\bar{z}\bar{z}} + \cancelto{0}{\partial_{\bar{z}} T_{\bar{z}z}} = 0\,.
\end{gathered} \tag{1.3.61}$$

This means that the stress tensor only has two non-zero components, which are a function of a single variable each: $T(z) \equiv -2\pi T_{zz}(z)$ is the "holomorphic part of the stress tensor", and $\bar{T}(\bar{z}) \equiv -2\pi T_{\bar{z}\bar{z}}(\bar{z})$ is the "anti-holomorphic part of the stress tensor", with a factor of 2π for convention.

One can show that the two-point function of the stress tensor is

$$\langle T(z)T(0)\rangle = \frac{c/2}{z^4}\,,\ \langle \bar{T}(\bar{z})\bar{T}(0)\rangle = \frac{c/2}{\bar{z}^4}\,, \tag{1.3.62}$$

where c is called the *central charge*. c is a measure of the number of degrees of freedom, and also appears in the transformation of the stress tensor under conformal transformation,

$$T'(z') = \left(\frac{dz'}{dz}\right)^{-2}\left(T(z) + \frac{c}{12}\left\{\frac{d^3z'/dz^3}{dz'/dz} - \frac{3}{2}\left(\frac{d^2z'/dz^2}{dz'/dz}\right)^2\right\}\right)\,, \tag{1.3.63}$$

where the expression in curly braces is called the Schwarzian derivative. c also appears in the two-dimensional conformal anomaly (temporarily using (x^0, x^1) coordinates),

$$\langle T^\mu_\mu\rangle = -\frac{c}{12}R\,, \tag{1.3.64}$$

where R is the scalar curvature of the geometry, which of course is zero in flat space, explicitly showing that conformal symmetry is only a true symmetry in flat space.

Once again we find new conserved currents thanks to our infinite dimensional conformal symmetry. Local conformal invariance means that any $J_z = \epsilon(z)T(z)$, $J_{\bar{z}} = 0$ is a conserved holomorphic current for any function $\epsilon(z)$ (similarly for anti-holomorphic currents).

We can now write down the Ward identities, similar to (1.3.36) but with a structure more appropriate for 2D CFTs and encompassing full conformal invariance. First, because only the global conformal transformations are a well-defined symmetry, the total variation of a correlation function under a local conformal transformation need not vanish as in (1.3.28). The integral around a ball encompassing all points in 2D becomes a contour integral on a circle surrounding all points. The variation of a correlation function of operators $O_i(z_i, \bar{z}_i)$ under an arbitrary infinitesimal conformal transformation is then

$$\begin{aligned}\delta_{\epsilon,\bar{\epsilon}}\langle \mathcal{O}_1\cdots\mathcal{O}_n\rangle = &-\frac{1}{2\pi i}\oint_C dz\,\epsilon(z)\langle T(z)\mathcal{O}_1\cdots\mathcal{O}_n\rangle\\ &+\frac{1}{2\pi i}\oint_C d\bar{z}\,\bar{\epsilon}(\bar{z})\langle \bar{T}(\bar{z})\mathcal{O}_1\cdots\mathcal{O}_n\rangle\end{aligned}\,, \tag{1.3.65}$$

where the contours encircle all the points. If we consider a conformal transformation $\epsilon_n(z) = z^{n+1}$, $\bar{\epsilon}_n(\bar{z}) = \bar{z}^{n+1}$, $n \in \mathbb{Z}$, i.e. the infinite dimensional basis of conformal transformations, we get the quantum generators of conformal transformations,

$$L_n \equiv \frac{1}{2\pi i} \oint dz z^{n+1} T(z)\,,^{16} \quad \bar{L}_n \equiv \frac{1}{2\pi i} \oint d\bar{z} \bar{z}^{n+1} \bar{T}(z)\,. \tag{1.3.66}$$

Their algebra is the same as (1.3.60), but with the addition of a "central term", yielding the Virasoro algebra:

$$\begin{aligned} [L_n, L_m] &= (n-m)L_{n+m} + \frac{c}{12} n(n^2-1)\delta_{n+m,0}\,, \\ \left[\bar{L}_n, \bar{L}_m\right] &= (n-m)\bar{L}_{n+m} + \frac{c}{12} n(n^2-1)\delta_{n+m,0}\,, \\ \left[L_n, \bar{L}_m\right] &= 0\,. \end{aligned} \tag{1.3.67}$$

In particular, the combination $L_0 + \bar{L}_0$ generates dilations $(z', \bar{z}') = (\lambda z, \lambda \bar{z})$,

$$[L_0 + \bar{L}_0, \mathcal{O}(0,0)] = \Delta \mathcal{O}(0,0)\,. \tag{1.3.68}$$

Primary and descendent operators in 2D: We are now ready to see one of the primary consequences of conformal invariance in 2D. We still have the operator-state correspondence, (1.3.37). We consider operators that are eigenfunctions of both L_0 and $\bar{L}_0$ separately,

$$[L_0, \mathcal{O}(0,0)] = h\mathcal{O}(0,0)\,,\; [\bar{L}_0, \mathcal{O}(0,0)] = \bar{h}\mathcal{O}(0,0)\,. \tag{1.3.69}$$

h and $\bar{h}$ are the holomorphic and anti-holomorphic dimensions; they show how an operator scales under independent dilations of z and $\bar{z}$. The total scaling dimension and spin of these operators are

$$\Delta = h + \bar{h}\,,\; m = h - \bar{h}\,. \tag{1.3.70}$$

The separation between holomorphic and anti-holomorphic parts of our objects allow us to focus on just e.g. the holomorphic generators and dimension (similar expressions will always exist for the anti-holomorphic ones).

The conformal generators $L_{\mp n}$, $n > 0$ act like an infinite family of raising and lowering operators, since

$$\begin{aligned} &[L_0, L_{-n}] = nL_{-n}\,,\; [L_0, L_n] = -nL_n \\ \Longrightarrow\; &[L_0, [L_{\mp n}, \mathcal{O}(0,0)]] = (h \pm n)\mathcal{O}(0,0)\,. \end{aligned} \tag{1.3.71}$$

[16]Note that the generators are defined via a contour integral, rather than an integral over a fixed time slice as in (1.3.26) (which in this case would be $\mathrm{Im}\, z$). The precise meaning for this will be discussed in section 1.3.4.

We reach the same conclusion as in section 1.3.2; there must exist operators that cannot be lowered anymore by either L_n or $\bar{L}_n$, which we call *primary operators*:

$$\text{primary:}\ [L_n, \phi(0,0)] = [\bar{L}_n, \phi(0,0)] = 0 \text{ for all } n > 0. \tag{1.3.72}$$

Under *any* finite conformal transformation, primary operators transform like

$$\text{primary:}\ \phi'(z', \bar{z}') = \left(\frac{dz'}{dz}\right)^{-h} \left(\frac{d\bar{z}'}{d\bar{z}}\right)^{-\bar{h}} \phi(z, \bar{z})\,. \tag{1.3.73}$$

In particular, the stress tensor is *not* primary, as it transforms according to (1.3.63). However, the Schwarzian derivative vanishes for global conformal transformations, which it must since the stress tensor is still a quasi-primary operator.

All the statements about quasi-primaries from section 1.3.2 follow through for primaries with the appropriate generalization. The states in our theory split into those that come from primary operators and descendent operators

$$\begin{aligned} \text{Primary:}\ & |h, \bar{h}\rangle \equiv \phi(0,0)|0\rangle\,, \\ \text{Descendants:}\ & L_{-n_1} \cdots L_{-n_k} \bar{L}_{-\bar{n}_1} \cdots \bar{L}_{-\bar{n}_{\bar{k}}} |h, \bar{h}\rangle\,, \\ & \text{dimensions } h + \sum_{i=1}^{k} n_i\,,\ \bar{h} + \sum_{i=1}^{\bar{k}} \bar{n}_i\,, \end{aligned} \tag{1.3.74}$$

and linear combinations of these. Thus, **the spectrum of primary operators determines the entire spectrum of states for a two-dimensional conformal field theory.**

Correlation functions: The two and three point functions of primary operators are fixed by global conformal invariance,

$$\begin{aligned} \langle \phi_1(z_1, \bar{z}_1) \phi_2(z_2, \bar{z}_2) \rangle &= \begin{cases} \frac{C}{z_{12}^{2h_1} \bar{z}_{12}^{2\bar{h}_1}} \text{ if } h_1 = h_2\,,\ \bar{h}_1 = \bar{h}_2 \\ 0 \text{ otherwise} \end{cases}, \\ \langle \phi_1(z_1, \bar{z}_1) \phi_2(z_2, \bar{z}_2) \phi_3(z_3, \bar{z}_3) \rangle &= C_{123} \frac{1}{z_{12}^{h_1+h_2-h_3} z_{23}^{h_2+h_3-h_1} z_{31}^{h_3+h_1-h_2}} \\ &\quad \times (z \to \bar{z}, h \to \bar{h})\,. \end{aligned} \tag{1.3.75}$$

We again have an operator product expansion, which determines all correlators in terms of the dimensions h, $\bar{h}$ and OPE coefficients. This yields an equivalent expressions for (1.3.47),(1.3.48), where we now sum over primary operators. The OPE is

$$\phi_1(z_1,\bar{z}_1)\phi_2(z_2,\bar{z}_2) = \sum_\phi C_{12\phi}\mathfrak{C}(z_{12},\bar{z}_{12},h_{1,2,\phi},\bar{h}_{1,2,\phi},L,\bar{L})\phi(z_2,\bar{z}_2)\,, \tag{1.3.76}$$

where we explicitly use combinations of L_{-n}, $\bar{L}_{-n}$ to generate all the descendants of the primary ϕ_i. Again, the function $\mathfrak{C}(\cdots)$ is determined entirely by the conformal Ward identities.

For the four-point function, in 2D there are two independent cross ratios (as in (1.3.46)), one each for z and $\bar{z}$ respectively. We can use conformal invariance to move three of the points to ∞, 1, and 0, so the four-point function becomes

$$\langle\phi_1(\infty,\infty)\phi_2(1,1)\phi_3(z,\bar{z})\phi_4(0,0)\rangle = \sum_\phi C_{12\phi}C_{34\phi}g^{12}_{34}(h_\phi,z)\bar{g}^{12}_{34}(\bar{h}_\phi,\bar{z})\,, \tag{1.3.77}$$

where we used the OPE for $\phi_1\phi_2$ and $\phi_3\phi_4$. $g^{12}_{34}(h_k,z)$ is the holomorphic Virasoro conformal block and is determined (in principle) by conformal invariance alone. No full Virasoro blocks are known, although they can be determined term-by-term in a power series expansion.

Summary: Conformal invariance in two dimensions becomes an infinite dimensional symmetry, which leads to us categorizing operators into primaries and their descendants. These operators also determine all states. The holomorphic and anti-holomorphic dependence factorizes, and all correlation functions are determined by the OPE coefficients and the (anti-) holomorphic dimensions of the primary operators.

1.3.4 Modular invariance

At first, conformal invariance in two dimensions seems to leave all the primary operators and their holomorphic/anti-holomorphic parts completely independent. But by transforming to a geometry where space is finite, rather than staying on the infinite 2D plane, we see that primaries are related to each other through another powerful symmetry called *modular invariance*. This is the symmetry that makes random matrix statistics more difficult to see in CFTs, so we need to understand it carefully.

Radial quantization and the cylinder: Up to this point we've been discussing a theory that lives on an infinite two-dimensional plane, due to the familiarity of that setting for standard quantum systems. However, we could also consider a theory on a cylinder with circumference L: the spatial coordinate is periodic $x = x + L$, while the time coordinate τ goes from $-\infty$ to ∞ (note that we are still in Euclidean signature). The Hilbert space is made up of states defined on fixed time slices $|\psi(\tau)\rangle$ and are evolved forward in time with the Hamiltonian H.

The reason our discussion of a theory on a two-dimensional plane is still relevant is because, as mentioned in section 1.3.2, the two geometries are related by a conformal transformation,

$$z = \frac{L}{2\pi} e^{-i\frac{2\pi}{L}(x+i\tau)}\,,\ \bar{z} = \frac{L}{2\pi} e^{i\frac{2\pi}{L}(x-i\tau)}\,. \tag{1.3.78}$$

So we can use everything we've learned on the two-dimensional Euclidean plane to also discuss a theory that lives on a cylinder, as in Figure 1.6. A fixed time slice on the cylinder corresponds to a circle of a given radius, while the position on the cylinder just gives the angular coordinate on that circle. The infinite past $\tau = -\infty$ gets mapped to the origin $z = 0$, and the infinite future gets mapped to the "point" at infinity.

This motivates us to define our states on the Euclidean plane *not* on a fixed time slice $x_0 = \operatorname{Im} z$, but instead to define them as living on concentric circles centered at the origin; "time" is now interpreted as the radius of the circle $|z|$, and we evolve our states using the dilation operator D. Instead of ordering the operators in correlation functions by $\operatorname{Im} z$, we order the operators based on their distance from the origin $|z|$, which we call "radial ordering." In fact, this definition of states was implicit in section 1.3.3, for example in the commutators in (1.3.67).

With this, we can see how the scaling dimensions of operators give us the spectrum of energies for the theory on the cylinder. The Hamiltonian on the cylinder and corresponding energies can be shown to be

$$H = \frac{2\pi}{L}\left(L_0 + \bar{L}_0 - \frac{c}{12}\right)\,, \quad E = \frac{2\pi}{L}\left(h + \bar{h} - \frac{c}{12}\right)\,, m = h - \bar{h}\,, \tag{1.3.79}$$

(where we also included the spin m for completeness). We recognize the dilation operator $D \equiv L_0 + \bar{L}_0$, which makes sense as dilations on the plane move us between concentric circles, which corresponds with moving between fixed time slices on the cylinder. The $\frac{2\pi}{L}$ essentially gives us the correct units, and we will often set $L = 2\pi$ or 1. The $-\frac{c}{12}$ comes from

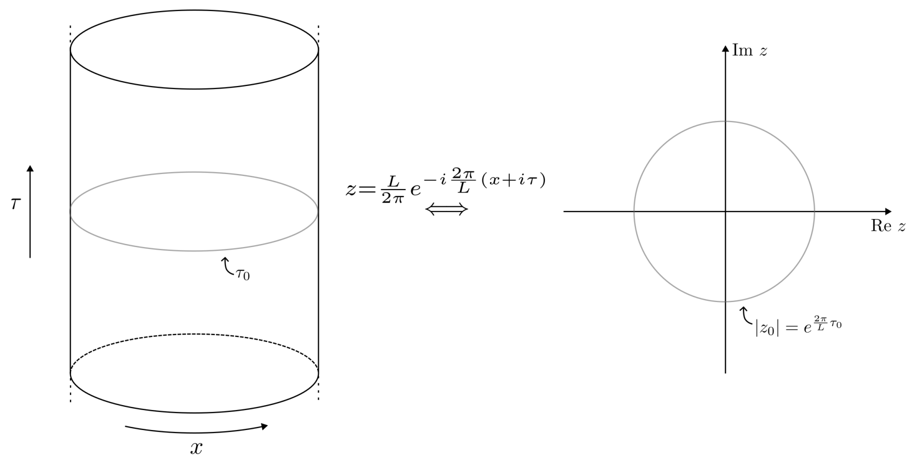

Figure 1.6: The mapping from the cylinder to the plane, showing the correspondence between time slices on the cylinder and circles of fixed radius.

the transformation rule of the stress tensor (1.3.63).[17] Depending on the context, we can thus categorize states in terms of their holomorphic and anti-holomorphic dimensions h, $\bar{h}$, or in terms of their energy and spin E, m.

In higher dimensions, a similar procedure holds; as we saw in (1.3.53), flat space is conformally equivalent to the higher dimensional cylinder. A fixed time slice corresponds to a sphere of fixed radius, and so we similarly define radial quantization by defining states on spheres of fixed radius.

The partition function in 2D CFTs: We can now consider the partition function, where we will discover a new symmetry. Let us (very briefly) consider our theory in Minkowski spacetime, where the spatial direction is a circle with circumference fixed to 2π using conformal invariance (i.e. on the cylinder). As in (1.2.6), the partition function for any quantum mechanical

[17] Specifically, if the vacuum on the plane has no energy i.e. $\langle T(z)\rangle = 0$, then

$$\begin{aligned} T_{\text{cyl}}(x+it) &= -\left(\frac{2\pi}{L}\right)^2 \left(T_{\text{plane}}(z)z^2 - \frac{c}{24}\right) \\ \implies \langle T_{\text{cyl}}(x+it)\rangle &= -\frac{c\pi^2}{6L^2} = \langle \bar{T}_{\text{cyl}}(x-it)\rangle \\ \implies \langle T^{00}\rangle &= -\frac{1}{2\pi}(\langle T_{\text{cyl}}\rangle + \langle \bar{T}_{\text{cyl}}\rangle) = -\frac{c\pi}{6L^2}\,, E_{\text{cyl}} = -\frac{c\pi}{6L} \end{aligned} \tag{1.3.80}$$

where in the last line, we used that $T(z) = -2\pi T_{zz}(z)$, and similar for $\bar{T}$. We see that on the cylinder, the vacuum has energy $-\frac{c\pi}{6L}$, or if we set $L = 2\pi$ then $E = -\frac{c}{12}$. The prescription in (1.3.79) correctly reproduces this, as the vacuum has scaling dimension 0.

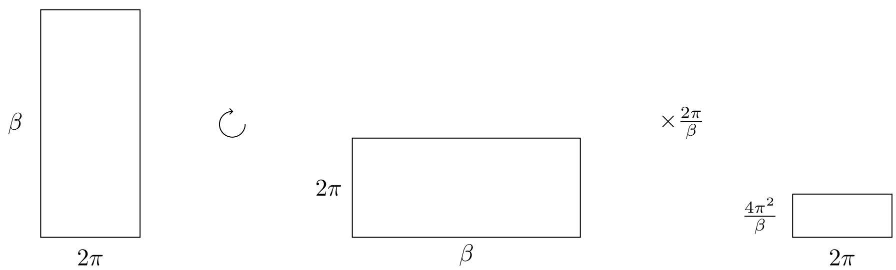

Figure 1.7: A cartoon representing the transformations that give modular invariance. The rectangles represent torii of a given width (spatial circumference) and height (Euclidean time/temperature circumference).

system is still

$$Z(\beta) \equiv \sum_n e^{-\beta E_n} = \mathrm{Tr}\, e^{-\beta H}\,, \tag{1.3.81}$$

where we can write the sum over energies as the trace of the Hamiltonian (using whatever basis we want).

Recall that the Euclidean time evolution operator in any quantum theory is $e^{-\tau H}$ as in (1.3.13), and that in terms of the path integral is (1.3.14). This gives the interpretation of the Boltzmann factor $e^{-\beta H}$ as evolving a state in Euclidean time by an amount equal to β. The trace then tells us that, in the path integral formulation, we integrate over all fields $\Phi(x)$ that are periodic under $\tau \to \tau + \beta$,

$$Z(\beta) = \int_{\Phi(\tau,\vec{x})=\Phi(\tau+\beta,\vec{x})} [d\Phi]\, e^{-S[\Phi(x)]} \tag{1.3.82}$$

(this holds for any number of dimensions, not just two). But if all of our fields are exactly periodic in this way, then there is nothing that distinguishes τ and $\tau + \beta$. This means that geometrically, **the partition function is defined by changing infinite Minkowski time into a periodic Euclidean time circle with circumference β, and doing the path integral.** In other words, a system that has a finite temperature lives on a geometry where the time coordinate is Euclidean and periodic.

In fact, our previous discussion about the transformation to the cylinder (1.3.78) means that by swapping time τ and space x in that transformation, $z = \frac{\beta}{2\pi} e^{\frac{2\pi}{\beta}(\tau+ix)}$, $\bar{z} = \cdots$, we have Euclidean time τ with period β, and an infinite spatial direction (just like we did in flat space). This is the exact geometry that arises when calculating the partition function for flat space! We call this geometry the "thermal cylinder", and we can find thermal correlation functions in flat space just by doing a conformal transformation to the thermal cylinder.

We quickly note that we can also do a conformal transformation to a thermal geometry in higher dimensions, however the spatial directions become the hyperbolic space $\mathbb{H}^{d-1}$. The thermal circle combined with hyperbolic space is a geometry that is conformally equivalent to so-called "Rindler space".[18] This means that thermal correlators in Rindler space can be obtained via conformal transformation of flat space correlators.

However, if our spatial direction is a circle and we calculate the partition function, replacing Minkowski time with the Euclidean circle results in a geometry that is not conformally equivalent to flat space, and new physics arises. Both the space and time directions are now Euclidean and on a circle, with periods 2π and β respectively. In other words our theory is on a torus. But in a Euclidean theory, there isn't anything that truly separates space and time so long as they have the same geometry, other than their arbitrary labels and how we define our states.[19] We're thus free to swap what we call "space" and "time"; doing so in this context means having a system on a spatial circle with circumference β, and we evolve it on a Euclidean time circle with circumference 2π.

Finally we use conformal invariance. Our theory is scale invariant, and so we can simultaneously scale the two circumferences in our system. By scaling both circumferences by $\frac{2\pi}{\beta}$, we have a system on a spatial circle with circumference $\beta \times \frac{2\pi}{\beta} = 2\pi$ (the same as what we started with), and we evolve it on a Euclidean time circle with circumference $2\pi \times \frac{2\pi}{\beta} = \frac{4\pi^2}{\beta}$. But this is just the partition function for our original system with a new temperature! **We come to the conclusion that in a conformal field theory,**

$$Z(\beta) = Z\left(\frac{4\pi^2}{\beta}\right) . \tag{1.3.84}$$

This constraint is extremely powerful; **the low temperature partition function (which is dominated by the lowest energy states) is equal to the high temperature partition function (which is dominated by the high energy states).**

[18] The metrics in the hyperbolic plane and Rindler space are

$$ds^2_{S^1\times\mathbb{H}^{d-1}} = d\tau^2 + \frac{1}{\rho^2}\left(d\rho^2 + dx_\perp^2\right) = \frac{1}{\rho^2}\left(\rho^2 d\tau^2 + d\rho^2 + dx_\perp^2\right) = \Omega(\rho) ds^2_{\text{Rindler}} \,. \tag{1.3.83}$$

[19] For the flat space partition function, the spatial direction is infinite and the time direction is on a circle, thus there is a proper distinction between the two.

In other words, one cannot simply have any arbitrary collection of primary operators; the low and high energy (dimension) operators are related. This can be explicitly captured by the famous *Cardy formula*. Recall that the density of states $\rho(E)$ of our theory is defined through

$$Z(\beta) = \int dE\, \rho(E) e^{-\beta E}\,. \tag{1.3.85}$$

The true density of states is a sum of Dirac delta functions, but we can often replace it with a smooth function to obtain the "coarse-grained" behaviour, similar to section 1.2.1. Now, as $\beta \to \infty$, the partition function is dominated by the vacuum state with energy $E_{\text{vac}} = -\frac{c}{12}$. Via modular invariance, this gives us the $\beta \to 0$ partition function,

$$\begin{aligned} Z(\beta) &\approx e^{\beta \frac{c}{12}}\,, \beta \to \infty \\ \implies Z(\beta) &\approx e^{\frac{4\pi^2}{\beta}\frac{c}{12}}, \beta \to 0\,. \end{aligned} \tag{1.3.86}$$

We can then invert the Legendre transform in (1.3.85) and take $E \to \infty$; via a saddle-point calculation, this is given by the $\beta \to 0$ partition function, and

$$\rho(E) = \int_{\epsilon - i\infty}^{\epsilon + i\infty} \frac{d\beta}{2\pi i} Z(\beta) e^{\beta E} \approx e^{2\pi\sqrt{\frac{c}{3}E}}\,,\, E \to \infty. \tag{1.3.87}$$

The conclusion is that the existence of the vacuum alone forces us to have a specific, exponentially large density of states at high energies. The "$\approx$" here means that this is only true as a coarse-grained statement; the exact density of states is of course a sum of delta functions, but its microcanonical average takes the approximate form in (1.3.87).

(1.3.84) is just the simplest example of modular invariance. The full version is found by adding an angular potential θ to the Boltzmann factor which couples to the spin of the states (i.e. one considers a grand canonical ensemble),

$$Z(\beta, \theta) = \sum_{m, E_m} e^{-\beta E_m + i\theta m} \tag{1.3.88}$$

It turns out this can also be interpreted geometrically as a path integral on a torus, but now periodic under $x + i\tau \to (x + 2\pi) + i\tau$ and $x + i\tau \to (x + \theta) + i(\tau + \beta)$. The partition function then depends on the ratio of the two (complex) periods, the "modular parameter" $\tau \equiv \frac{\theta}{2\pi} + i\frac{\beta}{2\pi}$, $\operatorname{Im}\tau > 0$, and full modular invariance becomes

$$Z(\tau) = Z\left(-\frac{1}{\tau}\right) = Z(\tau + 1). \tag{1.3.89}$$

The first equality, using the so-called S transformation $\tau \to -\frac{1}{\tau}$, is the same as (1.3.84) when $\tau = i\frac{\beta}{2\pi}$. The second equality, using the so-called T transformation $\tau \to \tau + 1$, is just a consequence of the fact that the spatial direction of our theory is a circle. These two equalities are called S duality and T duality respectively.

We can repeatedly apply these transformations to show that the CFT torus partition function has an entire group of symmetries,

$$Z(\tau) = Z\left(\frac{a\tau + b}{c\tau + d}\right), \quad a, b, c, d \in \mathbb{Z}\,, \; ad - bc = 1\,. \tag{1.3.90}$$

For example, $a = d = 0, b = -1, c = 1$ is the S transformation and $a = b = d = 1, c = 0$ is the T transformation. By considering these integers as matrices $\gamma \equiv \left(\begin{smallmatrix} a & b \\ c & d \end{smallmatrix}\right)$ they form a matrix group called $SL(2, \mathbb{Z})$. Modular invariance is then defined as invariance of the partition function under all $SL(2, \mathbb{Z})$ transformations.

Because of these dualities, the partition function for any τ can be determined if it is known for

$$\tau \in \mathcal{F} \equiv \left\{ \tau \,\middle|\, -\frac{1}{2} \leq \mathrm{Re}\,\tau \leq \frac{1}{2}\,, \mathrm{Im}\,\tau \geq 0\,, |\tau| \geq 1 \right\}. \tag{1.3.91}$$

$\mathcal{F}$ is called the "fundamental domain of $SL(2, \mathbb{Z})$." Using the language of cosets, this is denoted as $\mathcal{F} = \mathbb{H}/\mathrm{SL}(2, \mathbb{Z})$, which is the upper half plane $\mathbb{H}$ with all points connected by modular transformation identified as a single point.

Summary: Conformal invariance in two-dimensions provides us an exact way to characterize the energies on the cylinder. We find that these energies are highly constrained by considering the partition function, which possesses a property called modular invariance that relates low and high temperatures. This is made explicit in the Cardy formula, which gives the approximate high energy density of states due to the presence of the vacuum state.

1.4 Holography

Although chaotic phenomena in CFTs are interesting in their own right given how universal chaotic phenomena are in nature, in recent years a lot of the interest in chaotic CFTs comes from holography. Holography is a large and rich field, touching on everything from black holes, quantum information, thermalization, string theory, hydrodynamics, and much more. That said, we will focus only on the most relevant parts for motivating chaos in CFTs, plus some details that will be relevant for chapter 5. The motivation comes from the fact that certain primary states in CFTs are related to black holes in gravity, and black holes are known to be chaotic. We will clarify this relationship and its implications here.

Holography is a duality between two classes of systems: quantum gravitational theories in $d+1$ dimensions, and quantum field theories without gravity in d dimensions. The most famous type of holography is the *AdS/CFT correspondence*, which says that certain $d+1$ dimensional quantum gravity systems in a type of spacetime called *asymptotically AdS* are dual to regular d dimensional conformal field theories.

By a duality, we mean that there are ways of "translating" theoretical objects from one theory to another, producing equalities between calculations done in the gravity theory and those done in the CFT. These relationships are called the "dictionary".

To begin discussing this dictionary, we'll need to supplement our knowledge of CFTs with some basics about quantum gravity in asymptotically AdS spacetimes. In the process, we'll review the relevant features of general relativity, although a detailed knowledge of general relativity will not be necessary. We will generally work in Minkowski rather than Euclidean signature, i.e. we will have a timelike coordinate.

The most basic feature of classical general relativity is Einstein's equations, which relate the metric $g_{\mu\nu}(x)$ i.e. the geometry of spacetime, to the stress tensor $T_{\mu\nu}$ i.e. the distribution of matter and energy. The equations are

$$R_{\mu\nu} - \frac{1}{2}Rg_{\mu\nu} + \Lambda g_{\mu\nu} = 8\pi G T_{\mu\nu}\,. \tag{1.4.1}$$

$R_{\mu\nu}$ is the Ricci tensor and $R \equiv R^{\mu}{}_{\mu}$ is the scalar curvature; both are functions of the metric and measure the curvature of the geometry. Λ is the cosmological constant i.e. the energy of the vacuum, and G is Newton's constant. These equations can be derived as the equations of motion for the metric coming from an action containing the Einstein-Hilbert action and matter,

$$\begin{gathered} S_{EH}[g_{\mu\nu}(x)] = \frac{1}{16\pi G}\int d^d x\,\sqrt{-g}(R-2\Lambda)\,, \\ S[g_{\mu\nu}(x),\Phi(x)] = S_{EH}[g_{\mu\nu}(x)] + S_{\text{matter}}[g_{\mu\nu}(x),\Phi(x)] \end{gathered} \tag{1.4.2}$$

Einstein's equations show us how mass and energy affect the dynamics of a system. The metric tells us how free-falling particles move; particles with no forces acting on them follow geodesics $x(\lambda)$ i.e. paths that curve "as little as possible",

$$\begin{aligned} \frac{d^2x^\rho}{d\lambda^2} + \Gamma^\rho_{\mu\nu}\frac{dx^\mu}{d\lambda}\frac{dx^\nu}{d\lambda} &= 0\,, \\ \Gamma^\rho_{\mu\nu} \equiv \frac{1}{2}g^{\rho\sigma}\left(\frac{\partial g_{\nu\sigma}}{\partial x^\mu} + \frac{\partial g_{\mu\sigma}}{\partial x^\nu} - \frac{\partial g_{\mu\nu}}{\partial x^\sigma}\right) & \end{aligned} \tag{1.4.3}$$

where $\Gamma^\rho_{\mu\nu}$ is the Christoffel symbol, and λ is the parameter that parameterizes the path (for massive particles, we usually take λ to be time t).[20] Thus, matter and energy alter the movement of particles by changing the metric, and thus changing the movement of free-falling particles.

It's important to note that in a theory of *quantum* gravity, both the matter fields and the metric are supposed to be quantum fields. A given geometry/metric then corresponds to a particular state of the full quantum gravity theory. However, we will often use *the semi-classical approximation*, where we can do calculations with a small amount of matter that does not "back-react" and change the geometry via Einstein's equations. Thus the geometry, while still being a particular state of the quantum gravity theory, can be treated classically, while the matter is treated quantum mechanically.

The simplest solution to (1.4.1) is an empty universe with no cosmological constant, in which case the solution is just flat Minkowski space $g_{\mu\nu} = \eta_{\mu\nu}$ where particles follow traditionally straight lines. If we have a negative cosmological constant $\Lambda < 0$ instead, we get (empty) *Anti de Sitter (AdS) space*,

$$ds^2 = -\left(1 + \left(\frac{r}{R_{\text{AdS}}}\right)^2\right)dt^2 + \frac{dr^2}{1 + \left(\frac{r}{R_{\text{AdS}}}\right)^2} + r^2 d\Omega^2_{d-1} \tag{1.4.4}$$

R_{AdS} gives the curvature of the geometry and is related to Λ; from here it will be set equal to 1. We are using the equivalent of polar coordinates (1.3.52), where $r \geq 0$ is the radius and $d\Omega^2_{d-1}$ is the metric of a $d-1$ unit sphere. This spacetime has constant negative curvature everywhere; unlike Minkowski space where two parallel geodesics will always stay a fixed distance apart, or on a sphere where they will meet, in AdS they diverge away from each other, like the surface of a saddle, as in Figure 1.8.

One can show that the symmetries of the AdS metric are the group $\mathrm{SO}(d,2)$, the same size as the symmetry group of Minkowski space. Thus

[20] Specifically, massive particles follow time-like geodesics, i.e. $g_{\mu\nu}\frac{dx^\mu}{dt}\frac{dx^\nu}{dt} < 0$. Massless particles follow null geodesics, where $g_{\mu\nu}\frac{dx^\mu}{d\lambda}\frac{dx^\nu}{d\lambda} = 0$.

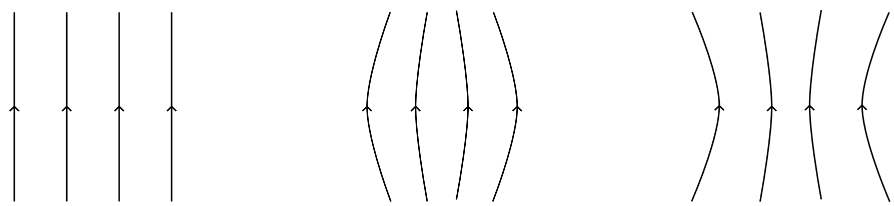

Figure 1.8: The three types of curvature, shown through their effect on parallel geodesics. In flat space, parallel geodesics stay a fixed distance apart. In positively curved space, parallel geodesics approach each other until they meet. In negatively curved space, parallel geodesics diverge away from each other. When embedded in three dimensional space, these geometries look like a flat plane, a sphere, and a saddle respectively.

AdS is maximally symmetric. This is, in fact, the same symmetry group as the conformal group for a d dimension Minkowski spacetime.

A fundamental aspect of any spacetime is the causal structure i.e. what regions of the geometry can be in communication with and affect each other. The causal structure of spacetime is determined by light cones, i.e. all the light-like rays that pass through a specific point. Two points are causally connected if they lie inside (or on the surface of) each other's light-cones, as then a signal can be sent between the points. We can do a coordinate transformation that is particularly useful to see the causal structure of AdS; set $r = \tan\theta$, $0 \leq \theta < \frac{\pi}{2}$, and we get

$$ds^2 = \frac{1}{\cos^2\theta}\left(-dt^2 + d\theta^2 + \sin^2\theta d\Omega^2_{d-1}\right) \tag{1.4.5}$$

The reason this gives us the causal structure is that light rays don't care about conformal factors like $\frac{1}{\cos^2\theta}$. So the causal structure of AdS space is given by what's inside the brackets of (1.4.5). This is topologically a solid cylinder (meaning it includes the inside); $\theta = \pi/2$ is the boundary of the cylinder, and corresponds to $r = \infty$, where the metric is

$$ds^2\big|_{\theta=\pi/2} \sim -dt^2 + d\Omega^2_{d-1} \tag{1.4.6}$$

which is just $\mathbb{R} \times S^{d-1}$, i.e. a d dimensional cylinder as in (1.3.53) where the length of the cylinder is time-like. If $d = 2$, this is just the boundary of a standard 3 dimensional cylinder, as in Figure 1.9. Any spacetime that matches this boundary structure is called asymptotically AdS; such spacetimes can be viewed as cylinders with more complicated geometry and dynamics going on in the interior.

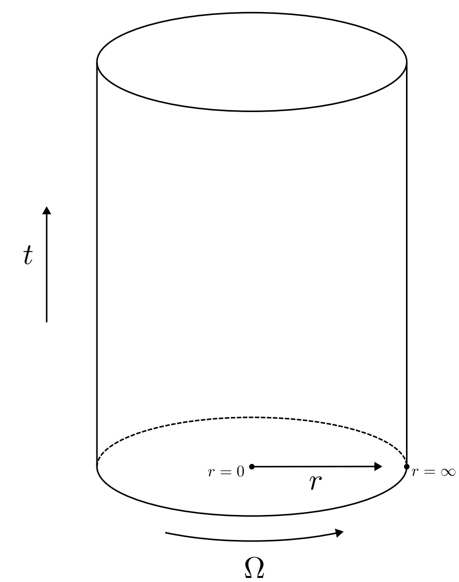

Figure 1.9: A representation of AdS_3. The boundary is at $r = \infty$. For general dimensions, one could still use this picture, but where every point is actually a $d-2$ dimensional sphere.

If we fire a light ray from the center of the cylinder $\theta = r = 0$, it takes finite time for the light ray to hit the boundary and reflect back to us. For this reason, AdS is often referred to as "being in a box". The fact that the boundary can be reached in finite time, and that the symmetry group of AdS is the exact same as that of the conformal group in d dimensions, are the first signs that perhaps a conformal field theory living on the boundary of an asymptotically AdS spacetime can describe the same physics as the gravitational system itself. This fact, along with many results and analyses to support it, has led physicists to conjecture the

AdS/CFT correspondence: Quantum gravity in asymptotically AdS spacetime "=" conformal field theory living on the boundary.

The gravitational spacetime is referred to as "the bulk", while the conformal field theory living on the boundary is just referred to as "the boundary". We should thus be able to calculate gravity quantities using the CFT technology from section 1.3 and vice-versa, after we use a conformal transformation to put the CFT on a cylinder.

While we could use any CFT to, in some sense, "define" a quantum gravity system, only certain CFTs will describe bulks that behave in the way we expect. In particular, we want to be able to treat the gravitational theory semi-classically. These CFTs are called *holographic CFTs*. Holographic CFTs with central charge c have the following properties:

- The central charge is large, $c \gg 1$.
- There are a finite number of "single-trace operators" $\mathcal{O}_i$ with $O(c^0)$ dimensions and spin equal to 0 or 1. Their two point functions are normalized as
$$\langle \mathcal{O}_i(x)\mathcal{O}(0)\rangle = \frac{1}{x^{2\Delta_i}}\,,$$
and their OPE coefficients are $O\left(\frac{1}{c}\right)$.
- For any collection of single-trace operators, there exists a "multi-trace" operator $\mathcal{O}_{i_1}\cdots\mathcal{O}_{i_n}$ with dimension $\Delta = \Delta_{i_1} + \cdots + \Delta_{i_n} + O\left(\frac{1}{c}\right)$.
- All operators with $O(c^0)$ dimension are either single or multi trace operators.
- Correlation functions of single- and multi-trace operators factorize at leading order in $1/c$, meaning that the correlation functions are given by "matching up" the single trace operators. For example,
$$\langle \mathcal{O}_1(x_1)\mathcal{O}_1(x_2)\mathcal{O}_3(x_3)\mathcal{O}_3(x_4)\rangle = \langle \mathcal{O}_1(x_1)\mathcal{O}_1(x_2)\rangle\langle \mathcal{O}_3(x_3)\mathcal{O}_3(x_4)\rangle + O\left(\frac{1}{c}\right).$$
The leading behaviour is the "universal mean field theory solution".

This approach to the correspondence, where one looks at the general properties that a CFT needs for it to have a good semi-classical bulk, is referred to as "bottom-up". This is in contrast to the "top-down" approach, where one starts with an exact, microscopic theory of quantum gravity (most often a string theory) and explicitly derives a duality between gravity and a conformal field theory. We are almost exclusively interested in the bottom-up approach, however we will sometimes look at top-down models.

We now give some important examples of this equality. The first is the relationship between fields in the bulk and operators on the boundary. To motivate this, lets consider a free scalar field, with an action given by (1.3.7). We assume that the field has small enough mass and low enough energy that it doesn't back-react. Classically, a scalar field in a curved spacetime obeys the Klein-Gordon equation,

$$(\Box_g - m^2)\phi(x) = 0\,,\, \Box_g \equiv \frac{1}{\sqrt{-g}}\partial_\mu\left(g^{\mu\nu}\sqrt{-g}\,\partial_\nu\right)\,. \tag{1.4.7}$$

Using the metric and coordinates in (1.4.4), we can solve this equation and look at how the field behaves as it approaches the boundary. One can show that the normalizable solution is

$$\phi(r,t,\Omega) \underset{r\to\infty}{\approx} r^{-\Delta}\psi(t,\Omega)\,,\ \Delta = \frac{d}{2} + \frac{1}{2}\sqrt{d^2+4m^2}\,. \tag{1.4.8}$$

Δ is actually similar to the scaling dimension of a CFT operator. We can see this by looking at the two-point function for the quantized field $\phi(x)$ as it approaches the boundary; one finds

$$\langle \phi(r_1,t_1,\Omega_1)\phi(r_2,t_2,\Omega_2)\rangle \underset{r\to\infty}{\approx} \frac{r_1^{-\Delta}r_2^{-\Delta}}{(\cos(t_1-t_2)-\cos\alpha)^{\Delta}} \tag{1.4.9}$$

where α is the angle between Ω_1 and Ω_2. This is exactly the two point function of primary operators for a CFT on the cylinder with scaling dimension Δ, multiplied by $r_1^{-\Delta}r_2^{-\Delta}$. This is one of the consequences of the "extrapolate dictionary":

$$\lim_{r\to\infty} r^{\Delta}\phi(r,t,\Omega) = \mathcal{O}_{\Delta}(t,\Omega)\,. \tag{1.4.10}$$

That is, every low-energy primary scalar operator on the boundary corresponds to a primary scalar field in the bulk. We can apply this to operators with spin as well; for example, the stress tensor on the boundary corresponds to the metric inside the bulk.

Black holes, coarse-graining, and chaos: The thread that ties together everything we've discussed so far (quantum chaos, conformal field theories, and holography) is found by considering the holographic dual of the CFT partition function and black holes in gravity.

Recall from (1.3.82) that the CFT partition function can be calculated as a path integral where the time coordinate is on a Euclidean circle,

$$Z_{\text{CFT}}(\beta) = \int_{\Phi(\tau,\vec{x})=\Phi(\tau+\beta,\vec{x})} [d\Phi]\, e^{-S[\Phi(x)]}$$

The holographic dual of this is the *gravity path integral* over a geometry whose boundary is also a Euclidean time circle, [21]

$$Z_{\text{CFT}}(\beta) = Z_{\text{grav}}(\beta) \equiv \int_{B_\beta} dg_{\mu\nu}\,[d\phi]\, e^{-S_{EH}[g_{\mu\nu}(x)]-S_{\text{matter}}[g_{\mu\nu}(x),\phi(x)]} \tag{1.4.11}$$

[21] In particular, the whole geometry now has to be Euclidean.

where we now also integrate over all metrics/geometries, and B_β are the boundary conditions for the geometry and matter fields (namely, that the geometry at the boundary matches the CFT geometry, and that the fields on the boundary are periodic on the Euclidean time circle). Often, in the semi-classical limit there will be a single geometry that dominates the path integral. For example at zero temperature $\beta \to \infty$ the path integral is dominated by empty AdS_{d+1}.

What about at sufficiently high temperature? This brings us to the boundary dual of a black hole. The simplest type of black hole with mass M in AdS_{d+1} is given by the metric

$$ds^2 = -f(r)dt^2 + \frac{dr^2}{f(r)} + r^2 d\Omega_{d-1}^2 \, , \; f(r) = r^2 + 1 - \frac{\alpha}{r^{d-2}} \, , \; \alpha = CM \quad (1.4.12)$$

where C is a known constant. This is the AdS version of the Schwarzchild black hole; it has a horizon at r_s where the function $f(r)$ is zero, $f(r_s) = 0$. The horizon size increases with mass, and any object that falls into this horizon can never escape.

As Hawking showed, black holes are thermal objects with a temperature $T \equiv \beta^{-1}$ given by their size/mass,

$$T = \frac{d - 2 + dr_s^2}{4\pi r_s} \quad (1.4.13)$$

It turns out that this fact has a beautiful holographic dual; **a black hole with inverse-temperature β in the bulk is holographically dual to a thermal state at inverse-temperature β on the boundary**. That is, the black hole geometry dominates the gravity path integral in (1.4.11), giving us the CFT partition function at finite temperature. In other words, we can calculate CFT correlation functions for a system at finite temperature, and this would be equal to quantum gravity correlation functions in a black hole geometry. The temperature needs to be appropriately high, otherwise one just has a thermal gas of matter in the bulk (or empty AdS at zero temperature), not a black hole.

This duality becomes more interesting when we use the fact that in a holographic CFT, the states created by operators with sufficiently large dimension (i.e. states with large energy) look just like thermal states: correlation functions in these states (rather than in the vacuum state) look like the correlation functions in a canonical ensemble (1.2.7). This tells us that in a holographic CFT, **high energy states in a CFT are holographically dual to black holes.**

In two-dimensional holographic CFTs, these high energy black hole states actually obey the Cardy formula (1.3.87). The minimum, *extremal energy* for a black hole state with spin m is $E_m^{(0)} \equiv \frac{2\pi}{L}\left(|m| - \frac{1}{12}\right)$, and

$$\rho_m(E) \approx e^{2\pi\sqrt{\frac{c}{3}E}}\,,\ E > E_m^{(0)} \tag{1.4.14}$$

where $\rho_m(E)$ is the density of states for spin m only.[22] Because the rest of the spectrum has a much smaller density of states, we will often refer to this as the *dense spectrum*. The part of the dense spectrum close to the lower bound is called the *near-extremal spectrum*.

So far, we've only talked about a single CFT partition function $Z_{\mathrm{CFT}}(\beta)$ and its holographic dual. If one has multiple partition functions multiplied together however, e.g. $Z_{\mathrm{CFT}}(\beta_1)Z_{\mathrm{CFT}}(\beta_2)$, the holographic dual is still just a single gravity path integral, but now the geometry has *two boundaries*, each on Euclidean time circles, $Z_{\mathrm{grav}}(\beta_1,\beta_2)$. Taking a semi-classical approximation, the gravity path integral doesn't factorize:

$$Z_{\mathrm{grav}}(\beta_1,\beta_2)\big|_{\text{semi-classical}} \neq Z_{\mathrm{grav}}(\beta_1)\big|_{\text{semi-classical}} Z_{\mathrm{grav}}(\beta_2)\big|_{\text{semi-classical}} \tag{1.4.15}$$

This non-factorization is similar behaviour as in section 1.2, where we took the coarse-grained average of the product of partition functions, leading to a spectral form factor that didn't factorize. The interpretation is that the semi-classical approximation in gravity doesn't give the full partition function or products of partition functions, but instead gives the coarse-grained average of them. What this means for black holes is that for high enough temperature, the gravity path integral is essentially a spectral form factor, and can tell us about the statistics of black hole states in gravity.

This comes to an important feature of holographic CFTs, and is one of the primary motivators of this thesis. In [32, 34] the two-boundary gravity path integral (the "wormhole amplitude") in two and three dimensions was calculated, showing that near-extremal black holes possess random matrix statistics. Not only that, but as we mentioned in section 1.2.2, black holes are maximally chaotic systems, i.e. the expectation value of the commutator we considered grows exponentially with $\lambda = \frac{2\pi}{\beta}$. Together this tells us a crucial fact:

Holographic CFTs are chaotic CFTs.

[22] This holds on either side of the duality, with energy interpreted as either the energy of (primary) operators, or the energy of black holes.

In other words, in order for the calculations in a CFT to match the calculations done in quantum gravity, the CFT must be quantum chaotic in both senses: the statistics of pairs of certain energies/dimensions should take the same form as random matrix theory, and small perturbations of a few degrees of freedom should grow exponentially fast. The former is measured by the spectral correlations in the density of states and partition function; the latter is measured by the thermal correlator of the commutator squared or the out-of-time-ordered correlator. In this thesis, we will investigate these phenomena in CFTs themselves.

Summary: The AdS/CFT correspondence says that conformal field theories in d dimensions are dual to certain quantum gravity theories in $d+1$ dimensions. Low-energy operators in the CFT are matched with quantum fields in gravity, with the scaling dimensions and masses related. The partition function in the CFT is given by the gravity path integral, and black holes in gravity are dual to thermal states and high energy states in the CFT. Gravity can calculate coarse-grained quantities in the CFT, and in particular the chaotic nature of black holes tells us that holographic CFTs are chaotic, containing random matrix statistics and scrambling.

1.5 Summary of results

Chapter 2: In the first two chapters, we analyze random matrix universality in the spectral correlations of chaotic two-dimensional CFTs with large central charge, and its interplay with symmetry. In this first chapter, our goal is to find what part of the CFT spectrum can exhibit random matrix universality despite the overwhelming amount of symmetry, and to show how these symmetries allow us to use the existence of random matrix universality in part of the spectrum to make predictions of another part.

We construct a partition function describing the fluctuations in the dense part of the spectrum of primary states, in a way that disentangles the chaotic properties of the spectrum from those which are a consequence of Virasoro symmetry. We then analyze this function using the harmonic analysis of modular invariant functions, where we decompose modular invariant functions (1.3.90) into a basis of modular invariant eigenfunctions of the Laplacian.[23] This basis contains two sectors: a continuous sector of analytically known functions called Eisenstein series, and a discrete sector of numerically known

[23]This is similar to the Fourier decomposition of periodic functions into a basis of plane waves, i.e. periodic eigenfunctions of the Laplacian

functions called Maass cusp forms. Here we focus on the simpler Eisenstein series, assuming that chaos is encoded entirely in the continuous sector.

This allows us to analyze the parts of the spectrum that are unconstrained by modular invariance. We argue that random matrix universality near the extremal/minimal energy of the dense spectrum is an independent feature of each spin sector separately. This is a non-trivial statement because the full spectrum in every spin sector is fully determined by only the spectrum of spin zero primaries and those of a single non-zero spin, a fact called "spectral determinacy". This leads to a linear ramp in the near-extremal (low temperature) spectral form factor at late times, as predicted by AdS_3 gravity.

We then describe an argument analogous to the one leading to Cardy's formula (1.3.87) for the averaged density of states, but in our case applying it to spectral correlations: assuming random matrix universality in the near-extremal spectrum in all spin sectors and using the S transform (1.3.84), we find similar random matrix universality in a large spin regime far from extremality.

Chapter 3: The focus of this chapter is on the discrete sector of the spectral decomposition, the Maass cusp forms. Both their eigenvalues and Fourier coefficients are sporadic discrete numbers with interesting statistical properties and relations to analytic number theory (features referred to as "arithmetic chaos"). We show that the near-extremal spectral form factor at late times is only sensitive to a statistical average over these erratic features. Nevertheless, complete information about their statistical distributions is encoded in the spectral form factor if we demand that the CFT contains random matrix universality in all independent spin sectors. We "bootstrap" the form of correlations between the cusp form basis functions corresponding to a universal linear ramp and show that they are unique up to subleading corrections. We observe that these correlations, which are fully determined by the assumption of quantum chaos, exactly match the known wormhole amplitude in pure AdS_3 gravity that first predicted random matrix universality in holographic CFTs.

Chapter 4: We study two novel approaches to efficiently calculate correlation function in higher dimensional CFTs, and describe applications to quantum chaos. This will allow us to explain and generalize various relations between hydrodynamics, scrambling, conformal blocks, shadow operators, and other parts of the structure of CFTs.

The first approach concerns the shadow operator formalism (1.3.55) and kinematic space techniques, which are tools that allow the computation of the operator product expansion and conformal blocks. We find a simpler reformulation of these tools; we observe that the shadow operator associated with the stress tensor can be written as the descendant of a field $\mathcal{E}$ with negative scaling dimension. Computations of stress tensor global conformal blocks can be systematically organized in terms of the "soft mode" $\mathcal{E}$, turning them into a simple diagrammatic perturbation theory at large central charge.

Our second (equivalent) approach concerns a theory of reparametrization modes linked to hydrodynamics. Due to the conformal anomaly in even dimensions, gauge modes linked to metric fluctuations acquire a hydrodynamic action, derived by using the generating function for stress tensor correlators (1.3.29). We show that these modes exhibit the same dynamics as the soft mode $\mathcal{E}$ that encodes the physics of the stress tensor shadow. We discuss the calculation of the conformal partial waves and the conformal blocks using our effective hydrodynamic theory. The separation of conformal blocks from shadow blocks is related to gauging of certain symmetries in the action of the soft mode.

As an application we study thermal physics in higher dimensions and argue that the theory of reparametrization modes captures the physics of scrambling in Rindler space. This is also supported by the observation of the pole skipping phenomenon in the energy density two-point function on Rindler space.

Chapter 5: We study a generalization of AdS/CFT where the CFT has a spatial boundary (a BCFT). A commonly proposed "bottom-up" holographic dual is an AdS spacetime with an additional boundary, an end-of-the-world brane attached to the CFT boundary. This duality has been used as a model for black hole microstates. We investigate when a holographic BCFT could be expected to possess such a holographic dual, and argue that the answer is almost never.

By studying Lorentzian BCFT correlators, we characterize constraints imposed on a BCFT by the existence of a bulk causal structure, namely the fact that light rays fired from the boundary can bounce off the end-of-the-world brane and return to the boundary. We argue that approximate 'bulk brane' singularities place restrictive constraints on the BCFT data (the operator dimensions and OPE coefficients) that are not expected to be true generically.

Chapter 2

Symmetries and spectral statistics in chaotic conformal field theories I: Eisenstein series and spectral determinacy

2.1 Introduction

A great deal of progress on understanding quantum chaos in conformal field theories (CFTs) has been made in the last decade, particularly thanks to holography. While many results for the consequences of chaos for *correlation functions* have been discovered (e.g., scrambling [21], the eigenstate thermalization hypothesis [42], and OPE coefficients [39]), the more traditional characteristic of quantum chaos, i.e., random matrix-like statistics in the coarse-grained spectrum of the theory [8, 11, 54, 55], has not been fully explored. In this work we are interested in the interplay between random matrix statistics in the CFT spectrum and the many symmetries and constraints that all two-dimensional CFTs posses.

The precise spectrum of any CFT is subject to highly non-trivial constraints such as the bootstrap equations [56]. These constraints can be applied to the coarse-grained spectrum, i.e., the spectrum averaged over microcanonical windows. An example in two-dimensional CFTs is the Cardy formula [57]; it gives a profile for the density of state at large energy that accurately describes an average over microcanonical windows of the true (discrete) density of states. Its derivation simply amounts to reinterpreting the vacuum state on a torus in the modular transformed channel using modular invariance. It is thus an example of a symmetry (modular invariance) constraining some part of the spectrum based on knowledge of another part.

In this chapter we focus on *correlations* in the spectrum of chaotic two-dimensional CFTs, such as those measured by the density of states two-point function, understood in the sense of microcanonical averaging. In quantum chaotic systems, such correlations obey the same statistics as an (appropriate) ensemble of random matrices. In [33, 34], it was shown that the *near-extremal correlations* of BTZ black hole microstates in AdS_3 gravity obey random matrix statistics; this suggests that a dual holographic two-dimensional CFT must have the same statistics described by such a wormhole amplitude. We wish to characterize in a precise sense the way in which two-dimensional CFTs can exhibit such a quantum chaotic spectrum. Since the CFTs of interest are quantum field theories and exhibit an enormous amount of symmetry, a careful analysis is needed to make the connection with (much simpler) random matrix theory.[24]

Symmetries and chaos. A signature of quantum chaos is the existence of universal correlations in the spectrum. When the quantum system enjoys a symmetry, parts of the spectrum are fixed by the symmetry, while other parts must be uncorrelated, and the correlations due to chaos tend to wash away. Therefore, one has to remove all consequences of the symmetry in order to be able to see the universal statistics of the chaotic spectrum. For example, for a system with a single conserved charge, one has to isolate different charge sectors, obtaining a universal description of each charge sector separately, whereas different sectors are uncorrelated [36]. In exploring the concept of randomness and statistical universality in two-dimensional CFTs, our first task is to take care of the large number of symmetries such systems enjoy:

(1) Virasoro symmetry: treating the Virosoro symmetry is standard – each state in the CFT is a primary of some conformal dimensions $(h, \bar{h})$ or a descendant of such a primary. The spectrum of descendants is fully determined by Virasoro symmetry. The full density of states is thus determined in terms of the density of primaries, which is the object we will focus on.[25]

[24] See also [58–61] for discussions and numerical results regarding the time scales associated with spectral form factors in CFTs, and in particular for rational theories where ergodicity can emerge in an approximate sense.

[25] The Virasoro symmetry is infinite dimensional, perhaps suggesting some degree of integrability. However, when we fix the symmetry completely, for large central charge the spectrum remains dense; the difference between the density of all states and that of Virasoro primaries only differs by replacing c with $c - 1$. Thus there is still an exponentially dense number of states that is not determined by symmetry. This is to be contrasted with integrable systems where fixing the charges determines the state uniquely. As explained below, the results of [34] provide an existence proof of CFTs with eigenvalue repulsion in the appropriate limit.

(2) Each conformal field theory has a conserved momentum, which we refer to as spin. In the spirit of the above comments, to see chaos we focus on the density of states for a fixed spin sector.

(3) Modular invariance: the primary density of states for fixed spin is not yet free of symmetry constraints. There are large conformal transformations, the modular transformations, which correlate the density of primaries of different conformal dimensions. To disentangle randomness from consequences of modular invariance, we decompose the partition function in terms of objects that are already modular invariant, thus enabling us to discover aspects of the theory which can be (pseudo-)random. As is described in detail in the next section, this decomposition utilizes the recent work on harmonic analysis of two-dimensional CFTs [62] (see also [45, 63]).

Some of these concepts are illustrated in figure 2.1. We will be focusing primarily on modular invariance in this chapter, and the ways in which it does or does not constrain the appearance of chaos in two-dimensional CFTs. Note that our goal is not to derive chaotic properties of CFTs, but rather to assume them and explore their interplay with symmetries and modular invariance. Because the existence of random-matrix like statistics in CFTs is motivated by holography, we now comment on our perspective on its implications.

Comments on 'ensemble averaging'. The presence of a nearly-continuous dense spectrum in gravity, together with the factorization problem [32, 64] and related developments in two-dimensional JT gravity (e.g., [65–68]), has led to the suggestion that three-dimensional gravity might be dual to an ensemble of CFTs [33, 34, 69, 70]. We now comment on these suggestions and outline the approach we follow.

Quantum mechanical systems exhibit statistical universalities referred to as "quantum chaos", which underlie the equilibrium properties of the system and its approach to equilibrium. For example, the high-energy spectrum is dense and can be approximated by a continuous density of states, whose low-point correlators are universal. For a single particle chaotic quantum system [15], one can check the predictions of quantum chaos by numerically diagonalizing the Hamiltonian of the system, binning the eigenvalues to create a continuous function, and calculating the density of states and its correlators. This is the sense in which we discuss chaotic properties, such as spectral statistics, of a single conformal field theory without resorting to any notion of ensembles of theories. Our main question is which aspects of the resulting density of states are universal, and how they are constrained or unconstrained by symmetry.

Quantum mechanical statistical universalities are argued for and described in an effective field theory language known as the Efetov sigma model [71, 72] (for a recent review see [73]), where they emerge as the low frequency description of the full system.[26] Often there is a canonical model which is used to exemplify these universalities, and that model (most commonly random matrix theory) often involves built-in randomness. Since the quantum chaotic properties are universal, the canonical model can be chosen for reasons of convenience and any of its special features (e.g., ensemble averaging) have no special significance beyond simplifying calculations.

2.1.1 Summary of results

Let us briefly summarize our two main findings regarding the interplay of modular invariance and quantum chaos. The first concerns the precise way in which modular invariance, when focusing on the near-extremal limit, *doesn't* constrain quantum chaotic universalities (namely random matrix statistics/eigenvalue repulsion) in the spectrum of different spin sectors, and is hence consistent with more general expectations about the interplay of quantum chaos and symmetries. The second finding provides an example where modular invariance can lead to new types of universal behavior of the spectrum. See also figure 2.1 for illustration.

Random matrix universality despite spectral determinacy. It was shown in [62], based on the same techniques we will use below, just how constraining modular invariance is: *knowledge of the light ($h + \bar{h} \leq \frac{c-1}{12}$), the spin 0, and the spin m spectrum for a single $m \geq 1$ completely determines the spectrum for all other spin sectors.* Following [62], we refer to this statement as spectral determinacy (see also [74]). This statement concerns the exact spectrum. One of our goals is to elucidate the extent to which it holds for the coarse-grained spectrum and its statistical properties. We will give arguments that in the near-extremal limit spectral determinacy does not

[26] An interesting sigma-model to describe some statistical properties of two-dimensional CFTs, namely of their operator product expansion (OPE) coefficients, was written down in [41], whereas here we are mainly interested in the operator spectrum. We hope that our results, perhaps in combination with the techniques developed in [41], can set the stage for a further understanding of the effective field theory of chaos in CFTs and its derivation from first principles.

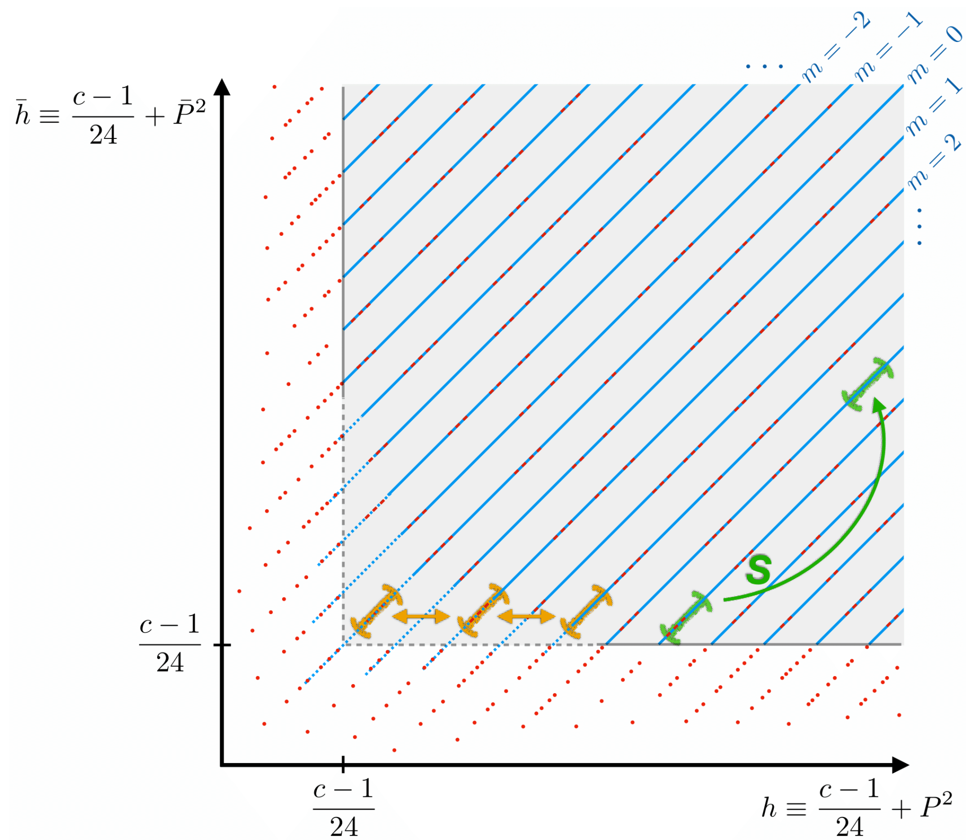

Figure 2.1: Cartoon of the spectrum of primary operators. The spectrum below the extremality bound (red dots outside the shaded region) is sparse and not chaotic. We remove it and all its modular images (red dots within the shaded region) from the primary partition function and focus on the statistics of the remaining dense spectrum after coarse-graining along fixed spin trajectories (blue). The first part of the chapter (section 2.3) demonstrates that chaos in different spin sectors near extremality (orange regions) contains independent information. The second part (section 2.4) derives eigenvalue repulsion far from extremality by assuming eigenvalue repulsion near extremality and performing a modular S-transformation (green regions).

constrain the coarse-grained spectrum in the same way. In particular, we will argue for the following statement (under some assumptions): *in the long time/near-extremal limit, universal short-ranged eigenvalue repulsion of a quantum chaotic spectrum in any finite number of spin sectors is not sufficient to infer nor exclude the same universality in all other spin sectors.* In other words, spectral determinacy is not constraining enough to prevent having random matrix statistics in each spin sector independently, nor powerful enough to infer random matrix statistics in every spin sector from a finite number of them.

Cardy-like formula for spectral correlations. Assuming random matrix universality and therefore short-ranged eigenvalue repulsion for each spin sector in the near-extremal limit, we see how modular transformations relate it to interesting statements about spectral correlations in the far-from-extremal regime. This is in the spirit of Cardy's derivation of the high energy behaviour of the (averaged) density of states, now applied to correlations in the spectrum. We show that the far-from-extremal spectrum also exhibits eigenvalue repulsion in a certain limit, demonstrating that random matrix universality applies in a larger part of the spectrum.

2.1.2 Outline

This chapter is organized as follows: in section 2.2 we define the part of the spectrum which has (almost) all symmetry constraints removed, and review harmonic analysis and spectral determinacy. In section 2.3 we analyze quantum chaotic universality in spectral correlations across spin sectors in the near-extremal limit, exploring the consequences of spectral determinacy. Section 2.4 discusses Cardy-like constraints on the spectrum far from extremality, using assumptions about a universal near-extremal spectrum. We end with a discussion in section 2.5 and refer to appendices for some details and derivations.

2.2 Modular invariant decomposition of the partition function

In this section we discuss the process of removing constraints of symmetry from the CFT spectrum, which results in the quantity of interest, the fluctuating part of the dense primary counting partition function. This is the quantity we use in the rest of the chapter to search for statistical universalities.

2.2.1 Dense primary counting partition function

Let $Z(x,y)$ denote the partition function of the two-dimensional CFT under consideration, which is obtained by a path integral on a torus with modular parameter $\tau = x + iy$:

$$Z(x,y) = \sum_{h,\bar{h}} e^{-2\pi y\left(h+\bar{h}-\frac{c}{12}\right)} e^{2\pi i x(h-\bar{h})} = \sum_m \int dE\, \rho^m(E)\, e^{-yE}\, e^{2\pi i x m}\,. \tag{2.2.1}$$

Throughout, we will assume that the CFT only has Virasoro symmetry and no additional currents (and $c > 1$). To enable statistical analysis we need a near-continuous density of states for sufficiently heavy operators, which is obtained in the limit of large central charge [75]. Following the above discussion, in order to strip the partition function from consequences of symmetry we will now improve it in two steps (following [62]):

1. First, we wish to discard all constraints on the spectrum which are purely due to Virasoro symmetry.[27] This means, we want to consider a primary-counting partition function, which does not separately count Virasoro descendants. While this is achieved by multiplying the partition function by $\prod_{n\geq 1} |1-e^{2\pi i n\tau}|^2 \equiv e^{\frac{\pi y}{6}}|\eta(\tau)|^2$, this prescription alone is not modular invariant. We achieve the same in a modular invariant way if we define
$$Z_{\mathrm{P}}(x,y) \equiv Z_0(x,y)^{-1} Z(x,y)\,, \tag{2.2.2}$$
where $Z_0(x,y) = 1/(y^{1/2}|\eta(x+iy)|^2)$ is the partition function of a free massless non-compact boson.

2. Next, we split the primary states into an above-extremal, 'non-censored' part (dimensions h and $\bar{h} > \frac{c-1}{24}$) with a near-continuous dense spectrum, and a below-extremal, 'censored' part (h or $\bar{h} \leq \frac{c-1}{24}$) which is sparse [76]. We will hereafter refer to such primaries and their spectrum as dense and censored respectively. The censored spectrum is not dense and not expected to be chaotic (see, e.g., [77]). We thus wish to focus only on the dense spectrum, but due to modular invariance the censored

[27] The fact that Virasoro descendants are not 'ergodic' was also shown explicitly in [58].

spectrum (particularly the vacuum) determines the coarse-grained behaviour of the dense spectrum. In order to focus on the pseudo-random aspects of the dense part of the spectrum we subtract off the 'modular completion' of the sparse part of the spectrum, i.e., all modular images of the below-extremal primaries [62, 76]. This defines:[28]

$$\widetilde{Z}_{\mathrm{P}}(x,y) \equiv Z_{\mathrm{P}}(x,y) - \hat{Z}_C(x,y)\,, \tag{2.2.3}$$

where the subscript C stands for censored. As we wish to discuss correlations in the dense spectrum, the correct object to consider is $\widetilde{Z}_{\mathrm{P}}(x,y)$. It computes the *deviations* from the universal dense average of the above-extremal, non-censored spectrum (e.g., due to the Cardy formula plus states dual to $SL(2,\mathbb{Z})$ black holes), with no censored primaries included. In effect, the modular completion defines our coarse-graining procedure: $\widehat{\rho}_C(E) = \rho_C(E) + \langle \rho_D(E) \rangle$, where '$D$' refers to the dense part of the full spectrum. With this prescription, subtracting the modular completion of the censored spectrum amounts to eliminating the latter while also removing the average density of states from the heavy spectrum.[29][30]

The definition results in the fluctuating part of the dense primary counting partition function, and is the object that can display quantum chaos. Finally, we write this object in terms of a decomposition into sectors with definite

[28]In [62] a similar object was defined using related but somewhat different rationale: if one averages (in some appropriate sense) over an ensemble of CFTs with fixed light spectrum, the subtracted part does not vary over the ensemble and therefore does not contribute to any correlations in the spectrum with respect to that ensemble average. Note that [62] subtracts only light states with $h + \bar{h} \leq \frac{c-1}{12}$ and their modular images, as such states render the partition function non-normalizable. As we are interested in the chaotic part of the spectrum we subtract a larger part, i.e., the censored, sparse spectrum and its modular completion; spectral determinacy applies in both cases. We thank Eric Perlmutter for making this distinction clear to us.

[29]A similar perspective is established in [78], motivated by the diagonal approximation of semi-classical periodic orbits.

[30]Because there does not exist a unique definition of modular completion, different definitions can in some sense be seen as different definitions of coarse-graining the spectrum. We focus on the kind introduced in [76], where the modular completion of each censored state results in a continuous density of states in the dense part of the spectrum. For example, the modular completion of the vacuum gives a continuous density of states for the dense spectrum that includes the well-known Cardy formula for the leading average density of states at high energies. Other censored states give additional contributions that are subleading at high energy and large central charge. Note that this is in the spirit originally suggested in [30] that the effective disorder average in gravity is related to the conventional one underlying quantum statistical mechanics.

spin:

$$\widetilde{Z}_{\mathrm{P}}(x,y) = \sum_{m\in\mathbb{Z}} e^{2\pi i m x}\, \widetilde{Z}^m_{\mathrm{P}}(y)\,. \tag{2.2.4}$$

This is not quite an ordinary partition function: the density of states it describes corresponds to *fluctuations* around the average density of states. Explicitly, the density of states

$$\widetilde{\rho}_{\mathrm{P}}(E) \equiv \rho_{\mathrm{P}}(E) - \widehat{\rho}_C(E) = \rho_D(E) - \langle \rho_D(E)\rangle \tag{2.2.5}$$

is the fluctuating density of states corresponding to the fluctuating partition function,

$$\widetilde{Z}^m_{\mathrm{P}}(y) = \frac{\sqrt{y}}{e^{\frac{\pi}{6}y}} \int_{E_m}^{\infty} dE\, \widetilde{\rho}^m_{\mathrm{P}}(E) e^{-yE}\,, \tag{2.2.6}$$

where we include the normalization factors from the non-compact boson. Thus, (2.2.4) is the modular-invariant object that can display quantum chaos. It is ‘fluctuating’ in the sense that $\widetilde{\rho}_{\mathrm{P}}(E)$ has a vanishing microcanonical average (in particular it has both positive and negative contributions).

Spectral decomposition: It is very useful to expand the fluctuating partition functions in a complete basis of normalizable modular invariant functions on the fundamental domain $\mathcal{F}$ [62] (see also [45, 78–80]). Such eigenfunctions consist of a continuous spectrum of Eisenstein series $E_s(y)$ with $s \in \frac{1}{2} + i\mathbb{R}$, and a discrete spectrum of Maass cusp forms $\nu_{n,\pm}(y)$:

$$\Delta_{\mathcal{F}} E_{\frac{1}{2}+i\alpha}(\tau) = \left(\frac{1}{4} + \alpha^2\right) E_{\frac{1}{2}+i\alpha}(\tau)\,, \quad \Delta_{\mathcal{F}} \nu_{n,\pm}(\tau) = \left(\frac{1}{4} + \left(R_n^{\pm}\right)^2\right) \nu_n(\tau)\,. \tag{2.2.7}$$

in addition to a constant function, $\Delta_{\mathcal{F}}\nu_0(\tau) = 0$. Note that there are both even $(+)$ and odd $(-)$ cusp forms (referring to their behaviour under $x \to -x$), so there are two sets of eigenvalues $\{R_n^{\pm}\}$. The cusp forms are only known numerically and their eigenvalues are erratically distributed; they are the focus of chapter 3.

After expanding the fluctuating part of the partition function in this modular invariant basis, the *expansion coefficients* are then unconstrained by modular invariance and their statistical properties are a good diagnostic of chaos. To write this, we refine the decomposition (2.2.4) slightly:

$$\begin{aligned} \widetilde{Z}_{\mathrm{P}}(x,y) = \widetilde{Z}^0_{\mathrm{P}}(y) + 2\sum_{m>0} \Big\{ &\cos(2\pi m x)\left[\widetilde{Z}^m_{\mathrm{P,disc.},+}(y) + \widetilde{Z}^m_{\mathrm{P,cont.}}(y)\right] \\ &+ \sin(2\pi m x) \widetilde{Z}^m_{\mathrm{P,disc.}-}(y)\Big\} \end{aligned} \tag{2.2.8}$$

where

$$
\begin{aligned}
\text{spin 0, continuous:} \quad & \widetilde{Z}^{0}_{\rm P}(y) = \mathrm{vol}(\mathcal{F})^{-\frac{1}{2}}\, z_0 + 2\sqrt{y}\int_{\mathbb{R}} \frac{d\alpha}{4\pi}\, z_{\frac{1}{2}+i\alpha}\, y^{i\alpha}\,,^{31} \\
\text{spin} > 0\text{, discrete:} \quad & \widetilde{Z}^{m>0}_{\rm P,disc.,\pm}(y) = \sum_{n\geq 0} z_{n,\pm}\, \nu^{m}_{n,\pm}(y)\,, \\
\text{spin} > 0\text{, continuous:} \quad & \widetilde{Z}^{m>0}_{\rm P,cont.}(y) = \int_{\mathbb{R}} \frac{d\alpha}{4\pi}\, z_{\frac{1}{2}+i\alpha}\, E^{m}_{\frac{1}{2}+i\alpha}(y)\,,
\end{aligned}
\tag{2.2.9}
$$

with $\mathrm{vol}(\mathcal{F}) = \frac{\pi}{3}$. Using the explicit basis functions for $m > 0$,

$$
\begin{aligned}
E^{m}_{\frac{1}{2}+i\alpha}(y) &= \frac{4\sigma_{2i\alpha}(m)}{m^{i\alpha}\Lambda(-i\alpha)}\,\sqrt{y}K_{i\alpha}(2\pi m y)\,, \\
\nu^{m}_{n,\pm}(y) &= a^{(n,\pm)}_{m}\,\sqrt{y}K_{iR^{\pm}_{n}}(2\pi m y)\,,
\end{aligned}
\tag{2.2.10}
$$

where $\Lambda(s) \equiv \Lambda(\frac{1}{2}-s) \equiv \pi^{-s}\Gamma(s)\zeta(2s)$. The cusp form Fourier coefficients are also erratically distributed.

We also obtain a decomposition into bases of Bessel functions by defining the spin-dependent overlaps

$$
\begin{aligned}
z^{m}(\alpha) &\equiv \frac{4\sigma_{2i\alpha}(m)}{m^{i\alpha}\Lambda(-i\alpha)}\, z_{\frac{1}{2}+i\alpha}\,, \\
z^{m}_{n,\pm} &\equiv a^{(n,\pm)}_{m}\, z_{n,\pm}\,, \\
\widetilde{Z}^{m>0}_{\rm P,cont.}(y) &= \int_{\mathbb{R}} \frac{d\alpha}{4\pi}\, z^{m}(\alpha) K_{i\alpha}(2\pi m y)\,, \\
\widetilde{Z}^{m>0}_{\rm P,disc.,\pm}(y) &= \sum_{n\geq 0} z^{m}_{n,\pm}\, K_{iR^{\pm}_{n}}(2\pi m y)\,.
\end{aligned}
\tag{2.2.11}
$$

This decomposition leads to a change of perspective: the density of states in any given spin sector (or the partition function) is an object which may exhibit familiar signatures of chaos such as eigenvalue repulsion, but it is the coefficients $z_{\frac{1}{2}+i\alpha}$ and z_n which encode the spectrum in a modular invariant way. These coefficients for different values of α and n are unrelated by symmetries and hence most natural to quantify chaos. The interplay of these objects is the main tool we use below.

[31] Here we imposed $\Lambda(i\alpha) z_{\frac{1}{2}+i\alpha} = \Lambda(-i\alpha) z_{\frac{1}{2}-i\alpha}$, which is a symmetry of the Eisenstein series.

The overlap coefficients in the decomposition (2.2.9) are given by:

$$\begin{aligned} z_{\frac{1}{2}+i\alpha} &\equiv \left(\widetilde{Z}_{\mathrm{P}},\, E_{\frac{1}{2}+i\alpha}\right) = \int_0^\infty dy'\,(y')^{-\frac{3}{2}-i\alpha}\,\widetilde{Z}_{\mathrm{P}}^{m=0}(y')\,, \\ z_n &= \frac{(\widetilde{Z}_{\mathrm{P}},\nu_n)}{(\nu_n,\nu_n)}\,. \end{aligned} \tag{2.2.12}$$

where the inner product used in this expression is defined in appendix A.1. We have used the 'unfolding trick' to write the Eisenstein series overlap in terms of the spin 0 component of the partition function. This is one aspect of spectral determinacy: the spin 0 spectrum is sufficient to determine all continuously labelled coefficients $z_{\frac{1}{2}+i\alpha}$.

2.2.2 Explicit spectral determinacy for nonzero spins

The modular invariant decomposition of the partition function into (continuous and discrete) eigenfunctions of the Laplacian implies relations between different spin partition functions, as they all can be written in terms of a joint set of coefficients $z_{\frac{1}{2}+i\alpha}$ and z_n. These relations can be presented in different ways; here we shall now introduce a representation in terms of a variable ξ, which we will see plays a role similar to energy. This will be particularly useful to make the statement of spectral determinacy more explicit, as is shown presently, as well as discuss the relation between spectral statistics in different spin sector in the next section.

In order to motivate the discussion below, recall that we are interested in the near-extremal and long time limit, in other words the behaviour near the cusp, $y \to \infty$. In that limit the spin $m > 0$ partition function receives equal contribution from each of the basis functions, as their behaviour in that limit is identical, i.e., $\sqrt{y}K_{i\alpha}(2\pi m y) \sim \frac{1}{2\sqrt{m}}\, e^{-2\pi m y}$ for large y. In other words the contribution is expected to be localized in some conjugate variable, which we now construct.

Let us consider the following representation of the Bessel functions (for $m > 0$):

$$K_{i\alpha}(2\pi m y) = \frac{1}{2}\int_{-\infty}^{\infty} d\xi\; e^{-2\pi m y \cosh\xi}\, \cos(\alpha\xi) \tag{2.2.13}$$

and the corresponding representation of the spin $m > 0$ components of the partition function:

$$\begin{aligned}\widetilde{Z}^m_{\mathrm{P,cont.}}(y) &= \int_{-\infty}^{\infty} \frac{d\alpha}{4\pi}\, z_{\frac{1}{2}+i\alpha}\, \frac{4\sigma_{2i\alpha}(m)}{m^{i\alpha}\Lambda(-i\alpha)}\, \sqrt{y} K_{i\alpha}(2\pi m y) \\ &= \frac{\sqrt{y}}{2\pi} \int_{-\infty}^{\infty} d\xi\, \mathcal{Z}^m_{\mathrm{P,cont.}}(\xi)\, e^{-2\pi m y \cosh \xi}\end{aligned} \tag{2.2.14}$$

where the information about the coefficients $z_{\frac{1}{2}+i\alpha}$ is now encoded in

$$\mathcal{Z}^m_{\mathrm{P,cont.}}(\xi) \equiv \int_{-\infty}^{\infty} d\alpha\, \cos(\alpha\xi)\, \frac{\sigma_{2i\alpha}(m)}{m^{i\alpha}\Lambda(-i\alpha)}\, z_{\frac{1}{2}+i\alpha}\,, \tag{2.2.15}$$

which is even in ξ. Similar equations can be written for the Maass cusp forms. To aid readability, we give these in appendix A.2 and focus here on the Eisenstein series. Inverting (2.2.15), we find

$$\frac{\sigma_{2i\alpha}(m)}{m^{i\alpha}\Lambda(-i\alpha)}\, z_{\frac{1}{2}+i\alpha} = \frac{1}{2\pi} \int_{-\infty}^{\infty} d\xi\, \cos(\alpha\xi)\, \mathcal{Z}^m_{\mathrm{P,cont.}}(\xi)\,. \tag{2.2.16}$$

To summarize, we can present the (continuous) part of the spectrum in terms of three equivalent quantities: (i) the partition function $\widetilde{Z}^m_{\mathrm{P,cont.}}(y)$, ($ii$) the transformed partition function $\mathcal{Z}^m_{\mathrm{P,cont.}}(\xi)$, and ($iii$) the coefficients $z_{\frac{1}{2}+i\alpha}$.

Spectral determinacy ($m > 0$). Using the above representation, we can express the spin m partition function (in ξ-space) as an integral transform of the spin m' partition function:

$$\boxed{\mathcal{Z}^m_{\mathrm{P,cont.}}(\xi) = \int_{-\infty}^{\infty} d\xi'\, \mathcal{K}^{m,m'}_{\mathrm{cont.}}(\xi,\xi')\, \mathcal{Z}^{m'}_{\mathrm{P,cont.}}(\xi')} \tag{2.2.17}$$

with the following universal kernels:

$$\mathcal{K}^{m,m'}_{\mathrm{cont.}}(\xi,\xi') = \frac{1}{2\pi} \int_{-\infty}^{\infty} d\alpha\, \cos(\alpha\xi) \cos\big(\alpha\xi'\big)\, \frac{\sigma_{2i\alpha}(m) m'^{\,i\alpha}}{\sigma_{2i\alpha}(m') m^{i\alpha}}\,. \tag{2.2.18}$$

An analogous relation should exist for the discrete part of the spectrum, see (A.2.4). Eq. (2.2.17) is the statement of spectral determinacy: $\mathcal{Z}^{m'}_{\mathrm{P,cont.}}(\xi)$ for some $m' > 0$ determines $\mathcal{Z}^m_{\mathrm{P,cont.}}(\xi)$ for all other spins $m > 0$. The transformation is also one-to-one and onto, as we can compose the kernels according to $\mathcal{K}^{m,m'} \circ \mathcal{K}^{m',m''} = \mathcal{K}^{m,m''}$. Thus, any limited information in one spin sector (for example, knowing only the spectrum in spin m for

$\xi \in [-\xi_0, \xi_0]$) is equivalent to limited information in any other spin sector in a way specified by the above.

In summary, we have found that knowledge of the partition function in a single (non-zero) spin sector, and the decomposition of that partition function into continuous and discrete part, suffices to recover the partition function in any other spin sector.

2.3 Random matrix universality across spin sectors

In this section, we study the statistics of the chaotic spectrum and specifically two-point correlations in the limit of nearby energy levels. Due to spectral determinacy the following is obvious: *if* random matrix universality is exhibited by some part of the spin m spectrum, we can infer this fact from *full* knowledge of the spectrum at spins 0 and a single $m' > 0$ alone. Naively, this seems to be in tension with the intuition that different spin sectors should independently exhibit quantum chaos. The goal of this section is to show that there is no inconsistency, thanks to the fact that random matrix universality *a priori* concerns the near-extremal part of the spectrum, which is not subject to spectral determinacy in isolation.

In the following discussion we focus on the part of the spectrum described by the Eisenstein series, which is more amenable to analytical arguments. The discrete cusp forms can *a priori* also be important for the physics we investigate, i.e., the statistical universalities we will discuss could be encoded fully or partially in the spectrum of cusp forms.[32] We return to this point in the discussion section, and in chapter 3 we will show that our results in the sector of Eisenstein series have an analog for the Maass cusp forms.

2.3.1 Random matrix universality at fixed spin

We begin by stating our assumptions and how they are motivated. One expects that the fixed-spin modular invariant primary partition function of dense states, $\widetilde{Z}_{\mathrm{P}}^{m}(y)$, exhibits random matrix universality in the near-extremal limit. This universality is a statement about two-point correlations in the spectrum, so it depends on two copies of the partition function evaluated at y_1 and y_2. The near-extremal limit then consists of taking not only $y_i \to \infty$,

[32]We thank Scott Collier for helpful comments, which clarified this point for us.

but additionally holding $\frac{y_1}{y_2}$ fixed. Universal random matrix behavior in this regime corresponds to the following form of correlations:

$$\begin{aligned}\langle \widetilde{Z}_{\mathrm{P}}^{m_1}(y_1)\, \widetilde{Z}_{\mathrm{P}}^{m_2}(y_2)\rangle_{\mathrm{ramp}} =& \frac{1}{2\pi}\, \frac{y_1 y_2}{y_1+y_2}\, \delta_{m_1 m_2}\, e^{-2\pi(m_1 y_1 + m_2 y_2)} + \dots \\ & \left(y_i \gg 1,\ \frac{y_1}{y_2} = \text{fixed}\right) .\end{aligned} \tag{2.3.1}$$

Note that all two-point functions in this chapter refer to connected correlators. We will suppress a corresponding subscript throughout. The subscript 'ramp' refers to the fact that the spectral form factor, defined by the analytic continuation $y_1 = \beta + iT$, $y_2 = \beta - iT$, exhibits a specific T-dependence for large times T:

$$\langle \widetilde{Z}_{\mathrm{P}}^{m_1}(\beta+iT)\, \widetilde{Z}_{\mathrm{P}}^{m_2}(\beta-iT)\rangle_{\mathrm{ramp}} \sim \frac{T^2}{4\pi\beta}\, \delta_{m_1 m_2}\, e^{-4\pi m_1 \beta} + \dots \quad (T \gg \beta \gg 1) \ . \tag{2.3.2}$$

Note that the partition function used for harmonic analysis, defined in (2.2.2), involves multiplication by the free boson partition function $Z_0(x, y)$, which not only removes Virasoro descendent states, but also changes the growth at large y by a factor $\sqrt{y}$ for each partition function and shifts the ground state energy by $\frac{\pi}{6}$. In order to recover the familiar form of the spectral form factor we remove these spurious factors when studying the large y limit, and consider instead

$$\begin{aligned}\frac{e^{\frac{\pi}{6}(y_1+y_2)}}{\sqrt{y_1 y_2}} \langle \widetilde{Z}_{\mathrm{P}}^{m_1}(y_1)\, \widetilde{Z}_{\mathrm{P}}^{m_2}(y_2)\rangle_{\mathrm{ramp}} =& \frac{1}{2\pi}\, \frac{\sqrt{y_1 y_2}}{y_1+y_2}\, \delta_{m_1 m_2}\, e^{-y_1 E_{m_1} - y_2 E_{m_2}} + \dots \\ & \left(y_i \gg 1,\ \frac{y_1}{y_2} = \text{fix}\right) .\end{aligned} \tag{2.3.3}$$

where $E_m = 2\pi\left(m - \frac{1}{12}\right)$ is the "ground state energy" for the spin m dense (BTZ black hole) spectrum. After analytic continuation to $y_{1,2} = \beta \pm iT$, this corresponds to removing a factor of T from the spectral form factor (2.3.2) and shifting the ground state energy, thus recovering the well-known linear 'ramp' (called like this and discussed in the context of black hole physics for the first time in [31]).

The expression (2.3.1) was argued for in holography [33–35] as it is the result of evaluating a two-boundary wormhole amplitude, which gives the leading gravitational contribution to the spectral form factor (this is also motivated by the black hole information problem [58, 81]). Random matrix behavior in holographic two-dimensional CFTs near extremality is also expected based on the fact that this limit is described by a reduction to the Schwarzian theory [82] (see also [83]): while the Schwarzian itself in the naive saddle point approximation is not sufficient to find a ramp in the spectral form factor, it is well understood that an alternative 'wormhole' saddle contribution to the two-disk amplitude does reproduce it [31, 32]. Finally, this is, of course, simply the expected behavior for the symmetry-unconstrained parts of the spectrum of generic chaotic quantum systems – an expectation that is borne out in a vast number of different systems and hence very universal.

To make the connection with traditional presentations, we change variables to energy eigenvalues (for fixed spin), where the above behavior translates into the universal form of eigenvalue repulsion for near-extremal energies:[33]

$$\begin{aligned}\langle\widetilde{\rho}_{\mathrm{P}}^{m_1}(E_1)\widetilde{\rho}_{\mathrm{P}}^{m_2}(E_2)\rangle_{\mathrm{ramp}} &= \int_{\epsilon-i\infty}^{\epsilon+i\infty} dy_1 dy_2 \left[\frac{e^{\frac{\pi}{6}(y_1+y_2)}}{\sqrt{y_1 y_2}}\langle\widetilde{Z}_{\mathrm{P}}^{m_1}(y_1)\,\widetilde{Z}_{\mathrm{P}}^{m_2}(y_2)\rangle_{\mathrm{ramp}}\right] e^{y_1E_1+y_2E_2} \\ &\approx -\frac{1}{(2\pi)^2}\frac{E_1-E_{m_1}+E_2-E_{m_2}}{\sqrt{E_1-E_{m_1}}\sqrt{E_2-E_{m_2}}\,(E_1-E_2)^2}\,\delta_{m_1m_2} \qquad (0<E_i-E_{m_i}\ll 1) \\ &\to -\frac{1}{2\pi^2\omega^2}\,\delta_{m_1m_2} \qquad (\omega\equiv E_1-E_2\ll E_i-E_{m_i})\end{aligned} \tag{2.3.4}$$

where $\widetilde{\rho}_{\mathrm{P}}^{m}(E)$ is the density of spin m dense primary states in the symmetry-unconstrained part of the spectrum described by $\widetilde{Z}_{\mathrm{P}}^{m}$. We refer to the limit taken in the second line as the *near-extremal limit*. In the last line we take additionally the small ω limit required to recover the familiar form of universal eigenvalue repulsion.

In the rest of this section, we study how information about the universal form of the spectral form factor is encoded in the spectral decomposition of the partition function.

2.3.2 Independence of the ramp in each spin sector

In this section, we present an analytic argument that demonstrates the independence of the ramp in each spin sector. By utilizing the definition of $\widetilde{Z}_{\mathrm{P,cont.}}^{m}(y)$, (2.2.15), and the kernels (2.2.18), we will show the following: *assuming that any finite collection of spin sectors exhibits a ramp near extremality is never sufficient to conclude the existence of a ramp in all other spin sectors.*

First, we study how the ramp in the usual representation (y variables) is encoded in the data amenable to spectral determinacy, $z_{\frac{1}{2}+\alpha}$ and $\mathcal{Z}_{\mathrm{P,cont.}}^{m}(\xi)$.

[33] We assume w.l.o.g. $E_1 > E_2$.

We will show that the spin 0 ramp is equivalent to a particular large α_i behaviour of $\left\langle z_{\frac{1}{2}+\alpha_1} z_{\frac{1}{2}+\alpha_2}\right\rangle$. Similarly, ramps in spin sectors $m > 0$ are equivalent to a particular small ξ_i behaviour of $\left\langle \mathcal{Z}^m_{\text{P,cont.}}(\xi_1)\mathcal{Z}^m_{\text{P,cont.}}(\xi_2)\right\rangle$.

We then use spectral determinacy to analyze how this data is interrelated. We will show that the presence of a ramp in the spin m sector cannot be deduced from a ramp in any other spin sector, and in fact no finite collection of spin sectors is sufficient to find a ramp in all other spin sectors.

Spin 0 ramp in α variables: We begin by analyzing the spin 0 spectrum. We express $\widetilde{Z}^0_{\text{P,cont.}}(y)$ in terms of $z_{\frac{1}{2}+i\alpha}$:

$$\widetilde{Z}^0_{\text{P,cont.}}(y) = \frac{\sqrt{y}}{4\pi}\int_{\mathbb{R}} d\alpha\, z_{\frac{1}{2}+i\alpha}\left[y^{i\alpha} + \frac{\Lambda(i\alpha)}{\Lambda(-i\alpha)}\, y^{-i\alpha}\right] = \frac{\sqrt{y}}{2\pi}\int_{\mathbb{R}} d\alpha\, z_{\frac{1}{2}+i\alpha}\, y^{i\alpha}\,, \tag{2.3.5}$$

where we used $\Lambda(s)E_s(\tau) = \Lambda(1-s)E_{1-s}(\tau)$. The spin 0 partition function is thus a Mellin transform of $z_{\frac{1}{2}+i\alpha}$. We now assume the ramp in the spin 0 sector:

$$\left\langle \widetilde{Z}^0_{\text{P,cont.}}(y_1)\widetilde{Z}^0_{\text{P,cont.}}(y_2)\right\rangle_{\text{ramp}} = \frac{1}{2\pi}\,\frac{y_1 y_2}{y_1+y_2} + \ldots \qquad \left(y_i \gg 1,\ \frac{y_1}{y_2} = \text{fix}\right). \tag{2.3.6}$$

We can use this spin 0 expression to compute its contribution to the overlap with the Eisenstein series using the unfolding trick (2.2.12):

$$\begin{aligned}\left\langle z_{\frac{1}{2}+i\alpha_1}\, z_{\frac{1}{2}+i\alpha_2}\right\rangle &= \int_0^\infty dy_1' dy_2'\, (y_1')^{-\frac{3}{2}-i\alpha_1}(y_2')^{-\frac{3}{2}-i\alpha_2}\left\langle \widetilde{Z}^0_{\text{P,cont.}}(y_1')\widetilde{Z}^0_{\text{P,cont.}}(y_2')\right\rangle \\ &\sim \frac{\pi}{\cosh(\pi\alpha_1)}\,\delta(\alpha_1+\alpha_2) \qquad (|\alpha_i| \to \infty)\,,\end{aligned} \tag{2.3.7}$$

where we used the ansatz (2.3.6). The result (2.3.7) is obtained by performing an exact Mellin transform of (2.3.6), disregarding any subleading corrections. The fact that this is really only an asymptotic condition for large $|\alpha_i|$ has two aspects to it:[34] transforming (2.3.7) back to y_i-variables, we evaluate the constraint $\delta(\alpha_1+\alpha_2)$, obtaining a single integral:

$$\left\langle \widetilde{Z}^0_{\text{P,cont.}}(y_1)\widetilde{Z}^0_{\text{P,cont.}}(y_2)\right\rangle_{\text{ramp}} \approx \frac{\sqrt{y_1y_2}}{4\pi}\int_{\mathbb{R}} d\alpha\, e^{i\alpha\log(y_1/y_2)}\,\frac{1}{\cosh(\pi\alpha)}\,. \tag{2.3.8}$$

[34]We thank E. Perlmutter for pointing out subtleties with the analytic continuation. See also [78] for a detailed discussion.

While this can be evaluated explicitly (giving (2.3.6)), let us understand the dominant contribution to the integral. In the Euclidean limit $y_i \to \infty$ with $\frac{y_1}{y_2} = \text{fix}$, the integral is dominated by small α and a saddle point at $\alpha = 0$ reproduces (2.3.7) up to subleading corrections. However, the Lorentzian spectral form factor implements the analytic continuation $y_{1,2} \to \beta \pm iT$ with $T \gg \beta \gg 1$. In this limit, we find $\log(y_1/y_2) \to \pm\pi i$. The integral then receives contributions from $\alpha \to \mp\infty$ and the large $|\alpha|$ asymptotics of (2.3.7) is the crucial ingredient needed to reproduce the linear ramp.

Spin $m > 0$ ramp in ξ variables: We now analyze the spin m ramp. Using (2.2.14), we have

$$\left\langle \widetilde{Z}^m_{\text{P,cont.}}(y_1)\widetilde{Z}^m_{\text{P,cont.}}(y_2)\right\rangle = \frac{\sqrt{y_1 y_2}}{4\pi^2}\int d\xi_1 d\xi_2\, e^{-2\pi m(y_1\cosh\xi_1 + y_2\cosh\xi_2)} \times\left\langle \mathcal{Z}^m_{\text{P,cont.}}(\xi_1)\mathcal{Z}^m_{\text{P,cont.}}(\xi_2)\right\rangle \tag{2.3.9}$$

Assuming the spin m ramp and taking $y_i \to \infty$, $\frac{y_1}{y_2} = \text{fixed}$ thus corresponds to taking the saddle-point $\xi_{1,2} \to 0$ ($\xi_1 \approx \xi_2$). Thus, the ramp in the usual y_i variables corresponds to a specific kind of correlations at small ξ_i, namely:

$$\left\langle \mathcal{Z}^m_{\text{P,cont.}}(\xi_1)\mathcal{Z}^m_{\text{P,cont.}}(\xi_2)\right\rangle \approx -\frac{\xi_1^2+\xi_2^2}{(\xi_1^2-\xi_2^2)^2} + \dots \qquad (\xi_i \to 0)\,, \tag{2.3.10}$$

which holds for any spin m. This is easily verified by plugging into (2.3.9) and evaluating by saddle point for large y_i. This looks similar to eigenvalue repulsion in traditional energy variables, particularly when we take $|\xi_1 - \xi_2| \ll \xi_i$, in which case (2.3.10) becomes $-\frac{1}{2(\xi_1-\xi_2)^2}$; this is actually expected, as the spectral form factor is related to correlations in the density of states as

$$\left\langle \widetilde{Z}^m_{\text{P}}(y_1)\widetilde{Z}^m_{\text{P}}(y_2)\right\rangle = \frac{\sqrt{y_1 y_2}}{e^{\frac{\pi}{6}(y_1+y_2)}}\int_{E_m}^{\infty} dE_1 dE_2\,\langle\widetilde{\rho}^m_{\text{P}}(E_1)\widetilde{\rho}^m_{\text{P}}(E_2)\rangle\, e^{-(y_1E_1+y_2E_2)}\,, \tag{2.3.11}$$

where $\widetilde{\rho}^m_{\text{P}}(E)$ is the density of spin m primary states counted by $\widetilde{Z}^m_{\text{P}}$.[35]

[35] Thus, when neglecting the Maass cusp forms, the ξ variables are related to energy via a simple (but spin-dependent) change of variables:

$$\mathcal{Z}^m_{\text{P}}(\xi) = 2\pi^2 m|\sinh\xi|\,\widetilde{\rho}^m_{\text{P}}\left(2\pi m\cosh\xi - \frac{\pi}{6}\right)\,. \tag{2.3.12}$$

Taking the appropriate limits, traditional eigenvalue repulsion in energy variables takes the same form in ξ variables.

To summarize, the universal ramp, which describes the regime of small energy differences, equivalently describes the asymptotics of correlations in $z_{\frac{1}{2}+i\alpha}$ and the small ξ statistics of $\mathcal{Z}^m_{\text{P,cont.}}(\xi)$.

Independence of the ramps: We now use (2.2.15) and (2.2.18) to see how these correlations are related across different spin sectors. We first focus on the imprint of the spin 0 ramp on spin m statistics, showing that this imprint is on an irrelevant regime for the spin m ramp. Then we focus on the imprint of spin m data onto the spin 1 statistics, showing that each ramp relies on different regimes of ξ_i in the spin 1 correlations.

First, for spin 0, we numerically analyze the imprint of the spin 0 ramp on the spin $m > 0$ spin sectors in section 2.3.3, and find that it gives a subleading correction. We conclude that the spin 0 ramp is independent of the other spin sectors.

We now look at how the spin $m > 0$ ramps are related to each other by focusing on how they appear in the spin 1 correlations. For transformations between spin m and spin 1, the kernels (2.2.17) transforming between spin sectors take a simple form:

$$\mathcal{K}^{m,1}_{\text{cont.}}(\xi,\xi') = \frac{1}{4}\sum_{\pm}\sum_{d|m}\delta\left(\xi \pm \xi' \pm \log\frac{d^2}{m}\right), \tag{2.3.13}$$

This yields the spin m correlations in terms of spin 1 correlations:

$$\boxed{\left\langle \mathcal{Z}^m_{\text{P,cont.}}(\xi_1)\mathcal{Z}^m_{\text{P,cont.}}(\xi_2)\right\rangle = \frac{1}{4}\sum_{\pm}\sum_{d_1,d_2|m}\left\langle \mathcal{Z}^1_{\text{P,cont.}}\left[\xi_1 \pm \log\frac{d_1^2}{m}\right]\mathcal{Z}^1_{\text{P,cont.}}\left[\xi_2 \pm \log\frac{d_2^2}{m}\right]\right\rangle} \tag{2.3.14}$$

This is an exact statement. It implies how a ramp of the l.h.s. would be encoded in the spin 1 statistics: it corresponds to a particular behavior for small ξ_i, which is equivalent to a sum of spin 1 correlations around $\xi = \pm\log\left(\frac{d^2}{m}\right)$ for all $d|m$.

This immediately proves what we set out to show: for example, the existence of a spin 1 ramp is insufficient to conclude the existence of the ramp for any other spin. For any $m > 1$, there is some divisor such that $\log\frac{d^2}{m}$ is outside the small ξ regime that the spin 1 ramp provides information for. In general, the existence of a spin m' ramp cannot be used to find the ramp for any other spin, as any ramp only gives a particular linear combination of spin 1 correlations.

Further, any finite collection of spins, with spin m being the largest, can only give information on correlations of $\mathcal{Z}^1_{\text{P,cont.}}[\xi]$ for $|\xi| < \log m$. This is insufficient to find the ramp for any spin $m' > m$, which requires knowledge of correlations for $\log m < |\xi_{1,2}| < \log m'$.[36] Therefore, assuming universal random matrix statistics in any finite collection of spin sectors is insufficient to conclude the same for all other spins just based on symmetries.

2.3.3 Signatures of the spin m ramp in other spin sectors (numerically)

Armed with the abstract argument of the previous subsection, we now put this on a firmer footing by numerically analyzing the imprint of the spin 0 and spin 1 ramps on the other spin sectors. This analysis will involve extrapolating the functional form of the ramp outside of the regime where it is strictly valid (large y, or small ξ). It should thus be taken with a grain of salt; however, our results will be consistent with the abstract argument given above, which we take as evidence that the analysis is justified *a posteriori*.

Signatures of a spin $m = 0$ ramp

We begin with the imprints of universal correlations in the near-extremal spin 0 spectrum onto other spin sectors and ask the following question: can we infer a ramp in the near-extremal spin m spectrum, by just assuming the existence of a ramp in the near-extremal spin 0 spectrum (subject to the caveat mentioned above)? We will give evidence that the answer is 'no'.

We begin with the 'ramp' in the spin 0 sector, which was given in (2.3.6). Such a spin 0 ramp determines the correlations of the overlap coefficients with Eisenstein series for large α; this was given in (2.3.7), which we reproduce here for convenience:

$$\begin{aligned}\left\langle z_{\frac{1}{2}+i\alpha_1}\, z_{\frac{1}{2}+i\alpha_2}\right\rangle \supset_0 \int_0^\infty dy_1' dy_2'\, (y_1')^{-\frac{3}{2}-i\alpha_1}(y_2')^{-\frac{3}{2}-i\alpha_2}\left\langle \widetilde{Z}^0_{\mathrm{P,cont.}}(y_1')\widetilde{Z}^0_{\mathrm{P,cont.}}(y_2')\right\rangle \\ = \frac{\pi}{\cosh(\pi\alpha_1)}\,\delta(\alpha_1+\alpha_2) + \ldots\end{aligned} \tag{2.3.15}$$

where "$\supset_0$" means that we only consider the contribution to the l.h.s., which comes from the ramp at spin 0, (2.3.6). This, of course, only contains partial information about the true microscopic spectrum. We wish to confirm that this partial information is insufficient to deduce the existence of a universal

[36]For example, assume a ramp for every spin up to $m = 10$; this only gives us information about the spin 1 correlations for a subset of $\xi_{1,2} \in [-\log 10, \log 10]$; thus, we wouldn't have all the necessary information to find the ramp for any spin $m' > 10$.

ramp at spin m. To this end, we use the result to compute the Eisenstein series contribution to the spectral form factor in the spin (m_1, m_2) sector:

$$\left\langle \widetilde{Z}^{m_1}_{\text{P,cont.}}(y_1)\widetilde{Z}^{m_2}_{\text{P,cont.}}(y_2)\right\rangle = \frac{1}{(4\pi)^2}\int d\alpha_1 d\alpha_2 \left\langle z_{\frac{1}{2}+i\alpha_1}\, z_{\frac{1}{2}+i\alpha_2}\right\rangle \\ \times E^{m_1}_{\frac{1}{2}+i\alpha_1}(y_1)\, E^{m_2}_{\frac{1}{2}+i\alpha_2}(y_2) \tag{2.3.16}$$

We analyze separately the cases where both spins are non-zero, and where one of them is zero.

(a) Both spins $m_1, m_2 \geq 1$: When neither spin in (2.3.16) is zero, we have

$$\begin{aligned}&\left\langle \widetilde{Z}^{m_1}_{\text{P,cont.}}(y_1)\widetilde{Z}^{m_2}_{\text{P,cont.}}(y_2)\right\rangle \\ &\quad\supset_0 \frac{\sqrt{y_1y_2}}{\pi}\int d\alpha\, \frac{\sigma_{2i\alpha}(m_1)\sigma_{-2i\alpha}(m_2)}{m_1^{i\alpha}m_2^{-i\alpha}\Lambda(i\alpha)\Lambda(-i\alpha)}\frac{K_{i\alpha}(2\pi m_1y_1)K_{-i\alpha}(2\pi m_2y_2)}{\cosh(\pi\alpha)} \\ &\quad= \frac{\sqrt{y_1y_2}}{\pi^2}\sum_{\substack{d_1|m_1\\ d_2|m_2}}\int d\alpha\, \frac{\alpha\tanh(\pi\alpha)}{|\zeta(2i\alpha)|^2}\left(\frac{m_2d_1^2}{m_1d_2^2}\right)^{i\alpha} K_{i\alpha}(2\pi m_1y_1)K_{-i\alpha}(2\pi m_2y_2)\end{aligned} \tag{2.3.17}$$

The integrand has poles at the following locations:

$$\text{poles:} \qquad \alpha = \pm\frac{i}{2}\,\eta_n \equiv \pm\frac{i}{4} \mp \frac{1}{2}\,\text{Im}(\eta_n)\,, \qquad \alpha = \frac{(2k-1)i}{2}\;,\ k\in\mathbb{Z} \tag{2.3.18}$$

where $\eta_n = \frac{1}{2}\pm i\{14.135\cdots, 21.022\cdots, 25.011\cdots, \ldots\}$ are the non-trivial zeros of the ζ-function. The second set of zeros is due to the factor $1/\cosh(\pi\alpha)$. The integrand falls off exponentially in all directions, so we can evaluate the integral by closing the contour either at $+i\infty$ or $-i\infty$. By Cauchy's theorem, we get

$$\left\langle \widetilde{Z}^{m}_{\text{P,cont.}}(y_1)\widetilde{Z}^{m}_{\text{P,cont.}}(y_2)\right\rangle \supset_0 2\pi i\Bigg[\sum_{\substack{\eta_n\\ \text{Im}(\eta_n)>0}}\text{Res}_{\alpha=\frac{i}{2}\eta_n}(\cdots) \\ + \sum_{k\geq 1}\text{Res}_{\alpha=\frac{(2k-1)i}{2}}(\cdots)\Bigg] \tag{2.3.19}$$

where $(\cdots)$ is the integrand in (2.3.17), including all the pre-factors. One can easily see that the values of these residues decay quickly as $|\eta_n|$ (for the first sum) or k (for the second sum) increases. It is therefore straightforward to evaluate these sums numerically by including sufficiently many terms.[37]

We find (numerically) for the contribution to the spin (m_1, m_2) spectral form factor due to the existence of a ramp at spin 0: for $y_i \gg 1$,

$$\boxed{\left\langle \widetilde{Z}^{m_1}_{\text{P,cont.}}(y_1)\widetilde{Z}^{m_2}_{\text{P,cont.}}(y_2)\right\rangle \supset_0 \lambda_{m_1}\,\delta_{m_1 m_2}\, e^{-2\pi(m_1 y_1 + m_2 y_2)}\sqrt{\frac{y_1 y_2}{y_1+y_2}} + \dots} \tag{2.3.20}$$

where the first few spin-dependent prefactors are

$$\lambda_1 = 0.761..\,, \quad \lambda_2 = 0.644..\,, \quad \lambda_3 = 0.613..\,, \quad \lambda_4 = 0.532..\,, \quad \lambda_5 = 0.548..\,, \tag{2.3.21}$$

Note that these proportionality constants are non-monotonic in spin due to their complicated dependence on number-theoretic properties of the spin. We show some of the numerical analysis leading to this conclusion in appendix A.3. Note that, given the simple universal form of (2.3.20), it is tempting to speculate that there might be an analytical argument to prove it.

Most importantly, (2.3.20) is *not* the form expected for a ramp (compare the non-exponential piece to (2.3.6)). It should instead be thought of as a subleading (in large y_i) correction to the spin m ramp. This shows that the imprint of the ramp in the spin 0 sector onto a higher spin sector is not a ramp, but merely a subleading correction to it. *Any potential ramp in the higher spin sector is therefore not due to a ramp at spin 0 plus symmetries.* This strengthens the analytic argument of the previous section.

(b) One spin $m_1 > 0$ and one vanishing spin $m_2 = 0$. Finally, if one spin is 0, we have

$$\begin{aligned}\left\langle \widetilde{Z}^{m_1}_{\text{P,cont.}}(y_1)\widetilde{Z}^{0}_{\text{P,cont.}}(y_2)\right\rangle &\supset_0 \frac{\sqrt{y_1 y_2}}{2\pi}\int d\alpha\, \frac{\sigma_{2i\alpha}(m_1)}{m_1^{i\alpha}\Lambda(-i\alpha)}\frac{K_{i\alpha}(2\pi m_1 y_1) y_2^{-i\alpha}}{\cosh(\pi\alpha)} \\ &= \frac{\sqrt{y_1 y_2}}{2\pi}\sum_{d_1|m_1}\int d\alpha\, \frac{K_{i\alpha}(2\pi m_1 y_1) y_2^{-i\alpha}}{\Gamma(-i\alpha)\zeta(-2i\alpha)\cosh(\pi\alpha)}\left(\frac{d_1^2}{m_1\pi}\right)^{i\alpha}\end{aligned} \tag{2.3.22}$$

This can be analyzed in the same way as (2.3.17) by residues. Unsurprisingly, one finds very small values (compared to those expected for a ramp), similar to the other unequal spin cases shown in figures A.1 and A.2.

[37] Roughly, including $\mathcal{O}(10-100)$ terms is sufficient to get an accuracy of $\mathcal{O}(10^{-5})$.

Signatures of a spin $m = 1$ ramp

We have argued in section 2.3.2 that for every m, $\mathcal{Z}^{m}_{\text{cont.}}(\xi)$ contains information about $\mathcal{Z}^{1}_{\text{P,cont.}}(\xi)$ that is not contained in any $\mathcal{Z}^{m'}_{\text{P,cont.}}(\xi)$ with $m' < m$. For illustration, we shall now make this abstract argument more concrete by repeating the analysis of section 2.3.3 for higher spin (which involves different manipulations): we shall assume the existence of universal eigenvalue repulsion in the spin $m = 1$ sector and analyze its imprint on other spin (m_1, m_2) sectors via spectral determinacy arguments (i.e., symmetries).

The universal ramp ansatz in the spin m sector is given by (2.3.10) in the ξ variables. The imprint of that expression onto the spin (m_1, m_2) sector is:

$$\begin{aligned}&\big\langle \widetilde{Z}^{m_1}_{\text{P,cont.}}(y_1)\widetilde{Z}^{m_2}_{\text{P,cont.}}(y_2)\big\rangle \\ &\qquad\supset_m \frac{\sqrt{y_1y_2}}{4\pi^2}\iint d\xi_1 d\xi_2\, e^{-2\pi(m_1y_1\cosh\xi_1+m_2y_2\cosh\xi_2)} \\ &\qquad\qquad\times\iint d\xi_1' d\xi_2'\,\mathcal{K}^{m_1,m}_{\text{cont.}}(\xi_1,\xi_1')\mathcal{K}^{m_2,m}_{\text{cont.}}(\xi_2,\xi_2')\left[-\frac{\xi_1'^2+\xi_2'^2}{(\xi_1'^2-\xi_2'^2)^2}\right]\end{aligned} \tag{2.3.23}$$

where the symbol "$\supset_m$" means that we only consider the contribution to the l.h.s. originating from a ramp at spin m.[38] For simplicity consider $m = 1$, where the kernels $\mathcal{K}^{m_i,m}_{\text{cont.}}$ reduce to a sum over delta-functions:

$$\begin{aligned}&\big\langle \widetilde{Z}^{m_1}_{\text{P,cont.}}(y_1)\widetilde{Z}^{m_2}_{\text{P,cont.}}(y_2)\big\rangle \\ &\quad\supset_{m=1} -\frac{\sqrt{y_1y_2}}{16\pi^2}\sum_{\substack{d_1|m_1\\ d_2|m_2}}\sum_{\pm}\iint d\xi_1 d\xi_2\,\frac{\big(\xi_1\pm\log\big(d_1^2/m_1\big)\big)^2+\big(\xi_2\pm\log\big(d_2^2/m_2\big)\big)^2}{\Big(\big(\xi_1\pm\log(d_1^2/m_1)\big)^2-\big(\xi_2\pm\log(d_2^2/m_2)\big)^2\Big)^2} \\ &\qquad\qquad\times e^{-2\pi(m_1y_1\cosh\xi_1+m_2y_2\cosh\xi_2)}\end{aligned} \tag{2.3.24}$$

For large y_i the integrals are dominated by a saddle point at small ξ_i. This can be straightforwardly evaluated numerically, and we find (within numerical accuracy):

$$\boxed{\big\langle \widetilde{Z}^{m_1}_{\text{P,cont.}}(y_1)\widetilde{Z}^{m_2}_{\text{P,cont.}}(y_2)\big\rangle \supset_{m=1} \sigma_0(m_1)\times\delta_{m_1m_2}\,\frac{1}{2\pi}\,\frac{y_1y_2}{y_1+y_2}\,e^{-2\pi m_1(y_1+y_2)}} \tag{2.3.25}$$

[38] Again, we extrapolate the validity of the ramp (valid at small ξ), which is only justified by the consistent result we find.

where $\sigma_0(m)$ is the number of divisors of m (including 1 and m). The source of this prefactor are the terms with $d_1 = d_2$. Some of our numerical analysis is again shown in appendix A.3 (in particular figure A.3). That is, the imprint of a ramp at spin 1 onto the spin m sector is $\sigma_0(m)$ times the ramp.[39][40] For our conclusions to hold, the factor $\sigma_0(m)$ is crucial: the functional dependence on y_i is indeed that of a ramp, so the discrepancy with random matrix universality is only due to the mismatching prefactor. However, this prefactor is always at least 2, so it never matches the random matrix theory expectation (which involves not just a linear ramp, but also a very specific normalization thereof). This is sufficient to conclude that a ramp in the spin 1 Eisenstein sector does not imply random matrix universality in higher spin sectors.

2.4 Cardy-like constraints on spectral correlations

With the knowledge that the ramp in each spin sector does indeed contain independent data despite spectral determinacy, we now take this as a starting point to find more information about the spectrum. Following the derivation of the Cardy formula, we will find that the existence of eigenvalue repulsion in the near-extremal spectrum predicts the same for a part of the spectrum far from extremality.

2.4.1 Review: modular invariance of the density of states

While modular invariance is most naturally formulated as an invariance of the partition function, following, e.g., [82, 84] we can write it as an invariance of the density of states of primaries. First, we define variables $(P, \bar{P})$ that are more suitable for applying modular transformations to the density of states directly:

$$h = \frac{c-1}{24} + P^2 \,, \quad \bar{h} = \frac{c-1}{24} + \bar{P}^2 \,. \tag{2.4.1}$$

The energy and spin variables we used previously are

$$E \equiv 2\pi \left(h + \bar{h} - \frac{c}{12} \right) \equiv 2\pi \left(P^2 + \bar{P}^2 - \frac{1}{12} \right) \,, \qquad \mathfrak{m} \equiv h - \bar{h} \equiv P^2 - \bar{P}^2 \,. \tag{2.4.2}$$

[39]As in the spin 0 case the numerical agreement is excellent, so one might expect there to be an analytical way to evaluate (2.3.24).

[40]We have not analyzed the imprint of the spin $m > 0$ ramps on the spin 0 sector.

It will be convenient to allow for positive and negative spins in this section. In addition, we define $\mathfrak{m} \in \mathbb{R}$ as the continuous spin, via $\rho(E) = \sum_{m\in\mathbb{Z}} \rho^m(E) = \int d\mathfrak{m}\, \rho(E,\mathfrak{m})$. The P variables can take both imaginary and real values, corresponding to different parts of the spectrum:

$$\begin{aligned} &\text{censored states:} \qquad 0 < -iP \leq \sqrt{\frac{c-1}{24}} \qquad \Leftrightarrow \qquad 0 \leq h \leq \frac{c-1}{24} \\ &\text{dense states:} \qquad 0 < P \qquad \Leftrightarrow \qquad h > \frac{c-1}{24} \end{aligned} \tag{2.4.3}$$

and similarly for $\bar{h}$. With these variables, we can write the CFT partition function as

$$\begin{aligned} Z(\tau,\bar\tau) &= \int_{-\infty}^{\infty} \frac{dP}{2}\frac{d\bar P}{2}\, \rho_{\mathrm{P}}(P,\bar P)\chi_{\mathrm{P}}(\tau)\bar\chi_{\bar{\mathrm{P}}}(\bar\tau)\,, \\ \chi_{\mathrm{P}}(\tau) &= \frac{e^{2\pi i\tau P^2}}{\eta(\tau)}\,, \quad \bar\chi_{\bar{\mathrm{P}}}(\bar\tau) = \frac{e^{-2\pi i\bar\tau \bar P^2}}{\eta(-\bar\tau)}\,, \end{aligned} \tag{2.4.4}$$

where $\rho_{\mathrm{P}}(P,\bar P)$ is the density of states of primary operators (we allow $(P,\bar P)$ to be negative, with $\rho_{\mathrm{P}}(P,\bar P)$ being even), and the Virasoro characters account for descendant states. As before, $\rho_{\mathrm{P}}(P,\bar P)$ is a sum of delta-functions, which now includes support on imaginary values of P [82].

In these variables, invariance of Z under the modular S-transform can be recast as the invariance of the density of states under a Fourier transform:

$$\rho_{\mathrm{P}}(P,\bar P) = 2\int_{-\infty}^{\infty} dP' d\bar P'\, e^{-4\pi i(PP'+\bar P\bar P')}\rho_{\mathrm{P}}(P',\bar P')\,. \tag{2.4.5}$$

This formulation of modular invariance makes the Cardy formula and the form of the asymptotic density of states in the lightcone limit ($\bar P > 0$ fixed, $P \to \infty$) more transparent; rather than having to work with the partition function (and complicated questions of convergence [61]) we can directly compute with the density of states.

For illustration, let us recall the derivation of the Cardy formula in these variables [82]: the contribution of the vacuum state to the density of states is $\rho_{\mathrm{P}}(P,\bar P) \supset \rho_{\mathrm{P,vac}}(P)\rho_{\mathrm{P,vac}}(\bar P)$ with

$$\rho_{\mathrm{P,vac}}(P) = \left[\delta\left(P - i\sqrt{\frac{c-1}{24}}\right) - \delta\left(P - i\sqrt{\frac{c-1}{24}-1}\right)\right] \,+\, (P \leftrightarrow -P)\,, \tag{2.4.6}$$

where the subtraction accounts for the null descendants of the vacuum. The modular S-transform of this contribution according to (2.4.5) gives the leading contribution to the density of states as $P, \bar{P} \to \infty$, i.e., the Cardy formula:

$$\rho_{\mathrm{P}}(P, \bar{P}) \approx 2 \exp\left(2\pi(P+\bar{P})\sqrt{\frac{c-1}{6}}\right) \qquad (P, \bar{P} \to \infty)\,. \tag{2.4.7}$$

2.4.2 S-dual of eigenvalue repulsion

Using the same ansatz for the primary partition function as section 2.3, we assume the near-extremal density of primaries exhibits random matrix statistics. The connected two-point function of the density of states is

$$\begin{aligned}\langle \rho_{\mathrm{P}}(P_1', \bar{P}_1')\rho_{\mathrm{P}}(P_2', \bar{P}_2')\rangle = \sum_{m_1, m_2 \in \mathbb{Z}} & F^{m_1,m_2}(P_1', \bar{P}_1', P_2', \bar{P}_2') \\ & \times \delta(P_1'^2 - \bar{P}_1'^2 - m_1)\delta(P_2'^2 - \bar{P}_2'^2 - m_2).\end{aligned} \tag{2.4.8}$$

In the near-extremal limit, we obtain the ramp by applying the change of variables in (2.4.2) to the expression for universal eigenvalue repulsion in (2.3.4):[41]

$$F^{m_1,m_2}(P_1', \bar{P}_1', P_2', \bar{P}_2') \approx -\frac{1}{2\pi^2}\frac{64|P_1'\bar{P}_1'P_2'\bar{P}_2'|}{\left(P_1'^2+\bar{P}_1'^2-P_2'^2-\bar{P}_2'^2\right)^2}\delta_{m_1,m_2} \qquad \begin{pmatrix} P_i', \bar{P}_i' \text{ near-extremal} \\ \omega \ll E_i - E_{m_i}\end{pmatrix} \tag{2.4.9}$$

which is expected to hold near extremality, defined by the

$$\text{near-extremal regime:} \qquad 0 < \min\left(P_i^2, \bar{P}_i^2\right) \ll 1 \tag{2.4.10}$$

and we also take $\omega \equiv 2\pi(P_1'^2 + \bar{P}_1'^2 - (P_2'^2 + \bar{P}_2'^2)) \ll E_i - E_{m_i} = 4\pi \min\left(P_i^2, \bar{P}_i^2\right)$, where we are using the expression for the small ω limit as in (2.4.10).[42]

We now take the modular S-transform of (2.4.9), first with respect to P_1', $\bar{P}_1'$, then with respect to the second set of variables. The S-transform is a

[41]This expression involves the Jacobian $\left|\frac{\partial(E_i, \mathrm{m}_i)}{\partial(P_i', \bar{P}_i')}\right| = 16\pi|P_i'\bar{P}_i'|$.

[42]We also assume that the divergence as $\omega \to 0$ of the gravity and RMT correlations is regulated (in RMT, the sine kernel regulates the divergence; in gravity, presumably more complicated wormhole configurations regulate the divergence).

Fourier transform, which we will evaluate by saddle point. Because we want the saddle point $(P'_{1*}, \bar{P}'_{1*})$ to lie in the near-extremal regime where (2.4.9) applies, the S-dual parameters $(P_i,\, \bar{P}_i)$ should lie *outside* the near-extremal limit. We achieve this by identifying the

$$\text{large spin, far-from-extremality regime:} \qquad \begin{array}{l} P_i^2 \gg \bar{P}_i^2 \gg 1 \\ (\Leftrightarrow\ \mathfrak{m}_i \gg \tau_i \gg 1\,) \end{array} \tag{2.4.11}$$

where, here and in the following, we take w.l.o.g. $\mathfrak{m}_i > 0$, and P_i^2 parametrically larger than $\bar{P}_i^2$.[43] (In appendix A.4 we give analogous expressions valid for any choice of signs for $\mathfrak{m}_i$.) In the bracket, we have written the condition in terms of the spin and (shifted) twist $\tau_i \equiv \frac{E_i}{2\pi} - \mathfrak{m}_i = 2\bar{P}_i^2 - \frac{1}{12} \approx 2\bar{P}_i^2$, thus showing how this regime translates into energy-spin variables. This regime is one of the most natural to consider when utilizing the S-transform [85]; it appears when we allow the conformal dimensions h, $\bar{h}$, or equivalently spin and twist, to approach infinity at different rates. Note that this is a distinct regime from that considered by the lightcone bootstrap [86], where the twist is bounded by extremality, $\tau \leq -\frac{1}{12}$.

This choice allows us to evaluate the Fourier transform (S-transform) despite our limited information about the density of states. Concretely, we wish to compute

$$\begin{aligned} \langle \rho_{\mathrm{P}}(P_1, \bar{P}_1)\rho_{\mathrm{P}}(P_2, \bar{P}_2)\rangle &\approx 4 \int dP'_1 d\bar{P}'_1 dP'_2 d\bar{P}'_2\, e^{-4\pi i(P'_1P_1 + \bar{P}'_1\bar{P}_1 + P'_2P_2 + \bar{P}'_2\bar{P}_2)} \\ &\quad \times \sum_{m_i \in \mathbb{Z}} F^{m_1,m_2}(P'_1, \bar{P}'_1, P'_2, \bar{P}'_2)\, \delta(P_1'^2 - \bar{P}_1'^2 - m_1)\delta(P_2'^2 - \bar{P}_2'^2 - m_2)\,. \end{aligned} \tag{2.4.12}$$

For details on the evaluation of these integrals in the regime (2.4.11), we refer to appendix A.4. The result is of the following form:

$$\begin{aligned} &\langle \rho_{\mathrm{P}}(E_1, \mathfrak{m}_1)\rho_{\mathrm{P}}(E_2, \mathfrak{m}_2)\rangle \\ &\approx 2 \sum_{m_i > 0} F^{m_1,m_2}\left(P_1\sqrt{\frac{m_1}{\mathfrak{m}_1}}, \bar{P}_1\sqrt{\frac{m_1}{\mathfrak{m}_1}}, P_2\sqrt{\frac{m_2}{\mathfrak{m}_2}}, \bar{P}_2\sqrt{\frac{m_2}{\mathfrak{m}_2}}\right) \left(\mathfrak{m}_1\mathfrak{m}_2 m_1 m_2\right)^{-1/4} \\ &\qquad \times \cos\left(4\pi\sqrt{m_1\mathfrak{m}_1} + \frac{\pi}{4}\right)\cos\left(4\pi\sqrt{m_2\mathfrak{m}_2} + \frac{\pi}{4}\right) \qquad (P_i^2 \gg \bar{P}_i^2 \gg 1)\,. \end{aligned} \tag{2.4.13}$$

[43] I.e., $P^2 = \Lambda P_0^2$, $\bar{P}_2 = \Lambda^v \bar{P}_0^2$, with $\Lambda \to \infty$, $0 < v < 1$.

Because $\mathfrak{m}_i = P_i^2 - \bar{P}_i^2 \gg 1$, we are guaranteed that $\bar{P}_i\sqrt{\frac{m_i}{\mathfrak{m}_i}}$ is small.[44] Ensuring the small ω condition where (2.4.9) applies, requires $\frac{\bar{P}_1^2}{P_1^2} - \frac{\bar{P}_2^2}{P_2^2} \ll \frac{\bar{P}_{1,2}^2}{P_{1,2}^2}$. We can then use the expression for F^{m_1,m_2} near extremality, i.e., (2.4.9); we find that the connected two-point function for $\mathfrak{m}_i \gg \tau_i \gg 1$ and $E_1 - E_2 \ll E_i$ is

$$\begin{aligned}\langle \rho_{\rm P}(E_1,\mathfrak{m}_1)\rho_{\rm P}(E_2,\mathfrak{m}_2)\rangle \approx &- \frac{1}{2\pi^2}\,\frac{\mathfrak{m}_1\mathfrak{m}_2}{\left(\mathfrak{m}_2\left(E_1 - 2\pi\,\frac{c-1}{12}\right) - \mathfrak{m}_1\left(E_2 - 2\pi\,\frac{c-1}{12}\right)\right)^2}\\ &\times \lim_{M\to\infty} \mathcal{S}_{\mathfrak{m}_1,\mathfrak{m}_2}(M)\end{aligned} \tag{2.4.14}$$

where

$$\mathcal{S}_{\mathfrak{m}_1,\mathfrak{m}_2}(M) \equiv \frac{1}{(\mathfrak{m}_1\mathfrak{m}_2)^{1/4}} \sum_{m=1}^{M} \frac{2}{\sqrt{m}} \cos\left(4\pi\sqrt{m\mathfrak{m}_1} + \frac{\pi}{4}\right)\cos\left(4\pi\sqrt{m\mathfrak{m}_2} + \frac{\pi}{4}\right). \tag{2.4.15}$$

The limit $M \to \infty$ of the expression $\mathcal{S}_{\mathfrak{m}_1,\mathfrak{m}_2}(M)$ is in fact not well defined without further regularization: as written, the sum does not converge. However, for $m_1 \neq m_2$ it also does not diverge either, but rather oscillates within a bounded window as a function of the cutoff M. Furthermore, the mean value of the oscillation tends to zero as $\mathfrak{m}_i$ grow large.[45] We illustrate this in figure 2.2. We belive that, upon implementing a proper method of coarse-graining over spins, one could derive asymptotic upper and lower bounds for (2.4.15) by applying techniques similar to the Tauberian theorems deployed in, e.g., [87]. However, since the variance we are considering is not strictly positive, we cannot easily apply such theorems and leave this problem to a future analysis. Finally, note that several approximations have been assumed in the computation presented here. A small correction of each term in $\mathcal{S}_{\mathfrak{m}_1,\mathfrak{m}_2}(M)$ turns this non-convergent series into a convergent one.[46] Since we assumed an approximate expression for the two-point function of the density of states and the latter is in fact a distribution, it is reasonable to expect for the above expressions to be regularized by subleading effects and by integration against test functions. It would be interesting to investigate this more rigorously.

[44] This is strictly true up to an asymptotic regime of large m_i, beyond which we assume the contributions are negligible. See appendix A.4 for details.

[45] This is also true if $\mathfrak{m}_1$ is held fixed and only $\mathfrak{m}_2$ grows large.

[46] In particular, any power of m^{-1} in front of the product of cosines that is strictly greater than 1/2 would produce a convergent sum. Similarly, methods such as Euler summation straightforwardly regularize the sum and give a definite result.

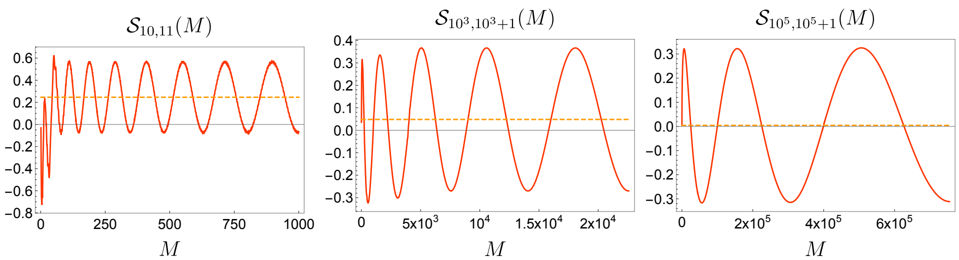

Figure 2.2: Plots of the non-convergent sum $\mathcal{S}_{\mathfrak{m}_1,\mathfrak{m}_2}(M)$ for $\mathfrak{m}_1 = \mathfrak{m}_2 - 1 \in \{10, 10^3, 10^5\}$ as a function of the cutoff M. We see that, although the limit $M \to \infty$ does not exist, the function oscillates within a bounded bandwidth. This is in stark contrast to the case $\mathfrak{m}_1 = \mathfrak{m}_2 \equiv \mathfrak{m}$, where $\mathcal{S}_{\mathfrak{m},\mathfrak{m}}(M)$ diverges. Note that for large $\mathfrak{m}_i$, the mean value around which the oscillations occur, tends to zero (dashed lines).

We can get a well defined result for (2.4.14) in the decompactification limit: by reintroducing units to spin, $m = \frac{2\pi}{L}n$ where L is the circumference of the cylinder, we replace $\sum_m \to \frac{L}{2\pi}\int_0^\infty dm$ in the limit $L \to \infty$. The integral over m can then be performed explicitly, and we find:

$$\boxed{\langle \rho_{\rm P}(E_1,\mathfrak{m}_1)\rho_{\rm P}(E_2,\mathfrak{m}_2)\rangle \approx -\frac{1}{2\pi^2}\frac{1}{(E_1-E_2)^2}\frac{L}{2\pi}\,\delta(\mathfrak{m}_1-\mathfrak{m}_2) \qquad \begin{pmatrix} |\mathfrak{m}_i| \gg \tau_i \gg 1, \\ |E_1-E_2| \ll E_i \end{pmatrix}} \tag{2.4.16}$$

This expression encodes eigenvalue repulsion in each spin sector, both the universal functional form and the correct prefactor as expected from random matrix theory. The regime of validity corresponds to the spectrum far from extremality.[47]

This shows that modular invariance extends the regime in which the statistics of primary operators follows random matrix universality; random matrix statistics for primary operators in the near-extremal spectrum implies the same statistics for primaries far from extremality.

2.5 Discussion

This chapter has two main results: first, while spectral determinacy implies very strong constraints between the spectra of primaries in different spin

[47]The absence of Dirac delta functions forcing $\mathfrak{m}_i$ to be discrete can be understood using the same reasoning as the lack of Dirac delta functions in the Cardy formula.

sectors, this does not preclude independent random matrix universality near extremality in each spin sector. Second, modular invariance can be used to argue for random matrix universality in a certain large spin regime far from extremality.

Our goal in the chapter was to identify a set of universal quantities for coarse-grained aspects of two-dimensional CFTs with large central charge. We have found that correlations between the coefficients of the modular invariant decomposition of the partition function provide such information (using a certain parametrization for the near-extremal spectrum). This opens the door to explaining these features along the lines of the Efetov sigma model [71–73]. Indeed, in the quantum mechanical case one can write a path integral for the spectral correlators of interest, and in the limit where it is universal this path integral is dominated by an ergodic mode. It would be very interesting to repeat this exercise for the quantities we have identified; we hope to return to this in the near future. Ultimately, it would be fascinating to find connections between the sigma-model describing random matrix statistics, and the sigma-models describing other properties of chaotic CFTs such as out-of-time-order correlators [88] or even hydrodynamics [89–91].

An important caveat in our analysis was the restriction to the continuous part of the $SL(2,\mathbb{Z})$ spectrum. For a ramp at spin 0 this restriction is irrelevant. We will see in chapter 3 how our analysis applies to the discrete cusp forms. Nevertheless we can already draw the following conclusion from studying just the Eisenstein series: if the universal ramp is encoded *at least partially*[48] in the correlations of Eisenstein series overlap coefficients of a particular spin sector, then spectral determinacy is in general not sufficient to conclude random matrix universality in the other spin sectors. Our conclusion would only fail to hold in cases where the ramp is encoded *solely* in the sector of Maass cusp forms, as we didn't analyze this sector here.[49] It would be interesting to study if there exist general criteria that force the ramp for $m > 0$ to be encoded in either the continuous or the discrete sectors alone.

With a view towards other future applications, we note that the formula expressing spectral determinacy (2.2.17), as a precise and explicit rephrasing of the constraints of modular invariance, may be useful in implementations of the modular bootstrap.

We used as a starting point the results from the gravitational analysis [33, 34] regarding the existence of random matrix statistics in each spin

[48]By "partially encoded" we mean that the coefficient of the ramp in the Eisenstein sector is not zero.

[49]Thus, we merely make an assumption of genericity, namely that there do not exist any constraints that prevent the ramp from being encoded in the continuous spectrum.

sector. However, one may hope to *derive* such statistics using the modular and conformal bootstraps, or show that such statistics is consistent with the universal properties of conformal field theories.[50] We have shown that such statistics is consistent with modular invariance, and thus have taken the first steps towards such a proof.

In our analysis of the modular S-transform of the spectral form factor, an extension of the saddle point analysis in section 2.4.2 outside of the decompactification limit would strengthen our claims regarding the extended regime of validity of random matrix universality. It would be interesting to develop more rigorous techniques to analyze this (e.g., along the lines of [85, 87]).

[50] One might analyze the accumulation of operators near extremality in CFTs with a twist gap, c.f., [92].

Chapter 3

Symmetries and spectral statistics in chaotic conformal field theories II: Maass Cusp Forms and Arithmetic Chaos

3.1 Introduction

In chapter 2, we began investigating the relationship between quantum chaos in two-dimensional CFTs and modular invariance. Motivated by the pure gravity wormhole amplitude found by Cotler and Jensen [33, 34] (see also [35]), we argued that random matrix statistics for the "near-extremal" part of the dense spectrum and the corresponding late time linear ramp is an independent feature of each spin sector separately. This is a non-trivial statement because the exact spectrum is fully determined by only the spectrum of spin zero primaries and those of a single non-zero spin. The focus of this analysis was on CFTs where the ramp is encoded solely in the continuous part of the basis of modular invariant functions. There exists a discrete part as well, the Maass cusp forms, that can also encode the ramp.

The cusp forms are interesting objects in their own right:

- Cusp forms arise as bound states for a particle moving in the fundamental domain of $SL(2,\mathbb{Z})$. This is a classically chaotic system, however due to its highly symmetric structure it does not obey random matrix statistics.
- Instead, their spectrum of eigenvalues $R_n^{\pm}$ is bounded from below and is Poisson distributed, i.e corresponds to independent draws from a known distribution.[51]

[51] We label the different cusp forms by an integer n and a sign '$\pm$', which refers to cusp forms of even and odd parity, respectively.

- Their Fourier coefficients $a_m^{(n,\pm)}$ for prime spin m are bounded by ± 2 and are also Poisson distributed independently drawn from known distributions. As a consequence of Hecke relations the Fourier coefficients for non-prime (composite) spins are polynomials of those with prime spins. This implies that the distributions of non-prime spin Fourier coefficients are also determined by the distributions for prime spins.

We sometimes refer to the collection of eigenvalues and Fourier coefficients as *cusp form data*. Together their statistical properties are sometimes referred to as *arithmetic chaos* [93–96].

A connection between arithmetic chaos and quantum chaos in CFTs is an intriguing possibility (first hinted at in [62]), particularly since quantum chaos in the wormhole amplitude is encoded solely in the cusp forms for all non-zero spins [78]. On the one hand, the fact that objects linked to chaos appear in the spectral decomposition of CFTs suggests that the two (very different) types of chaos may be linked in some way. On the other hand, arithmetic chaos is a property of the general modular invariant basis functions, not of the actual CFT spectrum, so it is also present in integrable CFTs. We intend to clarify the relation in this work.

Summary of results: In this chapter, we extend the techniques developed for the continuous $SL(2,\mathbb{Z})$ spectrum in chapter 2 to the cusp forms and identify the relationship between arithmetic and quantum chaos. We show that taking the near-extremal, late time limit automatically implements a statistical averaging over the cusp form data, in particular over their sporadic eigenvalues and erratic Fourier coefficients. On the one hand, this means that quantum chaos in 2d CFT depends only on statistical features of arithmetic chaos, not the detailed structure of the cusp form data. On the other hand, it is remarkable that full information about (i.e., all statistical moments of) the distributions of the cusp form data is encoded in the spectral form factor, assuming it exhibits a linear ramp in all spin sectors. We find the universal form these statistically averaged correlations in the cusp form sector must take to produce a ramp. As with the continuous sector, modular invariance does not spoil the independence of random matrix universality in each separate spin sector, since the statistical averaging proceeds differently in each spin sector; a linear ramp must be imposed as a separate assumption for each spin sector in order to fully and consistently determine the correlations in cusp form expansion coefficients.

By demanding that there be a linear ramp in every spin sector, we are able to "bootstrap" the exact cusp form correlations whose statistical

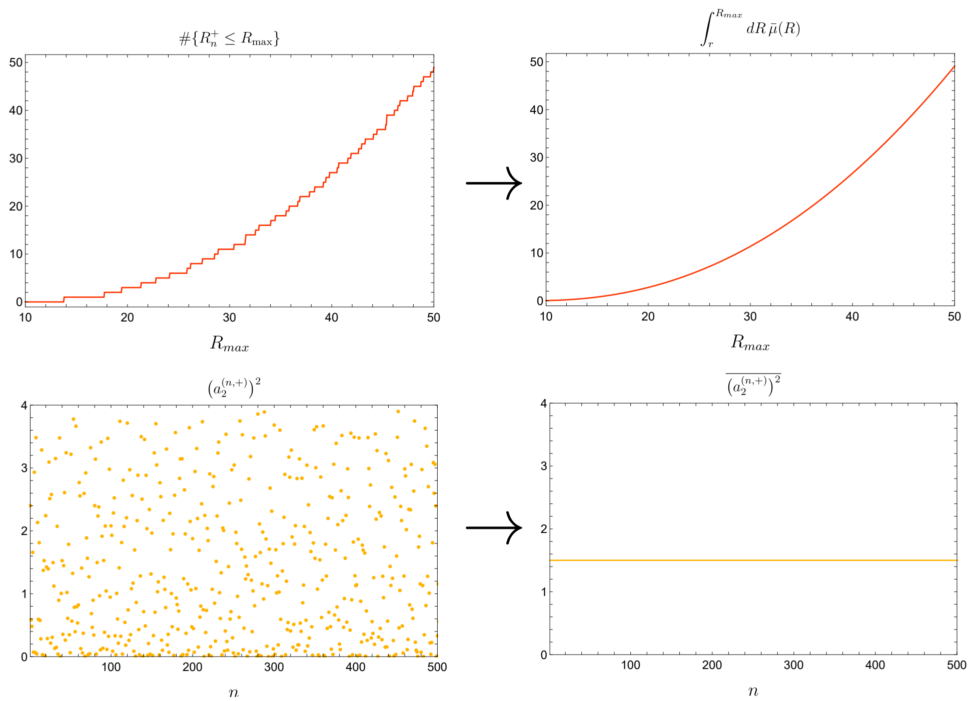

Figure 3.1: A depiction of the statistical approximation to cusp form data. The "spectral staircase" and the erratically distributed Fourier coefficients are replaced with their average values. We will justify this 'statistical' coarse-graining in the time regime that is relevant for random matrix universality. It should be distinguished from 'microcanonical' coarse-graining, which is always required to discuss correlations in the CFT spectrum.

averaging produces random matrix statistics independently in every spin sector. These correlations depend on all moments of the distributions of the Fourier coefficients for prime spin, and are related to well studied number-theoretic objects. In fact, these correlations are essentially universal and unique under some mild assumptions. The gravitational wormhole amplitude exhibits the same universality, while at the same time having the minimal subleading corrections (in the late time limit) to make it consistent with modular invariance [78]; under some related minimality assumptions our construction reproduces it exactly.

3.1.1 Outline

The chapter is organized as follows. In section 3.2 we review the setup of chapter 2, introducing the fluctuating part of the partition function and decomposing it in the complete basis of modular invariant functions. In section 3.3 we analyze how random matrix statistics appears in the cusp forms, and demonstrate its reliance on only arithmetic chaos. We derive an expression whose statistical average produces a ramp in each spin sector and show that it is unique under mild assumptions. In section 3.4 we then show that this expression exactly matches a calculation in AdS_3 gravity. In the discussion, we put forth some preliminary results on the spectral decomposition of the self-correlations in the spectrum, and how it differs from eigenvalue repulsion.

Conventions are collected in appendix A.1. We review statistical features of cusp forms in appendix B.1 and discuss some important mathematical properties in appendix B.2. Appendix B.3 concerns the imprint of linear ramps in a given spin sector onto other spin sectors.

3.2 Spectral decomposition of the ramp

We start by quickly reviewing the $SL(2,\mathbb{Z})$ spectral decomposition of the linear ramp and recollecting the work of chapter 2, in order to allow this chapter to stand on its own. In the next section we extend this analysis to the cusp forms, and in particular use statistical properties thereof (dubbed "arithmetic chaos") to simplify the analysis.

3.2.1 $SL(2,\mathbb{Z})$ spectral theory

Beginning from the full CFT partition function on a torus with modular parameter $\tau = x + iy$, $Z(x,y)$, in chapter 2 we introduced a fluctuating partition function $\widetilde{Z}_{\rm P}(x,y)$ by a series of steps intended to account for the symmetries of the problem:

- First, the partition function is divided by that of a single non-compact boson, $Z_0 = 1/(y^{1/2}|\eta(x+iy)|^2)$, to remove all Virasoro descendants in a modular invariant fashion.

- Then one realizes that the 'censored' part of the spectrum (i.e., states with h or $\bar{h} \leq \frac{c-1}{24}$, equivalently $E \leq 2\pi\left(|m| - \frac{1}{12}\right) \equiv E_m$) is not typically chaotic. Therefore, one subtracts off this part of the spectrum. In addition, one also removes the part of the dense spectrum ($h, \bar{h} > \frac{c-1}{24}$, equivalently $E > E_m$) that is determined from the censored spectrum by symmetries (such as modular S-transformations); together, these two parts are called the modular completion of the censored spectrum, $\widehat{Z}_C(x,y)$.

The resulting "fluctuating" partition function $\widetilde{Z}_{\rm P}(x,y)$ is the object that can display quantum chaos. Finally, we write this object in terms of a decomposition into sectors with definite spin:

$$\widetilde{Z}_{\rm P}(x,y) = \sum_{m\in\mathbb{Z}} e^{2\pi i m x}\, \widetilde{Z}_{\rm P}^{m}(y)\,. \tag{3.2.1}$$

Spectral decomposition: It is useful to expand the fluctuating partition functions in a complete basis of normalizable modular invariant functions on the fundamental domain $\mathcal{F}$ [62] (see also [45, 78–80]). Such eigenfunctions consist of a continuous spectrum of Eisenstein series $E_s(y)$ with $s \in \frac{1}{2} + i\mathbb{R}$, and a discrete spectrum of Maass cusp forms $\nu_{n,\pm}(y)$:

$$\Delta_{\mathcal{F}} E_{\frac{1}{2}+i\alpha}(\tau) = \left(\frac{1}{4} + \alpha^2\right) E_{\frac{1}{2}+i\alpha}(\tau)\,,\ \ \Delta_{\mathcal{F}} \nu_{n,\pm}(\tau) = \left(\frac{1}{4} + \left(R_n^{\pm}\right)^2\right) \nu_{n,\pm}(\tau)\,. \tag{3.2.2}$$

in addition to a constant function, $\Delta_{\mathcal{F}}\nu_0(\tau) = 0$. Note that there are both even (+) and odd (−) cusp forms, so there are two sets of eigenvalues $\{R_n^{\pm}\}$. These are randomly distributed, which we will quantify later.

After expanding the fluctuating part of the partition function in this modular invariant basis, the *expansion coefficients* are then unconstrained by modular invariance and their statistical properties are a good diagnostic of chaos. To write this, we refine the decomposition (3.2.1):

$$\widetilde{Z}_{\mathrm{P}}(x,y) = \widetilde{Z}^0_{\mathrm{P}}(y) + 2\sum_{m>0}\Big\{\cos(2\pi m x)\Big[\widetilde{Z}^m_{\mathrm{P,disc.},+}(y) + \widetilde{Z}^m_{\mathrm{P,cont.}}(y)\Big] + \sin(2\pi m x)\widetilde{Z}^m_{\mathrm{P,disc.}-}(y)\Big\} \tag{3.2.3}$$

where the spectrum consists of the following pieces:

$$\begin{aligned}
&\text{spin 0, continuous:} && \widetilde{Z}^0_{\mathrm{P}}(y) = \mathrm{vol}(\mathcal{F})^{-\frac{1}{2}}\, z_0 + 2\sqrt{y}\int_{\mathbb{R}} \frac{d\alpha}{4\pi}\, z_{\frac{1}{2}+i\alpha}\, y^{i\alpha}\,, \text{[52]}\\
&\text{spin} > 0\text{, discrete:} && \widetilde{Z}^{m>0}_{\mathrm{P,disc.},\pm}(y) = \sum_{n\geq 0} z_{n,\pm}\, \nu^m_{n,\pm}(y)\,,\\
&\text{spin} > 0\text{, continuous:} && \widetilde{Z}^{m>0}_{\mathrm{P,cont.}}(y) = \int_{\mathbb{R}} \frac{d\alpha}{4\pi}\, z_{\frac{1}{2}+i\alpha}\, E^m_{\frac{1}{2}+i\alpha}(y)\,,
\end{aligned} \tag{3.2.4}$$

with $\mathrm{vol}(\mathcal{F}) = \frac{\pi}{3}$. The modular invariant expansion coefficients are $\{z_0,\, z_{n,\pm},\, z_{\frac{1}{2}+i\alpha}\}$, and we are interested in their variance and how it encodes the linear ramp. Using the explicit basis functions for $m > 0$,[53]

$$\begin{aligned}
\nu^m_{n,\pm}(y) &= a^{(n,\pm)}_m \sqrt{y} K_{iR^{\pm}_n}(2\pi m y)\,,\\
E^m_{\frac{1}{2}+i\alpha}(y) &= \frac{2\, a^{(\alpha)}_m}{\Lambda(-i\alpha)}\sqrt{y}K_{i\alpha}(2\pi m y)\,, \qquad a^{(\alpha)}_m = \frac{2\sigma_{2i\alpha}(m)}{m^{i\alpha}}\,,
\end{aligned} \tag{3.2.6}$$

where $\Lambda(s) \equiv \Lambda(\frac{1}{2}-s) \equiv \pi^{-s}\Gamma(s)\zeta(2s)$. Here, we also defined the normalized Eisenstein series Fourier coefficient $a^{(\alpha)}_m$ in analogy with the cusp form Fourier coefficients.

We also trivially obtain a decomposition into bases of Bessel functions (both with continuous order, $K_{i\alpha}$, and sporadic discrete order, $K_{iR^{\pm}_n}$) by defining the *spin-dependent spectral overlap coefficients*:

$$\begin{aligned}
z^m_{n,\pm} &\equiv a^{(n,\pm)}_m\, z_{n,\pm}\,,\\
z^m(\alpha) &\equiv \frac{2\, a^{(\alpha)}_m}{\Lambda(-i\alpha)}\, z_{\frac{1}{2}+i\alpha}\,.
\end{aligned} \tag{3.2.7}$$

[52] Here we imposed $\Lambda(i\alpha)z_{\frac{1}{2}+i\alpha} = \Lambda(-i\alpha)z_{\frac{1}{2}-i\alpha}$, which is a symmetry of the Eisenstein series.

[53] Our conventions for Fourier coefficients are consistent with [62], but differ from [78]. For comparison, we give the translation:

$$\left(\mathtt{a}^{(s\equiv\frac{1}{2}+i\alpha)}_{j\equiv m}\right)_{\text{there}} = \left(a^{(\alpha)}_m\right)_{\text{here}}\,, \qquad \left(\mathtt{b}^{(n)}_{j\equiv m}\right)_{\text{there}} = \frac{\|\nu_{n,\pm}\|}{2}\left(a^{(n,\pm)}_m\right)_{\text{here}}\,. \tag{3.2.5}$$

The fact that $\{z_0,\, z_{n,\pm},\, z_{\frac{1}{2}+i\alpha}\}$ are independent of spin leads to *spectral determinacy* [62]: full knowledge of $\widetilde{Z}^m_{\text{P, cont./disc.,},\pm}(y)$ for only $m=0$ and a single non-zero spin determines the partition function for every other spin.[54] That the coefficients must be independent of spin will prove to be very important.

3.2.2 Linear ramp from correlations in spectral overlap coefficients

We are interested in the universal correlations that this fluctuating spectrum exhibits due to quantum chaos. In particular, a quantum chaotic CFT will have a universal asymptotic contribution to the variance of $\widetilde{Z}_{\text{P}}$, describing eigenvalue repulsion. This is often called the 'linear ramp' and corresponds to analytically continuing $y_1 \to \beta + iT$ and $y_2 \to \beta - iT$ and taking the large T limit of the spectral form factor. A linear ramp is captured in y_i variables by the following limiting behavior:

$$\begin{aligned}\left\langle \widetilde{Z}^{m_1}_{\text{P}}(y_1)\, \widetilde{Z}^{m_2}_{\text{P}}(y_2)\right\rangle_{\text{ramp}} =& \delta_{m_1 m_2}\left[\frac{1}{\pi}\frac{y_1 y_2}{y_1+y_2}\, e^{-2\pi|m_1|(y_1+y_2)}\right] + \dots \\ & \Big(y_i \gg 1,\ \frac{y_1}{y_2} = \text{fixed}\Big)\end{aligned} \tag{3.2.8}$$

where '...' denotes subleading terms in the large y_i limit. This should be read as a statement about each spin sector separately.

We note an important difference from chapter 2: here (and henceforth) the normalization for the ramp corresponds to the GOE universality class, where the slope of the ramp is given by $\frac{1}{\pi}$, matching the discussion in [78, 97]. This is in contrast to the normalization corresponding to the GUE universality class, given by $\frac{1}{2\pi}$, as in chapter 2 and [34]. The reason is that it was shown in [97] that every CFT contains an anti-linear, anti-unitary RT symmetry, implying that the relevant universality class for two-dimensional CFTs is GOE in every spin sector.

We wish to discuss how the ramp (3.2.8) translates into specific universal correlations between the coefficients of the spectral decomposition. This discussion should a priori be had for each spin sector individually. We first summarize the results from chapter 2.

[54] For partition functions that arise as Poincaré series, further constraints follow [78]. However, we do not assume this here.

Ramp for spin 0: For spins $m_1 = m_2 = 0$, the ramp is encoded in $\left\langle \widetilde{Z}^0_{\mathrm{P}}(y_1)\widetilde{Z}^0_{\mathrm{P}}(y_2)\right\rangle$, and in particular it is fully determined by correlations in the overlap coefficients with Eisenstein series:

$$\begin{aligned}
&\left\langle \widetilde{Z}^0_{\mathrm{P}}(y_1)\widetilde{Z}^0_{\mathrm{P}}(y_2)\right\rangle = 4\sqrt{y_1y_2}\int_{\mathbb{R}} \tfrac{d\alpha_1 d\alpha_2}{(4\pi)^2} \left\langle z_{\frac{1}{2}+i\alpha_1}\, z_{\frac{1}{2}+i\alpha_2}\right\rangle_{\text{spin 0 ramp}} y_1^{i\alpha_1}y_2^{i\alpha_2} + \ldots\,, \\
&\left\langle z_{\frac{1}{2}+i\alpha_1}\, z_{\frac{1}{2}+i\alpha_2}\right\rangle_{\text{spin 0 ramp}} \sim \frac{1}{2\cosh(\pi\alpha_1)} \times 4\pi\delta(\alpha_1+\alpha_2) \qquad (|\alpha_i| \to \infty)\,.
\end{aligned} \tag{3.2.9}$$

where terms subleading in the large y_i limit (denoted as '...') are required to obtain a modular invariant expression; these correspond to deviations from the asymptotic form given in the second line of (3.2.9).[55] While the correlations in $z_{\frac{1}{2}+i\alpha}$ will in general contain more information, the above should be understood as the *universal* contribution that is due to a ramp in the spin 0 sector.[56]

Ramp for non-zero spins: For non-zero spins, decomposing the ramp using (3.2.3) and noting that the leading term shown in (3.2.8) is even in spin, it is clear that the ramp could apriori be encoded in cross-correlations between any of the terms in (3.2.3) (subject to producing the correct parity). We will now discuss the form of the correlations that can encode a ramp in a single spin sector. However we will later stress the limitations of this approach when asking for linear ramps in more than one spin sector simultaneously, as these are not independent of each other and additional consistency conditions must be imposed.

Using the spectral decomposition of the partition function, we can write its even and odd parts for spin $m \geq 1$ in a basis of Bessel functions, where each individual term is still modular invariant by construction:

$$\begin{aligned}
\widetilde{Z}^m_{\mathrm{P},+}(y) &\equiv \sum_{n>0} z^m_{n,+}\,\sqrt{y}K_{iR_n^+}(2\pi m y) + \int_{\mathbb{R}} \frac{d\alpha}{4\pi}\, z^m(\alpha)\sqrt{y}K_{i\alpha}(2\pi m y)\,, \\
\widetilde{Z}^m_{\mathrm{P},-}(y) &\equiv \sum_{n>0} z^m_{n,-}\,\sqrt{y}K_{iR_n^-}(2\pi m y)\,.
\end{aligned} \tag{3.2.10}$$

[55]We thank E. Perlmutter for pointing out the importance of the large $|\alpha_i|$ limit, see [78] and chapter 2 for more details.

[56]Note that the correlation (3.2.9) is manifestly *diagonal* in the spectral parameters α_i. Such diagonality was proposed in [78] as a natural constraint analogous to Berry's diagonal approximation in the theory of periodic orbits. It is also a distinctive feature exhibited by the pure gravity result for the $\mathbb{T}^2 \times I$ amplitude [34].

We briefly review how the ramp could be encoded the Eisenstein series correlations. For the continuous part of the spectral decomposition, we can use the orthogonality of Bessel functions to invert the α-integral in (3.2.10):

$$z^m(\alpha) = \frac{2}{\pi}\,\alpha \sinh(\pi\alpha) \int_0^\infty \frac{dy}{y^{3/2}}\, K_{i\alpha}(2\pi m y) \widetilde{Z}^m_{\mathrm{P,cont.}}(y)\,. \tag{3.2.11}$$

This allows us to translate the universal expression for RMT eigenvalue repulsion, (3.2.8), into an expression for the correlations of $z^m(\alpha)$ coefficients by performing two correlated y-integrals of the form (3.2.11):

$$\langle z^{m_1}(\alpha_1) z^{m_2}(\alpha_2)\rangle_{\mathrm{ramp}} = 2\alpha_1 \tanh(\pi\alpha_1)\, \delta_{m_1 m_2}\, \left[\delta(\alpha_1 - \alpha_2) + \delta(\alpha_1 + \alpha_2)\right]\,. \tag{3.2.12}$$

This shows how a ramp for specific spin m can be encoded in the coefficients of the Eisenstein series, and the required correlations are again diagonal in the spectral parameter.[57] It is straightforward to verify this result explicitly by transforming (3.2.12) back to y-variables, which reproduces (3.2.8). We can equivalently write (3.2.12) as:

$$\begin{aligned} \left\langle z_{\frac{1}{2}+i\alpha_1} z_{\frac{1}{2}+i\alpha_2} \right\rangle_{\text{spin } m \text{ ramp}} =& \frac{\Lambda(-i\alpha_1)\Lambda(-i\alpha_2)}{2\big(a_m^{(\alpha_1)}\big)^2}\, \alpha_1 \tanh(\pi\alpha_1) \\ & \times \left[\delta(\alpha_1 - \alpha_2) + \delta(\alpha_1 + \alpha_2)\right] \end{aligned} \tag{3.2.13}$$

The fact that this relation depends explicitly on spin might be understood as follows: the existence of a ramp in each spin sector gives partial information about the correlation of the modular invariant coefficients in different regimes, roughly organized by scale of oscillation as function of α. The different regimes are spin-dependent, so (3.2.13) is to be understood as being valid only in the regime informed by the asymptotic form of the spin-m partition function.[58]

[57] Since $z^m(\alpha)$ is even in α by definition, we refer to the presence of the symmetrized sum of delta-functions in (3.2.12) as diagonal.

[58] To organize the information conveniently and discuss the relationship between all the statements implied by the ramp in different spin sectors, ref. [1] introduced a conjugate variable ξ; the existence of a ramp in each spin sector then is localized in that variable, in a different location for different spin sectors. The transformation to the ξ variables is roughly a Fourier transform, so localization in that variable translates to a definite scale of oscillatory behavior in the α variables.

3.3 Ramp from cusp forms – the statistical approximation

In this section we extend the above analysis to the cusp forms. The main tool we use is a continuous approximation to the sum over the cusp forms, which utilizes statistical information, known as "arithmetic chaos". We introduce the approximation in the context of a simple ansatz that yields ramps in a single spin sector from cusp form sums, and show how this is reproduced to good accuracy by the statistical approximation. This sets the stage for an improved ansatz, discussed in the next section, where we "assemble" ramps for *all* spin sectors simultaneously.

We would like to explore the type of correlations in the overlap coefficients, $\langle z_{n_1,\pm} z_{n_2,\pm}\rangle_{\text{ramp}}$, which yield a linear ramp through a sum over cusp forms:

$$\left\langle \widetilde{Z}^{m_1}_{\text{P,disc.},\pm}(y_1)\widetilde{Z}^{m_2}_{\text{P,disc.},\pm}(y_2)\right\rangle_{\text{ramp}} = \textstyle\sum_{n_1,n_2>0}\langle z_{n_1,\pm} z_{n_2,\pm}\rangle_{\text{ramp}}\, \nu^{m_1}_{n_1,\pm}(y_1)\nu^{m_2}_{n_2,\pm}(y_2)\,, \tag{3.3.1}$$

where the l.h.s. takes the universal form (3.2.8), and we recall $\nu^m_{n,\pm}(y) \equiv a^{(n,\pm)}_m \sqrt{y} K_{iR^\pm_n}(2\pi m y)$. Note that the sum is over erratic eigenvalues $R^\pm_n$ and erratic Fourier coefficients $a^{(n,\pm)}_m$. The first few eigenvalues are:

$$\begin{aligned} R^+_n &= 13.7798.., \quad 17.7386.., \quad 19.4235.., \quad 21.3158.., \quad 22.7859.., \ \dots \\ R^-_n &= \ \ 9.5337.., \quad 12.1730.., \quad 14.3585.., \quad 16.1381.., \quad 16.6443.., \ \dots \end{aligned} \tag{3.3.2}$$

These are sporadically distributed and become increasingly dense. The cusp form Fourier coefficients take a similarly erratic form (for fixed spin):

$$\begin{aligned} a^{(n,+)}_{m=2} &= +1.5493.., \quad -0.7655.., \quad -0.6928.., \quad +1.2875.., \quad +0.2677.., \ \dots \\ a^{(n,-)}_{m=2} &= -1.0683.., \quad +0.2893.., \quad -0.2309.., \quad +1.1619.., \quad -1.5402.., \ \dots \end{aligned} \tag{3.3.3}$$

where we normalized such that $a^{(n,\pm)}_{m=1} = 1$. The Fourier coefficients are distributed according to a Wigner semi-circle for prime spins $m \to \infty$. Studying the nearest neighbor spacings reveals that both the eigenvalues and the Fourier coefficients (for fixed spin) are Poisson distributed – a fact we shall refer to as *arithmetic chaos*; see Appendix B.1 for details and plots. In a sense, arithmetic chaos is more akin to an *integrable* rather than a chaotic structure. One of our goals is to elucidate the relationship between this randomness in the structure of the Maass cusp form expansion and the genuine *quantum chaos* described by the linear ramp in the spectral form factor. To reproduce the ramp from a sum over cusp forms, we will have to address this interplay.

A central ingredient in our analysis is a certain continuum approximation to the discrete sum over cusp forms; relatedly, we will argue that all cusp form data can be replaced with its statistical average, which we will explain in turn. Before giving details, let us summarize the steps we will follow:

1. To find $\langle z_{n_1,\pm} z_{n_2,\pm} \rangle$ such that the sum (3.3.1) yields a ramp, we first note that the linearly increasing density of eigenvalues $R_n^{\pm}$ allows us to approximate the sum by an integral over a continuous eigenvalue density. We will argue that this approximation becomes arbitrarily good for large y_i. Equivalently, we can think of the large y_i limit as implementing a statistical averaging over eigenvalues.

2. While less obvious, we will show that the large y_i limit also acts as a statistical averaging over the Fourier coefficients $a_m^{(n,\pm)}$. Since they appear squared in the spectral form factor, the cusp form sum is effectively only sensitive to their statistical variance. Thanks to certain Hecke relations, the information contained in the variances of Fourier coefficients for all spins m is equivalent to the information contained in the full distribution of those with prime m.

3. Using these statistical properties, we illustrate what kind of correlations $\langle z_{n_1,\pm} z_{n_2,\pm} \rangle$ can yield a ramp in a given spin sector. We then show how to get a ramp in *every* spin sector in a very constrained way. The correlations thus obtained come with a certain amount of freedom. We show that fixing this freedom in the simplest possible way leads to a result that matches the pure gravity wormhole amplitude [34].

Throughout this section we make extensive use of a database of 5832 even and 6282 odd Maass cusp forms (corresponding to eigenvalues $R_n^{\pm} < 400$), computed in [98] (see also [99] for a subset). We also assume the non-degeneracy of cusp forms, which is a widely believed but unproven conjecture.

3.3.1 Statistical treatment of the sum over eigenvalues $R_n^{\pm}$

A ramp can be encoded in the coefficients of Maass cusp forms; to extract this, we need to invert the discrete part of (3.2.10). This requires an appropriate regularization of the integrals over Bessel functions to ensure their orthogonality in the discrete solution space. We avoid this technical point for the moment by working with an approximate continuous representation. This will allow us to derive the solution. We will see that this representation utilizes many of the statistical properties of the cusp form, thus connecting arithmetic chaos to the expansion of the ramp in the cusp forms.

To start we define the density of cusp forms by $\mu_\pm(R)$, defined by

$$\widetilde{Z}^m_{\text{P,disc.},\pm}(y) = \int_{r_\pm}^\infty dR\, \mu_\pm(R)\, z^m_{R,\pm}\, \sqrt{y} K_{iR}(2\pi m y)\,, \quad \mu_\pm(R) = \sum_{n\geq 1} \delta(R - R_n^\pm)\,, \tag{3.3.4}$$

where $z^m_{R,\pm}$ is a smooth function of R such that $z^m_{R_n^\pm,\pm} \equiv z^m_{n,\pm}$. We will justify by construction that this is consistent with a ramp.

The asymptotic density of cusp forms can be approximated by a continuous function, using the 'Weyl law' (see for example [100, 101]):

$$\begin{aligned} \mu_+(R) &\approx \bar{\mu}_+(R) = \frac{1}{12}\, R - \frac{3}{2\pi}\, \log R + \frac{\log\left(\pi^4/2\right)}{4\pi} + \mathcal{O}\left(\frac{\log R}{R^2}\right)\,, \\ \mu_-(R) &\approx \bar{\mu}_-(R) = \frac{1}{12}\, R - \frac{1}{2\pi}\, \log R - \frac{\log 8}{4\pi} + \mathcal{O}\left(\frac{\log R}{R^2}\right)\,. \end{aligned} \tag{3.3.5}$$

The lower cutoff $r_\pm > 0$ in (3.3.4) is chosen appropriately such as to avoid over-counting of the constant cusp form. We review this approximation and various other statistical properties of the Maass cusp forms in appendix B.1, see in particular figure B.1. For the purpose of our analysis, the smooth approximation to the density of eigenvalues $R_n^\pm$ sometimes allows us to replace sums by integrals:

$$\sum_{n>0} f(R_n^\pm) \overset{?}{\approx} \int_{r_\pm}^\infty dR\, \bar{\mu}_\pm(R)\, f(R)\,, \tag{3.3.6}$$

which one might expect to hold for sufficiently smooth functions f. Clearly the approximation is better for functions f with support at larger values of R, since the eigenvalue density increases linearly with R; thus, more precisely, for any $\varepsilon > 0$ and sufficiently smooth functions f, there is a sufficiently large n_0 such that

$$\left| \sum_{n>n_0} f(R_n^\pm) - \int_{R_{n_0}}^\infty dR\, \bar{\mu}_\pm(R)\, f(R) \right| < \varepsilon\,. \tag{3.3.7}$$

Working with this continuous approximation, a calculation identical to (3.2.12) gives:

$$\left\langle z^{m_1}_{R_1,\pm} z^{m_2}_{R_2,\pm} \right\rangle_{\text{ramp}} \approx \frac{2R_1 \tanh(\pi R_1)}{\pi^2\, \bar{\mu}_\pm(R_1)^2}\, \delta_{m_1 m_2}\, \delta(R_1 - R_2)\,. \tag{3.3.8}$$

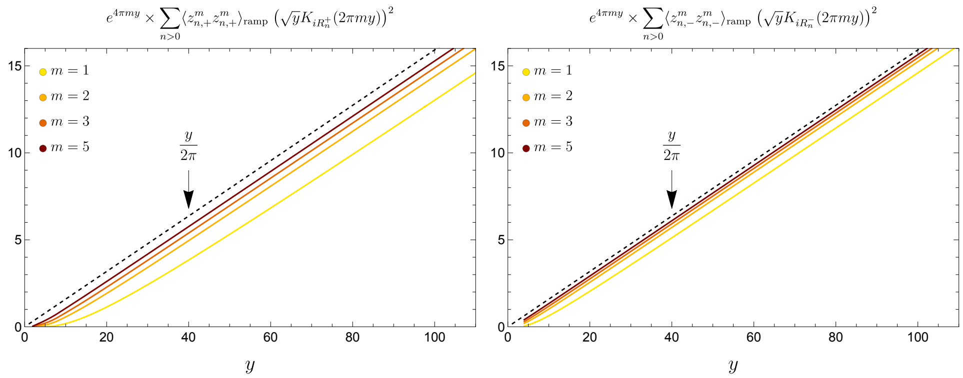

Figure 3.2: Numerical verification of the encoding of a linear ramp in correlations of even (left) and odd (right) Maass cusp forms, according to (3.3.10), for $y_1 = y_2 \equiv y$. The summation over n is performed up to some cutoff such that convergence is achieved within the displayable accuracy. The plots show that the sum converges to the ramp linear $y/(2\pi)$ up to an m-dependent constant that is subleading as $y \to \infty$.

One can immediately see that this approximate continuous expression translates into the following correlations for the discrete coefficients:

$$\left\langle z^{m_1}_{n_1,\pm}\, z^{m_2}_{n_2,\pm} \right\rangle_{\rm ramp} \approx \frac{2R^\pm_{n_1} \tanh\!\left(\pi R^\pm_{n_1}\right)}{\pi^2\, \bar{\mu}_\pm(R^\pm_{n_1})}\, \delta_{m_1 m_2}\, \delta_{n_1 n_2}\,. \tag{3.3.9}$$

or, equivalently, the cusp form sum (3.3.1) encoding a linear ramp should be of the form

$$\begin{aligned}\left\langle \widetilde{Z}^{m_1}_{\rm P,disc.,\pm}(y_1) \widetilde{Z}^{m_2}_{\rm P,disc.,\pm}(y_2) \right\rangle_{\rm ramp} \approx \sum_{n_1,n_2>0} &\left(\frac{2R^\pm_{n_1} \tanh\!\left(\pi R^\pm_{n_1}\right)}{\pi^2\, \bar{\mu}_\pm(R^\pm_{n_1})}\, \delta_{m_1 m_2} \delta_{n_1 n_2} \right) \\ &\times \sqrt{y_1} K_{iR_{n_1}}(2\pi m_1 y_1)\, \sqrt{y_2} K_{iR_{n_2}}(2\pi m_2 y_2)\end{aligned} \tag{3.3.10}$$

This is approximate in the following sense. To evaluate the sum we can proceed in two ways: (i) analytically, we can approximate the sum by an integral as in (3.3.6), which in turn recovers the *exact* ramp in *every* spin sector (by construction). The approximation is then due to replacing the sum by an integral. This approximation becomes increasingly good for $y_i \to \infty$ because the support of the Bessel functions shifts to larger values of $R^\pm_n$ where these are more dense. (ii) Numerically, we can confirm directly that the discrete sum (3.3.10) does also reproduce the ramp up to an error

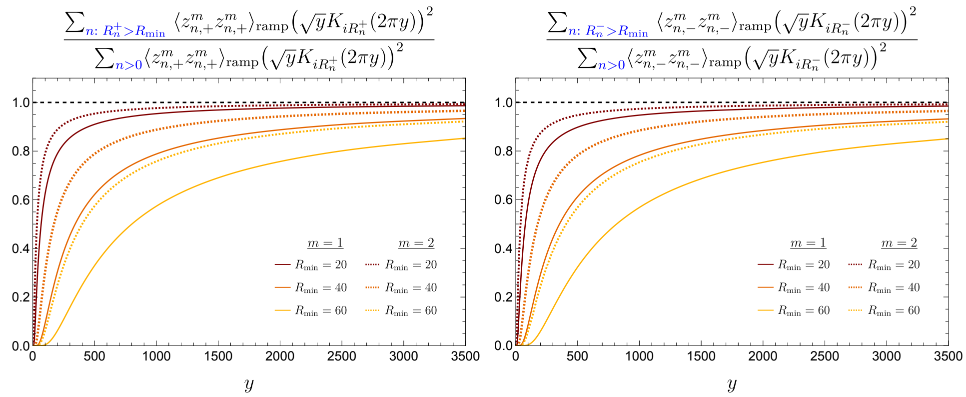

Figure 3.3: We quantify how the sum over cusp forms indexed by n depends on the terms with small n (and hence small $R_n^{\pm}$). We plot the ramp in the spectral form factor computed using only values of n for which $R_n^{\pm} > R_{\min}$ and normalize it by the complete result. Asymptotically as $y \to \infty$ this ratio converges to 1, no matter how many low-lying values of $R_n^{\pm}$ we exclude. We show the cases of even (left) and odd (right) cusp forms separately (they are almost indistinguishable). Solid lines correspond to spin $m = 1$, dashed lines to $m = 2$.

(a subleading constant shift) that goes to zero as $y_i \to \infty$.[59] Figure 3.2 illustrates the result (both for even and odd parity cusp forms). We see that the numerical evaluation of the Maass cusp form sum asymptotes to the expected linear ramp for large values of y_i (we only show the case $y_1 = y_2 \equiv y$, but other cross sections of the (y_1, y_2) plane were checked similarly).

Dominance of large $R_n^{\pm}$ as $y_i \to \infty$: We wish to comment more on the convergence of the sum over cusp forms indexed by n, (3.3.10), and the continuous approximation. As functions of y, the Bessel functions $K_{iR_n^{\pm}}(2\pi m y)$ have strong oscillations for $0 < 2\pi m y \lesssim R_n^{\pm}$, with amplitude of order $\sqrt{2\pi / R_n^{\pm}}\, e^{-\pi R_n^{\pm}/2}$, and subsequently decay exponentially like $\sqrt{1/(4my)}\, e^{-2\pi m y}$, independent of $R_n^{\pm}$. First, the exponential decay implies that the sum over n converges and can thus be truncated in numerical evaluation. More non-trivially, the sum is dominated by terms with increasingly large values of $R_n^{\pm}$. We verify this numerically in figure 3.3: we compare the

[59]The constant shift is the error introduced by the summands with small values of n, where the continuum approximation is worse. It is strictly subleading to the linear ramp for large y_i.

ramp computed using all relevant terms in the sum with the partial result obtained by dropping all terms with $0 < R_n^\pm < R_{\min}$. We observe that the ratio of these two quantities approaches 1 as $y \to \infty$, for any choice of $R_{\min}$. Another way to present the same result would be as follows: any partial sum over only low-lying $R_n^\pm$ converges to a finite constant (times the usual $e^{-2\pi m(y_1+y_2)}$) as $y_i \to \infty$, as the Bessel functions become independent of $R_n^\pm$. This is therefore subleading to the ramp:

$$\begin{aligned}\lim_{y_i\to\infty} e^{2\pi m(y_1+y_2)} &\sum_{n=1}^{n_{\max}} \langle z^m_{n,\pm} z^m_{n,\pm}\rangle_{\text{ramp}} \sqrt{y_1} K_{iR_n^\pm}(2\pi m y_1)\sqrt{y_2} K_{iR_n^\pm}(2\pi m y_2) \\ &= \frac{1}{4m}\sum_{n=1}^{n_{\max}} \langle z^m_{n,\pm} z^m_{n,\pm}\rangle_{\text{ramp}} = \text{const}(m, n_{\max}) < \infty\end{aligned} \tag{3.3.11}$$

for any $n_{\max}$. Effectively the sum over n is dominated by a window $R_{\min} \lesssim R_n^\pm \lesssim R_{\max}$ where both $R_{\min}$ and $R_{\max}$ increase with y. Thus using the continuous approximation, i.e., treating the eigenvalues $R_n^\pm$ statistically for large y, is valid.[60]

To summarize, the sum (3.3.10) can be (roughly) split into three pieces, which qualitatively contribute as follows to the spectral form factor:

$$\begin{array}{lll} (1)\ \ 0 < R_n^\pm \lesssim R_{\min}(y_i): & \text{subleading constant} & \\ (2)\ \ R_{\min}(y_i) \lesssim R_n^\pm \lesssim R_{\max}(y_i): & \text{linear ramp} & (3.3.12) \\ (3)\ \ R_{\max}(y_i) \lesssim R_n^\pm: & \text{exponentially small} & \end{array}$$

3.3.2 Statistical treatment of the Fourier coefficients $a_m^{(n,\pm)}$

Let us return to the sum over cusp forms, (3.3.1). We wish to address the following question: *what form of correlations $\langle z_{n_1,\pm} z_{n_2,\pm}\rangle$ yields the ramp* (3.3.10)*?* Naively, it seems that we have already answered this question in (3.3.9). However, that expression, taken literally, would via (3.2.7) give a different, *spin-dependent* form of $\langle z_{n_1,\pm} z_{n_2,\pm}\rangle$ for *every* spin, which clearly cannot be correct. *So how is* (3.3.10) *consistent with spin-independent correlations $\langle z_{n_1,\pm} z_{n_2,\pm}\rangle$?* To resolve this conundrum, we take a

[60] A final way of seeing this behaviour is to plot the integrand in the continuous approximation of the cusp form sum: $\bar{\mu}_\pm(R)\langle z^m_{n,\pm} z^m_{n,\pm}\rangle_{\text{ramp}}$ grows monotonically with n, while the Bessel functions decay very slowly as functions of R until $R \gtrsim 2\pi m y_i$. This leads to an integrand that peaks at a value of R that increases with y_i, in turn making the continuous approximation better.

detour to discuss properties of the Fourier coefficients $a_m^{(n,\pm)}$ of the cusp forms.

The Fourier coefficients are erratic, see (3.3.2). What does this mean for the validity of our continuous approximation to the eigenvalues? We have already seen that the sum over n can be split into three pieces, see (3.3.12). Both $R_{\min}$ and $R_{\max}$ increase indefinitely as $y_i \to \infty$, so the *density* of $R_n^\pm$, which are of interest to regime (2), increases as well. Summing over an increasingly dense set of $R_n^\pm$ acts as a *statistical coarse-graining* over the remaining n-dependent terms in the sum. In particular, the product of the Fourier coefficients appearing in the sum and the correlations $\langle z_{n_1,\pm} z_{n_2,\pm}\rangle$ get *averaged* over. We therefore expect to be able to replace the discrete erratic Fourier coefficients by their statistical distribution.

Distribution of Fourier coefficients: The statistical distribution of the Fourier coefficients is a well-known topic of mathematical research, and we review it in some detail in appendix B.1. Let us only point out the most crucial aspects. First, the asymptotic distribution of $a_m^{(n,\pm)}$ for fixed *prime* spins $m \equiv p$ is well known [102]:

$$\mu_p(x) = \begin{cases} \frac{(p+1)\sqrt{4-x^2}}{2\pi\left(\left(p^{1/2}+p^{-1/2}\right)^2 - x^2\right)} & \text{if } |x| < 2 \\ 0 & \text{otherwise} \end{cases} \tag{3.3.13}$$

For large prime spins, this approaches a Wigner semicircle $(2\pi)^{-1}\sqrt{4-x^2}$. Another notable feature is that the distribution suggests that $|a_p^{(n,\pm)}| < 2$ for all n, a property known as the Ramanujan-Petersson conjecture [102]. We are interested in moments of these distributions. Since the sum (3.3.1) features the squares of Fourier coefficients, a statistical feature of particular interest is their variance

$$\mathcal{N}_m^\pm \equiv \overline{\left(a_m^{(n,\pm)}\right)^2} \equiv \lim_{n_0\to\infty} \frac{1}{n_0} \sum_{n=1}^{n_0} \left(a_m^{(n,\pm)}\right)^2 , \tag{3.3.14}$$

which has the following exact value for prime spins:[61]

$$\mathcal{N}_p^\pm = \frac{p+1}{p} \qquad (p \text{ prime; exact}). \tag{3.3.16}$$

[61]It is interesting to note that since the Fourier coefficients for prime spins are Poisson distributed, as shown in appendix B.1, the variance in (3.3.14) already implies delta-functions in spin and eigenvalue index,

$$p_1, p_2 \text{ prime:} \qquad \overline{a_{p_1}^{(n_1,\pm)} a_{p_2}^{(n_2,\pm)}} = \overline{\left(a_{p_1}^{(n_1,\pm)}\right)^2}\, \delta_{n_1,n_2}\delta_{p_1,p_2} = \mathcal{N}_{p_1}^\pm\, \delta_{n_1,n_2}\delta_{p_1,p_2} . \tag{3.3.15}$$

See (B.1.5) for higher moments. We use the notation $\overline{(\cdots)}$ to denote *statistical* averaging (over n). This is independent of the *microcanonical* averaging, denoted by $\langle\cdots\rangle$, which we always use to discuss correlations in the coarse-grained CFT spectrum.

For non-prime spins m, the variances $\mathcal{N}_m^{\pm}$ are determined by the distributions for prime spins. Importantly, not only the variances of the distributions for prime spins, but also their *higher moments* are needed. The reason is that the Fourier coefficients themselves are determined as non-linear polynomials of those for prime spins by a certain Hecke algebra, see (B.1.9) for some examples. Statistical averaging over such polynomials requires knowledge of higher moments of the prime distributions. In summary, the following three pieces of information are equivalent:

$$\begin{gathered}\text{variances } \mathcal{N}_m^{\pm} \equiv \overline{\left(a_m^{(n,\pm)}\right)^2} \text{ of distributions of } \textit{all} \text{ spins } m \\ \Leftrightarrow \\ \textit{all} \text{ moments } \overline{\left(a_p^{(n,\pm)}\right)^k} \text{ of distributions of } \textit{prime} \text{ spins } p \\ \Leftrightarrow \\ \text{distributions (3.3.13) of } \textit{prime} \text{ spins}\end{gathered}$$

We review these statements in appendix B.1 and give examples in (B.1.9). Using the first 5832 even and 6282 odd Fourier coefficients, we find numerically for their variances as a function of spin m:

$$\begin{aligned}\mathcal{N}_m^+ &\approx \mathbf{1}\,,\, \mathbf{1.46}\,,\, \mathbf{1.27}\,,\, 1.65\,,\, \mathbf{1.13}\,,\, 1.84\,,\, \mathbf{1.07}\,,\, 1.72\,,\, 1.32\,,\, 1.63\,,\, \mathbf{1.02}\,,\ldots \\ \mathcal{N}_m^- &\approx \mathbf{1}\,,\, \mathbf{1.47}\,,\, \mathbf{1.30}\,,\, 1.68\,,\, \mathbf{1.16}\,,\, 1.89\,,\, \mathbf{1.09}\,,\, 1.76\,,\, 1.36\,,\, 1.68\,,\, \mathbf{1.04}\,,\ldots\end{aligned} \tag{3.3.17}$$

where values for prime m are printed in boldface (see tables B.1 and B.2 for more details).

Statistical averaging in the spectral form factor: Whenever the statistical averaging over n applies to our cusp form sum over n, it means that we can replace discrete erratic expressions by their statistical average. This amounts to a significant simplification for evaluating sums such as

This suggests that arithmetic chaos is linked to the diagonal approximation in the periodic orbit picture of [78]. The delta-function in the eigenvalue indices persists even for non-prime spins and is therefore tied to the effective statistical averaging implemented by the correlated cusp form sums (3.3.1). Note, however, that we will later average over summands involving higher moments of Fourier coefficients, which complicates the picture.

(3.3.1): for large y_i the *exact* squared Fourier coefficients (which oscillate erratically) can be replaced by their *mean value*, i.e., the variance of their distribution (3.3.13), thus 'forgetting' about the detailed sporadic values and only keeping track of statistical information. This explains how it was possible that the correlations $\langle z_{n_1,\pm} z_{n_2,\pm}\rangle$ that would follow from (3.3.9) would depend on spin in such an extremely fine tuned way as to cancel all erratic Fourier coefficients $a_{m_1}^{(n_1,\pm)} a_{m_2}^{(n_2,\pm)}$: the correlations $\langle z_{n_1,\pm} z_{n_2,\pm}\rangle$ do not actually need to cancel the Fourier coefficients exactly, but only *on average*. As we will see, this is indeed possible in a spin-independent way.

Focusing on a single spin sector, the fact that the Fourier coefficients only need to cancel on average means we would expect to reproduce the linear ramp in the spin m sector from

$$\left\langle \widetilde{Z}^m_{\text{P,disc.},\pm}(y_1) \widetilde{Z}^m_{\text{P,disc.},\pm}(y_2) \right\rangle_{\text{ramp naive}} \equiv \frac{1}{\mathcal{N}_m^\pm} \sum_{n>0} \left(\frac{2R_n^\pm \tanh(\pi R_n^\pm)}{\pi^2 \,\bar{\mu}_\pm(R_n^\pm)} \right) \times \left(a_m^{(n,\pm)}\right)^2 \sqrt{y_1} K_{iR_n^\pm}(2\pi m y_1) \sqrt{y_2} K_{iR_n^\pm}(2\pi m y_2) \tag{3.3.18}$$

This corresponds to correlations of the form[62]

$$\left\langle z_{n,\pm}\, z_{n,\pm} \right\rangle_{\text{spin } m \text{ ramp naive}} \equiv \frac{1}{\mathcal{N}_m^\pm} \frac{2R_n^\pm \tanh(\pi R_n^\pm)}{\pi^2 \,\bar{\mu}_\pm(R_n^\pm)} \approx \frac{24}{\pi^2 \,\mathcal{N}_m^\pm} \qquad (m \geq 1,\, n \gg 1) \tag{3.3.19}$$

We can check the validity of this claim numerically by computing the sum (3.3.18) and comparing it with the true form of the ramp. As can be seen in figure 3.4, for large y the correct linear ramp is approached, again up to a constant which is subleading for $y \to \infty$.

Evidently, (3.3.19) still depends on the spin m via the normalization $\mathcal{N}_m^\pm$, albeit much more weakly than had we tried to cancel the erratic Fourier coefficients in (3.3.18) exactly (term by term). It is therefore still not a good candidate for correlations $\langle z_{n,\pm} z_{n,\pm}\rangle$ that yield linear ramps independent of the choice of spin. And indeed, correlations of the form (3.3.19) only yield a ramp with the correct slope in the spin m sector. In other spin sectors m', we would need a similar form of correlations, but with a different normalization $1/\mathcal{N}_{m'}^\pm$. We will remedy this situation in the following subsection.

[62]The second approximation, $\frac{2R_n^\pm \tanh(\pi R_n^\pm)}{\pi^2 \,\bar{\mu}_\pm(R_n^\pm)} \approx \frac{24}{\pi^2}$, is valid asymptotically for very large n, i.e., for very large y_i. For all numerical results in this chapter, this approximation is not good enough and is not used.

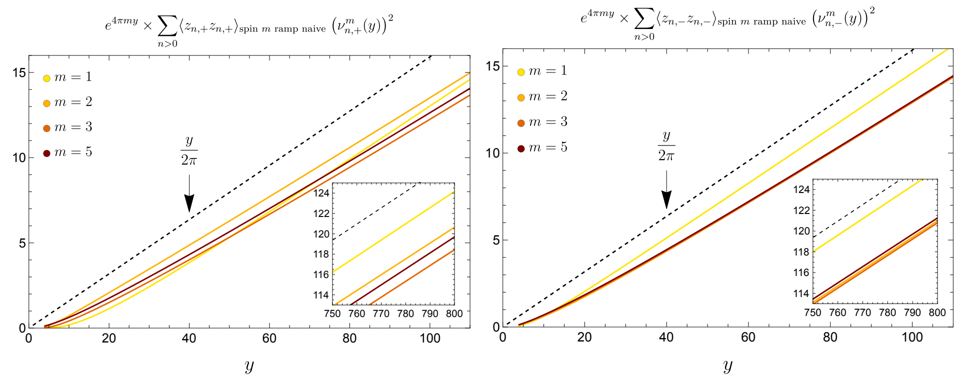

Figure 3.4: We compute the Maas cusp form sum using the variance of the Fourier coefficients instead of their exact values in (3.3.18). For large y increasingly many Fourier coefficients contribute to the sum over n, which means that their square can be increasingly well approximated by their variance. We therefore reproduce the linear ramp asymptotically (up to a subleading constant shift), c.f. figure 3.2. The left (right) shows the case of even (odd) parity cusp forms. In the odd case the ramps for different spins lie almost on top of each other. Insets show larger values of y.

3.3.3 Ramps in all spin sectors: number theory and uniqueness

As we have seen, (3.3.19) only encodes the ramp in the spin m superselection sector, but it 'contaminates' the slope of any putative ramp in other spin sectors. The basic assumption of quantum chaos, however, would be a linear ramp with the correct slope in *all* spin sectors. To achieve this, let us now take the statistical averaging one step further and improve the naive ansatz (3.3.19) such that it works *on average* for every spin sector, i.e., in a spin-independent way. We wish to write:

$$\boxed{\langle z_{n_1,\pm} z_{n_2,\pm} \rangle_{\text{ramp}} \approx \frac{2R^{\pm}_{n_1} \tanh\left(\pi R^{\pm}_{n_1}\right)}{\pi^2 \bar{\mu}_{\pm}(R^{\pm}_{n_1})} \, \delta_{n_1 n_2} \, f^{(n,\pm)} \approx \frac{24}{\pi^2} \, \delta_{n_1 n_2} \, f^{(n,\pm)}} \tag{3.3.20}$$

with a *spin-independent* function $f^{(n,\pm)}$ such that

$$\overline{\left(a^{(n,\pm)}_m\right)^2 f^{(n,\pm)}} = 1 \quad \text{for all } m \geq 1. \tag{3.3.21}$$

The effective averaging over n will then guarantee that in the limit $y_i \to \infty$, we recover the ramp *for all spins* m:

$$\begin{aligned}
&\sum_{n_1,n_2>0} \langle z_{n_1,\pm} z_{n_2,\pm}\rangle_{\text{ramp}}\; \nu^m_{n_1,\pm}(y_1)\nu^m_{n_2,\pm}(y_2) \\
&\quad\xrightarrow{y_i\to\infty} \sum_{n>0} \frac{24}{\pi^2}\, \overline{\left(a_m^{(n,\pm)}\right)^2 f^{(n,\pm)}}\, \sqrt{y_1} K_{iR_n^\pm}(2\pi m y_1)\, \sqrt{y_2} K_{iR_n^\pm}(2\pi m y_2) + \ldots \\
&\qquad = \frac{1}{\pi} \frac{y_1 y_2}{y_1+y_2}\, e^{-2\pi m(y_1+y_2)} + \ldots
\end{aligned} \tag{3.3.22}$$

where we replaced $\left(a_m^{(n,\pm)}\right)^2 f^{(n,\pm)}$ by its average according to (3.3.21) in the second line and then simply applied (3.3.10). We denote subleading terms by '. . .'.

We will refer to $f^{(n,\pm)}$ as the *arithmetic kernel* associated with the cusp form $\nu_{n,\pm}$. This name is inspired by the fact that any function satisfying (3.3.21) must obviously depend on all Fourier coefficients for all spins in a very fine-tuned way such that it produces just the right normalization for the ramp in every spin sector. It must, in a sense, encode all the information loosely referred to as *arithmetic chaos*, such as Hecke relations (B.1.8) and the statistical distribution of Fourier coefficients (3.3.13). Note that the ansatz (3.3.20) assumes diagonality in n_i. We will justify by construction that this is a consistent assumption. Note further that the condition (3.3.21) really only needs to hold asymptotically as a statement about the average over terms in the spectral form factor with large n.[63] Deviations for small n will only affect subleading terms in the late-time spectral form factor. We fix this ambiguity in the minmal way, i.e., by imposing (3.3.21) as an average over all n as written.

Given all the information encoded in 'arithmetic chaos', it is remarkable that such a function exists. We will now first write down this function, then explain why it works, and then derive it, showing that it is essentially unique (under the above assumptions). The arithmetic kernel satisfying (3.3.21) is given by

$$\boxed{f^{(n,\pm)} = \prod_{p \text{ prime}} \left[\frac{p+1}{p} - \frac{1}{p+1}\left(a_p^{(n,\pm)}\right)^2\right].} \tag{3.3.23}$$

[63] For example, we can imagine performing a 'moving average' over large but finite windows of n, which determine the cusp form sum over corresponding 'batches' of cusp forms, then for small n it is certainly allowed that the average fluctuates around 1.

Let us first confirm that this function satisfies (3.3.21). We do this in three steps:

1. **If $m \equiv p$ is prime:** Since the Fourier coefficients for prime spins are independently distributed, we only need to know the second and fourth moments of the distributions (3.3.13), which are easy to calculate. We immediately find:

$$\begin{aligned}\overline{\left(a_p^{(n,\pm)}\right)^2 f^{(n,\pm)}} = \left[\frac{p+1}{p}\,\overline{\left(a_p^{(n,\pm)}\right)^2} - \frac{1}{p+1}\,\overline{\left(a_p^{(n,\pm)}\right)^4}\right] \\ \times \prod_{\substack{p' \text{ prime} \\ p' \neq p}} \left[\frac{p'+1}{p'} - \frac{1}{p'+1}\,\overline{\left(a_{p'}^{(n,\pm)}\right)^2}\right] = 1\,,\end{aligned} \tag{3.3.24}$$

where every factor is individually 1 due to the following statistical facts:

$$p \text{ prime:} \qquad \overline{\left(a_p^{(n,\pm)}\right)^2} = \frac{p+1}{p}\,, \qquad \overline{\left(a_p^{(n,\pm)}\right)^4} = \frac{2p^2+3p+1}{p^3}\,. \tag{3.3.25}$$

2. **If $m = p^k$ is a prime power:** For prime power spins, we can analogously show that every factor in an expression similar to (3.3.24) is 1. For the first factor ($p' = p$) we need some more non-trivial facts about the Fourier coefficients, which follow from the Hecke multiplicativity rules (B.1.8). The required properties are (see appendix B.2 and in particular Lemma 4):

$$\begin{aligned} p \text{ prime:} \qquad & \overline{\left(a_{p^k}^{(n,\pm)}\right)^2} = \frac{p-p^{-k}}{p-1}\,, \\ & \overline{\left(a_{p^k}^{(n,\pm)}\right)^2\left(a_p^{(n,\pm)}\right)^2} = \frac{2(p+1)-p^{-k}(p+2+p^{-1})}{p-1}\,. \end{aligned} \tag{3.3.26}$$

Note that these properties encode *all* information about the distributions (3.3.13).

3. **Arbitrary m:** For any general integer m, there is a prime factorization $m = p_1^{k_1}\cdots p_r^{k_r}$. The Hecke multiplicativity rules (B.1.8) imply

$$m = p_1^{k_1}\cdots p_r^{k_r} \qquad \Rightarrow \qquad \left(a_m^{(n,\pm)}\right)^2 = \left(a_{p_1^{k_1}}^{(n,\pm)}\right)^2 \cdots \left(a_{p_r^{k_r}}^{(n,\pm)}\right)^2\,. \tag{3.3.27}$$

The property (3.3.21) follows factor by factor.

The arithmetic kernel $f^{(n,\pm)}$ has a deep number theoretical meaning in terms of Hecke L-functions. We elaborate on these fascinating mathematical properties in appendix B.2. We can also *derive* $f^{(n,\pm)}$ from physical requirements, i.e., by merely imposing (3.3.21) in all spin sectors. We sketch the derivation below, delegating details to appendix B.2.3.

Uniqueness of the arithmetic kernel: We will now derive the arithmetic kernel (3.3.23) by arguing that the requirement (3.3.21) fixes it *uniquely* (within an ansatz class). First recall that Fourier coefficients have multiplicative properties due to them being eigenvalues of Hecke operators. In particular, if the spin has a prime factor decomposition as in (3.3.27), since $a_{p^k}^{(n,\pm)}$ are independently distributed for different primes p it is useful to first solve the problem (3.3.21) for prime power spins, $m = p^k$. Consider an ansatz of the form

$$f_p^{(n,\pm)} = \sum_{r\geq 0} c_{p,r} \left(a_p^{(n,\pm)}\right)^{2r} \tag{3.3.28}$$

for prime p. Since we already assumed diagonality in eigenvalues $R_{n_i}^{\pm}$ in (3.3.20), odd powers of Fourier coefficients will average to zero, and we discard them in our ansatz. Such terms would not affect the construction of the universal ramp, but they would change the subleading behavior of the late time spectral form factor. Discarding odd powers in the ansatz can thus be viewed as a *minimality assumption* about the ansatz. It would be interesting to constrain such ambiguities further, using input from the off-diagonal sector.

The condition (3.3.21) yields an infinite linear system constraining the parameters $c_{p,r}$ in terms of moments of the distribution of Fourier coefficients. After some investigation (see appendix B.2.3), this system can be written as follows:

$$\sum_{r\geq 0} c_{p,r} \overline{\left(a_p^{(n,\pm)}\right)^{2(k+r)}} = \frac{(2k)!}{k!(k+1)!} \,. \tag{3.3.29}$$

Making extensive use of (i) Hecke relations and (ii) all moments of the distributions of prime Fourier coefficiens, the solution of this system for $m = p^k$ is unique:

$$c_{p,0} = \frac{p+1}{p} \,, \quad c_{p,1} = -\frac{1}{p+1} \,, \quad c_{p,r\geq 2} = 0 \,. \tag{3.3.30}$$

Using (3.3.27), the condition (3.3.21) for all m is then solved by

$$f^{(n,\pm)} = \prod_{p \text{ prime}} f_p^{(n,\pm)} = \prod_{p \text{ prime}} \left[\frac{p+1}{p} - \frac{1}{p+1}\left(a_p^{(n)}\right)^2\right] . \tag{3.3.31}$$

While we have made simplifying assumptions in the derivation of this kernel (see the discussion after (3.3.21)), its uniqueness within a large class of possibilities is remarkable. We show in the next subsection that the structure of the result (3.3.20), (3.3.23) is more than just a mathematical curiosity; it has a number theoretical interpretation and its simplicity is in fact intimately tied to a calculation in AdS_3 pure gravity.

3.4 Matching universal correlations to the AdS_3 wormhole

Our 'bottom-up' construction of the spectral overlap coefficients encoding the linear ramp was based on minimal assumptions about quantum chaos in all spin sectors and consistency with the symmetries of CFTs. We also assumed a certain minimality in the ansatz for the arithemtic kernel $f^{(n,\pm)}$, which then allowed us to fully determine it. In this section we compare this 'minimally consistent' arithmetic kernel with the wormhole amplitude found in AdS_3 pure gravity, which also exhibits such linear ramps. We find detailed agreement.

Demanding universal eigenvalue repulsion (i.e., a linear ramp) in every spin sector of the CFT, and assuming that for $m > 0$ this property is encoded in the cusp form sector alone, we constructed the following form of spectral correlations as the simplest consistent possibility:

$$\begin{aligned}
\left\langle z_{\frac{1}{2}+i\alpha_1}\, z_{\frac{1}{2}+i\alpha_2}\right\rangle_{\text{spin 0 ramp}} &= \frac{1}{2\cosh(\pi\alpha_1)} \times 4\pi\delta(\alpha_1+\alpha_2)\,, \\
\left\langle z_{n_1,\pm}\, z_{n_2,\pm}\right\rangle_{\text{spin } m>0 \text{ ramps}} &= \frac{24}{\pi^2}\, f^{(n,\pm)} \times \delta_{n_1,n_2}\,, \\
f^{(n,\pm)} &\equiv \prod_{p \text{ prime}} \left[\frac{p+1}{p} - \frac{1}{p+1}\left(a_p^{(n,\pm)}\right)^2\right]
\end{aligned} \tag{3.4.1}$$

By virtue of being spin-independent, these correlations provide a manifestly modular invariant encoding of a linear ramp in all spin sectors. (Of course, the 'bare' asymptotic ramp is not modular invariant by itself, so the subleading corrections produced by (3.4.1) are important.)

Let us now turn to gravity. The spectral decomposition of the $\mathbb{T}^2 \times I$ wormhole amplitude in AdS_3 pure gravity [33, 34] was given in [78], and provides an explicit example of a modular invariant spectral form factor that contains a ramp in the large y_i limit.[64] In our notation it corresponds to the

[64] We thank Scott Collier for private conversation on this result.

following non-zero variances:[65]

$$\begin{aligned}\left\langle z_{\frac{1}{2}+i\alpha_1} z_{\frac{1}{2}+i\alpha_2}\right\rangle_{\text{wormhole}} &= \frac{1}{2\cosh(\pi\alpha_1)} \times 4\pi\delta(\alpha_1+\alpha_2)\,, \\ \left\langle z_{n_1,\pm}\, z_{n_2,\pm}\right\rangle_{\text{wormhole}} &= \frac{1}{2\cosh\left(\pi R^{\pm}_{n_1}\right)}\,\frac{1}{\|\nu_{n,\pm}\|^2} \times \delta_{n_1 n_2}\,,\end{aligned} \tag{3.4.2}$$

where the cusp form norms are computed with respect to the Petersson inner product (see appendix B.2 for more details, and figure B.5 for concrete values). The second line is meant to indicate that both the even and odd correlations as indicated give a ramp with correct normalization. In a CFT with parity symmetry, the even and odd ramps describe chaos in different parity superselection sectors.

Now compare our result (3.4.1) with (3.4.2). The continuous part of the correlations, which encodes the spin 0 ramp, matches immediately (which is by construction). More interestingly, the discrete correlations, which we constructed by imposing quantum chaotic universality consistently across spin sectors, also match the gravity result. To see this, we need an important fact from arithmetic number theory, which is derived and explained in appendix B.2. The central observation is that our arithmetic kernel $f^{(n,\pm)}$ is a particular meromorphic *symmetric square L-function* $L^{(n,\pm)}_{\nu\times\nu}(s)$ evaluated at $s=1$. For every single cusp form, this function provides a generalization of the Riemann zeta-function that encodes all the statistical properties and Hecke relations between different spin Fourier coefficients. The precise statement is:

$$f^{(n,\pm)} = \frac{\zeta(2)}{L^{(n,\pm)}_{\nu\times\nu}(s=1)} = \frac{\pi^2}{48\cosh\left(\pi R^{\pm}_{n}\right)\|\nu_{n,\pm}\|^2}\,. \tag{3.4.3}$$

The intermediate steps in this equation are reviewed in appendix B.2. This establishes equality of, on the one hand, the correlations found from demanding a 'bare' linear ramp in all spin sectors (taking into account the mechanism of statistical averaging over cusp forms and constructing a minimal spin-independent arithmetic kernel) in (3.4.1), and, on the other hand, the pure gravity result, (3.4.2).

It is interesting to note that the spin-0 ramp, encoded in the Eisenstein sector, can similarly be expressed in terms of a suitable L-function:

$$\left\langle z_{\frac{1}{2}+i\alpha_1}\, z_{\frac{1}{2}+i\alpha_2}\right\rangle_{\text{spin 0 ramp}} = \frac{\Lambda(i\alpha_1)\Lambda(i\alpha_2)}{2L_E^{(2\alpha_1)}(1)} \times 4\pi\delta(\alpha_1+\alpha_2)\,, \tag{3.4.4}$$

[65]To compare with [78], note that $\frac{\pi}{\cosh(\pi\alpha)} = \Gamma(\frac{1}{2}+i\alpha)\Gamma(\frac{1}{2}-i\alpha)$. To compare with [34], note that we introduced an additional factor of 2 in the wormhole amplitude to match the GOE universality class, c.f., [78, 97].

where $L_E^{(\alpha)}(s) = \zeta(s+i\alpha)\zeta(s-i\alpha)$ is the meromorphic continuation of a sum over Fourier coefficients. See appendix B.2.4 for more details.

To summarize, we have found that a linear ramp in *all spin sectors* $m \geq 1$ is encoded in the following sum over cusp forms in the near-extremal limit:

$$\sum_{n>0} \frac{1}{2\cosh\left(\pi R_n^{\pm}\right)} \frac{\nu_{n,\pm}^m(y_1)}{\|\nu_{n,\pm}\|} \frac{\nu_{n,\pm}^m(y_2)}{\|\nu_{n,\pm}\|} = \frac{1}{\pi} \frac{y_1 y_2}{y_1+y_2} e^{-2\pi|m|(y_1+y_2)} + \dots \quad \text{(for all } m\text{)} \tag{3.4.5}$$

The agreement of the wormhole amplitude with the 'minimal' realization of quantum chaos across spin sectors was called the *MaxRMT principle* in [78]. It amounts to the statement that the gravity amplitude is the *minimal* modular completion of a spectral form factor exhibiting linear ramps. More precisely, ref. [78] shows that the wormhole amplitude is the minimal extension of the 'bare' ramp, after imposing 'diagonal' and 'Hecke' projections onto correlated eigenvalues and eigenfunctions in the spectral decomposition of the spectral form factor.[66] Our investigation similarly imposed some minimality requirements: the main assumptions were the realization of quantum chaos in all spin sectors and modular invariance; we argued that these assumptions required a spin-independent form of the arithmetic kernel and then constructed the simplest consistent kernel from an ansatz (3.3.20) by solving the statistical constraints. By discarding from the ansatz any terms that would be invisible to our statistical condition (3.3.21), we fixed it fully and recovered the wormhole amplitude. This simplicity provides a statistical perspective based on arithmetic chaos on the MaxRMT principle of [78].

3.5 Discussion

To summarize, we note again that the Euclidean wormhole amplitude (3.4.2) describes a universal part of the spectral correlations in any individual chaotic CFT, which dominates the late time near-extremal limit. We constructed the same object 'bottom-up' by imposing quantum chaos (in the form of a linear ramp) in every spin sector separately and consistently balancing the imprints ramps in any given spin sector have on the slope of ramps in other spin sectors. We delineated the way in which a solution can be constructed

[66] The 'Hecke projection' of [78] refers to demanding equal correlations in the continuous and discrete sectors, which is indeed a remarkable feature of (3.4.2) after absorbing the cusp form norms into the normalization of Fourier coefficients. We explore this feature in more detail in [103].

based on statistical considerations of Maass cusp forms. A crucial role was played by the effective statistical averaging over erratic data defining the modular invariant Maass cusp forms. It is due to this averaging that, on the one hand, all statistical information about 'arithmetic chaos' is encoded in the collection of linear ramps, while, one the other hand, detailed erratic features of cusp forms are washed out and a single spin-independent form of chaotic correlations could be bootstrapped. There is some freedom in the constructed solution, which would affect subleading corrections to the spectral form factor; the match with the gravitational result was established by not making use of any of this freedom, i.e., fixing it in the minmal way. We conclude with some further comments.

Spectral determinacy

It was found in [78] that the spectral decomposition of the AdS_3 wormhole amplitude is such that the correlations in the Eisenstein series coefficients and those in the Maass cusp form coefficients are identical. We found the same result by imposing statistical universalities (quantum chaos) in all spin sectors and implementing them in a minimal way through a sum over cusp forms. This strengthens the spectral determinacy property of general two-dimensional CFTs [62], as in these examples *all* spin sectors exhibit identical correlations ('strong spectral determinacy' [78]). How is this consistent with one of the basic assumptions of quantum chaos, i.e., the *independence* of spectral universalities in each symmetry superselection sector? We take the following perspective: even though the statistical approximation required that our result (3.4.1) for spin $m > 0$ linear ramps had to be the same for all spins, it nevertheless encodes separate input from all spin sectors. This is manifest when we consider the arithmetic kernel $f^{(n,\pm)}$: it contains all squared Fourier coefficients for all spin sectors in a highly fine-tuned way such as to ensure the correct statistical property (3.3.21) for all spin sectors. For example, had we only imposed the ramp in some particular spin sector, then the naive ansatz (3.3.19) would have been sufficient. But this would have impacted the slope of the ramp in all other spin sectors. Finding the universal kernel that yields the correct slope for all spins required us to separately assume the existence of a ramp for all spins and input the corresponding information into the construction of $f^{(n,\pm)}$ in a correlated way.[67]

We can summarize this as follows: imposing random matrix universality

[67]Note also that we did not assume additional structures in the CFT partition function, such as it being a Poincaré sum over images of a seed function, which would lead to further constraints; see [78].

in just one given spin sector leaves a lot of freedom for the choice of the cusp form correlations $\langle z_{n,\pm} z_{n,\pm} \rangle$, thanks to statistical coarse-graining in the late time limit. It does by no means imply a linear ramp with the correct slope for any other independent spin sector. But imposing random matrix universality in *all* spin sectors, leads to enough constraints to determine a universal, spin-independent form for the correlations describing the leading order linear ramp. Further, the statistical conditions we investigated naturally led to a 'minimal' solution of this problem, which agrees with the gravity result.

Deriving chaos

A first-principles, bottom-up derivation of chaos in holographic CFTs still eludes us. While we now understand the relationship between quantum chaos and modular invariance better, quantum chaos is still a basic assumption that we show is consistent with other features of the 2d CFTs. This is contrasted with the wormhole amplitude in gravity, which can be derived from first principles. Some standard properties of holographic CFTs might be sufficient for such a derivation, in particular the assumptions that yield a dense spectrum above the extremal limit (large central charge, no conserved currents, and a twist gap). A promising path towards this would be the construction of an Efetov sigma model as in [41, 73], similar to how chaos is derived in the SYK model [104]. It would be fascinating to see if such an approach can be adopted using recent discussions of random matrix ensembles for 2d CFT operator data and OPE coefficients, which furnish approximate solutions to the bootstrap equations [40, 46, 105].

The plateau

In chaotic quantum mechanics the universal form of eigenvalue correlations is expected to take the random matrix form for sufficiently close energy levels, depending on the universality class (see, e.g., [11]). For the GUE universality class, this is

$$\langle \rho(E+\omega/2)\rho(E-\omega/2)\rangle = \langle \rho(E)\rangle^2 + \langle \rho(E)\rangle \delta(\omega) - \frac{\sin^2\left(\pi\omega\langle\rho(E)\rangle\right)}{(\pi\omega)^2} \,. \tag{3.5.1}$$

The first term describes the disconnected part, the third the famous sine-kernel which gives rise to the ramp in the time domain. We now wish to discuss the second term, i.e., the tautological "self-correlations", to provide comparison with the chaotic case – eigenvalue repulsion and the ramp – discussed before. In quantum chaotic systems this term gives rise to the eventual plateau for sufficiently long times (or equivalently for sufficiently close eigenvalues), but this term is even more universal as it also exists in integrable systems. Systems with Poissonian statistics are completely described by the first two terms in (3.5.1), up to non-universal terms at early times.[68]

While the ramp appears to a natural object in the spectral decomposition, and can be described as analogous to the "diagonal approximation" [78] in a periodic orbit expansion (i.e., the correlations in spectral eigenvalues, α and $R_n^{\pm}$, are diagonal), we will see that the plateau is perhaps less natural. This is consistent with the analogy with the semi-classical periodic orbits, for which the plateau is non-perturbative. Note also that in gravity calculations, the plateau is much more difficult to obtain than the ramp; in JT gravity it arises from an infinite sum of wormhole geometries [106, 107]. We will now offer a few comments on the spectral decomposition of the plateau, leaving a full analysis for future work.

Self-correlations: First, we comment on the expected height of the plateau in a quantum chaotic system, and see how this is reproduced in our language with the fluctuating partition function $\widetilde{Z}_{\mathrm{P}}^{m}(y)$. Recall that the density of states for the fluctuating partition function is just the density of states for the dense spectrum minus its average, $\widetilde{\rho}_{\mathrm{P}}(E) = \rho_D(E) - \langle \rho_D(E) \rangle$. This means that the second and third terms in (3.5.1) have to do with the correlation of the fluctuating partition function. Thus the height of the plateau we expect from considering the fluctuating partition function is just that of a standard partition function (multiplied by $\frac{\sqrt{y_1 y_2}}{e^{\frac{\pi}{6}(y_1+y_2)}}$ from the definition of $\widetilde{Z}_{\mathrm{P}}$). Focusing on the second term in (3.5.1):

$$\begin{aligned}
\langle \widetilde{\rho}_{\mathrm{P}}^{m_1}(E_1) \widetilde{\rho}_{\mathrm{P}}^{m_2}(E_2) \rangle_{\text{plateau}} &= \langle \rho_D^{m}(E_1) \rangle \delta(E_1 - E_2) \delta_{m_1 m_2} \\
\Rightarrow \quad \langle \widetilde{Z}_{\mathrm{P}}^{m_1}(y_1)\, \widetilde{Z}_{\mathrm{P}}^{m_2}(y_2) \rangle_{\text{plateau}} &= \frac{\sqrt{y_1 y_2}}{e^{\frac{\pi}{6}(y_1+y_2)}} \langle Z_{\mathrm{P,D}}^{m_1}(y_1 + y_2) \rangle \delta_{m_1 m_2} \\
&\equiv \frac{\sqrt{y_1 y_2}}{e^{\frac{\pi}{6}(y_1+y_2)}}\, \delta_{m_1 m_2} \int_{E_{m_1}}^{\infty} dE\, \langle \rho_D^{m_1}(E) \rangle e^{-(y_1+y_2)E}\,,
\end{aligned} \tag{3.5.2}$$

[68] If we discuss multiple independent Hamiltonians, the self-correlations exist for identical matrices (tautologically) but are absent for distinct random matrices.

where $\langle \rho_D^m(E_1) \rangle$ is the average density of spin m Virasoro primaries.[69] Note that the plateau coefficient is given by $Z^m_{\mathrm{P,D}}$, which is *not* the modular invariant, fluctuating, dense partition function. It is just the standard partition function for the dense primaries of spin m; in particular it is not modular invariant.

By taking $y_i \to \infty$, we can estimate the plateau height:[70]

$$\left\langle \widetilde{Z}^m_{\mathrm{P}}(y_1) \widetilde{Z}^m_{\mathrm{P}}(y_2) \right\rangle_{\text{plateau}} \approx \langle \rho_D^m(E_m) \rangle \frac{\sqrt{y_1 y_2}}{y_1 + y_2} e^{-2\pi |m| (y_1 + y_2)} . \tag{3.5.4}$$

Comparing (3.5.4) to the ramp, we see that the ramp and plateau become equal to each other when $\sqrt{y_1 y_2} \sim T = \langle \rho_D^m(E_m) \rangle \equiv \Delta(E_m)^{-1}$, i.e., when at times of order the inverse mean-level spacing at threshold energy, as expected from general considerations.

Spectral decomposition: We can now analyze how the plateau appears in the Eisenstein series; the cusp forms come with new technical issues, and we relegate their discussion to appendix B.3.3. For the spin 0 case, we plug (3.5.4) into the usual integral transform (similar to (3.2.11)):

$$\left\langle z_{\frac{1}{2}+i\alpha_1} \, z_{\frac{1}{2}+i\alpha_2} \right\rangle_{\text{spin 0 plateau}} \approx 2i\pi^2 \langle \rho_D^0(E_0) \rangle \frac{1}{\sinh(\pi \alpha_1)} \delta(\alpha_1 + \alpha_2 - i) \, . \tag{3.5.5}$$

The most interesting feature of this expression is that it is not diagonal in α_i.[71]

[69] We use the average density from [61], given by

$$\langle \rho_D^m(E_1) \rangle \approx \frac{1}{2\pi} \frac{2}{1 + \delta_{m_1,0}} \frac{1}{\frac{E_1}{2\pi} + \frac{c}{12}} \exp\left\{ 2\pi \sqrt{\frac{c-1}{3} \left(\frac{E_1}{2\pi} + \frac{c}{12} \right)} \right\} . \tag{3.5.3}$$

[70] This is obtained via Laplace's method; the integral is dominated by the global maximum at $E_i = E_{m_i}$, as the local maximum for large y_i lies outside the region of integration as long as $y_1 + y_2 \gtrsim c \gg 1$.

[71] The appearance of unfamiliar delta function of a complex argument is due to our function space including functions that grow exponentially in y, see for example the discussion in [82].

For the spin $m_i > 0$ case, we find similarly:[72]

$$\langle z^{m_1}(\alpha_1) z^{m_2}(\alpha_2)\rangle_{\text{plateau}} \approx -4\pi^2 m \langle \rho_D^m(E_m)\rangle \times \mathcal{D}\left(\frac{1}{(\alpha_1-\alpha_2)^2} + \frac{1}{(\alpha_1+\alpha_2)^2}\right)\delta_{m_1 m_2} \quad (\alpha_i \to \infty) \tag{3.5.7}$$

Again, the correlations for the plateau in any spin sector are not diagonal (there is no delta-function imposing $\alpha_1 = \pm\alpha_2$). From the perspective of [78], this means the plateau does not come from the diagonal approximation analogous to the semi-classical periodic orbits, as one would expect.

Similar to our discussion of the ramp, we can ask if (3.5.7) should be improved by imposing a plateau consistently across all spin sectors. We leave such an analysis to the future, but discuss the question of the imprint of a plateau in a given spin sector onto other spin sectors, using numerical evidence, in appendix B.3.2.

[72] This should be understood as a distribution, i.e.,

$$\int \mathcal{D}\frac{1}{x^2}\phi(x) \equiv \int \frac{1}{x^2}\big(\phi(x) - \phi(0) - x\phi'(0)\big) = \int -\log|x|\phi''(x)\,. \tag{3.5.6}$$

Such a procedure is necessary as the Fourier transform of $|\xi|$ only makes sense as a distribution i.e. when integrated against test functions, and the resulting distribution cannot be defined without some method of regularizing the singularity at $\alpha_1 \pm \alpha_2 = 0$. The first method is by subtracting the first two terms in the Taylor series so that the singularity becomes removable; the second is to use integration by parts and discard boundary terms, which makes the singularity integrable.

Chapter 4

Reparametrization modes, shadow operators, and quantum chaos in higher-dimensional CFTs

4.1 Introduction

Chaos in dynamical systems is a crucial phenomenon explaining thermalization in many-body systems. There is a large number of manifestations of quantum and classical chaos, which can be roughly separated into early- and late-time characteristics. At long times the asymptotic approach to equilibrium is described in the framework of an effective field theory of the long-lived modes, hydrodynamics.

In this chapter we discuss some early-time manifestations of quantum chaos. The relevant phenomena are characterized by a so-called scrambling time of order the logarithm of the total number of degrees of freedom, and can be quantified by the exponential growth of certain out-of-time-order correlation functions (OTOCs) [16–19, 48, 108–111]. The associated growth rate is dubbed the Lypaunov exponent, which was shown to be bounded from above using only general principles of quantum field theory [48].

Thus, maximally chaotic theories are special. For example, theories dual to Einstein gravity are maximally chaotic, which leads to the intuition that a detailed understanding of maximal, or near-maximal chaos can perhaps be utilized to explain the emergence of a holographic dual to many-body strongly interacting systems.

Another, perhaps related, special property of maximally chaotic theories is the existence of an effective field theory of a single mode, sometimes referred to as the 'soft mode', the 'scramblon', or the 'reparametrization mode'. This is somewhat surprising since we are away from the long time limit justifying the use of the hydrodynamic effective description. Rather, the small parameter controlling the effective theory of the soft mode is the inverse of large number of degrees of freedom, which also controls the thermodynamic limit.

The first example of such an effective description is the Schwarzian theory, describing the low energy limit of the SYK model [17, 22], or the boundary dynamics of Jackiw-Teitelboim gravity [112–114]. Based on this example [53] suggested a general effective field theory description of maximal chaos in theories with conserved energy, by extrapolating hydrodynamics to the relevant short time regime. This description was named "quantum hydrodynamics" due to its formal similarity with classical hydrodynamics.

Given the success of the Schwarzian theory, reparametrization modes have also been used in two-dimensional CFTs for various applications such as conformal blocks [115, 116] and OTOCs (in thermal states) [88, 117]. While all these applications are clearly related to the physics of stress tensor conservation, a detailed understanding of this connection is missing. In this work we aim to explore the physics of reparametrization modes from the point of view of conformal representation theory, thus elucidating the connection between numerous different calculations in the literature. In order to uncover the general principles, it is convenient to work in an arbitrary number of (even) dimensions.

Summary. In this chapter we aim to provide a detailed understanding of the underlying physics of the reparametrization mode in CFTs. We clarify the connection with a number of other approaches to the computation and organization of conformal correlators. We argue that the reparametrization mode can be understood as a "longitudinal" (pure gauge) contribution to the *shadow operator associated with the stress tensor*. The shadow of the stress tensor is a formal operator of dimension 0, which allows for a convenient projection of correlation functions onto their contribution coming from exchanges of the stress tensor and its descendants alone [118, 119]. This connection explains why the reparametrization mode is useful for the computation of global or Virasoro conformal blocks.

We discuss two approaches to defining the soft mode in higher dimensional CFTs, and describe its quadratic action. The first relates the soft mode to the shadow of the energy momentum tensor, and the second defines it directly in terms of reparametrizations. The two approaches are shown to be equivalent, and generalize the Schwarzian in one dimension, and the Alekseev-Shatashvili action [115, 120] in two dimensions.

We then describe the coupling of the soft modes to external operators. In any CFT, the projection (fusion) of two primary probe operators into a stress tensor is described by the operator product expansion (OPE). The basic three-point fusion into a stress tensor is universally captured by the bilinear *stress tensor OPE blocks*. These operators, depending on two insertion points, have previously been studied in the context of *kinematic space*, where they appear naturally [121, 122]. We argue that they can be thought of as the "vertices" coupling reparametrization modes to external operators. In low dimensional examples, these vertices have previously been understood as reparametrized two-point functions.

We use our machinery to describe conformal blocks in arbitrary even dimensions. The basic ingredients we develop calculate simply the conformal partial waves, a certain combination of the stress energy block and its shadow. We argue that to isolate the physical block from its shadow, certain symmetries we call "conformal redundancies" need to be gauged. We demonstrate that this prescription give the correct answer in two dimensions, and make comments on those symmetries in higher dimensional CFTs.

Finally, we use our novel understanding of reparametrization modes and conformal kinematics to draw some conclusions about thermal physics in higher dimensions. Both a pole skipping analysis of energy-energy correlation functions, and the propagation of reparametrization modes between bilocal OPE block operators, lead us to a derivation of the Lyapunov exponent and butterfly velocity describing theories which exhibit maximal chaos in Rindler space. As in two dimensions, maximal chaos is, of course, not universal. Our analysis only captures the stress tensor contribution to the out of time order correlator. This establishes a connection between our consideration of conformal representation theory, and the "quantum hydrodynamic" description of maximally chaotic theories.

Outline. In §4.2 we study conformal kinematics as encoded in global conformal blocks and conformal partial waves. We provide a convenient reformulation of the shadow operator formalism for the stress tensor conformal block in terms of a vector mode with negative dimension, and use it to calculate the associated conformal partial wave in arbitrary even dimensions. We show in §4.3 that this negative dimension "shadow mode" can be understood as a reparametrization mode very similar to the one that occurs in the Schwarzian theory or two-dimensional CFTs. We derive a quadratic action for this mode from the conformal anomaly. We study the theory of reparametrizations in more detail for the case of two-dimensional theories in §4.4, with particular interest in the conformal map to the thermal cylinder.

In §4.5 we generalize this analysis to higher dimensions by mapping the Rindler wedge to a hyperbolic spacetime, thus creating a state with non-zero temperature. In §4.5.2 we demonstrate pole skipping of the energy-energy two-point function in CFTs in an arbitrary number of dimensions. The pole skipping location allows us to read off a maximal Lyapunov exponent $\lambda_L = \frac{2\pi}{\beta}$ and the Rindler space butterfly velocity $v_B = \frac{1}{d-1}$. We finish with comments and questions in §4.6.

4.2 Global conformal blocks and the shadow of the stress tensor

We begin our discussion with an exploration of global conformal blocks for CFTs in an arbitrary number of dimensions. Specifically, in this section we review and extend the kinematic space perspective on OPE blocks as bilocal operators. We offer a novel point of view on OPE blocks and conformal partial waves based on a reformulation of the shadow operator formalism. We will see that the shadow operators associated with conserved currents have special properties, which make them closely related to the reparametrization mode, i.e., the basic ingredient of the EFT of quantum chaos in the two-dimensional case [88, 115]. In the process we identify the soft mode in higher-dimensional CFTs and its coupling to matter (which is given by the OPE blocks). For the remainder of this section, we will work in Euclidean flat spacetime. The map to thermal physics in hyperbolic space and the relation with quantum chaos will be explored in subsequent sections.

4.2.1 Review of kinematic space and OPE blocks

We will be interested in the operator product expansion (OPE) of nearby operators. In order to efficiently organize the kinematic constraints that describe the universal aspects of the OPE in CFTs, it is useful to introduce the space on which pairs of operators live.

Kinematic space. One definition of the kinematic space $\mathcal{M}_\diamond^{(d)}$ of d-dimensional CFTs is as the space of pairs of either timelike or spacelike separated points. The former naturally define causal diamonds with a spherical base region, i.e. the intersection of the two points' light cones, so this space is clearly the same as the space of causal diamonds. A moment's thought reveals that this is in fact also isomorphic to the space of *spacelike* separated points, which define spacelike hyperbolas in one-to-one correspondence with causal diamonds.[73] More invariantly, we can define kinematic space as the coset

$$\mathcal{M}_{\Diamond}^{(d)} \equiv \frac{SO(2,d)}{SO(1,d-1)\times SO(1,1)}\,. \tag{4.2.1}$$

Here, $SO(2,d)$ is the conformal group in d spacetime dimensions. We mod out the group which leaves the objects in consideration invariant. For instance, in order to understand $\mathcal{M}_{\Diamond}^{(d)}$ as the space of codimension-2 spheres (i.e., causal diamonds), the coset should be understood as follows: The stabilizer of a given sphere consists of the group $SO(1,d-1)$ of rotations and special conformal transformations leaving the sphere on a fixed time slice invariant, as well as a group $SO(1,1)$ that corresponds to evolving the time slice along the conformal Killing flow inside the causal diamond. The resulting space is $2d$-dimensional with half of the directions being spacelike and the other half being timelike. For instance, in $d=2$, the above coset factors into two copies of de Sitter space $dS_2 \equiv SO(2,1)/SO(1,1)$. We refer the reader to [121, 122] for more extensive studies of this construction and the associated geometry.

For most of this chapter we will be working in Euclidean signature. In that case, the picture of kinematic space as the space of spacelike separated points is most natural, as it can easily be analytically continued. As a coset, we define the kinematic space of a Euclidean CFT as

$$\mathcal{M}_{\Diamond,E}^{(d)} \equiv \frac{SO(1,d+1)}{SO(1,d-1)\times SO(2)}\,, \tag{4.2.2}$$

with the stabilizer group corresponding to the subgroup leaving pairs of (Euclidean) points invariant under rotations, special conformal transformations, and the modular flow whose only two fixed points are the two points under consideration.[74] Most objects that we discuss in this chapter naturally live on the space (4.2.2).

OPE blocks as kinematic space operators. Consider now a Euclidean CFT. An immediate question about the space of pairs of points (x^μ, y^μ), is

[73] This is obvious in embedding space. See Appendix A.2 of [122] for details.

[74] The modular flow leaving two points (x^μ, y^μ) invariant is generated by the conformal Killing vector

$$K^\mu(x,y;\xi) = -\frac{2\pi}{(y-x)^2}\left[(y-\xi)^2(x^\mu-\xi^\mu)-(x-\xi)^2(y^\mu-\xi^\mu)\right]\,.$$

In Lorentzian or Euclidean signature, the conformal Killing vector looks identical, but the inner product is taken with either the Lorentzian or Euclidean metric.

whether there exist natural operators on this space, i.e., bilocal operators in the CFT. This is indeed the case, and we get an important hint from the operator product expansion (OPE) of two operators V, W. The latter can be written as a sum over conformal families of primary operators and their descendants, which V and W have non-trivial three-point overlap with. Schematically, we write as $x^\mu \to y^\mu$:

$$V(x)W(y) = \frac{1}{|x-y|^{\Delta_V+\Delta_W}} \sum_{\mathcal{O}} C_{VW\mathcal{O}}\, |x-y|^{\Delta} \left[\mathcal{O}(y) + \text{descendants}\right]. \tag{4.2.3}$$

In the following we will restrict to pairwise equal operators, $V = W$, for simplicity. Since we will eventually be interested in the OPE block associated with stress tensor exchanges, only identical external operators give a non-trivial result. We will refer to the sum over descendants as the *OPE block* $\mathfrak{B}_{\mathcal{O}}(x,y)$:

$$V(x)V(y) \equiv \frac{1}{|x-y|^{2\Delta_V}} \sum_{\mathcal{O}} C_{VV\mathcal{O}}\, \mathfrak{B}_{\mathcal{O}}(x,y). \tag{4.2.4}$$

The OPE is concerned with the limit $x^\mu \to y^\mu$. However, in abuse of language we will often refer to OPE blocks even if the two points (x^μ, y^μ) are not near each other. In fact, we will make more precise the fact that it is sensible and useful to study bilocal OPE blocks in the form of an integral over the associated conformal primary. We define:[75]

$$\mathfrak{B}_{\mathcal{O}}(x,y) \equiv \frac{k_{d-\Delta,\ell}}{\pi^{d/2} C_{\mathcal{O}}} \int d^d\xi\; I^{\mu_1\cdots\mu_\ell}_{VV\mathcal{O}}(x,y;\xi)\; \mathcal{O}_{\mu_1\cdots\mu_\ell}(\xi)\,, \tag{4.2.5}$$

where $C_{\mathcal{O}}$ is the coefficient in the two-point function of $\mathcal{O}$, Δ is its operator dimension, and

$$k_{\Delta,\ell} = \frac{\Gamma(\Delta-1)}{\Gamma(\Delta+\ell-1)} \frac{\Gamma(d-\Delta+\ell)}{\Gamma(\Delta-\frac{d}{2})} \tag{4.2.6}$$

is a normalization factor.[76] The constant in (4.2.5) is chosen to give a convenient normalization (c.f., [121]). The kernel is determined by conformal

[75]Eq. (4.2.5) is written with Euclidean signature in mind, where the integration region is all of $\mathbb{R}^d$ (see Appendix C.1 for details about this notation). A natural Lorentzian generalization, appropriate for studying the OPE with x^μ and y^μ timelike separated, involves integration over the causal diamond defined by x^μ and y^μ. However, in order to avoid subtleties regarding convergence and making the expression well-defined, we leave the interesting Lorentzian case for future work.

[76]Note in particular the stress tensor case: $k_{d,2} = [d(d-1)\Gamma(d/2)]^{-1}$ and $k_{0,2} = -(-)^{d/2}\Gamma(d+2)\Gamma(\frac{d}{2}+1)$.

symmetry, and can be thought of as a normalized three-point function between VV, and an auxiliary operator $\widetilde{\mathcal{O}}$ with dimension $\widetilde{\Delta} = d - \Delta$:

$$I^{\mu_1 \cdots \mu_\ell}_{VV\mathcal{O}}(x, y; \xi) = \frac{1}{C_{VV\mathcal{O}}} \frac{\langle V(x)V(y)\widetilde{\mathcal{O}}^{\mu_1 \cdots \mu_\ell}(\xi)\rangle}{\langle V(x)V(y)\rangle}\,, \tag{4.2.7}$$

which is independent of the operator V and OPE coefficient $C_{VV\mathcal{O}}$. The operator $\widetilde{\mathcal{O}}$ is known as the *shadow* of $\mathcal{O}$. One of the insights of [121, 122] was the realization that the sum over descendants in the OPE (4.2.4) is in fact equivalent to the integral (4.2.5). We will derive this below using related methods.

Despite our preference for the Euclidean setup, the smeared representation of the OPE block still has to be enjoyed with care (similarly for the Lorentzian OPE with spacelike separated points). Since we take the integral in (4.2.5) to cover all of Euclidean spacetime, we are making a subtle mistake: we include contributions for which the $V \times V$ OPE in $\langle V(x)V(y)\widetilde{\mathcal{O}}(\xi)\rangle$ appearing in the kernel (4.2.7) is not valid! For instance, in radial quantization, a more careful analysis would require $|\xi| > |x|, |y|$. It was understood in [119] that the effect of this carelessness is that the OPE block computed as in (4.2.5) will end up being contaminated by certain unphysical *shadow contributions* that need to be projected out. These shadow contributions are almost as desired (they have the same conformal properties as the actual physical OPE block, including the same eigenvalue under the conformal Casimir), if it weren't for unphysical short distance behavior. Instead of doing the conformal integrals more carefully, we will therefore have to deal with the task of projecting out shadow contributions at the end of various computations. We will discuss this projection and its physical interpretation in more detail in the following.

4.2.2 Conformal blocks, shadow blocks, and partial waves

The integral representation of the OPE blocks can be used to decompose four-point functions into more primitive building blocks. Consider the Euclidean four-point function of two pairs of operators, V and W. Using the OPE (4.2.3) for VV and for WW, the four-point function decomposes into *conformal blocks* $G^{(\ell)}_{\Delta}$ associated with the exchange of different primary operators $\mathcal{O}$ and their descendants:

$$\langle V(x_1)V(x_2)W(x_3)W(x_4)\rangle = \frac{1}{x_{12}^{2\Delta_V} x_{34}^{2\Delta_W}} \sum_{\mathcal{O}} C_{VV\mathcal{O}}\, C_{WW\mathcal{O}}\, G^{(\ell)}_{\Delta}(u, v)\,, \tag{4.2.8}$$

where (Δ, ℓ) are the dimension and spin of the internal operator $\mathcal{O}$ and $x_{ij} \equiv x_i - x_j$. In the following we will drop the i subscript. The conformal block is a purely kinematical object and only depends on the conformally invariant cross ratios

$$u = \frac{x_{12}^2 x_{34}^2}{x_{13}^2 x_{24}^2}\,, \qquad v = \frac{x_{14}^2 x_{23}^2}{x_{13}^2 x_{24}^2}\,. \tag{4.2.9}$$

In terms of OPE blocks, we can write the conformal block associated with exchanges of global conformal descendants as a two-point function of bilinears:

$$G_\Delta^{(\ell)}(u,v) = \langle \mathfrak{B}_\mathcal{O}(x_1,x_2)\, \mathfrak{B}_\mathcal{O}(x_3,x_4)\rangle_{\text{phys.}} \tag{4.2.10}$$

where the subscript "phys." indicates that we need to project out the shadow contributions mentioned at the end of the previous section (see below for details). Apart from being manifestly conformally invariant, the conformal blocks have other defining features. They are eigenfunctions of the $SO(2,d)$ conformal Casimir operator $\mathcal{C}_2 = L_{AB}L^{AB}$ with eigenvalue $-C_{\Delta,\ell} = \Delta(d-\Delta) - \ell(\ell+d-2)$. Below we will be interested in the block associated with the stress tensor, where $C_{d,2} = 2d$. In terms of the cross ratios (u,v) the Casimir reads

$$\begin{aligned} \frac{1}{2}\,\mathcal{C}^2 = \big(u(1+v) - (1-v)^2\big)\partial_v\, v\,\partial_v - (1-u+v)u\,\partial_u\, u\,\partial_u \\ +2(1+u-v)uv\,\partial_u\partial_v + d\,u\,\partial_u\,. \end{aligned} \tag{4.2.11}$$

Note that the shadow of a primary $\mathcal{O}$ has a conformal block associated with it, which shares the same eigenvalue $C_{\widetilde{\Delta},\ell} = C_{\Delta,\ell}$. We will refer to this object as the *shadow block* associated with the auxiliary operator $\widetilde{\mathcal{O}}$, and denote it as $G^{(\ell)}_{d-\Delta}$.

Conformal partial waves. More explicitly, we can write an integral representation of the shadow operator associated with a symmetric-traceless operator $\mathcal{O}$ [118, 119]:

$$\widetilde{\mathcal{O}}^{\mu_1\cdots\mu_\ell}(x) \equiv \frac{k_{\Delta,\ell}}{\pi^{d/2}} \int d^d y\; \frac{\prod_{i=1}^{\ell}\big(\delta^{\mu_i\nu_i}(x-y)^2 - 2(x-y)^{\mu_i}(x-y)^{\nu_i}\big)}{\big((x-y)^2\big)^{d-\Delta+\ell}}\; \mathcal{O}_{\nu_1\cdots\nu_\ell}(y) \tag{4.2.12}$$

where we take the normalization from [118] such that the operation of forming the shadow squares to the identity ($\widetilde{\widetilde{\mathcal{O}}} = \mathcal{O}$).

The shadow block is simply the conformal block associated with the shadow operator. Both the shadow operator and its block are usually not physical. They present formal tools that are useful for computations. In order to get physical results, one needs to make sure to project out shadow contributions at the end of calculations.

For our purposes it will often be convenient to consider a particular linear combination of block and shadow block. We will refer to this as the (normalized) *conformal partial wave (CPW)* and define it as

$$f_\Delta^{(\ell)}(u,v) \equiv \frac{1}{k_{d-\Delta,\ell}} \frac{\Gamma(\frac{\Delta+\ell}{2})^2}{\Gamma(\frac{d-\Delta+\ell}{2})^2}\, G_\Delta^{(\ell)}(u,v) + \frac{1}{k_{\Delta,\ell}} \frac{\Gamma(\frac{d-\Delta+\ell}{2})^2}{\Gamma(\frac{\Delta+\ell}{2})^2}\, G_{d-\Delta}^{(\ell)}(u,v)\,. \tag{4.2.13}$$

Both terms in $f_\Delta^{(\ell)}$ are conformally invariant and eigenfunctions of the Casimir with eigenvalue $C_{\Delta,\ell}$. They are distinguished by their short distance behavior:

$$G_\Delta^{(\ell)} \overset{u\to 0,\, v\to 1}{\sim} u^{\frac{\Delta-\ell}{2}}(1-v)^\ell + \ldots \qquad\qquad G_{d-\Delta}^{(\ell)} \overset{u\to 0,\, v\to 1}{\sim} u^{\frac{d-\Delta-\ell}{2}}(1-v)^\ell + \ldots \tag{4.2.14}$$

The advantage of the conformal partial wave combination is that it is single-valued and arises naturally in computations in the shadow formalism. Indeed, the two-point function $\langle \mathfrak{B}_\mathcal{O}(x_1,x_2)\,\mathfrak{B}_\mathcal{O}(x_3,x_4)\rangle$ before projection is proportional to the CPW $f_\Delta^{(\ell)}$. The projection onto the physical block in (4.2.10) corresponds to dropping the shadow block which has the wrong short distance behavior.

To summarize, conformal blocks are two-point functions of bilinear blocks $\mathfrak{B}_\mathcal{O}(x,y)$. These are global blocks in the sense that they correspond to a single stress tensor exchange. We discuss corrections to this leading answer later on. If we work in Euclidean signature, a monodromy projection onto the physical block is always necessary. At the level of the conformal blocks, this can be implemented as explained in [119] by simply projecting onto the conformally invariant part of $f_\Delta^{(\ell)}$ with the correct monodromy.

The stress tensor block. In this chapter we mainly study OPE blocks of the stress tensor (see however §4.2.5 for more general conserved currents). In this case, the shadow of the stress tensor is a fiducial operator with spin 2 and dimension $\widetilde{\Delta}_T = d - \Delta_T = 0$.

The block associated with stress tensor exchanges will simply be written as $G_d^{(2)}(u,v)$. In terms of the OPE blocks, we can write the contribution from the stress tensor and its descendants to the four-point function as

$$\langle V(x_1)V(x_2)W(x_3)W(x_4)\rangle\big|_T = \frac{C_{VVT}C_{WWT}}{x_{12}^{2\Delta_V}\,x_{34}^{2\Delta_W}}\,\big\langle \mathfrak{B}_T(x_1,x_2)\,\mathfrak{B}_T(x_3,x_4)\big\rangle_{\text{phys.}} \tag{4.2.15}$$

If we compute this two-point function of bilinears without doing the projection onto the physical part, we would again find a combination of the identity block and its shadow proportional to (4.2.13).

4.2.3 A reformulation of the shadow operator formalism

We will now explain our main results regarding a novel formulation of the shadow operator formalism for the global stress tensor block. The main technical observation will be the fact that the shadow of the stress tensor (which has vanishing conformal dimension) formally can be written as the descendant of a vector with dimension minus one. Subsequently we give an alternative interpretation of the vector as a "soft" diffeomorphism mode.

The stress tensor shadow as a total derivative. Consider the shadow of the stress tensor:

$$\widetilde{T}^{\mu\nu}(x) \equiv \frac{k_{d,2}}{\pi^{d/2}} \int d^d\xi \; I^{\mu\rho}(x-\xi)\; I^{\nu\sigma}(x-\xi)\; T_{\rho\sigma}(\xi)\,, \tag{4.2.16}$$

where $I^{\mu\rho}(x) \equiv \eta^{\mu\rho} - \frac{2}{x^2}\, x^\mu x^\rho$ is the inversion tensor. We observe that the operator $\widetilde{T}^{\mu\nu}$ can formally be written as a symmetric-traceless derivative:[77]

$$\boxed{\begin{aligned} \widetilde{T}_{\mu\nu}(x) &\equiv 2C_T\, \frac{\pi^{d/2}}{k_{0,2}}\, \mathbb{P}^{\;\rho\sigma}_{\mu\nu}\; \partial_\rho \mathcal{E}_\sigma(x)\,, \\ \mathcal{E}_\sigma(x) &= \frac{1}{2C_T}\frac{k_{0,2}k_{d,2}}{\pi^d} \int d^d\xi\; (x-\xi)^\alpha\, I^{\beta}_{\sigma}(x-\xi)\, T_{\alpha\beta}(\xi)\,, \end{aligned}} \tag{4.2.17}$$

where we employ the symmetric-traceless projector

$$\mathbb{P}^{\;\rho\sigma}_{\mu\nu} = \frac{1}{2}\left(\delta^\rho_\mu \delta^\sigma_\nu + \delta^\rho_\nu \delta^\sigma_\mu\right) - \frac{1}{d}\,\eta_{\mu\nu}\,\eta^{\rho\sigma}\,. \tag{4.2.18}$$

In other words, we formally write the stress tensor shadow as the descendent of a fiducial vector field with dimension $\Delta_{\mathcal{E}} = -1$ and spin $\ell_{\mathcal{E}} = 1$. Our main task will be to study this mode in its own right. As we will argue, it allows for a useful reformulation of the technology we have described so far, and it relates it to an effective field theory of reparametrizations.

Eq. (4.2.17) provides a nonlocal definition of $\mathcal{E}_\mu(x)$ in terms of the stress tensor. However, we would like to establish a local propagator for this mode.

[77] See also (C.1.3) for useful relevant identities and p. 194 of [123] for a more abstract way of writing this expression. The normalization in (4.2.17) is chosen for later convenience.

This can be achieved by observing that the two-point function $\langle \widetilde{T}_{\mu\nu}\widetilde{T}_{\rho\sigma}\rangle$ can be written as a total derivative in much the same spirit as $\widetilde{T}_{\mu\nu}$ itself: by conformal invariance, we have[78]

$$\begin{aligned}\langle \widetilde{T}_{\mu\nu}(x)\widetilde{T}_{\rho\sigma}(y)\rangle &= 2C_T\,\frac{k_{d,2}}{k_{0,2}}\,\mathbb{P}^{\alpha\gamma}_{\mu\nu}\,\mathbb{P}^{\beta\delta}_{\rho\sigma}\,I_{\alpha\beta}(x-y)I_{\gamma\delta}(x-y)\\ &= -C_T\,\frac{k_{d,2}}{k_{0,2}}\,\mathbb{P}^{\alpha\gamma}_{\mu\nu}\,\mathbb{P}^{\beta\delta}_{\rho\sigma}\,\partial^{(x)}_{\gamma}\partial^{(y)}_{\delta}\left[I_{\alpha\beta}(x-y)\,(x-y)^2\,\log\left(\mu^2(x-y)^2\right)\right]\,.\end{aligned} \tag{4.2.19}$$

We interpret the expression in square brackets as the two-point function of $\mathcal{E}_\mu$:

$$\langle \widetilde{T}_{\mu\nu}(x)\widetilde{T}_{\rho\sigma}(y)\rangle = 4C_T^2\,\frac{\pi^d}{k_{0,2}^2}\,\mathbb{P}^{\alpha\gamma}_{\mu\nu}\,\mathbb{P}^{\beta\delta}_{\rho\sigma}\,\partial^{(x)}_{\gamma}\partial^{(y)}_{\delta}\langle\mathcal{E}_\alpha(x)\,\mathcal{E}_\beta(y)\rangle \tag{4.2.20}$$

where we defined the "logarithmic" two-point function of the *stress tensor shadow mode* $\mathcal{E}_\mu$ as

$$\boxed{\langle\mathcal{E}_\alpha(x)\mathcal{E}_\beta(y)\rangle = -\frac{1}{C_T}\,\frac{k_{0,2}k_{d,2}}{4\pi^d}\,I_{\alpha\beta}(x-y)\,(x-y)^2\,\log\left[\mu^2\,(x-y)^2\right]} \tag{4.2.21}$$

Here, μ^2 is an energy scale that we need to introduce to write a sensible expression. Note that this scale drops out after taking the symmetric-traceless derivatives – formally it is an ambiguity in writing the above expression as a derivative. Similarly, any rescaling of the arbitrary scale μ^2 results in the addition of analytic terms to the propagator, which drop out in physical quantities. We can view it as a hint that this theory is secretly a theory of the conformal anomaly. This connection will be made more precise in §4.3.1.[79]

Except for this arbitrary scale, one can write other ambiguity terms that leave (4.2.19) invariant, such as constant shifts of the propagator proportional to the inversion tensor $I_{\alpha\beta}$. These will turn out to be irrelevant for the physics we discuss.

[78] We use a convention where

$$\langle T_{\mu\nu}(x)T_{\rho\sigma}(y)\rangle = 2C_T\,\mathbb{P}^{\alpha\gamma}_{\mu\nu}\,\mathbb{P}^{\beta\delta}_{\rho\sigma}\,I_{\alpha\beta}(x-y)I_{\gamma\delta}(x-y)\frac{1}{(x-y)^{2d}}\,.$$

[79] The necessity of introducing such a scale is also reminiscent of logarithmic conformal field theory [124–126]: our field $\mathcal{E}_\mu$ looks much like a logarithmic primary. We thank D. Grumiller for pointing this out and note that it would be interesting to explore this further.

Coupling to external operators. With the propagator (4.2.21) at hand, we now need to understand the coupling to external probe operators. To this end, we observe that $\widetilde{T}_{\mu\nu}$ acts as a source for $T^{\mu\nu}$. We can thus use it to write the following dimensionless projector onto the conformal family of the stress tensor [119]:

$$\begin{aligned} |\widetilde{T}| &\equiv \frac{1}{2C_T}\frac{k_{0,2}}{\pi^{d/2}}\int d^d\xi\; \widetilde{T}_{\mu\nu}(\xi)\,|0\rangle\langle 0|\,T^{\mu\nu}(\xi) \\ &= -\int d^d\xi\;\left\{\frac{1}{d}\,\partial_\rho\mathcal{E}^\rho(\xi)\,|0\rangle\langle 0|T^\mu_\mu(\xi) + \mathcal{E}_\nu(\xi)\,|0\rangle\langle 0|\,\partial_\mu T^{\mu\nu}(\xi)\right\} \end{aligned} \tag{4.2.22}$$

where we used (4.2.17) and integrated by parts the second term. We similarly define the projector $|T|$ such that we have the following properties: (i) the projector is invariant under taking its shadow, $|\widetilde{T}| = |T|$; (ii) it squares to itself, $|T|^2 = |T|$; and (iii) the insertion into correlation functions involving other stress tensors is trivial, $\langle T(x)\ldots\rangle = \langle T(x)|T|\cdots\rangle$. A few more details about these properties are given in Appendix C.1.

The stress tensor OPE block follows from applying this projector to a state associated with the insertion of a pair of external primaries V:

$$\begin{aligned} |\widetilde{T}|V(x)V(y)\rangle = -\int d^d\xi\,\Big\{\frac{1}{d}\,|\partial_\rho\mathcal{E}^\rho(\xi)\rangle\langle T^\mu_\mu(\xi)V(x)V(y)\rangle \\ + |\mathcal{E}_\nu(\xi)\rangle\,\partial_\mu\langle T^{\mu\nu}(\xi)V(x)V(y)\rangle\Big\} \\ \equiv \langle V(x)V(y)\rangle \times |\mathcal{B}^{(1)}_{\mathcal{E},V}(x,y)\rangle\,, \end{aligned} \tag{4.2.23}$$

which defines the normalized bilinear $\mathcal{B}^{(1)}_{\mathcal{E},V}(x,y)$ that describes the coupling of $\mathcal{E}^\mu$ to a bilinear pair of primaries. We have factored out normalization factors in order to conform with conventions in lower dimensions. The conformal Ward identity determines the divergence and the trace of the three-point function $\langle T^{\mu\nu}(\xi)\,V(x)V(y)\rangle$, which is nonzero due to contact terms. These can be parameterized as (see, for example, [123])[80]

$$\begin{aligned}\langle T^\mu_\mu(\xi)V(x)V(y)\rangle &= -\Delta_V\,\left[\delta^{(d)}(\xi-x)+\delta^{(d)}(\xi-y)\right]\,\langle V(x)V(y)\rangle\,,\\ \partial_\mu\langle T^{\mu\nu}(\xi)\,V(x)V(y)\rangle &= -\left[\delta^{(d)}(\xi-x)\,\partial^\nu_{(x)}+\delta^{(d)}(\xi-y)\,\partial^\nu_{(y)}\right]\,\langle V(x)V(y)\rangle\,.\end{aligned} \tag{4.2.25}$$

Plugging into (4.2.23) gives

$$\begin{aligned}|\mathcal{B}^{(1)}_{\mathcal{E},V}(x,y)\rangle = \frac{1}{\langle V(x)V(y)\rangle}\,&\left\{\frac{\Delta_V}{d}\,|\partial_\rho\mathcal{E}^\rho(x)+\partial_\rho\mathcal{E}^\rho(y)\rangle\langle V(x)V(y)\rangle\right.\\ &\left.+\Big(|\mathcal{E}_\nu(x)\rangle\,\partial^\nu_{(x)}+|\mathcal{E}_\nu(y)\rangle\,\partial^\nu_{(y)}\Big)\langle V(x)V(y)\rangle\right\}\end{aligned} \tag{4.2.26}$$

Using the explicit form of the scalar two-point function, $\langle V(x)V(y)\rangle \propto (x-y)^{-2\Delta_V}$, we immediately obtain the bilinear coupling (which we now write as an operator identity):

$$\boxed{\mathcal{B}^{(1)}_{\mathcal{E},V}(x,y) = \Delta_V\,\left\{\frac{1}{d}\left(\partial_\mu\mathcal{E}^\mu(x)+\partial_\mu\mathcal{E}^\mu(y)\right)-2\,\frac{(\mathcal{E}(x)-\mathcal{E}(y))^\mu\,(x-y)_\mu}{(x-y)^2}\right\}} \tag{4.2.27}$$

Note that the only way $\mathcal{B}^{(1)}_{\mathcal{E},V}(x,y)$ depends on the operator V is through an overall factor Δ_V. We decide to keep this factor as part of the definition of the bilocal.

Our proposal is that this bilinear of local fields $\mathcal{E}^\mu(x)$ is identical to the stress tensor OPE block:[81]

$$\boxed{\mathcal{B}^{(1)}_{\mathcal{E},V}(x,y) = C_{VVT}\;\mathfrak{B}_T(x,y).} \tag{4.2.28}$$

[80]There are well known ambiguities in the parametrization of these anomalies. Another common parametrization is [127]:

$$\begin{aligned}\langle T^\mu_\mu(\xi)V(x)V(y)\rangle &= 0\,,\\ \partial_\mu\langle T^{\mu\nu}(\xi)\,V(x)V(y)\rangle &= -\left[\delta^{(d)}(\xi-x)\,\partial^\nu_{(x)}+\delta^{(d)}(\xi-y)\,\partial^\nu_{(y)}\right]\,\langle V(x)V(y)\rangle\\ &\quad+\frac{\Delta_V}{d}\partial^\nu_{(\xi)}\left[\delta^{(d)}(\xi-x)+\delta^{(d)}(\xi-y)\right]\,\langle V(x)V(y)\rangle\,.\end{aligned} \tag{4.2.24}$$

Plugging this into (4.2.23) gives the same result (4.2.27).

[81]Note that the OPE coefficient C_{VVT} is fixed by the conformal Ward identity: $C_{VVT} = \frac{\Delta_V\,d\,\Gamma(\frac{d}{2})}{\pi^{d/2}(d-1)}$.

Both objects are bilinear operators. The l.h.s. contains local insertions of $\mathcal{E}^\mu$; we think of it as the vertex coupling bilinear operators to the mode $\mathcal{E}_\mu$. The r.h.s. is the OPE block (i.e., a nonlocal smearing of the stress tensor). In order to make sense of this equation, one needs to know the propagator of $\mathcal{E}^\mu$, which we provided in (4.2.21). Inside correlation functions, one can then check the identity.

Application to four-point functions. We can also use the shadow operator formalism directly in correlation functions to derive the bilinear couplings of the mode $\mathcal{E}^\mu$. To this end, we insert both of the projectors $|T|$ and $|\widetilde{T}|$ in a four-point function:

$$\begin{aligned}\langle V(x_1)V(x_2)W(x_3)W(x_4)\rangle &= \langle V(x_1)V(x_2)|T|\widetilde{T}|W(x_3)W(x_4)\rangle_{\text{phys.}} \\ &= \frac{1}{4C_T^2}\frac{k_{0,2}^2}{\pi^d}\iint d^d\xi\, d^d\xi'\ \langle V(x_1)V(x_2)T^{\mu\nu}(\xi)\rangle\langle\widetilde{T}_{\mu\nu}(\xi)\widetilde{T}_{\rho\sigma}(\xi')\rangle \\ &\qquad\qquad \langle T^{\rho\sigma}(\xi')W(x_3)W(x_4)\rangle_{\text{phys.}}\end{aligned} \tag{4.2.29}$$

Writing both instances of $\widetilde{T}$ as descendants of $\mathcal{E}$, we can then follow a similar procedure as in the previous paragraph: we integrate both derivatives by parts and use the conformal Ward identity (4.2.25) twice to localize the integrals. As a result, the above expression reduces to a two-point function of bilinears:

$$\langle V(x_1)V(x_2)W(x_3)W(x_4)\rangle\big|_T = \langle VV\rangle\langle WW\rangle \times \langle\mathcal{B}^{(1)}_{\mathcal{E},V}(x_1,x_2)\mathcal{B}^{(1)}_{\mathcal{E},W}(x_3,x_4)\rangle_{\text{phys.}} \tag{4.2.30}$$

This shows very directly that the global stress tensor block should be computed by the two-point function of $\mathcal{B}^{(1)}_{\mathcal{E},V}$, which is just a simple linear combination of $\mathcal{E}$-propagators. By comparing with (4.2.15) we also verify (4.2.28). We will now investigate these claims in more detail.

4.2.4 Conformal partial waves in arbitrary even dimensions

As the most immediate application of our reformulation of the shadow operator formalism, we will now illustrate how to compute global conformal blocks. We already know from (4.2.10) that these should be computed by two-point functions of OPE blocks. Note that we will work in Euclidean signature, so we expect to find conformal partial waves.

Let us compute the two-point function of bilinears, using the "vertices" (4.2.27) and the propagator (4.2.21). No conformal integrals need to be done. The calculation simply consists of taking a linear combination of the $\mathcal{E}^\mu$-propagator and its derivatives. This straightforward calculation yields:

$$\boxed{\left\langle \mathcal{B}^{(1)}_{\mathcal{E},V}(x_1,x_2)\,\mathcal{B}^{(1)}_{\mathcal{E},W}(x_3,x_4)\right\rangle = -\frac{8\Delta_V\Delta_W}{C_T}\,\frac{k_{0,2}k_{d,2}}{4\pi^d}\left(\frac{4}{d}+\frac{1-v}{u}\,\log v\right)} \tag{4.2.31}$$

which is written in terms of the cross ratios (4.2.9). *We claim that* (4.2.31) *is proportional to the global stress tensor conformal partial wave $f^{(\ell=2)}_{\Delta=d}$ in arbitrary even dimension.* In odd dimensions (4.2.31) corresponds to just the shadow block. We will later see in more detail why a soft mode theory of physical conformal blocks is difficult to obtain in odd dimensions. Note that (4.2.31) is simpler than perhaps expected. Let us therefore understand it in more detail.

As a first consistency check, note that (4.2.31) is an eigenfunction of the Casimir (4.2.11) with eigenvalue $-2d$, as expected for any linear combination of stress tensor block and shadow block. Note further that (4.2.31) is not just any such linear combination but a very particular one which has the feature that it is single-valued (since $0<u,v<1$).

Comparison with known blocks in even dimensions. Let us now compare with known results for global conformal partial waves in various dimensions, distinguishing even and odd dimensions. For even dimensions, these were computed in [118, 128] for more general situations (arbitrary internal and external operators) in terms of hypergeometric functions. Note that these objects are increasingly complicated in higher dimensions. Closed form expressions are available in $d=2,4,6$ in [128]. In the special case of the stress tensor block for pairwise equal external operators, their results are indeed proportional to (4.2.31). For instance, in $d=2,4$ the blocks and shadow blocks associated with stress tensor exchanges between pairwise equal primary operators take the following form (the case of $d = 6$ is similar):

$$
\begin{aligned}
&\triangleright\ d=2: \text{ physical block:} \quad G_2^{(2)} = 3\left[\frac{z-2}{z}\log(1-z)-2\right]+\text{c.c.}\\
&\qquad\qquad\ \ \text{shadow block:} \quad G_0^{(2)} = \frac{1}{4}\left[\frac{z-2}{z}\log(1-\bar{z})\right]+\text{c.c.}\\
&\triangleright\ d=4: \text{ physical block:} \quad G_4^{(2)} = 10\left[-\frac{\bar{z}}{z}\,\frac{z^2-6z+6}{(z-\bar{z})}\log(1-z)+3\right]+\text{c.c.}\\
&\qquad\qquad\ \ \text{shadow block:} \quad G_0^{(2)} = \frac{1}{18}\left[\frac{\bar{z}}{z}\,\frac{z^2-6z+6}{(z-\bar{z})}\log(1-\bar{z})\right]+\text{c.c.}
\end{aligned}
\tag{4.2.32}
$$

where $u \equiv z\bar{z}$ and $v \equiv (1-z)(1-\bar{z})$ and "*c.c.*" denotes complex conjugation (recall that in Euclidean signature, $\bar{z} \equiv z^*$). One can readily verify the short distance behavior (4.2.14) and the fact that the CPW (4.2.13) is proportional to (4.2.31).

Compared to the very complicated and strongly dimension-dependent general results of [118], our expression (4.2.31) for the stress tensor CPW is remarkably simple. This simplicity of the stress tensor partial wave – and the existence of a simple expression that is valid in any dimension – is a new result as far as we are aware.

4.2.5 Generalization: conserved currents with higher spin

Our discussion focuses on the OPE block associated with the stress tensor. While it is unclear how to generalize it to OPE blocks of arbitrary internal primaries, the generalization to conserved currents is straightforward. Consider a symmetric-traceless conserved current $J_{\mu_1\cdots\mu_\ell}$ (i.e., $\Delta_J = d+\ell-2$). Its shadow is

$$
\widetilde{J}^{\mu_1\cdots\mu_\ell}(x) \equiv \frac{k_{\Delta_J,\ell}}{\pi^{d/2}}\int d^d\xi\ \frac{1}{(x-\xi)^{2(2-\ell)}}\left(\prod_{i=1}^{\ell} I^{\mu_i\nu_i}(x-\xi)\right) J_{\nu_1\cdots\nu_\ell}(\xi)\,,
\tag{4.2.33}
$$

where the product of inversion tensors is understood to inherit symmetries and tracelessness from contraction with the current. As one easily verifies, this can be written as a symmetric-traceless derivative:

$$\widetilde{J}_{\mu_1\cdots\mu_\ell} = \frac{k_{\Delta_J,\ell}}{\pi^{d/2}} \left(\partial_{(\mu_1}\mathcal{E}^{(J)}_{\mu_2\cdots\mu_\ell)} - \text{traces}\right) ,$$
$$\text{where} \quad \mathcal{E}^{(J)}_{\mu_2\cdots\mu_\ell}(x) = \int d^d\xi \, \frac{(x-\xi)^{\nu_1}}{(x-\xi)^{2(2-\ell)}} \left(\prod_{i=2}^{\ell} I^{\nu_i}_{\mu_i}(x-\xi)\right) J_{\nu_1\cdots\nu_\ell}(\xi)\,. \tag{4.2.34}$$

where the bracket around indices means complete symmetrization, and we subtract traces such as to obtain an object that is traceless in any two indices.

Starting from the observation that the shadow of any symmetric-traceless conserved current can be written as a descendant of some fiducial field $\mathcal{E}^{(J)}$ with $(\Delta_{\mathcal{E}^{(J)}}, \ell_{\mathcal{E}^{(J)}}) = (1-\ell_J, \ell_J - 1)$, one could formulate a theory similar to the one for our reparametrization mode. Note that this can be thought of as taking a result of [122] to the next level: there it was observed that the smeared representation of OPE blocks for conserved currents localizes onto just a time slice of the full causal diamond. Our result shows that the OPE blocks for conserved currents allow for an even more local description: they can be computed in terms of reparametrization modes (or other symmetry generating modes), which completely localize to the two insertion points of the original operators in the OPE. In other words, the computation of global conformal blocks in these cases reduces to evaluating a local exchange diagram of symmetry generating modes $\mathcal{E}^{(J)}_{\mu_2\cdots\mu_\ell}$. This makes the evaluation of any conformal integrals unnecessary and should simplify various calculations in the literature.

We will not pursue this more general case further. For clarity of presentation, we have only discussed the stress tensor case with $\ell = 2$. However, from (4.2.34) it is clear that it should be possible to generalize our entire discussion to conserved currents with higher spin. It would be interesting to see if a simple expression for the associated conformal partial waves in arbitrary dimension can be obtained, analogous to (4.2.31).

4.3 A theory of reparametrization modes in higher dimensions

We have identified a soft mode $\mathcal{E}_\mu$ in higher dimensional CFT, and its coupling to matter. These ingredients are related to the shadow of the energy momentum operator in the manner described, and were sufficient to elucidate the connection between propagation of the soft mode between bilinear operators and the computation of global conformal blocks or conformal partial waves.

We will now explore further the observation that the soft mode can equivalently be understood as a reparametrization mode that sources the stress tensor. Using this insight, in this section we take preliminary steps towards writing an effective action for this mode which reproduces the above results. Specifically, we will discuss the linearized action, which is sufficient to reproduce the above results.

4.3.1 Effective action from the conformal Ward identity

Consider an infinitesimal reparametrization $x^\mu \to x^\mu + \epsilon^\mu(x)$ which provides a source for the stress tensor via $\delta g_{\mu\nu} = -(\partial_\mu \epsilon_\nu + \partial_\nu \epsilon_\mu) \equiv -2\partial_{(\mu}\epsilon_{\nu)}$. In the special case where $\epsilon^\mu(x)$ is a conformal Killing vector, we can subsequently perform a conformal transformation to remove this source. In order to make this manifest, we work with the source $\delta' g_{\mu\nu} = -2\partial_{(\mu}\epsilon_{\nu)} + \frac{2}{d}\,\eta_{\mu\nu}(\partial.\epsilon)$, where $\partial.\epsilon \equiv \partial_\sigma \epsilon^\sigma$, which vanishes on conformal transformations. Of course, we recognize this combination as being of exactly the same form as the shadow of the stress tensor, see (4.2.17). But now, we wish to study the dynamics of the *reparametrization mode* $\epsilon^\mu(x)$ by thinking of it as a source for the stress tensor in the spirit of effective field theory. To this end, we work with the connected generating functional $W[\epsilon]$, which is defined in terms of the partition function of the Euclidean CFT, $Z_0 = \int [d\Phi]\, e^{-S_{CFT}}$, as

$$e^{-W[\epsilon]} = \frac{1}{Z_0} \int [d\Phi]\, e^{-S_{CFT} - \int \frac{1}{2}\,\delta' g_{\mu\nu} T^{\mu\nu}}\,. \tag{4.3.1}$$

Let us use a convention where $T^{\mu\nu}$ is traceless and symmetric. The quadratic action for the reparametrization mode then reads as

$$W_2[\epsilon] = -\frac{1}{2}\int d^d x\, d^d y\; \partial_\mu \epsilon_\nu(x)\; \partial_\rho \epsilon_\sigma(y)\; \langle T^{\mu\nu}(x) T^{\rho\sigma}(y)\rangle_{\text{conn.}}\,. \tag{4.3.2}$$

We wish to integrate by parts one of the derivatives and use the conformal Ward identity in even dimensions [129]:

$$\partial_\mu \langle T^{\mu\nu}(x) T^{\rho\sigma}(y)\rangle_{\text{conn.}} = C_T\, n_d \left\{ \partial^\nu \partial^\rho \partial^\sigma - \frac{d-1}{d}\,\eta^{\nu(\rho}\partial^{\sigma)}\,\Box - \frac{1}{d^2}\,\eta^{\rho\sigma}\partial^\nu \Box \right\} \Box^{\frac{d-2}{2}}\,\delta^{(d)}(x-y)\,, \tag{4.3.3}$$

where $n_d = -2^{2-d}\,\pi^{d/2}/\Gamma(d+2)\Gamma(\frac{d}{2})$. Note that in odd dimensions there is no such anomalous contribution and the quadratic action we define here simply vanishes. This should be tied to the fact that the conformal blocks are more complicated in odd dimensions. Plugging (4.3.3) into the action W_2 gives:

$$\boxed{W_2[\epsilon] = -C_T\, n_d\, \frac{d-1}{4d} \int d^d x\ \epsilon^\mu(x) \left(\eta_{\mu\nu}\,\Box - \frac{d+2}{d}\,\partial_\mu\partial_\nu\right) \Box^{\frac{d}{2}}\ \epsilon^\nu(x)} \tag{4.3.4}$$

We can now discuss the resulting propagator for our soft mode. In order to invert the kernel, we can pass to momentum space where $\partial_\mu \to ik_\mu$. The momentum space propagator follows immediately after inverting the integration kernel:

$$\langle \epsilon^\mu(k)\epsilon^\nu(-k)\rangle = -\frac{1}{C_T\, n_d}\,\frac{2d}{d-1} \left(\eta^{\mu\nu}\, k^2 - \frac{d+2}{2}\, k^\mu k^\nu\right) (-k^2)^{-\frac{d+4}{2}}\,. \tag{4.3.5}$$

Note that the scaling $(-k^2)^{-\frac{d+2}{2}}$ is what one would formally expect for the momentum space two-point function of dimension-(-1) operators [130]. We will make this more precise now. In fact, by Fourier transforming back to position space, we can recover the result of our reformulation of the shadow operator formalism! Let us now see how this works.

The Fourier transform of (4.3.5) is naively divergent, so we need to regularize it. This is done by first reducing the divergence for small momenta:

$$\begin{aligned}
\langle \epsilon^\mu(x)\epsilon^\nu(0)\rangle &= -\frac{1}{C_T\, n_d}\,\frac{2d}{d-1} \int \frac{d^dk}{(2\pi)^d}\, e^{ikx} \left(\eta^{\mu\nu}\, k^2 - \frac{d+2}{2}\, k^\mu k^\nu\right) (-k^2)^{-\frac{d+4}{2}} \\
&= -\frac{1}{C_T\, n_d}\,\frac{1}{2(d-1)} \int \frac{d^dk}{(2\pi)^d}\, e^{ikx} \left(\eta^{\mu\nu}\,\Box_{(k)} - 2\,\partial^\mu_{(k)}\partial^\nu_{(k)}\right) (-k^2)^{-\frac{d}{2}} \\
&= \frac{1}{C_T\, n_d}\,\frac{1}{2(d-1)} \left(\eta^{\mu\nu}\, x^2 - 2\, x^\mu x^\nu\right) \int \frac{d^dk}{(2\pi)^d}\, e^{ikx}\, (-k^2)^{-\frac{d}{2}}\,,
\end{aligned} \tag{4.3.6}$$

where we integrated by parts the k-derivatives thus converting them into a position space tensor structure. In the last line we recognize the inversion tensor $I_{\mu\nu}(x) = \eta_{\mu\nu} - 2\,\frac{x^\mu x^\nu}{x^2}$.

Next, we use differential regularization [131, 132] to replace $|k|^{-d}$ by a regulated expression with a well-defined Fourier transform:

$$|k|^{-d}\Big|_{\text{reg.}} \equiv -\frac{1}{2(d-2)}\,\Box_{(k)} \left(\frac{\log\!\left(|k|^2\mu^{-2}\right)}{|k|^{d-2}}\right)\,, \tag{4.3.7}$$

where $\Box_{(k)}$ can again be replaced by a factor of $(-x^2)$, using integration by parts. In writing the regularized expression it is necessary to introduce an arbitrary energy scale μ^2. We note the following Fourier transform of the regulated expression:

$$\int \frac{d^d k}{(2\pi)^d}\, e^{ikx}\, \frac{\log\big(|k|^2\mu^{-2}\big)}{|k|^{d-2}} = -\frac{d-2}{2^{d-1}\pi^{d/2}\Gamma(\frac{d}{2})}\,\frac{1}{x^2}\Bigg[\log\left(\mu^2 x^2\right) - \log 4 + \gamma - \psi\left(\frac{d-2}{2}\right)\Bigg] \tag{4.3.8}$$

We can clearly drop the three constant terms in the square bracket as these can be absorbed into a redefinition of the arbitrary scale μ (in abuse of notation, we will denote the redefined μ by the same letter). Putting all these pieces together, we find:

$$\langle \epsilon^\mu(x)\epsilon^\nu(0)\rangle = -\frac{1}{C_T}\,\frac{k_{0,2}k_{d,2}}{4\pi^d}\, I^{\mu\nu}(x)\, x^2\ \log\left(\mu^2 x^2\right) \tag{4.3.9}$$

This is precisely the propagator (4.2.21) that we derived from the shadow operator formalism upon identifying the reparametrization mode ϵ^μ in terms of the mode $\mathcal{E}^\mu$ whose descendant is the stress tensor shadow! At least at the level of two-point functions, we conclude that the reparametrization mode and shadow mode are the same:

$$\epsilon^\mu(x) = \mathcal{E}^\mu(x)\,. \tag{4.3.10}$$

In the following we argue for this relation more generally.

4.3.2 Monodromy projection and symmetries of the quadratic action

We have now established that the reparametrization modes ϵ^μ exhibit the same dynamics as the shadow modes $\mathcal{E}^\mu$ whose derivative is the shadow of the stress tensor. However, we are not done yet, as we still need to implement the monodromy projection onto the physical contributions to correlation functions. We now argue that the monodromy projection can be understood in terms of the symmetries of the effective action.

Note that the quadratic action (4.3.4) can be written as follows:

$$W_2[\epsilon] = -\frac{C_T\, n_d}{2}\int d^d x\, \mathbb{P}^{\rho\sigma}_{\mu\nu}\partial_\rho\epsilon_\sigma(x)\ \left[\partial^\lambda\partial^{(\mu} - \frac{d-1}{d}\,\Box\,\eta^{\lambda(\mu}\right]\partial^{\nu)}\,\Box^{\frac{d-2}{2}}\epsilon_\lambda(x)\,. \tag{4.3.11}$$

This way of writing the action makes the connection with the shadow operator, as well as some important symmetry properties manifest. The first factor $(\mathbb{P}_{\mu\nu}^{\rho\sigma}\partial_\rho\epsilon_\sigma)$ is just the symmetric traceless source associated with infinitesimal reparametrizations, $-\frac{1}{2}\,\delta' g_{\mu\nu}$. In other words, it is proportional to the longitudinal shadow operator dual to the stress tensor, c.f., (4.2.17). The second factor in (4.3.11) can be thought of as the stress tensor itself, expressed as an operator in our effective field theory. Indeed, we have from the definition of the shadow transform:

$$\begin{aligned} T^{\rho\sigma}(x) \equiv \widetilde{\widetilde{T}}^{\rho\sigma}(x) &\equiv \frac{k_{0,2}}{\pi^{d/2}}\,\frac{1}{2C_T}\int d^d y\,\langle T^{\rho\sigma}(x) T^{\mu\nu}(y)\rangle\,\widetilde{T}_{\mu\nu}(y) \\ &= C_T\,n_d\,\mathbb{P}_{\mu\nu}^{\rho\sigma}\left[\partial^\lambda\partial^{(\mu} - \frac{d-1}{d}\,\Box\,\eta^{\lambda(\mu}\right]\partial^{\nu)}\,\Box^{\frac{d-2}{2}}\,\mathcal{E}_\lambda(x)\,, \end{aligned} \tag{4.3.12}$$

where we wrote $\widetilde{T}_{\mu\nu}$ in terms of $\mathcal{E}^\mu$ using (4.2.17), and then integrated by parts using the Ward identity (4.3.3). In short, the action (4.3.11) can be simply understood as the coupling $W_2[\epsilon] \propto \int \delta' g_{\mu\nu}\,T^{\mu\nu}[\epsilon]$, where $T^{\mu\nu}[\epsilon]$ should be understood as in (4.3.12). This is, of course, not surprising, but it is useful to think about this standard coupling in terms of the reparametrization modes as it makes the connection with shadow operators very clear.

Symmetries of the quadratic action. The action (4.3.11) is useful for analyzing the symmetries. The two factors corresponding to the shadow of the stress tensor and the stress tensor itself, give rise to two sets of symmetries $\epsilon_\mu \to \epsilon_\mu + \delta\epsilon_\mu$:

- The source/shadow of the stress tensor $(-\frac{1}{2}\,\delta' g_{\mu\nu})$ is invariant under:

$$\delta\epsilon_\mu = K_\mu \quad \text{with} \quad \partial_{(\mu}K_{\nu)} - \frac{1}{d}\,\eta_{\mu\nu}(\partial.K) = 0\,, \tag{4.3.13}$$

  that is, $\delta\epsilon_\mu$ is a conformal Killing vector. There are the usual $\frac{1}{2}(d+1)(d+2)$ solutions to this, which are a manifestation of the $SO(d+1,1)$ conformal symmetry:

$$K_\mu(x) = a_\mu - \omega_{[\mu\nu]}x^\nu + \lambda\,x^\mu + x^2 I_{\mu\nu}(x)\,b^\nu\,, \qquad I_{\mu\nu} = \eta_{\mu\nu} - 2\,\frac{x_\mu x_\nu}{x^2}\,, \tag{4.3.14}$$

  which parametrize translations (a^μ), rotations ($\omega_{[\mu\nu]}$), scale transformations (λ), and special conformal transformations (b^μ).

- The stress tensor part $T^{\mu\nu}$ as in (4.3.12) is invariant under $\delta\epsilon_\mu$ with

$$\mathbb{P}_{\mu\nu}^{\rho\sigma}\left[\partial^\lambda\partial^{(\mu} - \frac{d-1}{d}\,\Box\,\eta^{\lambda(\mu}\right]\partial^{\nu)}\,\Box^{\frac{d-2}{2}}\,\delta\epsilon_\lambda = 0\,. \tag{4.3.15}$$

We refer to these symmetries as *conformal redundancies.* They represent an invariance of the definition of the energy-momentum tensor in terms of the reparametrization mode.

Projecting out the shadow modes. We have now reached the point where we can present a proposal for separating the physical block from the unphysical shadow block, at the level of our effective field theory. In order for the reparametrization mode to describe exchanges of the physical stress tensor, but not of its shadow operator, we need to supplement our effective field theory with an appropriate gauge symmetry, such that the physical stress tensor is a gauge invariant operator but its shadow is not.[82] In other words, we now wish to gauge precisely the *conformal redundancies* (4.3.15). Correspondingly, the propagation of the shadow operator in physical correlation functions will be forbidden. *In low-dimensional cases we verify below that this corresponds to the prescription of omitting gauge modes in the quadratic action.*

Note that the stress tensor can be written as a convolution of its shadow, with a known kernel which is proportional to the 2-point function $\langle T_{\mu\nu}T_{\rho\sigma}\rangle$, see (4.3.12). The conformal redundancies can be characterized equivalently as zero modes of that kernel – those are symmetries which act non-trivially on the shadow yet leave the result of the convolution, the stress tensor, invariant. While we leave a complete characterization of the conformal redundancies (especially for the non-linear action), for future work, this suggest a direct connection with the phenomenon of pole skipping (to be discussed further below).

4.3.3 Coupling reparametrizations to external operators

Obviously, it is also possible to derive the bilinear couplings to external operators, (4.2.27), from the reparametrization mode technique. This strategy is the immediate generalization of the way matter fields are coupled to the Schwarzian mode in one dimension [22, 112, 113], and holomorphic reparametrizations are coupled to primary operators in CFT$_2$ [88, 115]: we start with the conformal two-point function and perform a reparametrization. To linear order in the reparametrization, we obtain the bilinear coupling (4.2.27).

Let us make this more precise. We start with the coupling of the probe operators to sources, which is invariant under coordinate transformations

[82] We thank Kristan Jensen for useful conversations on this issue.

$x^\mu \to x'^\mu$. It follows that

$$\int d^d x\, d^d y\, \langle V(x)V(y)\rangle J(x)J(y) = \int d^d x' d^d y'\; \langle V(x')V(y')\rangle\; J(x')J(y')$$
$$= \int d^d x\, d^d y\; \langle V(x')V(y')\rangle\, [\Omega(x)\Omega(y)]^{\frac{\Delta}{2}}\; J(x)J(y) \tag{4.3.16}$$

where $\Omega(x)$ is the conformal factor, related to the Jacobian by $\left|\frac{\partial x'}{\partial x}\right| = \Omega^{d/2}$, and we also used $J(x') = J(x)\,\Omega^{(\Delta-d)/2}$. From this we can read off the full nonlinear coupling of finite reparametrizations to pairs of scalar operators V. It is given by the reparametrized two-point function:

$$\overline{\mathcal{B}}_V(x,y) \propto \left|\frac{\partial x'}{\partial x}\right|^{\frac{\Delta}{d}} \left|\frac{\partial y'}{\partial y}\right|^{\frac{\Delta}{d}} \frac{1}{(x'(x)-y'(y))^{2\Delta}} \tag{4.3.17}$$

These objects are natural bilinear operators in the theory (local operators in kinematic space).

An infinitesimal reparametrization $x^\mu \to x'^\mu = x^\mu + \epsilon^\mu(x)$ gives a conformal factor $\Omega(x) = 1 + \frac{2}{d}\,\partial_\rho \epsilon^\rho(x)$. This is related to the Jacobian of the transformation by $\left|\frac{\partial x'}{\partial x}\right| = 1 + \partial_\rho \epsilon^\rho$. The perturbative couplings of infinitesimal reparametrizations follow from this structure by expanding (4.3.17) in ϵ:

$$\overline{\mathcal{B}}_{\epsilon,V}(x,y) = \langle V(x)V(y)\rangle\, \left[1 + \mathcal{B}^{(1)}_{\epsilon,V}(x,y) + \mathcal{B}^{(2)}_{\epsilon,V}(x,y) + \ldots\right] \tag{4.3.18}$$

where $\mathcal{B}^{(1)}_{\epsilon,V}(x,y)$ is the same object as derived in (4.2.27) where we identify the logarithmic primary $\mathcal{E}_\mu$ with the reparametrization mode ϵ_μ. By expanding (4.3.17) to higher orders, we obtain higher order couplings involving n instances of ϵ_μ. The coupling at n-th order in ϵ_μ is of the form

$$\mathcal{B}^{(n)}_{\epsilon,V} = \frac{1}{n!}\left(\mathcal{B}^{(1)}_{\epsilon,V}\right)^n + \text{lower order in } \Delta_V\,. \tag{4.3.19}$$

For $n=1$ these bilinears describe the physics of a single stress tensor exchange in the OPE. This is the leading answer at large C_T. What is the meaning of higher order couplings $\mathcal{B}^{(n)}_{\epsilon,V}$? In two-dimensional CFTs, it is natural to expect that multi-ϵ exchanges correspond to Virasoro contributions to the conformal block. An example of a calculation where (4.3.19) was used for all n (and "lower orders in Δ_V" are not needed), is the exponentiation of the light-light block, where all external operators are light compared to the central charge [133]. This was verified for $d = 2$ in [115] using reparametrization mode techniques. In that case ladder exchange diagrams of reparametrization modes dominate. We review the two-dimensional calculation in Appendix C.2. It would be interesting to explore similar statements in higher dimensions, where one might expect a similar exponentiation to occur [134]. In higher dimensions, we expect that multi-ϵ diagrams compute multi-stress tensor exchanges. These are not universal in $d > 2$, but there might well exist certain contributions (such as "lowest twist" contributions) or kinematic regimes where a universal answer exists. Such exchanges were recently considered in [135–138]. It would be interesting to explore the relation with our formalism.

4.4 Two-dimensional CFTs

In this section we investigate in more detail the two-dimensional case, expanding on previous results of [88, 115] (see also [117]). In $d = 2$ we use complex coordinates $(z, \bar{z})$. Most of our discussion will be in Euclidean signature, where $\bar{z} = z^*$. For more details about conventions, see Appendix C.1.

4.4.1 Zero temperature

In $d = 2$, the stress tensor has components $T \equiv -2\pi T_{zz}$ and $\overline{T} \equiv -2\pi T_{\bar{z}\bar{z}}$. Similarly, the shadow of the stress tensor has non-zero components $\widetilde{T} \equiv -2\pi \widetilde{T}^{zz}$ and $\widetilde{\overline{T}} \equiv -2\pi \widetilde{T}^{\bar{z}\bar{z}}$. The shadow of the holomorphic stress tensor can be written as follows:

$$\widetilde{T}(z, \bar{z}) = \frac{2}{\pi} \int d^2 z' \, \frac{(z - z')^2}{(\bar{z} - \bar{z}')^2} \, T(z') \tag{4.4.1}$$

and similarly for the shadow $\widetilde{\overline{T}}$ of the anti-holomorphic stress tensor $\overline{T}$. It is straightforward to write these shadow currents as symmetric-traceless derivatives:

$$\widetilde{T} = -\frac{c}{3} \, \bar{\partial} \mathcal{E} \qquad \text{with} \qquad \mathcal{E} \equiv \frac{6}{\pi \, c} \int d^2 z' \, \frac{(z - z')^2}{(\bar{z} - \bar{z}')} \, T(z') \, , \tag{4.4.2}$$

and similarly for $\widetilde{\overline{T}} = -\frac{c}{3} \partial \overline{\mathcal{E}}$. The central charge appearing in (4.4.2) is related to the usual central charge in two dimensions by $c = 4\pi^2 C_T$. Instead of shadow operators, we can think, as discussed above, in terms of holomorphic and anti-holomorphic reparametrizations $(z, \bar{z}) \to (z + \epsilon, \bar{z} + \bar{\epsilon})$.

The reparametrization modes have an action as described in §4.3. The $d = 2$ version of the Euclidean propagator (4.3.9) (or (4.2.21)) takes the following form:

$$\mathcal{G}^E_{\mathcal{E}}(1,2) \equiv \langle \mathcal{E}(z_1,\bar{z}_1)\mathcal{E}(z_2,\bar{z}_2)\rangle = \frac{6}{c}\,(z_1-z_2)^2\,\log\left[\mu^2(z_1-z_2)(\bar{z}_1-\bar{z}_2)\right] \tag{4.4.3}$$

There is a similar expression for $\langle\overline{\mathcal{E}}\overline{\mathcal{E}}\rangle$, while mixed propagators vanish, $\langle\mathcal{E}\,\overline{\mathcal{E}}\rangle = 0$. In the same way, we can use the bilinear coupling (4.2.27), viz.,

$$\mathcal{B}^{(1)}_{\mathcal{E},V}(z_1,\bar{z}_1;z_2,\bar{z}_2) = \frac{\Delta_V}{2}\left[\partial\mathcal{E}_1 + \partial\mathcal{E}_2 - 2\,\frac{\mathcal{E}_1-\mathcal{E}_2}{z_1-z_2}\right] + \text{anti-holo.}\,, \tag{4.4.4}$$

to compute the conformal partial wave in $d = 2$. We can further exploit holomorphic factorization in two dimensions by recognizing $\mathcal{B}^{(1)}_{\mathcal{E},V}$ as the sum of two decoupled holomorphic and anti-holomorphic terms. This is useful for coupling the fields $\mathcal{E}$ and $\overline{\mathcal{E}}$ to spinning primaries with holomorphic and anti-holomorphic dimensions $(h,\bar{h})$:

$$\begin{aligned}\mathcal{B}^{(1)}_{\mathcal{E},h}(1,2) &\equiv h\,\left[\partial\mathcal{E}_1 + \partial\mathcal{E}_2 - 2\,\frac{\mathcal{E}_1-\mathcal{E}_2}{z_1-z_2}\right]\,,\\ \mathcal{B}^{(1)}_{\overline{\mathcal{E}},\bar{h}}(1,2) &\equiv \bar{h}\,\left[\bar{\partial}\overline{\mathcal{E}}_1 + \bar{\partial}\overline{\mathcal{E}}_2 - 2\,\frac{\overline{\mathcal{E}}_1-\overline{\mathcal{E}}_2}{\bar{z}_1-\bar{z}_2}\right]\,.\end{aligned} \tag{4.4.5}$$

Since the general case is straightforward to deal with (see [88] for details), we will simply assume the external primaries to be holomorphic, i.e., $\bar{h} = 0$. Holomorphic fields only couple to the mode $\mathcal{E}$, and we can discard $\overline{\mathcal{E}}$ for ease of notation.

Monodromy projection splits the soft mode propagator. The result for the global block computation is identical to (4.2.31) with $u = z\bar{z}$ and $v = (1-z)(1-\bar{z})$, so we will not repeat it here. Instead, we observe that in two dimensions a simple split into physical and shadow contributions occurs. For instance, (4.4.3) separates into a sum of a (holomorphic) *physical part* (computing the physical block) and a *shadow part* (computing the shadow block):

$$\mathcal{G}^E_{\mathcal{E}} = \mathcal{G}^E_{\mathcal{E},\,\text{phys.}} + \mathcal{G}^E_{\mathcal{E},\,\text{shad.}} \quad \text{with} \quad \begin{cases}\mathcal{G}^E_{\mathcal{E},\,\text{phys.}} = \dfrac{6}{c}\,(z_1-z_2)^2\,\log\left[\mu(z_1-z_2)\right]\\[2ex] \mathcal{G}^E_{\mathcal{E},\,\text{shad.}} = \dfrac{6}{c}\,(z_1-z_2)^2\,\log\left[\mu(\bar{z}_1-\bar{z}_2)\right]\end{cases} \tag{4.4.6}$$

These two parts of the propagator are distinguished by their monodromy around $z_{12}=0$: as $z_{12}\to e^{2\pi i}z_{12}$, the physical (shadow) propagator maps to itself plus (minus) $\frac{12\pi i}{c}\,z_{12}^2$.

Using these two separate propagators, the two-point function of holomorphic bilinears $\mathcal{B}^{(1)}_{\mathcal{E},h}$ now computes the physical and the shadow blocks separately. We find for the global identity block and shadow block between pairs of equal operators:

$$\begin{aligned}
G^{(\ell=2)}_{\Delta=2} &= \big\langle \mathcal{B}^{(1)}_{\mathcal{E},h}(1,2)\,\mathcal{B}^{(1)}_{\mathcal{E},h'}(3,4)\big\rangle_{\text{phys.}} = \frac{2hh'}{c}\; z^2\;\; {}_2F_1(2,2,4,z)\,,\\
G^{(\ell=2)}_{\tilde{\Delta}=0} &= \big\langle \mathcal{B}^{(1)}_{\mathcal{E},h}(1,2)\,\mathcal{B}^{(1)}_{\mathcal{E},h'}(3,4)\big\rangle_{\text{shad.}} = \frac{24hh'}{c}\;\frac{\bar{z}}{z}\;\; {}_2F_1(-1,-1,-2,z)\\
&\qquad\qquad\qquad\qquad\qquad\qquad\qquad\;\; \times{}_2F_1(1,1,2,\bar{z})\,,
\end{aligned} \tag{4.4.7}$$

which is computed using the two parts of the propagator (4.4.6) respectively, and we defined $z=\frac{z_{12}z_{34}}{z_{13}z_{24}}$. Note that the arbitrary scale μ has dropped out, as it must. The first line of the previous equation is, of course, just the well-known leading contribution at large c to the Virasoro identity block.

Monodromy projection as gauging a symmetry. It is intriguing to see that at least in two dimensions, the separation between physical and shadow contributions already occurs at the level of the reparametrization mode propagator. We can thus implement the monodromy projection onto the physical piece at a very early stage: we simply discard the shadow part of the propagator $\mathcal{G}^{E}_{\mathcal{E}}$. Let us see this property at the level of the quadratic action. In $d=2$, the latter reads as

$$W_2[\epsilon,\bar{\epsilon}] = \frac{c}{24\pi}\int d^2z\;\left[\bar{\partial}\epsilon\;\partial^3\epsilon \quad+\quad \text{anti-holo.}\right] \tag{4.4.8}$$

Following the general discussion above, consider the symmetries $\epsilon\to\epsilon+\delta\epsilon$ of this action:

- The first factor, $\bar{\partial}\epsilon$, should be thought of as the source (or the shadow $\widetilde{T}$). It is invariant under
$$\delta\epsilon = \Lambda_{\text{h}}(z) \tag{4.4.9}$$
for arbitrary holomorphic functions Λ_{h}. These are chiral conformal transformations in two dimensions.

- The second factor, $\partial^3\epsilon$, is proportional to the stress tensor $T[\epsilon]$ and it is invariant under
$$\delta\epsilon = \Lambda_0(\bar{z}) + \Lambda_1(\bar{z})\,z + \Lambda_2(\bar{z})\,z^2\,. \tag{4.4.10}$$

> These $\bar{z}$-dependent $SL(2)$ transformations were dubbed conformal redundancies above. In order to separate the physical from the shadow block, they should be understood as a gauge invariance of the theory. Gauging these is equivalent to imposing the presence of the stress tensor as a gauge invariant operator, while projecting out its shadow, as discussed above in the general case.

We can implement these ideas very explicitly in the present case, when we derive the propagator for ϵ via Fourier transform. For momenta $(k, \bar{k}) = (k^0 + ik^1, k^0 - ik^1)$ conjugate to the coordinates $(\bar{z}, z)$, we have:

$$\langle \epsilon(k, \bar{k})\, \epsilon(-k, -\bar{k}) \rangle = \frac{12\pi}{c} \frac{1}{\frac{k^0+ik^1}{2} \left(\frac{k^0-ik^1}{2} \right)^3} \tag{4.4.11}$$

To Fourier transform, we first integrate k^1 along the real line. We perform this integral via contour integration and *only pick up the contribution from the "physical" pole $k^1 = ik^0$. The "unphysical" pole at $k^1 = -ik^0$ is associated with the transformations* (4.4.10)*, which we want to gauge; this means we should drop the corresponding contributions to the propagator.* This gives:

$$\langle \epsilon(x)\epsilon(0) \rangle_{\text{phys.}} = \int_{\substack{\text{pole} \\ k^1 = ik^0}} \frac{d^2k}{(2\pi)^2} \, \langle \epsilon(k, \bar{k})\, \epsilon(-k, -\bar{k}) \rangle \, e^{ik.x} = \frac{6}{c} \, z^2 \, \log(\mu z) + \dots \tag{4.4.12}$$

where "..." denotes (both finite and divergent) analytic terms. We have thus recovered the physical propagator of (4.4.6). Taking into account the "shadow pole" $k^1 = -ik^0$ in the above Fourier transform, we could have also obtained the shadow part of the propagator. This shows that (in two dimensions) the *monodromy projection is equivalent to gauging the transformations* (4.4.10)*. A convenient way of doing this, at least in low dimensions, is by simply omitting the corresponding modes in the Fourier transform.*

This elucidates the monodromy projection onto the physical part of the propagator (and hence the conformal blocks etc.) at the level of the reparametrization mode, and links it to gauging a particular symmetry. While the projection onto the physical block has to be done by hand in position space, in momentum space the separation happens very naturally: the physical and shadow contributions simply come from different poles in the momentum space propagator, and imposing the gauge symmetry explicitly sets the contribution from those poles to zero.

4.4.2 Finite temperature

In two dimensions it is straightforward and instructive to study thermal physics by mapping to the cylinder via

$$(z, \bar{z}) = \left(\frac{\beta}{2\pi} e^{-i\frac{2\pi}{\beta}u},\ \frac{\beta}{2\pi} e^{i\frac{2\pi}{\beta}\bar{u}} \right) . \tag{4.4.13}$$

For simplicity we set $\mu = \frac{2\pi}{\beta} = 1$. We further write $u = \tau + i\sigma$ where $\tau \in [0, 2\pi)$ denotes the compact direction, i.e., the thermal circle. The holomorphic bilinear coupling on the cylinder is simply

$$\mathcal{B}^{(1)}_{\mathcal{E},h}(u_1, \bar{u}_1; u_2, \bar{u}_2) = h \left[\partial\mathcal{E}_1 + \partial\mathcal{E}_2 - \frac{\mathcal{E}_1 - \mathcal{E}_2}{\tan\frac{u_{12}}{2}} \right] , \tag{4.4.14}$$

Finite temperature propagator and monodromy projection. In order to get the physical reparametrization mode propagator, it is most convenient to follow the same strategy as in the flat space case: we start from the quadratic action to obtain the propagator in momentum space. When Fourier transforming back to position space, we omit modes that correspond to the (finite temperature version of the) gauge symmetry (4.4.10). Let us see this explicitly.

The quadratic action (4.4.8), after mapping to the thermal cylinder, reads as follows:

$$W_2[\epsilon, \bar{\epsilon}] = \frac{c}{24\pi} \int d^2u \ \left\{ \bar{\partial}\epsilon \ (\partial^2 + 1)\partial\epsilon \ + \ \text{anti-holo.} \right\} . \tag{4.4.15}$$

In the following we shall focus on the "holomorphic" first term. The "anti-holomorphic" second term can be treated in complete analogy.

Note that (4.4.15) looks slightly different from the action in [88, 115] because it is written covariantly and at this stage still contains shadow contributions. The action of [88, 115] is recovered by replacing $\partial \to \partial_\tau$; of course, this is a rather ad hoc prescription. We will now argue that the above action is completely equivalent to that of [88, 115], as long as one gauges the appropriate symmetry associated with invariances of the stress tensor.

The action (4.4.15) for ϵ is invariant under anti-holomorphic transformations $\epsilon \to \epsilon + \Lambda_{\mathrm{h}}(u)$ just like the flat space action (4.4.8). The additional $SL(2)$ invariance now takes the form

$$\epsilon \to \epsilon + \delta\epsilon \, , \qquad \delta\epsilon = \Lambda_0(\bar{u}) + \Lambda_1(\bar{u})\, e^{iu} + \Lambda_{-1}(\bar{u})\, e^{-iu} \, . \tag{4.4.16}$$

The stress tensor

$$T[\epsilon] = \frac{c}{12}\partial(\partial^2 + 1)\epsilon \tag{4.4.17}$$

is invariant under these transformations. In the Fourier transform below, we will therefore omit modes corresponding to these transformations in order to obtain a physical result.

The momentum space propagator corresponding to (4.4.15) is:

$$\langle \epsilon(\omega_E, k)\, \epsilon(-\omega_E, -k) \rangle = \frac{12\pi}{c} \frac{1}{\frac{\omega_E + ik}{2}\, \frac{\omega_E - ik}{2} \left[\left(\frac{\omega_E - ik}{2} \right)^2 - 1 \right]}\,, \tag{4.4.18}$$

where (ω_E, k) are the Euclidean frequency and momentum conjugate to (τ, σ). This propagator can now be Fourier transformed back to position space. This involves two steps:[83] first, we need to perform a contour integral over k, picking up residues at the poles $k \in \{\pm i\omega_E,\, -i(\omega_E \pm 2)\}$. Second, we need to sum over frequencies $\omega_E \in \mathbb{Z}$. Gauging the invariances of the stress tensor means that in this process we should not include modes associated with the transformations (4.4.16). This means that in the contour integral over k, we only include the "physical" pole $k = i\omega_E$. In the subsequent sum over frequencies we omit the frequencies $\omega_E \in \{-1, 0, 1\}$ as they again correspond to the shadow contributions. The contribution from the residue at $k = i\omega_E$ yields the desired result of [88, 115]:

$$\begin{aligned} \langle \epsilon(\tau, \sigma)\, \epsilon(0, 0) \rangle \Big|_{\substack{\text{pole} \\ k = i\omega_E}} &= \frac{24}{c} \left[\sin^2\left(\frac{\tau + i\sigma}{2} \right) \log\left(1 - e^{i\,\mathrm{sgn}(\sigma)(\tau + i\sigma)} \right) \right. \\ &\qquad \left. - \frac{1}{4} + \frac{3}{8}\, e^{i\,\mathrm{sgn}(\sigma)(\tau + i\sigma)} \right] \\ &\equiv \mathcal{G}^{E,\text{th.}}_{\mathcal{E},\text{phys.}} \end{aligned} \tag{4.4.19}$$

The last two terms are analytic and are pure gauge in the sense that they do not contribute to physical correlation functions. We could choose to discard them. The above propagator is $\mathcal{G}^{E}_{\mathcal{E},\text{phys.}}$ in the thermal state. It could also be obtained without any Fourier transform by conformally transforming $\mathcal{G}^{E}_{\mathcal{E},\text{phys.}}$ and imposing translational invariance and normalizability for $|\sigma| \to \infty$ as a boundary condition.

One can similarly check that the remaining poles $k \in \{-i\omega_E,\, -i(\omega_E \pm 2)\}$ give contributions that reproduce precisely the thermal version of the shadow propagator $\mathcal{G}^{E}_{\mathcal{E},\text{shad.}}$:

$$\langle \epsilon(\tau, \sigma)\, \epsilon(0, 0) \rangle \Big|_{\substack{\text{other} \\ \text{poles}}} = \tfrac{24}{c}\, \sin^2\left(\tfrac{\tau + i\sigma}{2} \right) \log\left(1 - e^{-i\,\mathrm{sign}(\sigma)(\tau - i\sigma)} \right) \equiv \mathcal{G}^{E,\text{th.}}_{\mathcal{E},\text{shad.}}\,. \tag{4.4.20}$$

[83] The details are analogous to calculations done in [88].

The physical propagator was already written down in [88, 115]. Its shadow counterpart follows naturally from our analysis. The sum of these terms, $\mathcal{G}_{\mathcal{E}}^{E,\text{th.}} = \mathcal{G}_{\mathcal{E},\text{phys.}}^{E,\text{th.}} + \mathcal{G}_{\mathcal{E},\text{shad.}}^{E,\text{th.}}$, can be understood as the thermal version of the general result (4.4.6) by means of a conformal transformation. Note that the propagators $\mathcal{G}_{\mathcal{E},\text{phys.}}^{E,\text{th.}}$ and $\mathcal{G}_{\mathcal{E},\text{shad.}}^{E,\text{th.}}$ are single-valued and normalizable for large spatial separations.

Finally, we remark that the physical and shadow parts are distinguished as usual by their monodromies. On the cylinder, we can focus on the monodromies around the thermal τ-circle at fixed non-zero values of σ. For instance, fixing $\sigma_{12} \equiv \delta \to 0^+$, the monodromies are:

$$\mathcal{G}^E_{\mathcal{E},\left\{\substack{\text{phys.}\\ \text{shad.}}\right\}} \overset{\tau\to\tau+2\pi}{\longrightarrow} \mathcal{G}^E_{\mathcal{E},\left\{\substack{\text{phys.}\\ \text{shad.}}\right\}} \pm 2\pi i \left[\frac{24}{c}\sin^2\left(\frac{\tau_{12}}{2}\right)\right] . \tag{4.4.21}$$

General remarks. Note that the physical contribution to the reparametrization mode propagator (which eventually leads to Lyapunov growth of OTOCs) comes from a single pole at $k = i\omega_E$. Not coincidentally, *this is precisely the pole that gives rise to pole skipping in the energy-momentum tensor two-point function, which will be discussed in §4.5.2. This leads us to conjecture that the projection onto the physical reparametrization mode propagator can be achieved in momentum space by simply only keeping the contribution from the pole that was responsible for pole skipping.*

Finally, note that this simple prescription is quite reminiscent of similar methods developed by [139] in the context of conformal blocks. We can think of the projection of the momentum space integral onto a single pole in terms of multiplication of the propagator (4.4.18) with a phase factor that imposes the gauge symmetry and removes the unphysical "shadow poles". Employing a notation more similar to [140], one has to multiply the momentum space expression for $\langle \epsilon(\omega_E, k)\, \epsilon(-\omega_E, -k)\rangle$ with the phase function that vanishes at the unphysical "shadow poles" and is normalized to 1 at the physical poles. In the thermal case this function is

$$B(\omega_E, k) \equiv \frac{\sin(\pi(ik-\omega_E))\, \sin(\pi i k)}{\sin(2\pi\omega_E)\, \sin(\pi\omega_E)} . \tag{4.4.22}$$

Multiplication with this function in momentum space achieves the projection onto physical modes only by means of removing the unphysical poles. Indeed, one easily verifies that the Fourier transform of the projected propagator, $B(\omega_E, k)\, \langle \epsilon(\omega_E, k)\, \epsilon(-\omega_E, -k)\rangle$, is precisely (4.4.19) without any shadow contributions.

Having set up the building blocks of the effective theory of the reparametrization mode in two dimensions in thermal states, more interesting calculations can be performed with it. These include the "light-light" Virasoro block and its exponentiation [133], the "heavy-light" Virasoro block [141] and $1/c$ corrections to it [142], application to OTOCs [21, 143], higher-point blocks [144] and OTOCs [145, 146], and so on. Some of these calculations have been done for two-dimensional CFTs using the reparametrization mode formalism in [88, 115, 116], so we will not repeat them here. It would, of course, be very interesting to find new applications of this formalism, as it promises to simplify calculations considerably (see §4.6 for some suggestions). In §4.5 we will return to applications in thermal states for higher dimensions, in particular focusing on OTOCs in Rindler space.

4.5 Application: thermal physics and OTOCs in higher dimensions

It is well known that an observer who is stationary with respect to Rindler time perceives the Minkowski vacuum state as thermal. Since the Rindler wedge of Euclidean spacetime $\mathbb{R}^d$ is conformal to a spacetime with hyperbolic spatial slices, $S^1 \times \mathbb{H}^{d-1}$, it is thus clear that a simple conformal map is sufficient for studying thermal states and quantum chaos of CFTs living on a hyperbolic space [147]. The temperature thus obtained is fixed in terms of the size of the S^1, or equivalently the curvature of the hyperbolic space; we set it to $\beta = 2\pi$ for most of this section.

In the following, we discuss thermal out-of-time-ordered correlators in higher dimensions by various means. We start with a discussion of the OTOC based on analytically continuing the stress tensor conformal blocks (as computed by reparametrization modes). Then, we will discuss the phenomenon of pole skipping, thus establishing an even closer connection with the stress tensor two-point function.

In both cases we observe maximal Lyapunov exponent and butterfly velocity. As in two dimensions, this should be thought of as the stress tensor contribution to the OTOC, which may or may not dominate. For instance, both the maximal Lyapunov exponent and the butterfly velocity in planar $\mathcal{N} = 4$ SYM theory receive corrections at finite couplings. This can be understood using conformal Regge theory, which takes into account contributions to the OTOC other than the stress tensor exchanges. The true Lyapunov exponent is then given by the Regge intercept associated with the leading Regge trajectory [20, 48, 148].

4.5.1 OTOCs from conformal blocks in higher dimensions

In this subsection we demonstrate how to compute global stress tensor contributions to OTOCs in higher-dimensional Rindler space. The connection with our reparametrization mode formalism is as follows: we have shown in previous sections how a single reparametrization mode exchange computes global conformal blocks. We can now use these directly to study thermal physics. The basic observation is that Rindler space (a simple coordinate transform of flat Minkowski space) is conformally equivalent to a space $S^1 \times \mathbb{H}^{d-1}$. We can thus study thermal physics on hyperbolic space using just conformal symmetry arguments. We mostly repeat and expand the analysis of [149], where Rindler OTOCs were computed from the global stress tensor block (note also the relevant papers [148, 150] that appeared while our work was nearing completion).

We start with the observation that the hyperbolic space metric is conformally equivalent to Rindler space:

$$\begin{aligned} ds^2_{S^1\times\mathbb{H}^{d-1}} &= d\tau^2 + \frac{1}{\rho^2}\left(d\rho^2 + dx_\perp^2\right) = \frac{1}{\rho^2}\left(\rho^2 d\tau^2 + d\rho^2 + dx_\perp^2\right) \\ &\equiv \Omega(\rho)^2\, ds^2_{\text{Rindler}} \end{aligned} \tag{4.5.1}$$

where $x_\perp^i \in \mathbb{R}^{d-2}$. The conformal factor $\Omega(\rho) = \frac{1}{\rho}$ will be important when translating results back to Rindler space. In order to make the connection with chaos, it is most natural to work in the "radar coordinate" $\rho = e^{\frac{2\pi}{\beta}\sigma}$. The (right) Rindler wedge is in turn related to Euclidean Minkowski space $ds^2 = \eta_{\mu\nu}\, dx^\mu dx^\nu$ by the coordinate transformation

$$x^\mu = \left(\frac{\beta}{2\pi}\, e^{\frac{2\pi}{\beta}\sigma}\, \sin\left(\frac{2\pi}{\beta}\tau\right),\, \frac{\beta}{2\pi}\, e^{\frac{2\pi}{\beta}\sigma}\, \cos\left(\frac{2\pi}{\beta}\tau\right),\, x_\perp^i\right)\,, \tag{4.5.2}$$

where real Rindler time would be denoted as $t_{\text{R}} = -i\tau$. It is therefore straightforward to study thermal physics in hyperbolic space by performing a coordinate transformation to Rindler space and then a conformal transformation. In the following we set $\beta = 2\pi$.

The quickest way to getting the thermal OTOC is by recalling our result for the global stress tensor CPW in arbitrary dimension, (4.2.31), and the physical conformal blocks associated with it. As these are simply scalar functions, all we need for the thermal setup in hyperbolic space are the

Rindler expressions for the cross ratios u and v. These follow immediately from their definition (4.2.9) using the observation that

$$x_{ij}^2 = -2\, e^{\sigma_i+\sigma_j} \left[\cos\tau_{ij} - \cosh \mathbf{d}(i,j)\right] , \tag{4.5.3}$$

where $\mathbf{d}(i,j)$ is the $SO(d-2,1)$ invariant geodesic distance in the hyperbolic space $\mathbb{H}^{d-1}$ (see (C.1.6) for an explicit expression).

We wish to study a four-point function of pairwise equal operators inserted at (almost) coincident points. We thus set $\mathbf{d}(1,2) = \mathbf{d}(3,4) = 0$ and $\mathbf{d}(1,3) = \mathbf{d}(1,4) = \mathbf{d}(2,3) = \mathbf{d}(2,4) \equiv \mathbf{d} = \text{const}$. We furthermore analytically continue to real time $\tau_j \to i t_{\mathrm{R},j} + \delta_j$ with $t_{\mathrm{R},1} = t_{\mathrm{R},2} = t$ and $t_{\mathrm{R},3} = t_{\mathrm{R},4} = 0$ where δ_i are small regulators in Euclidean time. We thus get for the cross ratios:

$$\begin{aligned} u &= \frac{[\cos\delta_{12} - 1]\,[\cos\delta_{34} - 1]}{[\cosh(t - i\delta_{13}) - \cosh\mathbf{d}]\,[\cosh(t - i\delta_{24}) - \cosh\mathbf{d}]} \sim e^{-2t}\ \delta_{12}^2\delta_{34}^2 + \ldots \\ v &= \frac{[\cosh(t - i\delta_{14}) - \cosh\mathbf{d}]\,[\cosh(t - i\delta_{23}) - \cosh\mathbf{d}]}{[\cosh(t - i\delta_{13}) - \cosh\mathbf{d}]\,[\cosh(t - i\delta_{24}) - \cosh\mathbf{d}]} \sim 1 + e^{-t+\mathbf{d}}\ \delta_{12}\delta_{34} + \ldots \end{aligned} \tag{4.5.4}$$

For late times $t \gg \frac{2\pi}{\beta}$, $u \approx 0$, which is precisely the short distance limit that allows us to easily distinguish the physical block from the shadow block, c.f. (4.2.14). In terms of the complex variables $(z, \bar{z})$, we have in this limit

$$z \sim -e^{-t+\mathbf{d}}\ \delta_{12}\delta_{34}\,, \qquad \bar{z} \sim -e^{-t-\mathbf{d}}\ \delta_{12}\delta_{34}\,. \tag{4.5.5}$$

This is, of course, completely analogous to the two-dimensional case with geodesic distance replacing the one spatial direction.

We already know that the physical block behaves in the short distance limit as [118]

$$G_{\Delta=d}^{(\ell=2)} \ \overset{u\to 0}{\sim}\ u^{\frac{d-2}{2}}\,(1-v)^2\ {}_2F_1\left(\frac{d+2}{2}, \frac{d+2}{2}, d+2; 1-v\right) . \tag{4.5.6}$$

The OTOC configuration corresponds to sending $\delta_i \to 0$ under the condition that $\delta_1 > \delta_3 > \delta_2 > \delta_4$. As far as the multi-valued function (4.5.6) is concerned, this simply means analytically continuing the cross ratio v and taking it around the origin, while holding u fixed. We abbreviate this operation as $(u, v) \to (u, e^{-2\pi i}v)$. Under this analytic continuation around the branch point of the conformal block, the latter picks up a monodromy, which leads to the Lyapunov behavior. The setup is illustrated in Fig. 4.1.

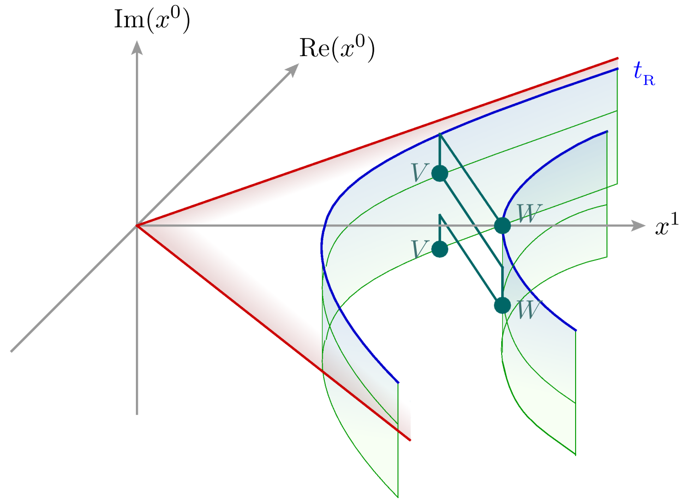

Figure 4.1: Out-of-time-order configuration in Rindler space. Inside the red shaded Rindler wedge we show two Rindler time trajectories in blue, which are at constant geodesic separation. The four operators are inserted at the green dots. We show the out-of-time-ordered configuration by including a small amount of imaginary time.

Under the analytic continuation described above, the hypergeometric function in (4.5.6) picks up a (imaginary[84]) monodromy $\sim (1-v)^{-d-1}$. The Euclidean block analytically continued to the Lorentzian OTOC configuration then scales as[85]

$$\frac{\langle V(t,\mathbf{d})W(0,0)V(t,\mathbf{d})W(0,0)\rangle_{\text{conn.}}}{\langle VV\rangle\langle WW\rangle} \sim G^{(\ell=2)}_{\Delta=d}(u\to 0, v\to e^{-2\pi i}v)$$
$$\sim u^{\frac{d-2}{2}}(1-v)^{-d+1} \sim \frac{1}{\delta_{12}\delta_{34}}\, e^{t-(d-1)\,\mathbf{d}}\,. \tag{4.5.7}$$

It follows that the Lyapunov exponent and butterfly velocity are $\lambda_L = 1$ and $v_B = \frac{1}{d-1}$, respectively, measured in units of $\frac{2\pi}{\beta}$.

Example in four dimensions. As an explicit example, consider the stress tensor conformal block in $d=4$, written down in (4.2.32). Under analytic

[84]The coefficient of the monodromy term is $2\pi i\, d!\,(d+1)!\,\Gamma(\frac{d}{2}+1)^{-4}$.

[85]Notation here is somewhat imprecise with regards to spatial insertion points. We mean a configuration where V operators are inserted a geodesic distance $\mathbf{d}$ away from W operators.

continuation to the second sheet described above, $(1-z) \to e^{-2\pi i}(1-z)$, while $\bar{z}$ is held fixed. We find:

$$G_4^{(2)} \to -10\left\{\frac{\bar{z}}{z}\frac{z^2-6z+6}{z-\bar{z}}\left[\log(1-z)-2\pi i\right]-6+\frac{z}{\bar{z}}\frac{\bar{z}^2-6\bar{z}+6}{\bar{z}-\bar{z}}\log(1-\bar{z})\right\}$$
$$\sim e^{t-3\mathbf{d}} \tag{4.5.8}$$

where we took the limit $t-\mathbf{d} \gg \frac{\beta}{2\pi}$ in the second step. From the exponential growth we can immediately see the Lyapunov exponent is $\lambda_L = 1$ and the butterfly velocity is $v_B = \frac{1}{3}$.

4.5.2 Chaos exponents from pole skipping in higher dimensions

A different motivation for the effective field theory of the soft mode revolves around the phenomenon of pole skipping, pointed out in [151] and further discussed in [53, 88, 152–155]. This is a phenomenon that exists in maximally chaotic theories whose Lypaunov behaviour is dominated by a single effective mode. We focus on higher-dimensional CFTs on hyperboilc (or equivalently Rindler) space. These are known to be maximally chaotic under the assumption that the stress tensor block dominates [149]. This analysis provides a nice consistency check with our discussion so far and generalizes [88].

The quantity we will discuss is the energy-energy conformal two-point function. While this is more complicated to compute than two-point functions of scalar operators, it is necessitated by the absence of chaos-related pole skipping in scalar two-point functions. The latter do display pole skipping, but not in a way that can be related to exponentially growing modes in an obvious way [154, 155]. While this work was nearing completion, a pole skipping analysis from the bulk point of view was done in [150], providing results consistent with our findings.

Thermal energy-energy correlator in CFT$_d$

We use the previously discussed fact that thermal physics in hyperbolic space can be understood by means of a conformal transformation of a Rindler wedge. To set the stage for the discussion of pole skipping in higher dimensions, we start by working out the energy-energy two-point function on $S^1 \times \mathbb{H}^{d-1}$.

We invite the reader to skip the derivation and jump to the result for the energy-energy correlator in momentum space, (4.5.19).

Position Space. We start by analyzing the thermal energy-energy two-point function on $S^1 \times \mathbb{H}^{d-1}$ in position space. We use the embedding space formalism [156] (see also Appendix C.1 for more details on conventions). We embed $S^1 \times \mathbb{H}^{d-1}$ in $\mathbb{R}^{1,d+1}$. The latter is a Minkowski spacetime with coordinates X^A, and the embedding space metric is $\eta_{AB} = \mathrm{diag}(-1, 1, \dots, 1)$.[86] A point in $S^1 \times \mathbb{H}^{d-1}$ will be parametrized as

$$P^A_{\mathrm{H}} \equiv (P^I_{\mathrm{H}}, P^{II}_{\mathrm{H}}, P^\mu_{\mathrm{H}}) = \left(\frac{1+\rho^2+x_\perp^2}{2\rho} \, , \, \frac{1-\rho^2-x_\perp^2}{2\rho} \, , \, \sin\tau \, , \, \cos\tau \, , \, \frac{x_\perp^i}{\rho} \right) , \tag{4.5.9}$$

which lies on the projective null cone, $P_{\mathrm{H}} \cdot P_{\mathrm{H}} = 0$, and thus parametrizes a CFT spacetime point. The normalized scalar two-point function on $S^1 \times \mathbb{H}^{d-1}$ for a dimension Δ operator is

$$\mathcal{G}_\Delta(P_1, P_2) \equiv \frac{1}{(-2P_1 \cdot P_2)^\Delta} = \frac{1}{(-2\cos(\tau_1 - \tau_2) + 2\cosh \mathbf{d}(1,2))^\Delta} \, , \tag{4.5.10}$$

where $\mathbf{d}(1,2)$ is the spatial hyperbolic distance in $\mathbb{H}^{d-1}$ between the two points (see (C.1.6) for an explicit expression).

Since we will be interested in the chaos-related features of the energy-energy correlator, let us also record the stress-tensor two-point function (c.f., [157]):

$$\begin{aligned} \mathcal{G}_{\mu\nu,\rho\sigma}(P_1,P_2) &\equiv \left\langle T_{\mu\nu}(P_1) T_{\rho\sigma}(P_2) \right\rangle_{S^1\times\mathbb{H}^{d-1}} \\ &= 2C_T \, \mathbb{P}^{AB}_{\mu\nu}(P_1) \mathbb{P}^{CD}_{\rho\sigma}(P_2) \frac{\partial}{\partial Z_1^A} \frac{\partial}{\partial Z_1^B} \frac{\partial}{\partial Z_2^C} \frac{\partial}{\partial Z_2^D} \\ &\qquad \left[\frac{((P_1\cdot P_2)(Z_1\cdot Z_2) - (P_1\cdot Z_2)(P_2\cdot Z_1))^2}{(-2P_1\cdot P_2)^{d+2}} \right] , \end{aligned} \tag{4.5.11}$$

where $Z_{1,2}$ are auxiliary vectors allowing for a compact notation. The projectors appearing in the above expression are defined as

$$\mathbb{P}^{AB}_{\mu\nu}(P) = \frac{\partial P^{(A}}{\partial x^\mu_{\mathrm{R}}} \frac{\partial P^{B)}}{\partial x^\nu_{\mathrm{R}}} - \frac{1}{d} \eta^{AB} \eta_{CD} \frac{\partial P^C}{\partial x^\mu_{\mathrm{R}}} \frac{\partial P^D}{\partial x^\nu_{\mathrm{R}}} \tag{4.5.12}$$

[86] We denote the complete set of $\mathbb{R}^{1,d+1}$ indices as $A = (I, II, \mu)$ where the Minkowski index is $\mu = (0, m) = (0, 1, i)$.

where $x^\mu_{\mathrm{R}} = (\tau, \rho, x^i_\perp)$ denotes the Rindler coordinates.

We will be interested in the Fourier transform of the energy-energy correlator $\mathcal{G}_{00,00}(P_1, P_2)$. In order to apply known technology for performing this Fourier transform, we write the energy-energy two-point function in terms of the following auxiliary quantity:

$$\mathcal{G}^{a,b}_\Delta(P_1, P_2) \equiv \frac{1}{(-2a\,\cos(\tau_1 - \tau_2) + 2b\,\cosh \mathbf{d}(1,2))^\Delta}\,. \tag{4.5.13}$$

This is just the scalar two-point function (4.5.10) taken slightly off-shell by the parameters a, b. We can write the Euclidean energy-energy correlator in terms of this quantity as follows:

$$\begin{aligned}\mathcal{G}_{00,00}(P_1, P_2) = C_T \Bigg[&\mathcal{G}^{a,b}_{d+2}(P_1, P_2) \\ &+ \frac{1}{4d(d+1)} \left(\frac{2(d-1)}{d}\,\partial_a \partial_b - \frac{1}{d}(\partial_a^2 + \partial_b^2) \right) \mathcal{G}^{a,b}_d(P_1, P_2) \\ &+ \frac{1}{16(d-2)(d-1)d(d+1)}\,\partial_a^2 \partial_b^2 \mathcal{G}^{a,b}_{d-2}(P_1, P_2) \Bigg]_{a,b\to 1}\end{aligned} \tag{4.5.14}$$

This can be simply checked – we provide some details in Appendix C.3.1. This way of writing $\mathcal{G}_{00,00}$ will turn out to be very convenient.

Momentum Space. The next step in our calculation will be to find the Fourier transform of the energy-energy two-point function $\mathcal{G}_{00,00}$. The rewriting in terms of scalar propagators as in (4.5.14) reduces this to a simpler task: we only need to compute the Fourier transform of the slightly off-shell scalar two-point function $\mathcal{G}^{a,b}_\Delta$ defined in (4.5.13). This has been previously achieved in the on-shell case where $a = b = 1$. We can therefore closely follow the calculation as presented in [158].

In order to Fourier transform, we first need to identify a suitable set of basis functions to expand in. Since we work on a spacetime $S^1 \times \mathbb{H}^{d-1}$, a basis of functions $f_{\omega,k,p_\perp}$ should be eigenfunctions of the Laplacian

$$\Box_{S^1\times\mathbb{H}^{d-1}} = \partial_\tau^2 + \Box_{\mathbb{H}^{d-1}} = \partial_\tau^2 + \rho^2 \left(\rho^{d-3} \partial_\rho \frac{1}{\rho^{d-3}} \partial_\rho + \Box_{\mathbb{R}^{d-2}} \right)\,. \tag{4.5.15}$$

These basis functions are characterized by the momenta $(\omega_E, k, p^i_\perp)$ conjugate to $(\tau, \rho, x^i_\perp)$. A suitable set of orthonormal basis functions is given by

$$f_{\omega,k,p_\perp}(P) = \left(\frac{4k\,\sinh(\pi k)}{\pi} \right)^{1/2} \rho^{\frac{d-2}{2}}\, K_{ik}(|p_\perp|\,\rho)\, e^{i(\omega_E \tau + p_\perp\cdot x_\perp)}\,. \tag{4.5.16}$$

These have eigenvalues $(-\omega_E^2\,,\,-k^2 - \frac{(d-2)^2}{4}\,,\,-p_\perp^2)$ with respect to ∂_τ^2, $\Box_{\mathbb{H}^{d-1}}$, and $\Box_{\mathbb{R}^{d-2}}$. Note that there is another set of solutions of the same form, but with $J_{ik}(i|p_\perp|\,\rho)$ instead of $K_{ik}(|p_\perp|\,\rho)$. These are not normalizable, so we discard them. However, below we will discuss imaginary values for the momentum k, in which case the regular solutions are precisely these Bessel-J functions.

With respect to this basis of orthonormal functions, we find that the momentum space expression for $\mathcal{G}_\Delta^{a,b}$ is given by the following:

$$\mathcal{G}_\Delta^{a,b}(P_1,P_2) = \frac{1}{(2\pi)^d}\sum_{\omega_E}\int_0^\infty dk \int d^{d-2}p_\perp\, \mathcal{G}_\Delta^{a,b}(\omega_E,k)\, f_{\omega_E,k,p_\perp}(P_1) \times f^*_{\omega_E,k,p_\perp}(P_2)\,, \tag{4.5.17}$$

where

$$\mathcal{G}_\Delta^{a,b}(\omega_E,k) = \frac{\pi^{d/2}}{\Gamma(\Delta)}\frac{a^{\omega_E}}{b^{\Delta+\omega_E}}\frac{\Gamma(\alpha)\Gamma(\alpha^*)}{\Gamma(\omega_E+1)}\,{}_2F_1\left(\alpha,\,\alpha^*,\,\omega_E+1;\,\frac{a^2}{b^2}\right)_{\text{reg.}} \tag{4.5.18}$$

with $\alpha \equiv \frac{1}{2}(\Delta - \frac{d-2}{2} + ik + \omega_E)$. The subscript "reg." refers to the fact that the expression needs to be regularized in the limit as $a,b\to 1$ whence the hypergeometric function is naively divergent. We will describe this regularization below. The derivation of (4.5.18) is analogous to the case of on-shell scalar two-point functions in [158]. We review some of the details in Appendix C.3.2.

By combining (4.5.18) with (4.5.14) (in momentum space) we can now immediately infer the desired correlation function. Taking derivatives with respect to a and b as in (4.5.18), we find for the *energy-energy two-point function on* $S^1\times\mathbb{H}^{d-1}$:

$$\boxed{\mathcal{G}_{00,00}(\omega_E,k) = \frac{C_T\,\pi^{d/2}\,(d-2)\,\Gamma(-\frac{d}{2})}{8\,(d+1)\,\Gamma(d)}\left(k^2+\left(\frac{d}{2}\right)^2\right)\left(k^2+\left(\frac{d-2}{2}\right)^2\right) \times \left.\frac{\Gamma\left[\frac{1}{2}\left(\omega_E \pm ik + \frac{d-2}{2}\right)\right]}{\Gamma\left[\frac{1}{2}\left(\omega_E \pm ik - \frac{d-6}{2}\right)\right]}\right|_{\text{reg.}}} \tag{4.5.19}$$

Here and henceforth, any double sign "$\pm$" inside a function's argument means that one should multiply by all possible signs; for example, $\Gamma(x\pm y)\equiv\Gamma(x+y)\Gamma(x-y)$. Further, the expression is divergent for even dimensions due to the factor $\Gamma(-\frac{d}{2})$. This can be dealt with by performing dimensional regularization and keeping the finite term. We discuss this regularization in some more detail in Appendix C.3.3.

Pole skipping

Given the momentum space expression for the energy-energy correlator, we now wish to discuss the pole skipping phenomenon as described in [53]. There, it was argued that it is interesting to consider the analytic continuation of the energy-energy correlator to complex frequencies and momenta. The latter has lines of poles, which are however lifted at certain special points. These special points allow one to read off the Lyapunov exponent and butterfly velocity in case of chaotic theories.

Our discussion below will generalize the study of pole skipping in two-dimensional CFTs [88, 159]. As we shall see, a very similar pole skipping is observed in arbitrary dimensions and it is sensibly related to the Lyapunov exponent and butterfly velocity characterizing the OTOC. We discuss even and odd dimensions separately.

Odd dimensions. For simplicity, we first focus on the odd-dimensional case, where we do not need any further regularization of (4.5.19).

First note that the pole structure of (4.5.19) comes from the following singular part:

$$\mathcal{G}_{00,00}(\omega_E, k)\Big|_{\text{singular}} \sim \Gamma\left[\frac{1}{2}\left(\omega_E + ik + \frac{d-2}{2}\right)\right]\Gamma\left[\frac{1}{2}\left(\omega_E - ik + \frac{d-2}{2}\right)\right] \tag{4.5.20}$$

The two Γ-functions in the denominator manifestly don't have any zeros (for finite values of the arguments) and hence do not contribute any poles to the two-point function. This singular piece (4.5.20) has...

$$\text{...lines of simple poles at:} \qquad k = \pm i\left[\frac{d-2}{2} + 2n + \omega_E\right] \qquad (n = 0, 1, 2, \ldots) \tag{4.5.21}$$

We will refer to these as the *pole lines*.

In addition, the propagator $\mathcal{G}_{00,00}(\omega_E, k)$ has *zero lines*. These are of two types: there are four vertical lines due to the vanishing of the prefactor $(k^2 + (\frac{d}{2})^2)(k^2 + (\frac{d-2}{2})^2)$, leading to...

$$\text{...lines of simple zeros at:} \quad k = \pm i\,\frac{d}{2} \quad \text{and} \quad k = \pm i\,\frac{d-2}{2}\,. \tag{4.5.22}$$

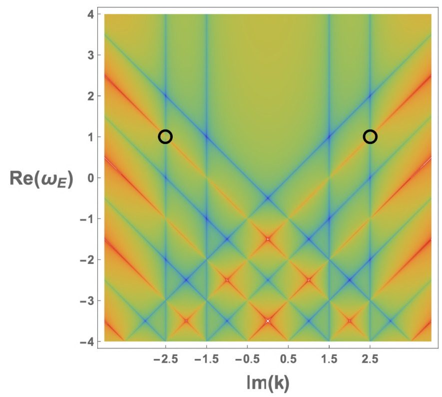

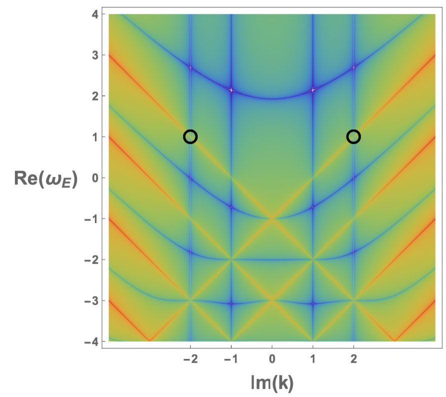

Figure 4.2: Plots of $\log|\mathcal{G}_{00,00}(\omega_E, k)|$ in $d = 5$ (left) and $d = 4$ (right). The "warm" lines (orange/red) correspond to poles. The "cold" lines (blue) correspond to zeros. The four vertical zero lines are due to the polynomial prefactors in (4.5.19) and (4.5.26). Pole skipping occurs when zero lines and pole lines intersect. In order to make a connection with exponentially growing modes in quantum chaos, one should focus on the upper half plane, where pole skipping is observed at precisely two locations (black circles): $(\omega_E, k)_{\text{skip}} = (1, \pm i\frac{d}{2})$. Note that in the even dimensional case (right figure) the precise shape of the zero lines (but not the pole skipping locations) depend on ambiguous contact terms.

Furthermore, the denominator of (4.5.19) has simple poles, leading at the level of the correlation function to...

$$\text{...lines of simple zeros at:} \qquad k = \pm i\left[\frac{d-6}{2} - 2m - \omega_E\right] \qquad (m = 0, 1, 2, \ldots) \tag{4.5.23}$$

The situation is best understood by drawing a density plot of $\mathcal{G}_{00,00}(\omega_E, k)$, see the left panel of Fig. 4.2. This illustrates clearly the structure of zeros and poles (for the example of $d = 5$).

We are interested in the pole skipping phenomenon, i.e., the locations where pole lines and zero lines intersect and the pole is lifted. As we can easily see, this happens infinitely often. However, let us focus on the upper half plane, $\text{Re}(\omega_E) > 0$, where poles correspond to exponentially growing modes relevant to chaos. In the upper half plane the zero lines (4.5.2) never intersect with pole lines (4.5.21) and pole skipping is solely due to the vertical zero lines (4.5.23). Furthermore, only the line $k = \pm i\frac{d}{2}$ intersects with the pole lines indexed by $n = 1$. In order to get exponential growth, our conventions will single out the following pole skipping locations as the relevant one:

$$(\omega_E, k)_{\text{skip}} = \left(1,\ \pm i\,\frac{d}{2}\right). \tag{4.5.24}$$

For later reference, we also record the other three locations where $n = 1$ pole lines are skipped due to intersection with the vertical zero lines:

$$(\omega_E, k)^{(s)}_{\text{skip}} = \left(0,\ \pm i\,\frac{d-2}{2}\right). \tag{4.5.25}$$

The meaning of the superscript $^{(s)}$ is supposed to indicate that these pole skipping locations are related to “shadow” contributions to the soft mode propagator.

We will demonstrate below how to determine the Lyapunov exponent of chaotic CFTs from (4.5.24). It is crucial to stress that this particular pole skipping occurs for complex frequency in the *upper* half plane, thus leading to exponentially growing modes. This is a feature of the stress tensor correlator, which is absent in discussions of other two-point functions that also display pole skipping, but only in the lower half plane and not related to quantum chaos in any immediate way (c.f. [154, 155]).

Even dimensions. In even dimensions, the regularization of the expression (4.5.19) leads to a slightly more complicated result. We offer the full expression in Appendix C.3.3. For now, let us simply quote the result (C.3.9) for the special case of $d = 4$:

$$\begin{aligned}\mathcal{G}_{00,00}(\omega_E, k)^{(d=4)}_{\text{finite}} = -\frac{C_T\,\pi^2}{240}\,(k^2+4)(k^2+1)\Bigg\{&\psi\left(\frac{\omega_E + ik + 1}{2}\right)\\ &+\psi\left(\frac{\omega_E - ik + 1}{2}\right)\Bigg\}\end{aligned} \tag{4.5.26}$$

A section of this function is plotted in the right panel of Fig. 4.2.

As is clear from inspection, the lines of poles are precisely the same as in odd dimensions, (4.5.21). Also, the vertical lines of zeros due to the polynomial prefactor are identical to (4.5.2). Only the additional lines of zeros (the analog of (4.5.23)) are more complicated and in fact depend on contact terms. As far as pole skipping is concerned, we will mostly be interested in the intersection of pole lines and vertical zero lines, which are identical to the odd dimensional case and independent of the regularization and contact terms; unsurprisingly, they lead to pole skipping at the same location as in odd dimensions, (4.5.24).

Lyapunov exponent and butterfly velocity from pole skipping. Let us focus on the $n = 0$ trajectory in the upper half plane (for any $d \geq 3$), where the pole skipping happens at $(\omega_E, k)_{\text{skip}} = (1, \pm i\frac{d}{2})$. We wish to interpret these locations as characterizing the Lyapunov exponent and butterfly velocity in Rindler space. In order to interpret this, we will now give two arguments – one abstract and one very concrete. We will set the transverse momenta $p_\perp^i = 0$ for simplicity.

As an abstract interpretation of the pole skipping on the $n = 0$ trajectory, note that the pole skipping at $(\omega_E, k)_{\text{skip}} = (1, \pm i\frac{d}{2})$ corresponds to the following eigenvalues of the Laplacian (4.5.15) on $S^1 \times \mathbb{H}^{d-1}$:

$$\left(\omega_E^2,\ -k^2 - \frac{(d-2)^2}{4}\right)_{\text{skip}} = (1,\ d-1)\,, \tag{4.5.27}$$

where we neglect the transverse directions. As in the flat space case, we interpret the first eigenvalue as saying that there is an imaginary frequency mode, corresponding to exponential growth with Lyapunov exponent 1 in units of $\frac{2\pi}{\beta}$. Similarly, we interpret the second eigenvalue as the inverse of the butterfly velocity in the same units. That is, $v_B = \frac{1}{d-1}$ in accordance with [149].[87]

In order to give a more concrete interpretation, we can evaluate the basic "Fourier" modes (4.5.16) at the pole skipping location in a long-time (Lyapunov) and short-distance (flat space) limit. Obviously, the time dependence of (4.5.16) is just a plane wave, which evaluated at $\omega_E = \pm i$ gives exponential modes $e^{\mp\tau}$ associated with a Lyapunov exponent $\lambda_L = 1$. In order to extract the butterfly velocity, we study the u-dependence of (4.5.16) at the pole skipping location for spatially nearby points ($\rho \to 0$). One subtlety is that the Bessel function K_{ik} evaluated at $k = i\,\frac{d}{2}$ is not regular at short distances. In order to get a sensible interpretation, we replace it by the regular solution to the Laplacian on $S^1 \times \mathbb{H}^{d-1}$, eq. (4.5.15), which takes the form of (4.5.16) with Bessel-J functions instead of Bessel-K. At the pole skipping location these hyperbolic eigenfunctions behave as

$$\rho^{\frac{d-2}{2}} J_{ik}(i|p_\perp|\,\rho)\Big|_{(\omega_E,k)\to(1,-i\frac{d}{2})} \overset{\rho\to 0}{\sim} \quad \rho^{d-1}\,. \tag{4.5.28}$$

Writing $\rho = e^\sigma$, this behavior clearly corresponds to a butterfly velocity $v_B = \frac{1}{d-1}$ as expected for chaos in Rindler space.

[87] As a side remark, note that the other vertical zero line, leading to pole skipping at $(\omega_E, k) = (0, \pm i\frac{d-2}{2})$ has eigenvalues $\left(\omega_E^2,\ -k^2 - \frac{(d-2)^2}{4}\right)_{\text{skip}} = (0, 0)$. This seems unrelated to Lyapunov growth.

4.6 Conclusions and outlook

Summary. Motivated by recent studies of reparametrization modes in the low energy SYK model and two-dimensional CFTs, we set out to provide a more general understanding of the dynamics of such modes in CFTs of arbitrary dimension. We have established a variety of connections between reparametrization modes, the conformal anomaly, the shadow operator formalism for conserved currents, and OPE block techniques in kinematic space. These connections explain in detail how the reparametrization modes are related to the physics of stress tensor contributions to conformal blocks and provide an interesting new perspective on all these topics.

The simplest example for a physical computation is the exchange of a single reparametrization mode in a four-point function. At large central charge this is indeed the dominant contribution. It computes the single-stress tensor exchange in the global conformal block. Exchanges of multiple reparametrization modes are expected to compute multi-stress tensor exchanges. In $d = 2$ these compute the stress tensor contribution to the Virasoro identity block; in the "light-light" regime, the dominant diagrams are ladder diagrams.

As an immediate application, we also studied CFTs in thermal states by exploiting the equivalence of physics in the Rindler wedge and thermal physics of CFTs living on a hyperbolic space. By investigating pole skipping in the thermal energy-energy two-point function in arbitrary dimensions, we confirmed the expected behavior of out-of-time-ordered correlation functions and derived the chaos exponents for maximally chaotic CFTs on hyperbolic space.

Questions and future directions. Some interesting opportunities for future research are now available. While we provided a quadratic action for the reparametrization mode, we have not yet found a way to complete it nonlinearly. In one dimension, the nonlinear completion is the Schwarzian action [17, 22]; in two dimensions the nonlinear completion is the Alekseev-Shatashvili action [115, 120]. We wonder if it might be possible to obtain a nonlinear action in higher (even) dimensions by performing a coadjoint orbit quantization of kinematic space (4.2.1). It was already shown in [160] that higher-dimensional kinematic space is indeed a coadjoint orbit of the conformal group. It would be interesting to explore this further in light of the new perspective provided by the present chapter.[88]

[88] See also [161, 162] for other relations of kinematic space with theories of reparametrizations in $d = 2$.

So far, all our detailed understanding of chaotic theories in terms of few effective degrees of freedoms (reparametrization modes) describes theories that saturate the chaos bound of [48]. It will be interesting to understand how the reparametrization mode theory should be modified such as to capture corrections to the maximal Lyapunov exponent. It is clear that the pole skipping phenomenon is special to maximally chaotic theories (for instance, as we have shown, it occurs in any conformal field theory, irrespective of integrability, chaoticity etc.). It would be interesting if there exists a suitable generalization of the pole skipping phenomenon which provides an effective field theory description of modes other than just stress tensor contributions and is thus capable of capturing corrections to maximal chaos.

It will be interesting to apply the theory of reparametrization modes to study stress tensor conformal blocks at large central charge. These are particularly interesting in the context of holography, where they describe the leading universal physics of graviton exchanges in the bulk. Various known results have already been reproduced, illustrating the utility and simplicity of the formalism. It should now be used to find novel results – for example, one can imagine studying conformal blocks in new kinematic regimes (e.g., the late time regime [163], the light cone regime [164], etc.), or higher-point conformal blocks in various channels [144, 165, 166]. Furthermore, not much is known about the higher-dimensional conformal blocks beyond the global single-stress tensor exchanges (see however [135–137]).

Some technicalities about the formulation of the shadow operator formulation in terms of the reparametrization mode deserve better understanding. For instance, much of our formulation is restricted to an even number of spacetime dimensions: the quadratic action for the reparametrization mode only exists due to the conformal anomaly in even dimensions. We anticipate that the non-existence of a simple theory of reparametrizations in odd dimensions might be related to various other complications in that case. For instance, even global conformal blocks are very complicated in odd dimensions [118]. On the other hand, the pole skipping phenomenon discussed in §4.5.2 does occur both in even and odd dimensions.[89] It would be good to understand what this means for the existence or non-existence of a simple theory of reparametrizations in odd dimensions.

[89] Note, however, that the technical details are quite different in the two cases.

Chapter 5

Looking for (and not finding) a bulk brane

5.1 Introduction

Is every consistent theory of quantum gravity a 'string theory'? There are many ways to attempt to ask this question (or even just to define the terms). Since string theory involves non-perturbative higher-dimensional objects or branes, in the context of AdS/CFT one way of asking this question is to study whether, given a holographic conformal field theory (CFT), defect operators in the CFT are described by gravitational branes in the dual bulk. That is, does every holographic CFT have a well-behaved spectrum of branes? As a step in this general direction, in this chapter we ask if, given a holographic CFT, every conformal boundary condition is properly described by the bulk gravitational effective field theory, allowing for the addition of a semi-classical 'end-of-the-World (ETW)' brane[90].

A closely related—but more concrete—ambition is to sharpen the holographic dictionary for boundary conformal field theories (BCFT). That is, given a holographic CFT, what additional assumptions—if any—must be made for an associated BCFT to be described by the bulk gravitational effective field theory (again allowing for the addition of semi-classical branes)? And can we explicitly write the mapping between solutions of the boundary bootstrap and semi-classical bulk+brane actions?

Sharpening the holographic dictionary for BCFTs is timely. Recent works [168–178] have employed a BCFT as a model of a lower-dimensional gravitational system coupled to an auxiliary CFT. A BCFT is then a concrete and calculable model for studying Euclidean wormholes and islands. In these works, it has been assumed that the BCFT has a good holographic dual with

[90]In the literature, the term "end-of-the-world brane" is sometimes also applied to higher-dimensional duals of holographic BCFTs in which the spacetime caps off smoothly over large distances due to shrinking internal space directions; see e.g. [167]. In this work, we will use this term to connote a localized, semi-classical gravitating brane which constitutes a boundary for a given spacetime.

an ETW brane. Furthermore, it has been suggested that one might be able to minimally UV-complete coarse-grained gravitational theories by adding ETW branes to the theory [179, 180]. But just how realistic or typical are well-behaved ETW branes in a theory of gravity?

A similar program for sharpening the duality between CFTs and bulk gravitational effective field theory was initiated in [181]. There, the conformal bootstrap was used to argue that any CFT such that

(i) simple correlators factorize in a $1/c$ expansion; and

(ii) the spectrum is gapped such that below some large Δ_{gap} the only operators are simple light operators and their multi-trace composites

is dual to a bulk theory of semi-classical Einstein gravity. A great deal of subsequent work on the holographic bootstrap has strengthened and refined this claim, for example [182–193].

To begin the parallel program for BCFTs, we first note that the holographic CFT bootstrap typically begins with the assumption that the bootstrap can be studied in a $1/c$ expansion about a universal mean field theory solution (MFT) determined by the CFT two-point function. For example, a scalar four-point function would have the schematic form

$$\langle \phi\phi\phi\phi \rangle = \sum \langle \phi\phi \rangle^2_{Univ} + \mathcal{O}(1/c) \,, \tag{5.1.1}$$

where $\langle \phi\phi \rangle_{Univ}$ is the universal CFT two-point function.

In contrast to a CFT, the BCFT two-point function is not universal and kinematically behaves similarly to a CFT four-point function [194–196]. Moreover, unlike for the holographic CFT, there is no restriction from the BCFT or its gravitational dual that this two-point function should be perturbatively close to a known universal solution like the MFT. Thus, before attempting to understand an analogous correspondence between bulk+brane interactions and perturbative solutions to the BCFT bootstrap, we must first understand the leading order, non-perturbative backreaction of the boundary on the bulk gravitational solution.

To understand what is special about the leading order solution for a BCFT with a simple bulk dual, we will argue that it is useful to rotate to Lorentzian/Minkowski signature, since the Lorentzian BCFT two-point function can probe the *bulk causal structure*. When the BCFT has a semi-classical gravitational dual, the bulk causal structure often implies the existence of new approximate singularities in the BCFT[91] (see Figure 5.1).

[91] We don't expect these to be true singularities of the BCFT. Rather, much like the

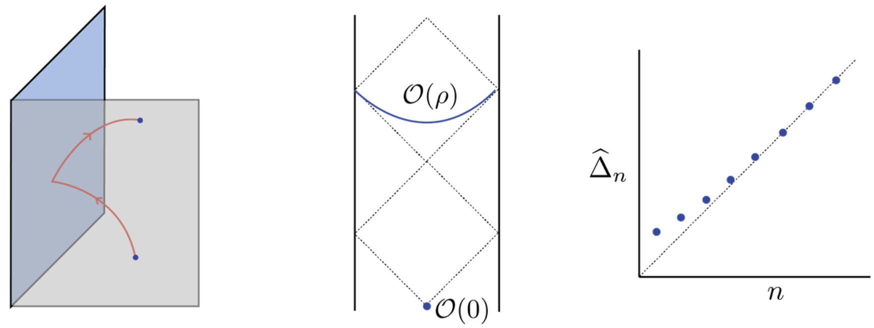

(a) (b) (c)

Figure 5.1: (a) A light ray leaving the boundary and returning to the boundary at a later time (in this example reflecting off an ETW brane); (b) The bulk causal structure then implies new 'bulk brane' singularities in the BCFT to the future of a BCFT operator; (c) The bulk brane singularities require a careful alignment of operator dimensions appearing on the boundary of the BCFT.

Similar singularities for scattering at bulk points in a CFT have been noted before, and their CFT origins were discussed in detail in [197].[92]

On the BCFT side, these new bulk singularities can only be obtained through the careful alignment of boundary operator dimensions over some large range of dimensions up to a 'boundary gap' $\widehat{\Delta}_{\text{gap}}$. The careful alignment of these operators makes such a bulk causal structure fragile. We find no constraints from the CFT being holographic that fix these specific dimensions.

From the fragility of the bulk causal structure, we suggest that holographic boundary conditions are sparse in the space of all boundary conditions for a holographic CFT. On top of the assumptions already necessary for our CFT to be holographic, we must further make a new set of assumptions about the boundary condition itself. Namely, we would like to conjecture that a holographic CFT with a boundary condition whose

(i) correlators factorize in an expansion about a (non-universal) free bulk solution; and

semi-classical singularities predicted by scattering at a bulk point, these will be flattened out at the scale of the gap when the gravitational theory becomes non-local [197]. A similar phenomenon is observed in the two-point function of a holographic CFT at finite temperature; singularities due to null geodesics which wrap the photon sphere of the bulk black hole are resolved by tidal effects in string theory [198].

[92]Lorentzian CFT correlation functions and the singularities from bulk points have been used as a powerful diagnostic of bulk geometry [199–201].

(ii) boundary operator spectrum is gapped such that below some large $\widehat{\Delta}_{\rm gap}$ the only operators are simple light operators and their multi-trace composites;

is dual to a bulk theory of semi-classical gravity with the possible addition of an ETW brane with a local action. It is the first of these conditions that this chapter suggests is not generic and must be assumed, although there are subtleties related to this point that appear when we study more complicated top-down constructions of holographic BCFTs. The second condition, and the necessity and sufficiency of these two conditions together, will *not* be addressed in this chapter.

This chapter is structured as follows. We begin with a review of BCFTs and their holographic duals in section 5.2, as well as establishing notation to be used in the rest of the chapter. A reader familiar with BCFTs can easily skip this section or reference it when the notation we use is not obvious. To understand what a holographic BCFT looks like in terms of its spectrum of boundary operators, in section 5.3 we examine the simplest possible model: empty AdS cut off by an ETW brane. We take the operator spectrum found in our simple model and explain its meaning in section 5.4 by studying the bulk causal structure and the Lorentzian continuation of BCFT two-point functions. We establish a general correspondence between the boundary operator spectrum and the bulk causal structure in section 5.5; this leads to our conjecture about necessary and sufficient conditions for a holographic BCFT. We examine our conjecture in top-down models and introduce some necessary caution regarding the strongest version of our claims in section 5.6. We conclude with a discussion in section 5.7.

5.2 Review of BCFT

Critical phenomena involving a boundary are described by boundary conformal field theories, which involve generalizations of the many familiar concepts and tools of conformal field theories. To arrive at a BCFT, one typically introduces a boundary to a known CFT where the space ends. One may also introduce additional degrees of freedom living on the boundary, which can be coupled to the CFT degrees of freedom. A complete specification of the theory then involves imposing boundary conditions for the the bulk degrees of freedom, as well as dynamics for the boundary excitations. If this can be done in a manner that maximally preserves conformal invariance, or by flowing to a conformal fixed point, the resulting theory is a BCFT. For a given CFT, there may be many different possible choices of conformally-invariant

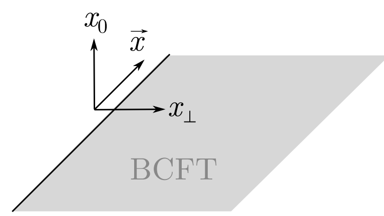

Figure 5.2: A BCFT on a half-plane $\mathbb{R}^{d-1} \times \mathbb{R}^{+}$. Here, x_0 and $\vec{x}$ are coordinates parallel to the boundary; $x_\perp$ is a coordinates perpendicular to the planar boundary, which sits at $x_\perp = 0$.

boundary conditions (or conformal fixed points), each of which is described by a different BCFT.

Symmetries The most basic tool in studying a BCFT is conformal representation theory: the excitations of the theory organize themselves into representations of a reduced conformal symmetry group that is left unbroken by the new boundary. When the BCFT lives on the half-plane $\mathbb{R}^{d-1} \times \mathbb{R}_+$ with a planar boundary, the unbroken symmetry is $\mathrm{SO}(d,1) \subset \mathrm{SO}(d+1,1)$, which is the set of transformations that maps the half-plane back to itself. We will use coordinates on this space given by $x = (x_0, \vec{x}, x_\perp)$, where $x_0, \vec{x}$ are Euclidean coordinates parallel to the boundary and $x_\perp$ is our coordinate orthogonal to the planar boundary. We depict these coordinates in Figure 5.2.

CFT Operators and Boundary Operators Because a BCFT only modifies the CFT along the boundary, the spectrum of CFT operators and their algebra remains unchanged. Localized on the boundary, however, we have new *boundary operators*, $\hat{\mathcal{O}}_I$. These operators are organized into representations of $\mathrm{SO}(d,1)$, which are partially labeled by a boundary conformal dimension $\hat{\Delta}_I$. The boundary conformal dimension is just the usual eigenvalue of the unbroken d-dimensional dilation operator (which dilates both along and away from a point on the boundary). As is familiar, any such representation has a primary and descendants and we use this structure to organize our description of the BCFT in much the same way as we do for CFTs.

State-Boundary Operator Map By the usual logic of the state-operator mapping, there is a one-to-one map between boundary operators of the

BCFT and states of the theory quantized on a half-sphere D^{d-1}. This follows from the half-plane picture by using an infinite dilation to map back to a point on the boundary. Alongside the state-boundary operator map, we still also have the regular CFT state-operator map when we quantize the theory on a sphere S^{d-1} which does not intersect the boundary.

The state-boundary operator map allows us to write a *boundary operator expansion* (BOE), whereby any CFT operator can be written as a sum over boundary operators

$$\mathcal{O}_i(x) = \frac{\mathcal{A}_i}{(2x_\perp)^\Delta} + \sum_J \frac{\mathcal{B}_{iJ}}{(2x_\perp)^{\Delta_i - \Delta_J}} \widehat{C}[x_\perp, \partial_{\vec{x}}] \widehat{\mathcal{O}}_J(x_0, \vec{x}) \,, \tag{5.2.1}$$

where the sum over J is over boundary primary operators and the differential operator $\widehat{C}$ which contributes the contributions of descendants is fixed by conformal invariance. Likewise, the BCFT inherits the regular OPE from the CFT without a boundary:

$$\mathcal{O}_i(x)\mathcal{O}_j(y) = \sum_k \frac{\mathcal{C}_{ij}^k}{|x-y|^{\Delta_i + \Delta_j - \Delta_k}} C[x-y, \partial_y] \mathcal{O}_k(y) \,. \tag{5.2.2}$$

Correlation Functions Because of the reduced symmetry, BCFT correlation functions involving CFT operators away from the boundary are less constrained than those of a CFT without a boundary. A useful 'trick' for characterizing the kinematic constraints on a BCFT correlator is to view the correlator as doubled with operator insertions mirrored across the boundary (each copy carrying half the conformal weight of the original operator).

Following the logic of doubling, one can easily see that a scalar CFT operator has a one-point function that behaves kinematically like a CFT two-point function

$$\langle \mathcal{O}(x) \rangle = \frac{\mathcal{A}_\mathcal{O}}{(2x_\perp)^\Delta} \,, \tag{5.2.3}$$

where the coefficient $\mathcal{A}_\mathcal{O}$ which determines the size of the vacuum expectation value is a free parameter of the theory, unlike in a CFT, because we choose not to change the normalization of our CFT operators.

Likewise, the two-point function of scalar operators in a BCFT behaves much like a CFT four-point function and thus no longer fixed by conformal invariance. It can be written in terms of an undetermined function of a single conformally-invariant cross-ratio,

$$\langle \mathcal{O}(x)\mathcal{O}(y) \rangle = \frac{1}{|4x_\perp y_\perp|^\Delta} \mathcal{G}(\xi) \,, \tag{5.2.4}$$

where the cross-ratio can be defined as

$$\xi = \frac{(x-y)^2}{4x_\perp y_\perp} = \frac{(x_0-y_0)^2 + (\vec{x}-\vec{y})^2 + (x_\perp - y_\perp)^2}{4x_\perp y_\perp} \,. \tag{5.2.5}$$

5.2.1 Boundary Bootstrap

The function $\mathcal{G}(\xi)$ that appears in (5.2.4) must decompose into irreducible representations of the conformal symmetry. There are two ways to perform this decomposition. We can take the operators near to each other, $\xi \to 0$, and use the CFT OPE to fuse the two operators into a sum of bulk operators. We can then evaluate the sum over local operators in the BCFT. The result is an expansion in terms of bulk conformal blocks g^B [195, 196, 202]:

$$\text{Bulk Channel :} \qquad \mathcal{G}(\xi) = \sum_i a_i \, g^B_{\Delta_i}(\xi) \,, \tag{5.2.6}$$

where i labels CFT bulk primaries and the coefficients a_i are the product of the bulk OPE coefficient and one-point function coefficient of $\mathcal{O}_i$,

$$a_i = \mathcal{C}^i \mathcal{A}_i \,, \tag{5.2.7}$$

where we suppress the $\mathcal{O}$ appearing in the OPE coefficient. Alternatively, we can take the operators to the boundary, $\xi \to \infty$, and use the BOE to expand each operator as a sum of boundary operators. We then evaluate the two-point functions of the resulting summed boundary operators, which are fixed by conformal invariance. The result is an expansion in terms of boundary blocks g^b [195, 196, 202]:

$$\text{Boundary Channel :} \qquad \mathcal{G}(\xi) = \sum_I b_I \, g^b_{\hat{\Delta}_I}(\xi) \,, \tag{5.2.8}$$

where I labels boundary primary operators and b_I is the square of their BOE coefficients

$$b_I = {\mathcal{B}_I}^2 \,. \tag{5.2.9}$$

The equivalence of the expansions in terms of either the boundary conformal blocks or bulk conformal blocks,

$$\sum_{\mathcal{O}'} a_i g^B_{\Delta_i}(\xi) = \sum_I b_I g^b_{\hat{\Delta}_I}(\xi) \,, \tag{5.2.10}$$

is a BCFT version of *crossing symmetry* and gives bootstrap equations that can be studied with analogous tools as in the CFT case [196, 202]. We depict the crossing symmetry visually in Figure 5.3.

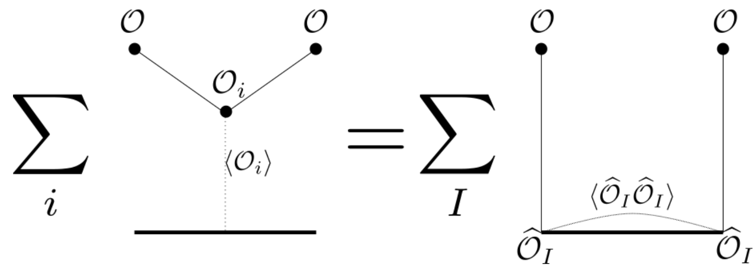

Figure 5.3: Pictorial representation of 5.2.10. The thick line represents the boundary; thin lines represent fusion of external operators into bulk or boundary operators; dotted lines represent correlators.

Scalar Blocks As shown in [195], the scalar conformal blocks, obtained by solving the Casimir equation for the full and reduced conformal symmetry, are

$$g^B_\Delta(\xi) = \xi^{\Delta/2-\Delta_{\text{ext}}}{}_2F_1\left(\frac{\Delta}{2},\frac{\Delta}{2};\Delta-\frac{d}{2}+1;-\xi\right) \tag{5.2.11}$$

$$g^b_{\widehat{\Delta}}(\xi) = \xi^{-\widehat{\Delta}}{}_2F_1\left(\widehat{\Delta},\widehat{\Delta}-\frac{d}{2};2\widehat{\Delta}+2-d;-\xi^{-1}\right)\,, \tag{5.2.12}$$

where Δ_{ext} is the dimension of the external operators.

There are branch point singularities in $\mathcal{G}(\xi)$ at $\xi\to 0,\infty$. As in [202], we take the branch cut to run from $(-\infty,0)$, so that the Lorentzian continuation ξ lives on the cut plane $\mathbb{C}\backslash(-\infty,0)$.

Radial Coordinates We can also introduce radial coordinates [203, 204], which will simplify some of our expressions:

$$\xi = \frac{(1-\rho)^2}{4\rho}\,. \tag{5.2.13}$$

This takes the cut ξ-plane to the unit disk $|\rho|<1$, with $\xi\in(0,\infty)$ mapped to $\rho\in(0,1)$. The boundary block is then

$$g^b_{\widehat{\Delta}}(\rho) = \left[\frac{4\rho}{(1-\rho)^2}\right]^{\widehat{\Delta}}{}_2F_1\left(\widehat{\Delta},\widehat{\Delta}-\frac{d}{2}+1;2\widehat{\Delta}+2-d;\frac{-4\rho}{(1-\rho)^2}\right) \tag{5.2.14}$$

$$= (4\rho)^{\widehat{\Delta}}{}_2F_1\left(\widehat{\Delta},\frac{d-1}{2};\widehat{\Delta}-\frac{d}{2}+\frac{3}{2};\rho^2\right)\,, \tag{5.2.15}$$

where on the second line, we used a quadratic transformation of the hypergeometric function ${}_2F_1$.

5.2.2 Holographic BCFT

Bottom-Up Models

In [205, 206] (following [207, 208]) it was proposed that the holographic dual of a BCFT should be a bulk geometry, $\mathcal{M}$, terminated by an ETW brane, $\mathcal{B}$, that acts as an additional infrared boundary for the gravitational theory. The new boundary $\mathcal{B}$ meets the standard asymptotically AdS boundary at the location of the BCFT boundary (see Figure 5.4). The gravitational sector of the bulk+brane theory is proposed to have an action that now includes a standard Gibbons-Hawking boundary term on the brane

$$S_G = \frac{1}{16\pi G_N}\int_{\mathcal{M}} \sqrt{-g}(R-2\Lambda) + \frac{1}{8\pi G_N}\int_{\mathcal{B}} \sqrt{-h}(K-T)\,, \tag{5.2.16}$$

where h is the induced metric on the brane, K is the trace of the extrinsic curvature, and T is the tension of the ETW brane. One also expects the same bulk AdS matter action as the original CFT without a boundary as well a new matter action living on the ETW brane:

$$S = S_G + \int_M \mathcal{S}^m_{AdS} + \int_B \mathcal{S}^m_{ETW}\,. \tag{5.2.17}$$

The residual SO$(d,1)$ symmetry of the BCFT fixes the bulk geometry to take the highly-constrained form

$$ds^2 = dr^2 + e^{2A(r)} ds^2_{AdS_d}\,, \tag{5.2.18}$$

where a lower-dimensional AdS$_d$ is warped over a radial direction with some warp factor $A(r)$. The warp factor is determined by whatever vacuum expectation values are sourced by the ETW matter action $\mathcal{S}^m_{ETW}$, but must asymptotically approach that of empty AdS$_{d+1}$ where $A(r) = \ln\cosh(r)$ as $r \to -\infty$. (We will work in coordinates where the AdS radius $L = 1$.) The ETW brane will sit on some constant radial slice $r = r_0$, fixed by the combination of the tension T and the particular warp factor $A(r)$.

Top-Down Models

The bottom-up proposal of [205, 206] is known to be too simple to fully describe some explicit top-down constructions of holographic duals that have been derived for 'microscopic' BCFTs. In these cases, there is a more complicated bulk geometry with a non-trivial internal space. The internal space allows the bulk geometry to cap off smoothly in the infrared instead of ending on a brane. A few known top-down constructions of holographic BCFT are worth noting here:

- In [209, 210], the authors present general half-BPS solutions of 6-dimensional type 4b supergravity, including those with a single $\mathrm{AdS}_3 \times S^3$ asymptotic region, expected to be dual to BCFT_2. The geometric ansatz for these solutions is a warped product $\mathrm{AdS}_2 \times S^2$ fibred over a Riemann surface Σ. The solutions constructed in [209] are referred to as the AdS_2-cap and AdS_2-funnel; a more general class of solutions is found in [210], involving Riemann surfaces Σ with additional boundary components and handles. It is conjectured that these solutions should correspond to supersymmetric configurations of self-dual strings and 3-branes, though this identification and the corresponding class of BCFTs is not well-understood.

- Half-BPS solutions of 11-dimensional supergravity with a single $\mathrm{AdS}_4 \times S^7$ region, corresponding to stacks of semi-infinite M2-branes ending on M5-branes, have been constructed in [211, 212].

- In [213–215], half-BPS solutions of type IIB supergravity, corresponding to configurations of D3-branes ending on D5-branes and NS5-branes, were constructed. Solutions with a single asymptotic $\mathrm{AdS}_5 \times S^5$ region furnish a holographic description of the $U(N)$ $\mathcal{N} = 4$ super Yang-Mills theory with $OSp(4|4)$-preserving boundary conditions, classified by Gaiotto and Witten in [216, 217].

We discuss explicit top-down models in more detail in section 5.6.2.

Holographic BCFT Dictionary

Here we review the holographic dictionary for a scalar bulk field in a BCFT. We explain how to construct bulk operators in bottom-up models and how to extract their corresponding boundary operator expansion data. We follow closely the treatment in [218], although we will use slightly different conventions.

Consider a bulk scalar field operator $\phi(\vec{y}, u, r)$ of mass M. By the standard AdS/CFT dictionary, this field is dual to a CFT operator $\mathcal{O}_\Delta$ of dimension

$$\Delta = \frac{1}{2}\left(d + \sqrt{d^2 + 4M^2}\right) . \tag{5.2.19}$$

At leading order, the bulk field satisfies the free wave equation on the warped background

$$\left(\Box_{\mathcal{M}} - M^2\right)\phi = 0 \, . \tag{5.2.20}$$

We can write a solution of this wave equation in the form

$$\sum_n \bar{\psi}_n(r)\hat{\phi}_n(\vec{y},w), \tag{5.2.21}$$

where the $\hat{\phi}_n$ are fields of mass m_n which satisfy the Klein-Gordon equation $\Box_d\hat{\phi}_n = m_n^2\hat{\phi}_n$ in AdS$_d$. Substituting the mode expansion into (5.2.20) we find that the radial modes $\bar{\psi}_n(r)$ must solve

$$\bar{\psi}_n''(r) + dA'(r)\bar{\psi}_n'(r) + e^{-2A(r)}m_n^2\bar{\psi}_n(r) - M^2\bar{\psi}_n(r) = 0, \tag{5.2.22}$$

To completely determine the mode expansion, we must also specify a complete set of boundary conditions. As we are looking for the bulk operator, we require that our solution be normalizable as we approach the AdS boundary

$$\bar{\psi}_n(r) \underset{r\to\infty}{=} e^{-r\Delta}\,(1+\ldots) \tag{5.2.23}$$

and furthermore choose that the leading term is unit normalized. A second boundary condition is specified on the bulk brane, where the specific condition is determined by the terms appearing in the brane action. Together, these two boundary conditions determine the correct modes ψ_n and eigenvalues m_n, giving the bulk scalar operator

$$\phi(\vec{y},u,r) = \sum_n \psi_n(r)\hat{\phi}_n(\vec{y},w)\,. \tag{5.2.24}$$

The last step in writing down (5.2.24) is to fix the correct rescaling of the mode functions $\psi_n = c_n\bar{\psi}_n$. The rescaling is determined by enforcing the canonical commutation relations for the bulk field (see Appendix D.1). Note that with this proper normalization in place, the mode functions have the asymptotic form $\psi_n(r) = c_n e^{-r\Delta} + \ldots$.

Having derived the bulk scalar operator, we can now take the boundary limit to obtain the dual CFT operator. The mode expansion in terms of the AdS$_d$ operators directly gives the dual boundary operator expansion [218]. However, it is even cleaner to relate the bulk modes to boundary operators by considering the bulk and boundary two-point functions, which we will do in the following.

Holographic Two-Point Function Consider the bulk two-point function in our mode expansion:

$$\begin{aligned}\langle\phi(\mathbf{x}_1)\phi(\mathbf{x}_2)\rangle &= \sum_{n,m}\psi_n(r_1)\psi_m(r_2)\left\langle\hat{\phi}_n(x_1,u_1)\hat{\phi}_n(x_2,u_2)\right\rangle \\ &= \sum_{n,m}\psi_n(r_1)\psi_m(r_2)G^{(AdS_d)}_{\Delta_n}(x_1,u_1;x_2,u_2).\end{aligned} \tag{5.2.25}$$

Using the known form of the AdS$_d$ two-point function (see e.g. [219],

$$G_{\Delta}^{(AdS_d)}(\xi) = \mathcal{C}_{\Delta,d-1}2^{-2\Delta}\xi^{-\Delta}\,{}_2F_1(\Delta,\Delta-d/2+1,2\Delta-d+2,-1/\xi) \quad (5.2.26)$$

where

$$\mathcal{C}_{\Delta,d-1} = \frac{\Gamma(\Delta)}{2\pi^{\frac{d-1}{2}}\Gamma(\Delta-d/2+3/2)}\,, \quad (5.2.27)$$

one can compute the CFT two-point function in the standard way:

$$\langle\mathcal{O}_1\mathcal{O}_2\rangle = \lim_{r_1,r_2\to\infty}\cosh^{2\Delta}(r)\frac{1}{\mathcal{C}_{\Delta,d}}\left\langle\phi(X_1)\phi(X_2)\right\rangle. \quad (5.2.28)$$

Because the AdS$_d$ bulk-to-bulk propagator (5.2.26) and boundary conformal block (5.2.12) are identical (up to a constant), we immediately find

$$\langle\mathcal{O}_1\mathcal{O}_2\rangle = \frac{1}{\mathcal{C}_{\Delta,d}}\sum_n\left(\lim_{r_1,r_2\to\infty}\cosh^{2\Delta}(r)\psi_n(r_1)\psi_n(r_2)\right)\mathcal{C}_{\Delta_n,d-1}2^{-2\Delta}g^b_{\Delta_n}(\xi), \quad (5.2.29)$$

which we can rewrite as

$$\langle\mathcal{O}_1\mathcal{O}_2\rangle = \frac{1}{\mathcal{C}_{\Delta,d}}\sum_n c_n^2\mathcal{C}_{\Delta_n,d-1}2^{-2\Delta_n}g^b_{\Delta_n}(\xi). \quad (5.2.30)$$

From comparing this expression to (5.2.8), we conclude two things:

1. The spectrum of boundary operators appearing in the BOE of $\mathcal{O}_\Delta$ is given by
$$\left\{\Delta_n = \frac{1}{2}\left(d-1-\sqrt{(d-1)^2+4m_n^2}\right)\right\}. \quad (5.2.31)$$

2. The BOE coefficients are given by
$$\mathcal{B}_n = \frac{1}{2^{\Delta_n}}\sqrt{\frac{\mathcal{C}_{\Delta_n,d-1}}{\mathcal{C}_{\Delta,d}}}c_n\,. \quad (5.2.32)$$

5.3 Simplest Bulk Model

To understand the leading-order free two-point function in a holographic theory, we begin by studying the simplest possible bottom-up model: empty AdS terminated by an ETW brane. In our radial coordinates (5.2.18), the AdS$_d$ foliation of AdS$_{d+1}$ takes the form

$$ds^2 = dr^2 + \cosh^2(r)\left(\frac{d\vec{y}^2+du^2}{u^2}\right). \quad (5.3.1)$$

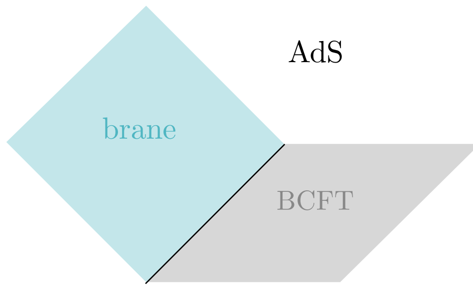

Figure 5.4: Our simple model in which the bulk is locally AdS_{d+1}, but is terminated by an ETW brane. We depict here the AdS_d foliation of AdS_{d+1}.

The location of the brane is given by some $r = r_0$, determined by the tension. See Figure 5.4. It will also sometimes be useful to change to an 'angular' coordinate using $\tanh(-r) = \cos(\varphi)$ so that

$$ds^2 = \csc^2\varphi \left[d\varphi^2 + \left(\frac{d\vec{y}^2 + du^2}{u^2} \right) \right] , \tag{5.3.2}$$

simplifying the conformal structure of the metric.

We consider a free scalar field, ϕ, whose dual CFT operator has dimension Δ. We will need to impose boundary conditions at the location of the brane. As a simple choice, we choose Neumann boundary conditions on the field, $\partial_r \phi(r_0) = 0$, although the qualitative features of our results will not depend on this specific choice. Using the mode expansion explained in section 5.2.2,

$$\phi(\vec{y}, u, r) = \sum_n c_n \bar{\psi}_n(r) \hat{\phi}_n(\vec{y}, u) , \tag{5.3.3}$$

we find the two independent radial solutions of the EOM to be

$$\psi_{n(1)}(r) = \sin^{d/2}(\varphi) P_\nu^\mu(\cos\varphi), \tag{5.3.4}$$

$$\psi_{n(2)}(r) = \sin^{d/2}(\varphi) \left(\frac{1-\cos\varphi}{1+\cos\varphi} \right)^{\frac{\mu}{2}} {}_2F_1\left(\nu+1, -\nu, \mu+1, \frac{1-\cos\varphi}{2} \right), \tag{5.3.5}$$

where we have chosen to use our angular coordinate φ, while ν and μ are

$$\nu = \Delta_n - \frac{d}{2}, \tag{5.3.6}$$

$$\mu = \Delta - \frac{d}{2}. \tag{5.3.7}$$

The asymptotic behaviour of these solutions as $r \to \infty$ is

$$\psi_{n(1)} \sim e^{-r(d-\Delta)}, \quad \psi_{n(2)} \sim e^{-r\Delta}, \tag{5.3.8}$$

which is what we expect from the non-normalizable and normalizable solutions of the wave equation, respectively.

Taking into account our boundary condition on the brane, only the modes $\psi_{n(1)}$ which satisfy $\psi'_{n(1)}(r_0) = 0$ are admissible. Since each radial function $\psi_{n(1)}(r)$ is related to a corresponding co-dimension 1 field $\phi_n(\vec{y}, w)$, with a dimension Δ_n given by Eq. (5.2.31), we expect that the condition $\psi'_{n(1)}(r_0) = 0$ will restrict the spectrum of $\Delta_n s$ to take on only a discrete set of values.

In the limit of large Δ_n, we can explicitly solve the equation $\psi'_{n(1)}(r_0) = 0$ for Δ_n to obtain

$$\Delta_n = \frac{d-1}{2} + \frac{\left(n + \frac{1}{2}\left(\Delta - \frac{d}{2}\right) + \frac{1}{4}\right)\pi}{\arccos(\tanh(r_0))} \quad n \in \mathbb{Z} \quad (\text{large } \Delta_n). \tag{5.3.9}$$

In our angular coordinates, where the brane sits at φ_0, this simplifies to

$$\Delta_n = \frac{d-1}{2} + \frac{\left(n + \frac{1}{2}\left(\Delta - \frac{d}{2}\right) + \frac{1}{4}\right)\pi}{\varphi_0} \quad n \in \mathbb{Z}\,. \tag{5.3.10}$$

Note that, in $d = 2$, the position r_0 of the brane is understood to be related to the defect entropy $\log g$ of the CFT by [206]

$$\log g = \frac{r_0}{4G}, \tag{5.3.11}$$

which gives

$$\Delta_n^{d=2} = \frac{1}{2} + \frac{\left(n + \frac{\Delta}{2} - \frac{1}{4}\right)\pi}{\arccos(\tanh(2G\log g))} \quad n \in \mathbb{Z}. \tag{5.3.12}$$

It remains to calculate the scaling coefficients c_n appearing in (5.2.24) by enforcing the equal time canonical commutation relations. Following Appendix D.1, we compute c_n from the mode normalization

$$\int_{r_0}^{\infty} dr \cosh^{d-2}(r)\psi_n(r)\psi_m(r) = \frac{1}{c_n^2}\delta_{nm}\,. \tag{5.3.13}$$

Using the explicit expressions for $\psi_n(r)$ in Eq. (5.3.5), we can solve for c_n in the asymptotic limit of large n, which is the same limit in which we evaluated the scaling dimensions Δ_n of the operators ϕ_n. This gives the expression

$$\begin{aligned} c_n \approx & \frac{\pi^{1/4}\sqrt{(1+\mu)}}{2}\sqrt{\frac{\Gamma(\mu+1/2)}{\Gamma(\mu+2)\Gamma(2\mu+1)}}\left(\frac{2}{\arccos(\tanh r_0)}\right)^{\mu+1} \\ & \times\left(\frac{\pi}{4}(4n+2\mu+1)\right)^{\mu+1/2}, \end{aligned} \tag{5.3.14}$$

with $\mu = \Delta - d/2$, as before.

From Eq. (5.2.32), we can then compute the the BOE coefficients by plugging in the above c_n into the expression

$$\mathcal{B}_n = \frac{1}{2^{\Delta_n}}\sqrt{\frac{\mathcal{C}_{\Delta_n,d-1}}{\mathcal{C}_{\Delta,d}}}c_n\,. \tag{5.3.15}$$

In the large n limit, we can write this as

$$\mathcal{B}_n = 2^{-\frac{n}{\varphi_0}}n^{\Delta-\frac{d+1}{4}}B+\dots \tag{5.3.16}$$

with B a constant independent of n:

$$B = e^{\frac{3}{4}-\frac{d}{4}}\pi^{-\frac{d}{4}+\Delta+\frac{1}{2}}2^{\frac{\pi(d-2\Delta-1)}{4\varphi}-\frac{d-1}{2}}\varphi^{\frac{d-1}{4}-\Delta}\left[\Gamma(\Delta)\Gamma(-d/2+\Delta+1)\right]^{-1/2} \tag{5.3.17}$$

We conclude from this simple model that the information about the bulk geometry, namely—given our restricted assumptions—the location of ETW brane at φ_0, appears in two places:

1. The asymptotic spacing of boundary operator dimensions $\gamma = \lim_{n\to\infty}\Delta_{n+1}-\Delta_n = \frac{\pi}{\varphi_0}$.
2. The asymptotic growth of the BOE coefficients $\mathcal{B}_n \sim \exp\left(\frac{n}{\varphi_0}\ln 2\right)$.

What is not yet clear is why the information about the brane is encoded in this particular way and how it generalizes to a lesson about all BCFTs with good bulk duals. To make this next step, we must turn to the Lorentzian structure of two-point functions in a (holographic) BCFT.

5.4 Lorentzian BCFT Singularities

In this section, we will consider the singularities associated with a scalar two-point function in a Lorentzian BCFT. We start by discussing the field theory setup and the expected structure of kinematic singularities. For BCFTs with a simple holographic dual, we consider the apparent singularities that arise from the bulk causal structure. In particular, we consider the bulk null rays that are reflected off the brane, and compute the cross-ratio of the return locus for these rays.

5.4.1 BCFT Singularities

In Euclidean signature, a CFT correlator has singularities whenever two operators become coincident (and is analytic otherwise). Similarly, a Euclidean BCFT correlation function will have singularities only when operators approach each other, or when they approach the boundary. (We can think of this as an operator approaching their mirrored double across the boundary.)

In terms of a scalar BCFT two-point function, and our cross ratio ξ defined in (5.2.5), the singularity when the two operators approach each other corresponds to the limit $\xi \to 0$. In this limit, the correlator will diverge like

$$\langle \mathcal{O}(x)\mathcal{O}(y)\rangle = \frac{1}{|x-y|^{2\Delta}} + \dots \tag{5.4.1}$$

or, correspondingly, $\mathcal{G}(\xi) \sim \xi^{-\Delta}$. When the operators approach the boundary, in the limit $\xi \to \infty$, the correlator diverges like

$$\langle \mathcal{O}(x)\mathcal{O}(y)\rangle = \frac{\mathcal{A}^2}{|4x_\perp y_\perp|^{\Delta}} + \dots \tag{5.4.2}$$

or, correspondingly, $\mathcal{G}(\xi) \sim \mathcal{A}^2$. Unlike the CFT case, there is no third Euclidean singularity, which could be thought to correspond to the operator $\mathcal{O}(y)$ approaching the mirror of $\mathcal{O}(x)$.

In Lorentzian signature, we similarly expect a singularity when $\mathcal{O}(y)$ approaches the lightcone of $\mathcal{O}(x)$ at the cross-ratio $\xi = 0$. We can also continue the Lorentzian two-point function around the branch point at $\xi = 0$ to the timelike region $\xi < 0$. Here there is another possible singularity where the $\mathcal{O}(y)$ approaches the reflection of the lightcone of $\mathcal{O}(x)$ off the boundary at $\xi = -1$. This is known as the *Regge Limit* of the BCFT [202] and it has been shown that the BCFT diverges here at worst as $\mathcal{G}(\xi) \sim (\xi+1)^{-\Delta}$. This is exactly the singularity one would expect from approaching the lightcone of the 'mirror' of $\mathcal{O}(x)$. We depict the Lorentzian causal structure and the corresponding cross-ratios in Figure 5.5.

When we change to radial coordinates, placing $\mathcal{O}(y)$ in the timelike region to the future of $\mathcal{O}(x)$, but before the reflected lightcone, corresponds to $\rho = e^{i\varphi}$ for $\varphi \in [0, \pi]$. At one end $\rho = 1$ ($\varphi = 0$) is the lightcone of $\mathcal{O}(x)$

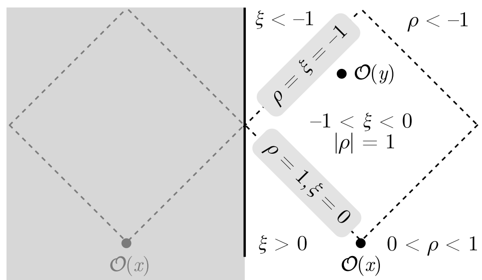

Figure 5.5: We depict various regions of the Lorentzian interval for a BCFT in terms of various cross-ratios. Importantly we note that the causal diamond bounded by the lightcone of the operator $\mathcal{O}(x)$ and its reflection off the boundary is described by the radial cross-ratio ρ living on the unit circle. It interpolates between the initial lightcone at $\rho = e^{i0}$ and the reflected ligthcone at $\rho = e^{i\pi}$.

at $\xi = 0$ and at the other end $\rho = -1$ ($\varphi = \pi$) is the reflected lightcone of $\mathcal{O}(x)$ at $\xi = -1$. We also indicate the ρ-regions in Figure 5.5.

It has been argued that a CFT correlation function should only have singularities at points corresponding to Landau diagrams [197] where null particles interact at local vertices. By the same logic, we expect the only singularities of a BCFT two-point function to be that on the lightcone and its reflection. We do not not attempt to prove this statement in general, but we can follow [197], and show that it holds in a 2D BCFT.

BCFT Singularities in 2D In two dimensions one can perform a conformal transformation to map the unit ρ disk into the interior of the unit disk in a new coordinate q, hitting the boundary only at $q = \pm 1$. We depict the region in Figure 5.6. One can then show that the two-point function converges everywhere in the interior of the unit q disk; the convergent region includes the region where the two-operators are timelike separated, except the point $q = \pm 1$ corresponding to the expected BCFT lightcone. We give a more complete derivation of this result in Appendix D.3.

5.4.2 Bulk Singularities

The location of the BCFT singularities we have just listed are universal and kinematic, in the sense they can be read off the behaviour of individual conformal blocks without consulting the spectrum. But for a BCFT with a simple holographic dual, a new type of singularity can emerge: an insertion

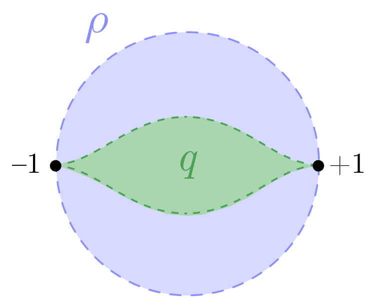

Figure 5.6: Relation between the radial ρ variable and the new coordinate q.

now generates a lightcone in the *gravitational bulk* as well as the boundary. Bulk light-rays can head into the infrared gravitational geometry and return some time later to the boundary, indicating new singularities in the BCFT. When the bulk geometry is 'shallow' (for example, when the geometry ends on a brane with a large negative tension), these singularities may even occur before the boundary light ray has returned.

To illustrate this behaviour, we begin by examining our simple toy model where empty AdS is terminated by an ETW brane. We can re-write our angular metric (5.3.2) in the form

$$\mathrm{d}s^2_{\mathrm{Euc}} = \frac{1}{\sin^2\theta \sin^2\varphi}\left(\mathrm{d}\tau^2 + \cos^2\theta \mathrm{d}\Omega^2_{d-2} + \mathrm{d}\theta^2 + \sin^2\theta\, \mathrm{d}\varphi^2\right) , \qquad (5.4.3)$$

by turning the AdS$_d$-radial coordinate on the slices into a second angular coordinate θ.[93] The angular radial coordinate θ on the slices takes values $\theta \in [0, \pi/2]$ with 0 being the boundary of AdS. Recall that the other coordinate ϕ takes values in the range $\varphi \in [0, \varphi_b]$ and is found from the coordinate change $\cos\varphi = \tanh(-r)$. $\mathrm{d}\Omega^2_{d-2}$ is the line element on the $\mathbb{S}^{d-2}$ that parametrizes the rest of the AdS$_d$ slice. Ignoring the conformal factor, we can see that the angular coordinates (θ, φ) together form part of an $\mathbb{S}^2$. By continuing to Lorentzian time, we arrive at the metric

$$\mathrm{d}s^2_{\mathrm{Lor}} = \frac{1}{\sin^2\theta \sin^2\varphi}\left(-\mathrm{d}t^2 + \cos^2\theta \mathrm{d}\Omega^2_{d-2} + \mathrm{d}\theta^2 + \sin^2\theta\, \mathrm{d}\varphi^2\right) . \qquad (5.4.4)$$

We will perform our bulk causal calculations in these coordinates.

[93]By radial coordinate, we mean the global AdS$_d$-radial coordinate on the slices. These global AdS coordinates can be obtained simply by switching to polar coordinates on the slice, with an origin on the boundary.

Figure 5.7: (a) A 2D spatial-slice of AdS_3 cutoff by an ETW brane. (b) The same spatial slice conformally mapped to part of the two-sphere. The path of a null geodesic is marked in red.

To begin, we restrict ourselves to consider null rays travelling on the 2-sphere at a fixed position on the $\mathbb{S}^{d-2}$ in (5.4.4). This is a straightforward affair. Consider a null ray $x^\mu(\lambda) = (t(\lambda), \theta(\lambda), \varphi(\lambda)))$, with affine parameter λ. The conformal factor drops out, leaving a simple null geodesic equation

$$-\dot{t}^2 + \dot{\theta}^2 + \sin^2\theta\,\dot{\varphi}^2 = 0\ . \tag{5.4.5}$$

We are free to take $\dot{t} = 1$, so that affine time elapsed simply measures distance along the sphere, and the calculation of the return locus reduces to a problem of spherical trigonometry. Without loss of generality, we take the initial insertion to lie at $x^\mu = (0, \theta_0, 0)$. The null ray will head off into the bulk with some initial direction $\dot{\theta}_0 = \dot{\theta}(0)$, bounce off the brane at $\varphi = \varphi_b$, and return to the boundary $\varphi = 0$ at some angle θ_1 and time $\Delta t = d$ measured by the distance travelled.

To simplify the kinematics further, we can *double* the width of the wedge to $2\varphi_b$. There is now no need to consider the reflection off the brane, since the light ray sails smoothly through the mirror and arrives at the reflected boundary. It follows immediately from spherical trigonometry[94] that the initial position θ_0, direction $\dot{\theta}_0$, return angle θ_1 and elapsed time $\Delta t = d$ are related by

$$\cos d = \cos\theta_0\cos\theta_1 + \sin\theta_0\sin\theta_1\cos\varphi_b\ . \tag{5.4.6}$$

We show the spatial path of one of these null geodesics in Figure 5.7.

To compute the cross-ratio, ξ, for this locus, note that the flat BCFT coordinates are related to our polar coordinates $x_1 = e^{it}\cos\theta$ and $x_\perp = e^{it}\sin\theta$. Plugging in (5.4.6), the analytically continued cross-ratio is

$$\xi = \frac{(e^{i\Delta t}\cos\theta_1 - \cos\theta_0)^2 + (e^{i\Delta t}\sin\theta_1 - \sin\theta_0)^2}{4e^{i\Delta t}\sin\theta_1\sin\theta_0} = -\sin^2\varphi_b\ . \tag{5.4.7}$$

[94] Specifically, the spherical law of cosines.

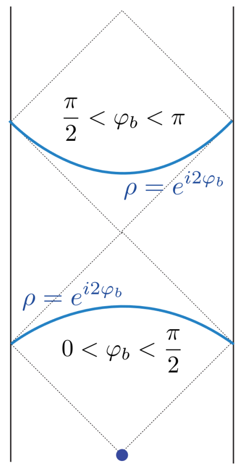

Figure 5.8: An illustration of two example return loci for branes of different tension/causal depth. When the brane tension is positive, φ_b is greater than $\pi/2$ and null geodesics return to the boundary along a curve in the upper causal diamond. When the brane tension is negative, φ_b is less than $\pi/2$ and null geodesics return to the boundary along a curve in the lower causal diamond.

This is pleasingly simple. In terms of our radial cross-ratio (5.2.13), it is even simpler:

$$\rho = e^{i2\varphi_b} \ . \tag{5.4.8}$$

We show the return locus for varying φ_b in Figure 5.8.

We conclude that the bulk causal structure of our simple ETW brane model predicts a singularity in the BCFT at the cross-ratio (5.4.8). This occurs away from the expected BCFT singularities at $\rho = 1, 0, -1$.

General warp factor We can repeat the same argument with minor modifications for a more general warped background plus ETW brane as in (5.2.18). In this case, one only needs to find the appropriate angular coordinate to put the metric in the form

$$\mathrm{d}s^2_{\mathrm{Lor}} = \frac{1}{\sin^2\theta f(\varphi)}\left(-\mathrm{d}t^2 + \cos^2\theta \mathrm{d}\Omega^2_{d-2} + \mathrm{d}\theta^2 + \sin^2\theta\, \mathrm{d}\varphi^2\right) \ , \tag{5.4.9}$$

for some function $f(\varphi)$ determined by the warp factor $A(r)$. Because the causal structure does not depend on this unknown conformal factor, we again find the return locus to be

$$\rho = e^{i2\varphi_b} \ . \tag{5.4.10}$$

where $\varphi_b = \int_{-\infty}^{r_b} e^{-A(r)} dr$. We note, in particular, that the causal structure of the bulk and of the return locus to the boundary is independent of the Euclidean distance to the brane. In contrast to this work, the Euclidean distance is what appears in holographic calculation of boundary entropy in 2D CFTs, for example, and many calculations of entanglement entropy.

General geodesics While calculating null geodesics which are not at a fixed position on the $\mathbb{S}^{d-2}$ would be slightly more challenging, there is no need to go to the trouble. The BCFT two-point function is a function only of a single cross-ratio, up to a conformally-covariant pre-factor. Thus, having mapped part of the null cone to the locus $\rho = e^{i2\varphi_b}$, we can conclude that null geodesics with non-zero momentum on the sphere must also return at another point on the sphere with the same cross-ratio. Or, in other words, we can map any two unit vectors on the AdS_d slices into each other by a conformal transformation and so all of the null rays are equivalent.

5.5 Looking for a Bulk Brane

In section 5.3 we showed how the bulk geometry of a simple ETW brane model is encoded in the spectrum and BOE coefficients of the dual BCFT. And in section 5.4 we showed that the bulk causal structure also predicts new Lorentzian singularities in the BCFT from null rays that reflect off the bulk ETW brane. We now put these two sides of the coin together and explain how one entails the other.[95]

The boundary conformal block, written in terms of our radial cross-ratio (5.2.15), has a simple large dimension limit

$$\lim_{\hat{\Delta}\to\infty} g^b_{\widehat{\Delta}}(\rho) = (4\rho)^{\widehat{\Delta}} \frac{1}{(1-\rho^2)^{(d-1)/2}} \,. \tag{5.5.1}$$

We consider this large-dimension limit at the return time of the bulk null cone, (5.4.8), to see that

$$\lim_{\hat{\Delta}\to\infty} g^b_{\widehat{\Delta}}(e^{i2\varphi_b}) = 4^{\widehat{\Delta}} e^{i2\widehat{\Delta}\varphi_b} \frac{1}{(1-e^{i4\varphi_b})^{(d-1)/2}} \,. \tag{5.5.2}$$

When we plug in the asymptotic spacing of boundary operator dimensions in our simple model, (5.3.10),

$$\widehat{\Delta} = \widehat{\Delta}_0 + n\frac{\pi}{\varphi_b} \tag{5.5.3}$$

[95]Or heads from one to the other. Pun obviously intended.

we see that the block takes the form

$$\lim_{n\to\infty} g^b_{\widehat{\Delta}_n}(\rho) = e^{i2\widehat{\Delta}_0\varphi_b} 4^{\widehat{\Delta}_n} \frac{1}{(1-e^{i4\varphi_b})^{(d-1)/2}} \,.. \tag{5.5.4}$$

Thus the spacing of the boundary operator dimensions has exactly cancelled the n-dependence of the phase precisely at the return time of bulk null cone. These conformal blocks will then all add coherently at this point so that the sum over conformal blocks takes the form

$$e^{i2\widehat{\Delta}_0\varphi_b} 4^{\widehat{\Delta}_0} \frac{1}{(1-e^{i4\varphi_b})^{(d-1)/2}} \sum_n 2^{2n\frac{\pi}{\varphi_b}} b_n \tag{5.5.5}$$

Consequently, this sum can potentially diverge. To see that this is in fact the case, we plug in the large-n BOE coefficients from (5.3.16). Dropping the prefactor, near the return time at $\rho = \exp\left[i2\varphi_b(1+\epsilon)\right]$ the sum over n gives

$$\sum_n e^{2\pi i n\epsilon} n^{2\Delta - \frac{d+1}{2}} \,. \tag{5.5.6}$$

This is just a Fourier transform of the BOE coefficients. Doing the Fourier transform and extracting the singular contributions, we find Lorentzian singularities in the two-point function proportional to

$$\mathcal{G}(\rho) \sim \frac{1}{(\rho_b - \rho)^{2\Delta - \frac{d-1}{2}}} \frac{1}{(-1-\rho)^{\frac{d-1}{2}}} \,. \tag{5.5.7}$$

We conclude that the bulk causal structure has been mapped into a particular regular asymptotic spacing of the boundary operators that appear in the BOE.

From bulk points to bulk branes Our story is a very close analogue, both in spirit and technically, to the story in [197]. There the authors explained how the causal structure of the dual AdS vacuum leads to new singularities in CFT four-point functions. These result from local interactions that happen at a point in the AdS bulk geometry. The bulk point isn't expected to be a true singularity of the four-point function—these are believed to occur only where predicted by Landau diagrams in the boundary theory. Rather it is a resonance in the correlator that is smoothed out at the scale of the cut-off where bulk locality breaks down.

Similarly, we don't expect to find true new singularities in the BCFT two-point function. On the bulk side, we don't expect the brane to be exactly local. It will have some intrinsic width at which it will smear out bulk signals that reflect off the brane. On the boundary side, we only expect singularities where allowed by BCFT Landau diagrams. Thus, above some cutoff scale $\widehat{\Delta}_{\text{gap}}$ that determines the width of the brane we expect the careful alignment of boundary operator dimensions to break down. Above this dimension, operators contribute with incoherent phases, truncating the divergent sum in (5.5.6)

5.5.1 No bulk branes (at least generically)

We argued that we don't expect the bulk brane singularity to be a true singularity of the BCFT. Nevertheless, the validity of our semiclassical description, a bulk geometry terminated by an ETW brane, over a large range of scales requires the careful alignment of boundary operator dimensions up to some large $\widehat{\Delta}_{\text{gap}}$.

We conjecture that this careful alignment is not a generic feature of BCFTs, even when the underlying CFT has a good gravitational description. Thus, an operator spectrum and BOE coefficients consistent with a bulk ETW brane geometry must be another input or assumption about the particular boundary condition of the CFT, much in the way we have to assume features of the spectrum of a large c CFT such that it has a good semiclassical gravitational description.

We do know that the correlation functions of a BCFT become those of the underlying CFT when all insertions are far from the boundary. Thus, we do not claim that the geometry will break down everywhere in the bulk. Rather, our claim is that generically there cannot be the type of simple causal structure consistent with an ETW brane geometry. The lack of fine-tuned dimensions prohibits null-rays from leaving the boundary and returning in reasonably-short times.[96]

In the spirit of [181], we can formalize our conjecture as the following:

Conjecture 1. A holographic CFT with boundary condition B will have a good bulk dual provided

(i) correlation functions factorize about a (non-universal) free bulk solution; and

[96] Of course, if we are willing to wait sufficiently long times, we can produce a resonance in an arbitrary theory by waiting for the phases of any finite number of blocks to align in the future. It's not clear that these types of resonances should have a *simple* gravitational interpretation.

(ii) the boundary operator spectrum is gapped such that below some large $\widehat{\Delta}_{\text{gap}}$ the only operators are simple boundary operators and their multi-trace composites.

It is the first of these conditions—the existence of a consistent leading-order free bulk two-point function—that we are concerned with in this chapter and that we have argued shouldn't generically look like an ETW brane. Whether or not we might still expect a good bulk geometry, but without an ETW brane, we will discuss in section 5.6. We leave the examination of the second of these conditions to future work, but we note that aspects of this are challenging without a characterization of the space of solutions to (i).

Note that the causal structure of the four-point function in a holographic CFT also requires a similar alignment of operator dimensions. Specifically, in a holographic CFT one obtains "double-twist operators" due to the crossing equations and the presence of the identity operator; the stress tensor then fixes their anomalous dimensions, which asymptotically go to zero at both large spin and large central charge. These two facts explain the emergence of the "bulk point" [197], where scattering between CFT operators occurs in the bulk but not the boundary.

In a defect CFT, a similar story generically emerges [220]: for a defect of codimension q, there are boundary operators associated to derivatives of bulk primaries in the q directions transverse to the defect. Their anomalous dimension goes to zero at large "transverse spin" (i.e. the charge of the residual $\mathrm{SO}(q-1,1)$ symmetry). This control of the anomalous dimensions clearly vanishes in an interface or boundary CFT. We no longer have any transverse spin to work with when $q=1$, even though we still have operators given by derivatives of bulk primaries in the remaining transverse direction. To have a good bulk dual, these operators must possess non-trivial anomalous dimensions that aren't fixed by symmetry and universal properties alone. A BCFT is then a simple setting where there isn't quite enough symmetry to fix the form of the vacuum two-point function and it must be an input.

A useful analogy in holographic CFTs for when the free correlators are not fixed by symmetry is an excited state. Excited states in a holographic CFT will not generically have a good bulk geometry and hence will not have a good causal structure. Thus, we do not expect to see the approximate singularities of a local bulk geometry except in carefully chosen states. We suggest good ETW brane geometries are far from generic in the space of BCFTs in much the same way good bulk geometries are far from generic in the Hilbert space.

5.6 Beyond ETW branes

Our discussion so far has focused only on the bottom-up ETW brane proposal of [206]. However, we know this proposal is insufficient to fully describe various top-down models where the bulk geometry is more complicated. Moreover, while our evidence suggested that an ETW brane required finely-tuned boundary operator dimensions, we would like to be able to make a much more general conjecture: *without special finely-tuned dimensions the BCFT bulk will not be everywhere geometric.* To examine this stronger statement, we will elaborate below on constructions that go beyond the ETW brane proposal.

5.6.1 General Bulk Geometries

We explore first two simple toy models to build intuition for what happens when a BCFT is not terminated by an ETW brane, but terminates instead when extra dimensions pinch off.

First, let us consider a metric on $HS^2 \times \mathbb{R}^{0,1}$, with the form

$$ds^2 = -dt^2 + d\theta^2 + \sin^2\theta d\varphi^2 \,, \qquad t \in \mathbb{R}\,,\, \theta \in (0, \pi/2)\,,\, \varphi \in (0, 2\pi)\,. \quad (5.6.1)$$

We take this to be a model of an extra dimension pinching off in the IR bulk geometry where we view the angular direction φ as an extra compact direction and θ as a coordinate on the base, like the bulk radial coordinate. We are concentrating on what happens in the region where the extra dimension pinches off and we ignore the rest of the geometry for now. Nevertheless, one could imagine smoothly joining the hemisphere to close off a circle of constant radius fibered over AdS.

Suppose we have a massive scalar field ϕ, with mass M, on this geometry; the equation of motion is

$$M^2\phi = \Box\phi = -\partial_t^2\phi + \frac{1}{\sin\theta}\partial_\theta\left(\sin\theta\partial_\theta\right)\phi + \frac{1}{\sin^2\theta}\partial_\varphi^2\phi\,. \qquad (5.6.2)$$

We assume a simple boundary operator will correspond to some fixed momentum on the circle $\psi_m(\phi) = e^{im\varphi}$. One might worry that the last term in (5.6.2) will generate a potential for modes with non-zero angular momentum, leading to a different effective causal structure in the base space for different modes (ie. different boundary operators). More importantly, one might worry the potential will smear out the singularity of the returning signal that reflects off the end of the extra dimension. To see that this won't be the case, it's easiest to note that the causal structure corresponds to a high-energy limit where the potential becomes irrelevant—the pinching extra dimensions appear just like a hard wall when approached along the lightcone.

We can also make the above intuition more explicit. For some fixed m, the solutions of the equation of motion that are smooth as the sphere caps off all take the form

$$\psi_{\omega,m}(t,\theta,\varphi) = P^m_{l(\omega)}(\cos\theta)e^{i\omega t}e^{im\varphi}\,, \tag{5.6.3}$$

where $l(\omega) = \frac{1}{2}\left(\sqrt{4\omega^2 - 4M^2 + 1} - 1\right)$. Near the equator of the hemisphere, at large ω, the solutions behave as

$$\psi_{\omega,m}(t,\theta,\varphi) \approx \cos(\omega\theta + \pi)e^{i\omega t}e^{im\varphi} \tag{5.6.4}$$

and so this behaves just like a wave reflecting off a hard wall at $\theta = 0$. The ω modes all add up coherently at $t = 2\theta$ to generate the reflected lightcone.

We can further fix the allowed frequencies ω by imposing additional boundary conditions at the equator of the hemisphere (where we imagine joining onto the rest of the bulk solution). For example, we can set Neumann boundary conditions on the equator to find that the allowed asymptotic values of ω are precisely $\omega_n = 2n\,,\ n \in \mathbb{N}$. It's then possible to see the lightcone that has reflected off of both boundaries and refocused at the original location: after a time inverse to the regular operator spacing the modes again add up coherently.

Of course, this isn't the only type of characteristic behaviour we can construct. We can also consider a toy model where the extra dimension caps off slowly:

$$ds^2 = -dt^2 + dz^2 + \frac{1}{z^2}d\varphi^2\,, \qquad t \in \mathbb{R}\,,\ z \in \mathbb{R}_{\geq z_0}\,,\ \varphi \in (0, 2\pi)\,. \tag{5.6.5}$$

Here the radius of the extra dimension shrinks slowly like $1/z$, again generating an effective potential for angular modes on the extra-dimension, but this time with no hard end. At the other end, we terminate the geometry at some z_0 (where again we could imagine joining onto another bulk solution). In contrast to the previous example, here we expect that as we increase the energy of modes they will penetrate deeper and deeper into the infrared geometry. Thus, there is no natural scale that sets the return time for lightrays sent in the radial direction and no expected reflected lightcone.

To see this explicitly, we can solve the wave equation for a free, massive scalar field in this background. The solutions that don't diverge in the infrared take the form

$$\psi_{\omega,m}(t,z,\varphi) = U(\tfrac{M^2-\omega^2}{4m}, 0; mz^2)e^{i\omega t}e^{im\varphi}\,, \tag{5.6.6}$$

where $U(a, b, x)$ is the Tricomi (confluent hypergeometric) function. For large frequency (and sufficiently small z), we can rewrite these solutions as

$$\psi_{\omega,m}(t, z, \varphi) \approx \sqrt{\frac{2mz}{\pi\omega}} \cos\big(\omega z + \tfrac{\pi}{4}(1 - \omega^2/m)\big) e^{i\omega t} e^{im\varphi} \,. \tag{5.6.7}$$

In contrast to the previous example, we see here that there is a phase shift that depends on ω and so we will not have all of the reflected modes add coherently at the same time/position.

We can again further fix the allowed frequencies ω by imposing additional boundary conditions at z_0. For example, we can set Neumann boundary conditions at $z = 1$ to find that the asymptotic spacing of eigenvalues ω_n scales like $\omega_n - \omega_{n-1} \sim 1/\sqrt{n}$. This spacing is not regular, and thus we will not have a finite-time recurrence where a reflected lightcone could return.

Causal Depth The primary distinguishing feature of the above two examples is the difference in their *causal depth.* As in the ETW brane examples, when light rays sent into the geometry can return in finite time (a finite causal depth), we see a reflected lightcone, a corresponding divergence in the two-point function, and the careful alignment of asymptotic eigenvalues. On the other hand, when light rays sent into the geometry don't return in finite time, we no longer expect a reflected lightcone, nor a corresponding divergence in the two-point function or alignment of operator dimensions. The common intuition is that BCFTs will have a dual bulk geometry with a finite causal depth, whether they are terminated by an ETW brane or the closing off of extra compact dimensions, and should look more like the first of these very simple toy models.

Asymptotically AdS Toy Model

The comments above contain the essential features and physical intuition for the argument that individual Kaluza-Klein modes exhibit the same reflected singularity (in the case of finite causal depth), and consequently, that different CFT operators must exhibit the same resultant Lorentzian singularity.[97] To give additional support for this claim, we can explicitly analyze another toy model involving a free scalar field propagating on a background which is a static, asymptotically locally AdS geometry whose spatial slices are cigar-like,

[97]Although this argument is clearest when the form of the warping is relatively simple, as in the examples we have described, we might hope that something analogous should hold in any case where there are internal directions that degenerate.

as described by the metric

$$ds^2 = \frac{L^2}{z^2}\left(dz^2 - dt^2 + z^2 f(z)^2 d\theta^2\right) , \qquad \theta \in (0, 2\pi) , \tag{5.6.8}$$

where for convenience we choose

$$f(z) = \frac{1 - z^2}{2} . \tag{5.6.9}$$

One can verify that this choice makes the geometry non-singular at $z = 1$.

The explicit analysis of this problem is left to Appendix D.2, but we summarize the important features here. The eigenfunctions of the Klein-Gordon operator are of the variable-separated form $e^{im\theta}e^{i\omega t}\phi_{m,\omega}(z)$, where we interpret different KK modes of the internal S^1 (labelled by integer m) as corresponding to different operators in the dual quantum theory. The functions $\phi_{m,\omega}(z)$ are known (they involve linear combinations of *confluent Heun functions*, with linear dependence fixed by normalizability at $z = 0$), and the values of ω are quantized by the requirement of regularity at $z = 1$. To demonstrate that operators of differing m exhibit the same reflected singularity, which we expect to occur when the insertions are separated by $\Delta t = 2$ (the time for an ingoing null ray to travel from $z = 0$ to the IR wall at $z = 1$ and bounce back), it suffices to show that, for any fixed m, the quantized frequencies exhibit asymptotic spacing

$$\Delta\omega \equiv \lim_{n\to\infty} \omega_{n+1} - \omega_n = \frac{2\pi}{\Delta t} = \pi . \tag{5.6.10}$$

The form of the Green function as a sum over modes then fixes the desired singularity. Computing the spectrum numerically in various cases, we indeed appear to find that (5.6.10) holds across values of m; an example of this calculation can be seen in Figure 5.9. We interpret this as additional concrete evidence for our claim that CFT operators corresponding to KK modes of some bulk field should quite generally exhibit a common Lorentzian singularity associated with bulk causality.

5.6.2 Top Down Holographic BCFT

In the previous subsection, we have discussed how some of our conclusions may be generalized to plausible smooth bulk geometries involving an internal space which degenerates. We would now like to understand how these considerations might apply to fully-fledged top-down holographic constructions of AdS/BCFT. As mentioned in section 5.2.2, a number of such constructions

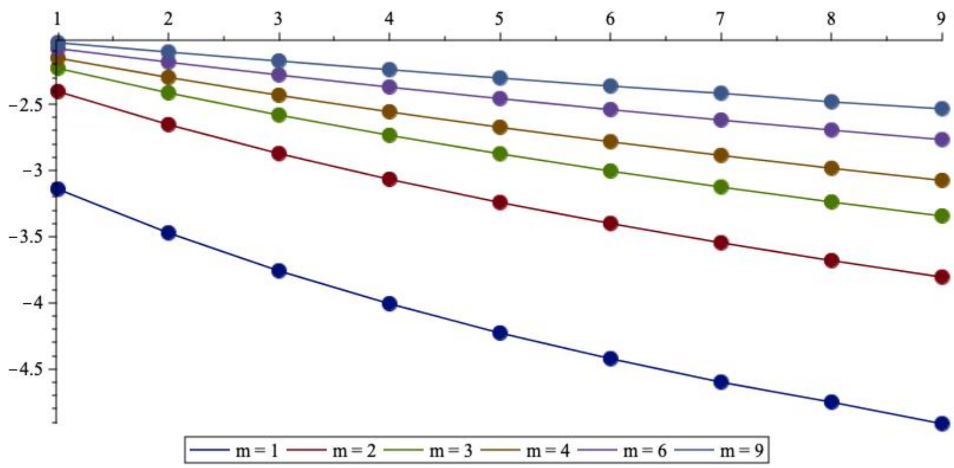

Figure 5.9: Plots of $\ln\left|\omega_{n+1} - \omega_n - \pi\right|$ versus n for various values of m in asymptotically AdS toy model with a free scalar field. We have chosen $ML = 1$ for concreteness.

are known [209–215], and it appears necessary to explain whether or not the existence of a smooth bulk in these cases entails the spectral fine-tuning we have argued for previously, and if not, how their causal structure is consistent with this conclusion. Since the spectrum of boundary operators with protected conformal dimensions is not known in these theories, and extracting this spectrum is not expected to be straightforward in general [221], our investigation will be on the side of the bulk causal structure.

Certainly, it is a possibility that the heuristic arguments of the previous subsection may not capture important structural aspects of the warped supergravity solutions describing the microscopic theories of interest. But in this section, we will attempt to address a different possibility, namely that the intersection of the bulk light cone of a boundary point with the asymptotic boundary may generically be small or empty in these theories. In this case, bulk causality would not directly introduce a spectral constraint of the type we have been concerned with, or would do so only for a very select subset of operators. In the language of the previous subsection, we might say that such solutions exhibit infinite causal depth. Unlike the simple toy models that we have considered, this is no longer necessarily a manifestation of a slowly shrinking internal space, but rather may reflect that a generic ingoing geodesic will follow a trajectory which may involve very complicated behaviour in the internal space.

We can illustrate this possibility by considering a concrete example, namely the "AdS_2-Cap" solution of six-dimensional $(0,4)$ ("type 4b") supergravity identified by Chiodaroli, D'Hoker, and Gutperle in [209]; this is expected to provide a fully back-reacted holographic description of a D1-D5 junction in 10 dimensions, where a D1-brane and a D5-brane wrapping a suitable four-manifold join to form a D1/D5 bound state. This solution has a single $\mathrm{AdS}_3 \times S^3$ asymptotic region, describing the near-horizon geometry for the D1/D5 bound state, while the D1-brane and the D5-brane each contribute a curvature singularity at fixed locations in the internal space, referred to as "caps". The resultant 6-dimensional metric is of the form

$$ds_6^2 = f_1^2 ds^2_{\mathrm{AdS}_2} + f_2^2 ds^2_{S^2} + \rho^2 dw d\bar{w} \,, \tag{5.6.11}$$

where $(w, \bar{w})$ are complex coordinates on a Riemann surface Σ, which we may take to be the upper half plane. One may use $SL(2,\mathbb{R})$ symmetry to fix the location of the $\mathrm{AdS}_3 \times S^3$ asymptotic region at $w = 0$ and the AdS_2-caps at $w = \pm 1$.

Equipped with this solution, one can proceed to study numerically the behaviour of ingoing null geodesics; we leave a more detailed discussion to Appendix D.4. In Figure 5.10 we display the behaviour of such null geodesics on the internal submanifold Σ, restricting to geodesics with no initial momentum in the S^2 direction for clarity; the geodesics are seen to initially orbit the caps, which appear to be attractor-like.

To attempt to confirm that the AdS-caps do indeed attract all ingoing null geodesics in the class we are considering, we can examine the geodesic equation in the vicinity of these caps, again restricting to the case with no momentum in the S^2 direction. (We choose the one at $w = 1$ for convenience). Denoting

$$x - 1 \equiv \epsilon_x \equiv \epsilon \cos\Theta \,, \qquad y \equiv \epsilon_y \equiv \epsilon \sin\Theta \,, \tag{5.6.12}$$

we obtain at leading order in small ϵ

$$\frac{\ddot{\epsilon}}{\epsilon} + \frac{\dot{\epsilon}^2}{\epsilon^2} = 2\frac{\dot{\epsilon}^2}{\epsilon^2} + \left(O(\epsilon)\frac{\dot{\epsilon}_x^2}{\epsilon^2} + O(\epsilon)\frac{\dot{\epsilon}_y^2}{\epsilon^2} + O(\epsilon)\frac{\dot{\epsilon}_x}{\epsilon}\frac{\dot{\epsilon}_y}{\epsilon} \right) \,, \tag{5.6.13}$$

from which it should follow that

$$\epsilon(s) \approx \epsilon_0 e^{cs} \,, \tag{5.6.14}$$

provided that ϵ remains sufficiently small that perturbation theory remains valid. That is, it appears that the geodesics will approach the AdS-cap exponentially, and in particular would not reach the precise location of the

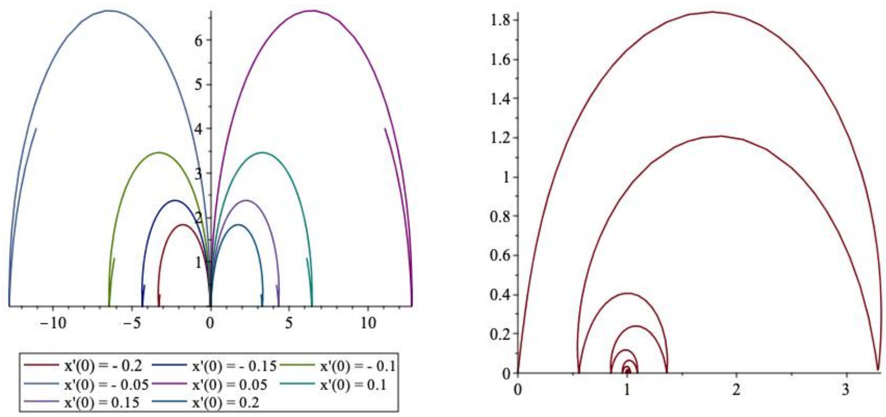

(a) Initial behaviour of ingoing null geodesics on internal submanifold Σ (with initial data in the x-direciton provided).

(b) Generic behaviour of ingoing null geodesic (in this case $x'(0) = 0.2$), which falls into and orbits the AdS-cap.

Figure 5.10: The AdS-cap curvature singularities at $w = \pm 1$ in the upper half-plane Σ appear to be attractor-like for ingoing null geodesics.

cap in finite affine parameter in the leading order calculation. We can confirm numerically that, at least for sufficiently small affine parameter, this is a good approximation (see Appendix D.4).

Based on this cursory analysis, it appears plausible that a significant portion of the bulk light cone has no intersection with the asymptotic boundary of the spacetime, instead getting trapped near the AdS-cap curvature singularities. It is in this sense that this example may be exhibiting what we have previously referred to as an infinite causal depth. Note that, in this case, this is not due to a slowly shrinking internal space; in fact, the AdS-caps are at finite proper distance from any point in the interior of the geometry, and the geometry in the vicinity of the AdS-cap is of the form

$$ds^2 \approx \frac{\sqrt{2}\mu_0}{\kappa}\sqrt{\kappa^2 + \mu_0^2 \sin^2\Theta}\left(d\epsilon^2 + \epsilon^2\left(d\Theta^2 + \frac{\kappa^2}{\mu_0^2}ds^2_{\mathrm{AdS}_2} + \frac{\kappa^2\sin^2\Theta}{\kappa^2 + \mu_0^2\sin^2\Theta}ds^2_{S^2}\right)\right), \tag{5.6.15}$$

where $\kappa > 0$ and μ_0 are the real parameters for our class of AdS_2-cap solutions. Rather, this is simply a seemingly generic property of null geodesics sent inward from the asymptotic boundary.

In general, we expect that the supergravity approximation should break down in the vicinity of these singularities, with string loop and α'-corrections becoming important. This may also be a generic feature of top-down constructions of holographic BCFT: generic causal probes will enter regions of the bulk where the effective description breaks down.

It is worth noting that, even in this example, there exist geodesics which return to the asymptotic boundary in short affine parameter as a result of finely-tuned initial conditions. For example, null geodesics sent radially inward from the equator of the asymptotic S^3 will avoid falling into either AdS-cap. In the BCFT, the radial coordinate cross-ratio describing the separation between endpoints of these geodesics is precisely

$$\rho = e^{\pm \frac{i\pi\mu_0}{2\kappa}}\,;. \tag{5.6.16}$$

(See Appendix D.4 for further details.) It is possible that this result is indicating the existence of more complicated operators localized on the internal dimensions which do exhibit a singularity, and that this again requires the existence of particular families of boundary operators (whose dimensions in this case have asymptotic spacing $|\Delta_{n+1} - \Delta_n| \sim \frac{4\kappa}{mu_0} n$).

Top-down models with finite causal depth

The above top-down BCFT example shows how the holographic dual can seem to develop an infinite causal depth and avoid the simplest causal constraints on the BOE spectrum. Here we show that this isn't the case for all known top-down constructions: we give an explicit example of a top-down BCFT with finite causal depth.

Our example will be an interface conformal field theory (ICFT) with a codimension one defect separating two different CFTs on either side of the defect. We can view the ICFT as a BCFT by folding the two sides on top of each other. Then the BCFT will look like a product of two non-interacting theories that are coupled only via the boundary condition.

The precise example we will consider here is the supersymmetric Janus solution found in [222]. In this Janus solution, the bulk geometry smoothly interpolates between two different asymptotic $\mathrm{AdS}_3 \times S^2 \times T^4$ regions. The dual ICFT is a marginal deformation of the two-dimensional D1/D5 $\mathcal{N} = (4,4)$ SCFT. The details of the geometry will not be important to our analysis and can be found in [222]. For our purposes, we note that the metric takes a form similar to the previously discussed top-down constructions:

$$ds_{10}^2 = f_1^2 ds_{AdS_2}^2 + f_2^2 ds_{S^2}^2 + \rho^2 dw d\bar{w} + f_3^2 ds_{T^4}^2\,, \tag{5.6.17}$$

where $w, \bar{w}$ are coordinates on a Riemann surface Σ with boundary. The various metric prefactors are functions on the Riemann surface.

Let us note that κ is bounded, $\kappa > 1$, and controls the warping of the AdS_2 slices of the bulk. In [222], it was shown that the boundary entropy is determined in terms of κ and takes the form

$$S_{bdy} = \frac{c}{3} \log \kappa \,, \tag{5.6.18}$$

where c is the central charge of the 2D CFT. With the bound on κ the boundary entropy is always positive.

In [223], the Euclidean two-point function was computed holographically and takes the form

$$\begin{aligned}\left\langle \mathcal{O}\left(x_\perp, t\right) \mathcal{O}\left(x'_\perp, t'\right)\right\rangle = & \frac{2^{3-2\Delta}}{\pi \kappa^{2\Delta}[\Gamma(\Delta-1)]^2} \frac{1}{\left|x_\perp x'_\perp\right|^{\Delta}} \sum_{n=0}^{\infty} \operatorname{sign}(\xi)^n \\ & \times (n+\Delta-1/2) \frac{\Gamma(n+2\Delta-1)}{\Gamma(n+1)} Q_{\widehat{\Delta}_n - 1}(|2\xi+1|)\,.\end{aligned} \tag{5.6.19}$$

The boundary operator dimensions $\widehat{\Delta}_n$ appearing in the calculation were found exactly in [223] and their asymptotic spacing is given by

$$\lim_{n\to\infty} \widehat{\Delta}_n - \widehat{\Delta}_{n-1} = \frac{1}{\kappa}\,. \tag{5.6.20}$$

From this careful alignment of boundary operator dimensions we can already conclude that these solutions have a finite causal depth.

To see the finite causal depth explicitly, we can go ahead and find the bulk singularity by looking at the asymptotics of the analytically continued two-point function. Again using our radial coordinates, ρ, we expand 5.6.19 when both points are spacelike separated on the same side of the defect. As already noted in [223], this gives an expansion in terms of $\rho^{n/\kappa}$.[98] Thus, when we analytically continue to the timelike region on the RHS where $\rho = e^{i\theta_R}$, we expect a singularity at a time

$$\theta_R = 2\pi\kappa\,. \tag{5.6.21}$$

This can be explicitly checked from the summation of the asymptotic expansion in [223], which gives a singularity of the form

$$\frac{1}{(1-\rho^{1/\kappa})^{2\Delta-1/2}}\,, \tag{5.6.22}$$

with the appropriate divergence at $\rho = e^{i2\pi\kappa}$.

[98] In the original author's notation, our radial coordinates is precisely their ζ.

We can also calculate the expansion when the two operators are timelike separated on opposite sides of the defect. We first insert the second operator in the spacelike region across the defect where $0 < -\rho < 1$. Here the expansion takes the schematic form

$$\sum_n c_n (-1)^n (-\rho)^{n/\kappa} \,. \tag{5.6.23}$$

We can then analytically continue $-\rho$ to live on the unit circle and find that the phases align when

$$\theta_L = \pi\kappa \,. \tag{5.6.24}$$

As expected, we find the singularity on the LHS of the defect at half the time it takes for it to return to the RHS.

5.7 Discussion

We have argued that a powerful probe of the putative bulk geometry of a BCFT is the Lorentzian two-point function. The two-point function is sensitive to the (approximate) causal structure of the bulk and is a probe of how null rays can reflect off the IR geometry and return to the boundary.

In the case that the bulk geometry is terminated by an ETW brane, we argued in section 5.3 that this is indicated in the two-point function of simple CFT operators by a fixed, careful alignment of the boundary operator dimensions appearing in the BOE. We suggest that there is no reason to expect such spacing generically in the possible boundary conditions for a given holographic CFT. Thus, we have argued that an ETW brane is not generically the correct bulk description of a boundary condition for a holographic CFT.

In certain cases, we also have a top-down construction of the dual geometry for a boundary condition of a holographic CFT. These geometries are not described by ETW brane geometries, but rather have extra compact dimensions that pinch off in the IR. We argued that simple geometries that cap off at a finite causal depth will also have a reflected lightcone that relies on a seemingly fragile alignment of boundary operator dimensions. However, in some of the more complicated geometries actually found in top-down constructions, it is more subtle. There it seems that many null geodesics may become trapped in the IR geometry and do not return at short times. These top-down constructions then might be more similar to our toy models without a finite causal depth.

The existence of top-down constructions with both finite and infinite causal depth make it less clear just how atypical the existence of a good bulk dual is for a BCFT. Because some examples seem to not have a finite causal depth when probed by simple CFT operators, they do not require the same careful alignment of boundary operator dimensions. Nevertheless, it would be a much stronger claim to then assume that any set of boundary dimensions could always be explained by a sufficiently-complex local bulk geometry. It seems more likely that these complicated geometries would be a small subset of even more complicated, non-local solutions. Moreover, by probing a geometry with more complicated operators that are localized in the extra dimensions, we might expect to be able to send light-like signals into the bulk that return to the boundary. These would then require constraints on the boundary spectrum of these more complicated operators, which also need not be generic in the space of boundary conditions.

Complex geometries and chaotic boundary spectra The trapping of light-like geodesics in the IR geometry of some top-down models bears a resemblance to the dynamics of chaotic systems. Insofar as the null geodesics explore the IR geometry ergodically and fail to return to the boundary, this picture is reminiscent of the chaotic motion of billiards on a Reimannian manifold. One possible correspondence is that there is a mapping between the irregular spectrum of light operators in the BCFT and the chaotic light-like trajectories in the bulk geometry. This seems to be a different manifestation of chaotic dynamics than usually discussed in holography and it would be interesting to understand this connection better[99]. Nevertheless, as stated above, we remain hesitant to suggest that any complicated spectrum could be mapped to a sufficiently complicated *local* bulk geometry.

Boundary vs. bulk causality In the ETW brane scenario, when the brane is close to the boundary, bulk null rays can reflect off the bulk brane and return to their point of origin more quickly than a null ray confined to the boundary. This is the region (in Figure 5.5) where $-1 < \xi < 0$. In a 2D CFT with the simplest AdS+ETW brane bulk, for example, this happens when the boundary entropy is negative.

There is some apparent (if perhaps naive) tension here with causality: a bulk observer can learn information about the boundary condition more quickly than they can causally probe the boundary of the CFT itself. On the

[99]The possibility that the "hard chaos" of such causal probes in the near-horizon region of a black hole could be a manifestation of scrambling appeared in [224].

other hand, these signals return in the causal future of the boundary point, so there is no sharp conflict with boundary causality. Moreover, it's important to note that information about the boundary condition isn't localized at the boundary itself. As just one obvious example, information about the boundary condition is encoded in one-point functions measurable arbitrarily far from the boundary.

There are other cases where a bulk singularity in the region $-1 < \xi < 0$ would actually be in conflict with boundary causality. In an ICFT (folded to be seen as a BCFT) a bulk singularity in this region between a RHS and LHS operator would correspond to a signal travelling acausally across the defect to the other side. We note that in section 5.6.2, our Janus solution did not have a singularity in this region precisely because $\kappa > 1$ (that is the boundary entropy was greater than zero).

It would be interesting to have top-down constructions where information about the boundary can be causally accessed more quickly via the bulk than via the CFT.

Top-down models and SUSY It is believed by some that supersymmetry is a necessary ingredient for the existence of holographic CFTs [225]. In our top-down constructions, it would be interesting to know what role, if any, supersymmetry plays in fixing the boundary operator spectrum so that it is consistent with the bulk geometry. This would be particularly interesting to consider in the ICFT of section 5.6.2 where we do see the careful tuning of asymptotic boundary operator dimensions.

Calculating BCFT two-point functions As we discussed in section 5.6.2, we do have top-down constructions of holographic BCFTs with strong evidence for the existence of a good bulk geometry. It would be useful to have BCFT calculations of two-point functions in these theories to confirm the correspondence with predictions from the bulk geometry.

Bootstrap constraints We have argued that the constraints on the boundary spectrum necessary for agreement with a simple bulk geometry appear fragile and are not expected to be generic. Moreover, the existence of more complicated top-down constructions also seems to imply that a fixed regular spacing cannot be the only allowed possibility. Nevertheless, we have not ruled out the possibility that the alignment of boundary operator dimensions follows from some simpler assumptions, perhaps by using an appropriate bootstrap argument. It would be interesting to explore this further.

2D CFTs In [226], it was shown that the entanglement entropy of an interval in a 2D BCFT is consistent with the AdS+ETW brane proposal, provided the assumption of vacuum block dominance in the BCFT. It is somewhat surprising that the bulk would reproduce the correct entanglement entropy, even if it fails to satisfy the constraints laid out in this chapter. One possible resolution is that the entanglement entropy is a rather weak probe of the bulk geometry in this setting. When in this disconnected phase, the entropy depends only on the boundary entropy and measures only the integrated distance to the brane. On the other hand, it would be interesting if the assumption of vacuum block dominance also placed constraints in the Lorentzian bulk brane regime we considered here.

Chapter 6

Conclusion

The last several years have seen an explosion in interest in and results for chaotic conformal field theories. Spurred on by the AdS/CFT correspondence, predictions for how we should expect a chaotic CFT to behave, or even what it means for a CFT to be chaotic, have lead to scores of fascinating results and perspectives on the matter.

The greatest hope for this thesis is that it succeeds in contributing to this activity. We have shown how random matrix statistics can manifest in CFTs and its relationship with some of their most stringent symmetries, discovering fascinating correspondences with results from gravity. We have shown how hydrodynamics is linked with scrambling, and how this link manifests in the standard structure of CFTs. These results are all universal, with essentially the only assumptions being (at most) that the CFTs have semi-classical gravity duals, and as such should hold for any chaotic CFT, providing a stable footing to launch future projects and essential properties that must be matched.

One of the strongest hopes for these projects is a first-principles derivation of all chaotic phenomena. While the description of scrambling in this thesis satisfies this hope, random matrix universality is still something we have to put in "by hand". The relationship between scrambling and random matrix universality, as phenomena acting on totally different time scales, also eludes us.

A single, unified description of chaotic CFTs, valid at all time scales and derived from the bottom up, in our eyes is the ultimate goal of studying these chaotic phenomena. We hope that the relationships in this thesis between chaotic phenomena and CFT symmetries and structure provide the keys, or at least some tantalizing hints, towards such a description.

Bibliography

[1] F. M. Haehl, C. Marteau, W. Reeves and M. Rozali, *Symmetries and spectral statistics in chaotic conformal field theories*, *Journal of High Energy Physics* **2023** (2023) 196.

[2] F. M. Haehl, W. Reeves and M. Rozali, *Symmetries and spectral statistics in chaotic conformal field theories II: Maass cusp forms and arithmetic chaos*, Sept., 2023. 10.48550/arXiv.2309.00611.

[3] F. M. Haehl, W. Reeves and M. Rozali, *Reparametrization modes, shadow operators, and quantum chaos in higher-dimensional CFTs*, *Journal of High Energy Physics* **2019** (2019) 102.

[4] W. Reeves, M. Rozali, P. Simidzija, J. Sully, C. Waddell and D. Wakeham, *Looking for (and not finding) a bulk brane*, *Journal of High Energy Physics* **2021** (2021) 2.

[5] L. A. N. Laboratory, "The Quantum Butterfly Effect — Discover Los Alamos National Laboratory}." https://discover.lanl.gov/publications/1663/2021-august/the-quantum-butterfly-effect/.

[6] E. Ott, *Chaos in Dynamical Systems*. Cambridge University Press, Cambridge, 2 ed., 2002, 10.1017/CBO9780511803260.

[7] C. Beck and F. Schögl, *Thermodynamics of Chaotic Systems: An Introduction*, Cambridge Nonlinear Science Series. Cambridge University Press, Cambridge, 1993, 10.1017/CBO9780511524585.

[8] L. D'Alessio, Y. Kafri, A. Polkovnikov and M. Rigol, *From quantum chaos and eigenstate thermalization to statistical mechanics and thermodynamics*, *Advances in Physics* **65** (2016) 239.

[9] E. P. Wigner, *Characteristic Vectors of Bordered Matrices With Infinite Dimensions*, *Annals of Mathematics* **62** (1955) 548.

[10] F. J. Dyson, *Statistical Theory of the Energy Levels of Complex Systems. I*, *Journal of Mathematical Physics* **3** (1962) 140.

[11] A. D. Mirlin, *Statistics of energy levels and eigenfunctions in disordered and chaotic systems: Supersymmetry approach*, *Proc. Int. Sch. Phys. Fermi* **143** (2000) 223.

[12] R. U. Haq, A. Pandey and O. Bohigas, *Fluctuation Properties of Nuclear Energy Levels: Do Theory and Experiment Agree?*, *Physical Review Letters* **48** (1982) 1086.

[13] G. Casati, F. Valz-Gris and I. Guarnieri, *On the connection between quantization of nonintegrable systems and statistical theory of spectra*, *Lettere al Nuovo Cimento (1971-1985)* **28** (1980) 279.

[14] M. V. Berry, *Quantizing a classically ergodic system: Sinai's billiard and the KKR method*, *Annals of Physics* **131** (1981) 163.

[15] O. Bohigas, M. J. Giannoni and C. Schmit, *Characterization of Chaotic Quantum Spectra and Universality of Level Fluctuation Laws*, *Physical Review Letters* **52** (1984) 1.

[16] S. H. Shenker and D. Stanford, *Black holes and the butterfly effect*, *Journal of High Energy Physics* **2014** (2014) 67.

[17] A. Kitaev, *A simple model of quantum holography.*, *Talks at KITP, April 7,and May 27* (2015) .

[18] Y. Sekino and L. Susskind, *Fast Scramblers*, *JHEP* **10** (2008) 065 [0808.2096].

[19] S. H. Shenker and D. Stanford, *Multiple Shocks*, *JHEP* **12** (2014) 046 [1312.3296].

[20] S. H. Shenker and D. Stanford, *Stringy effects in scrambling*, *Journal of High Energy Physics* **2015** (2015) 132.

[21] D. A. Roberts and D. Stanford, *Two-dimensional conformal field theory and the butterfly effect*, *Phys. Rev. Lett.* **115** (2015) 131603 [1412.5123].

[22] J. Maldacena and D. Stanford, *Comments on the Sachdev-Ye-Kitaev model*, 1604.07818.

[23] Y. Gu, X.-L. Qi and D. Stanford, *Local criticality, diffusion and chaos in generalized Sachdev-Ye-Kitaev models*, *Journal of High Energy Physics* **2017** (2017) 125.

[24] A. A. Belavin, A. M. Polyakov and A. B. Zamolodchikov, *Infinite Conformal Symmetry in Two-Dimensional Quantum Field Theory*, *Nucl. Phys. B* **241** (1984) 333.

[25] P. Di Francesco, P. Mathieu and D. Senechal, *Conformal Field Theory*, Graduate Texts in Contemporary Physics. Springer-Verlag, New York, 1997, 10.1007/978-1-4612-2256-9.

[26] J. M. Maldacena, *The Large N limit of superconformal field theories and supergravity*, *Int. J. Theor. Phys.* **38** (1999) 1113 [hep-th/9711200].

[27] E. Witten, *Anti de Sitter space and holography*, *Advances in Theoretical and Mathematical Physics* **2** (1998) 253.

[28] O. Aharony, S. S. Gubser, J. Maldacena, H. Ooguri and Y. Oz, *Large N field theories, string theory and gravity*, *Physics Reports* **323** (2000) 183.

[29] D. Harlow and D. Jafferis, *The factorization problem in Jackiw-Teitelboim gravity*, *Journal of High Energy Physics* **2020** (2020) 177.

[30] J. Pollack, M. Rozali, J. Sully and D. Wakeham, *Eigenstate Thermalization and Disorder Averaging in Gravity*, *Physical Review Letters* **125** (2020) 021601.

[31] J. S. Cotler, G. Gur-Ari, M. Hanada, J. Polchinski, P. Saad, S. H. Shenker et al., *Black holes and random matrices*, *Journal of High Energy Physics* **2017** (2017) 118.

[32] P. Saad, S. H. Shenker and D. Stanford, *A semiclassical ramp in SYK and in gravity*, 1806.06840.

[33] J. Cotler and K. Jensen, *AdS_3 wormholes from a modular bootstrap*, *JHEP* **11** (2020) 058 [2007.15653].

[34] J. Cotler and K. Jensen, *AdS3 gravity and random CFT*, *Journal of High Energy Physics* **2021** (2021) 33.

[35] L. Eberhardt, *Off-shell Partition Functions in 3d Gravity*, 2204.09789.

[36] D. Kapec, R. Mahajan and D. Stanford, *Matrix ensembles with global symmetries and 't Hooft anomalies from 2d gauge theory*, *JHEP* **04** (2020) 186 [1912.12285].

[37] A. Ghosh, H. Maxfield and G. J. Turiaci, *A universal Schwarzian sector in two-dimensional conformal field theories*, *JHEP* **05** (2020) 104 [1912.07654].

[38] P. Kraus and A. Maloney, *A cardy formula for three-point coefficients or how the black hole got its spots*, *Journal of High Energy Physics* **2017** (2017) 160.

[39] S. Collier, A. Maloney, H. Maxfield and I. Tsiares, *Universal dynamics of heavy operators in CFT$_2$*, *JHEP* **07** (2020) 074 [1912.00222].

[40] J. Chandra, S. Collier, T. Hartman and A. Maloney, *Semiclassical 3D gravity as an average of large-c CFTs*, *Journal of High Energy Physics* **2022** (2022) 69.

[41] A. Belin, J. de Boer, P. Nayak and J. Sonner, *Generalized spectral form factors and the statistics of heavy operators*, *JHEP* **11** (2022) 145 [2111.06373].

[42] N. Lashkari, A. Dymarsky and H. Liu, *Eigenstate thermalization hypothesis in conformal field theory*, *Journal of Statistical Mechanics: Theory and Experiment* **2018** (2018) 033101.

[43] Y. Hikida, Y. Kusuki and T. Takayanagi, *Eigenstate thermalization hypothesis and modular invariance of two-dimensional conformal field theories*, *Physical Review D* **98** (2018) 026003.

[44] A. Pérez and R. Troncoso, *Gravitational dual of averaged free CFT's over the Narain lattice*, *Journal of High Energy Physics* **2020** (2020) 15.

[45] S. Collier and E. Perlmutter, *Harnessing S-duality in $\mathcal{N}=4$ SYM & supergravity as SL(2, $\mathbb{Z}$)-averaged strings*, *JHEP* **08** (2022) 195 [2201.05093].

[46] A. Belin, J. de Boer, D. L. Jafferis, P. Nayak and J. Sonner, *Approximate CFTs and Random Tensor Models*, Aug., 2023. 10.48550/arXiv.2308.03829.

[47] "David Tong: Lectures on String Theory." http://www.damtp.cam.ac.uk/user/tong/string.html, 1, 2009.

[48] J. Maldacena, S. H. Shenker and D. Stanford, *A bound on chaos*, *JHEP* **08** (2016) 106 [1503.01409].

[49] D. Harlow, *Jerusalem lectures on black holes and quantum information*, *Reviews of Modern Physics* **88** (2016) 015002.

[50] R. M. Wald, *General Relativity*. Chicago Univ. Pr., Chicago, USA, 1984, 10.7208/chicago/9780226870373.001.0001.

[51] D. Simmons-Duffin, *TASI Lectures on the Conformal Bootstrap*, Feb., 2016.

[52] P. Ginsparg, *Applied Conformal Field Theory*, Nov., 1988. 10.48550/arXiv.hep-th/9108028.

[53] M. Blake, H. Lee and H. Liu, *A quantum hydrodynamical description for scrambling and many-body chaos*, *Journal of High Energy Physics* **2018** (2018) 127.

[54] E. P. Wigner, *Characteristic Vectors of Bordered Matrices With Infinite Dimensions*, *Annals of Mathematics* **62** (1955) 548.

[55] F. J. Dyson, *Statistical Theory of the Energy Levels of Complex Systems. I*, *Journal of Mathematical Physics* **3** (1962) 140.

[56] D. Poland, S. Rychkov and A. Vichi, *The Conformal Bootstrap: Theory, Numerical Techniques, and Applications*, *Rev. Mod. Phys.* **91** (2019) 015002 [1805.04405].

[57] J. L. Cardy, *Operator Content of Two-Dimensional Conformally Invariant Theories*, *Nucl. Phys. B* **270** (1986) 186.

[58] E. Dyer and G. Gur-Ari, *2D CFT Partition Functions at Late Times*, *JHEP* **08** (2017) 075 [1611.04592].

[59] N. Benjamin, E. Dyer, A. L. Fitzpatrick and Y. Xin, *The Most Irrational Rational Theories*, *JHEP* **04** (2019) 025 [1812.07579].

[60] J. Kudler-Flam, L. Nie and S. Ryu, *Conformal field theory and the web of quantum chaos diagnostics*, *JHEP* **01** (2020) 175 [1910.14575].

[61] B. Mukhametzhanov and S. Pal, *Beurling-Selberg extremization and modular bootstrap at high energies*, *SciPost Physics* **8** (2020) 088.

[62] N. Benjamin, S. Collier, A. L. Fitzpatrick, A. Maloney and E. Perlmutter, *Harmonic analysis of 2d CFT partition functions*, *JHEP* **09** (2021) 174 [2107.10744].

[63] H. Paul, E. Perlmutter and H. Raj, *Integrated Correlators in* $\mathcal{N} = 4$ *SYM via* $SL(2, \mathbb{Z})$ *Spectral Theory*, 2209.06639.

[64] J. M. Maldacena and L. Maoz, *Wormholes in AdS*, *JHEP* **02** (2004) 053 [hep-th/0401024].

[65] P. Saad, *Late Time Correlation Functions, Baby Universes, and ETH in JT Gravity*, 1910.10311.

[66] D. Stanford and E. Witten, *JT gravity and the ensembles of random matrix theory*, *Adv. Theor. Math. Phys.* **24** (2020) 1475 [1907.03363].

[67] D. Stanford, *More quantum noise from wormholes*, 2008.08570.

[68] A. Blommaert, T. G. Mertens and H. Verschelde, *Eigenbranes in Jackiw-Teitelboim gravity*, *JHEP* **02** (2021) 168 [1911.11603].

[69] A. Maloney and E. Witten, *Averaging over Narain moduli space*, *JHEP* **10** (2020) 187 [2006.04855].

[70] N. Afkhami-Jeddi, H. Cohn, T. Hartman and A. Tajdini, *Free partition functions and an averaged holographic duality*, *JHEP* **01** (2021) 130 [2006.04839].

[71] F. Wegner, *The mobility edge problem: Continuous symmetry and a conjecture*, *Zeitschrift für Physik B Condensed Matter and Quanta* **35** (1979) 207.

[72] K. B. Efetov, *Supersymmetry and theory of disordered metals*, *Adv. Phys.* **32** (1983) 53.

[73] A. Altland and J. Sonner, *Late time physics of holographic quantum chaos*, 2008.02271.

[74] J. Kaidi and E. Perlmutter, *Discreteness and integrality in Conformal Field Theory*, *JHEP* **02** (2021) 064 [2008.02190].

[75] T. Hartman, C. A. Keller and B. Stoica, *Universal spectrum of 2d conformal field theory in the large c limit*, *Journal of High Energy Physics* **2014** (2014) 118.

[76] C. A. Keller and A. Maloney, *Poincaré series, 3D gravity and CFT spectroscopy*, *Journal of High Energy Physics* **2015** (2015) 80.

[77] J.-M. Schlenker and E. Witten, *No ensemble averaging below the black hole threshold*, *JHEP* **07** (2022) 143 [2202.01372].

[78] G. Di Ubaldo and E. Perlmutter, *AdS_3/RMT_2 Duality*, 2307.03707.

[79] G. Di Ubaldo and E. Perlmutter, *AdS_3 Pure Gravity and Stringy Unitarity*, 2308.01787.

[80] E. D'Hoker and J. Kaidi, *Lectures on modular forms and strings*, 2208.07242.

[81] J. M. Maldacena, *Eternal black holes in anti-de Sitter*, *JHEP* **0304** (2003) 021 [hep-th/0106112].

[82] H. Maxfield, *Quantum corrections to the BTZ black hole extremality bound from the conformal bootstrap*, *Journal of High Energy Physics* **2019** (2019) 3.

[83] T. G. Mertens, G. J. Turiaci and H. L. Verlinde, *Solving the Schwarzian via the Conformal Bootstrap*, *JHEP* **08** (2017) 136 [1705.08408].

[84] A. Zamolodchikov and A. Zamolodchikov, *Liouville field theory on a pseudosphere*, *arXiv:hep-th/0101152* (2001) [hep-th/0101152].

[85] S. Pal and Z. Sun, *Tauberian-Cardy formula with spin*, *Journal of High Energy Physics* **2020** (2020) 135.

[86] Y. Kusuki, *Light cone bootstrap in general 2D CFTs and entanglement from light cone singularity*, *Journal of High Energy Physics* **2019** (2019) 25.

[87] B. Mukhametzhanov and A. Zhiboedov, *Modular invariance, tauberian theorems and microcanonical entropy*, *JHEP* **10** (2019) 261 [1904.06359].

[88] F. M. Haehl and M. Rozali, *Effective Field Theory for Chaotic CFTs*, *JHEP* **10** (2018) 118 [1808.02898].

[89] F. M. Haehl, R. Loganayagam and M. Rangamani, *Effective Action for Relativistic Hydrodynamics: Fluctuations, Dissipation, and Entropy Inflow*, *JHEP* **10** (2018) 194 [1803.11155].

[90] H. Liu and P. Glorioso, *Lectures on non-equilibrium effective field theories and fluctuating hydrodynamics*, *PoS* **TASI2017** (2018) 008 [1805.09331].

[91] M. Winer and B. Swingle, *Hydrodynamic Theory of the Connected Spectral form Factor*, *Phys. Rev. X* **12** (2022) 021009 [2012.01436].

[92] S. Pal, J. Qiao and S. Rychkov, *Twist accumulation in conformal field theory. A rigorous approach to the lightcone bootstrap*, 2212.04893.

[93] J. Bolte, G. Steil and F. Steiner, *Arithmetical chaos and violation of universality in energy level statistics*, *Physical Review Letters* **69** (1992) 2188.

[94] P. Sarnak, "Arithmetic Quantum Chaos." `http://web.math.princeton.edu/sarnak/Arithmetic%20Quantum%20Chaos.pdf`, 1993.

[95] D. A. Hejhal and B. N. Rackner, *On the Topography of Maass Waveforms for PSL(2,Z)*, *Exp. Math.* **1** (1992) 275.

[96] E. Bogomolny, B. Georgeot, M.-J. Giannoni and C. Schmit, *Arithmetical chaos*, *Physics Reports* **291** (1997) 219.

[97] C. Yan, *More on Torus Wormholes in 3d Gravity*, 2305.10494.

[98] H. Then, *Maaß cusp forms for large eigenvalues*, *Mathematics of Computation* **74** (2004) 363.

[99] T. LMFDB Collaboration, "The L-functions and modular forms database." `https://www.lmfdb.org`, 2023.

[100] G. Steil, *Eigenvalues of the Laplacian and of the Hecke operators for PSL(2,Z)*, .

[101] C. Matthies and F. Steiner, *Selberg's ζ function and the quantization of chaos*, *Phys. Rev. A* **44** (1991) R7877.

[102] P. Sarnak, *Statistical Properties of Eigenvalues of the Hecke Operators*, in *Analytic Number Theory and Diophantine Problems: Proceedings of*

a Conference at Oklahoma State University, 1984, A. C. Adolphson, J. B. Conrey, A. Ghosh and R. I. Yager, eds., Progress in Mathematics, (Boston, MA), pp. 321–331, Birkhäuser, (1987), DOI.

[103] F. M. Haehl, W. Reeves and M. Rozali, *Euclidean wormholes in two-dimensional CFTs from quantum chaos and number theory*, Sept., 2023. 10.48550/arXiv.2309.02533.

[104] A. Altland and D. Bagrets, *Quantum ergodicity in the SYK model*, *Nucl. Phys. B* **930** (2018) 45 [1712.05073].

[105] A. Belin and J. de Boer, *Random statistics of OPE coefficients and Euclidean wormholes*, *Class. Quant. Grav.* **38** (2021) 164001 [2006.05499].

[106] A. Blommaert, J. Kruthoff and S. Yao, *An integrable road to a perturbative plateau*, *JHEP* **04** (2023) 048 [2208.13795].

[107] P. Saad, D. Stanford, Z. Yang and S. Yao, *A convergent genus expansion for the plateau*, 2210.11565.

[108] A. I. Larkin and Y. N. Ovchinnikov, *Quasiclassical method in the theory of superconductivity*, *Sov.Phys.JETP* **28** (1969) 1200.

[109] S. Leichenauer, *Disrupting Entanglement of Black Holes*, *Phys. Rev.* **D90** (2014) 046009 [1405.7365].

[110] P. Hayden and J. Preskill, *Black holes as mirrors: Quantum information in random subsystems*, *JHEP* **09** (2007) 120 [0708.4025].

[111] N. Lashkari, D. Stanford, M. Hastings, T. Osborne and P. Hayden, *Towards the Fast Scrambling Conjecture*, *JHEP* **04** (2013) 022 [1111.6580].

[112] A. Almheiri and J. Polchinski, *Models of AdS_2 backreaction and holography*, *JHEP* **11** (2015) 014 [1402.6334].

[113] J. Maldacena, D. Stanford and Z. Yang, *Conformal symmetry and its breaking in two dimensional Nearly Anti-de-Sitter space*, 1606.01857.

[114] K. Jensen, *Chaos and hydrodynamics near AdS_2*, 1605.06098.

[115] J. Cotler and K. Jensen, *A theory of reparameterizations for AdS_3 gravity*, *JHEP* **02** (2019) 079 [1808.03263].

[116] K. Jensen, *Scrambling in nearly thermalized states at large central charge*, `1906.05852`.

[117] G. Turiaci and H. Verlinde, *On CFT and Quantum Chaos*, *JHEP* **12** (2016) 110 [`1603.03020`].

[118] F. A. Dolan and H. Osborn, *Conformal Partial Waves: Further Mathematical Results*, `1108.6194`.

[119] D. Simmons-Duffin, *Projectors, Shadows, and Conformal Blocks*, *JHEP* **04** (2014) 146 [`1204.3894`].

[120] A. Alekseev and S. L. Shatashvili, *Path Integral Quantization of the Coadjoint Orbits of the Virasoro Group and 2D Gravity*, *Nucl. Phys.* **B323** (1989) 719.

[121] B. Czech, L. Lamprou, S. McCandlish, B. Mosk and J. Sully, *A Stereoscopic Look into the Bulk*, *JHEP* **07** (2016) 129 [`1604.03110`].

[122] J. de Boer, F. M. Haehl, M. P. Heller and R. C. Myers, *Entanglement, holography and causal diamonds*, *JHEP* **08** (2016) 162 [`1606.03307`].

[123] E. S. Fradkin and M. Y. Palchik, *New developments in D-dimensional conformal quantum field theory*, *Phys. Rept.* **300** (1998) 1.

[124] V. Gurarie, *Logarithmic operators in conformal field theory*, *Nucl. Phys.* **B410** (1993) 535 [`hep-th/9303160`].

[125] M. R. Gaberdiel, *An Algebraic approach to logarithmic conformal field theory*, *Int. J. Mod. Phys.* **A18** (2003) 4593 [`hep-th/0111260`].

[126] M. Flohr, *Bits and pieces in logarithmic conformal field theory*, *Int. J. Mod. Phys.* **A18** (2003) 4497 [`hep-th/0111228`].

[127] H. Osborn, *Lectures on Conformal Field Theories in more than two dimensions*, 2018.

[128] F. A. Dolan and H. Osborn, *Conformal partial waves and the operator product expansion*, *Nucl. Phys.* **B678** (2004) 491 [`hep-th/0309180`].

[129] E. S. Fradkin and M. Y. Palchik, *Conformal Quantum Field Theory in D-dimensions*. Springer Netherlands, Dordrecht, 1996, 10.1007/978-94-015-8757-0.

[130] A. Bzowski, P. McFadden and K. Skenderis, *Implications of conformal invariance in momentum space*, *JHEP* **03** (2014) 111 [1304.7760].

[131] D. Z. Freedman, K. Johnson and J. I. Latorre, *Differential regularization and renormalization: A New method of calculation in quantum field theory*, *Nucl. Phys.* **B371** (1992) 353.

[132] J. I. Latorre, C. Manuel and X. Vilasis-Cardona, *Systematic differential renormalization to all orders*, *Annals Phys.* **231** (1994) 149 [hep-th/9303044].

[133] A. L. Fitzpatrick, J. Kaplan and M. T. Walters, *Universality of Long-Distance AdS Physics from the CFT Bootstrap*, *JHEP* **08** (2014) 145 [1403.6829].

[134] H. Maxfield, *A view of the bulk from the worldline*, Dec., 2017. 10.48550/arXiv.1712.00885.

[135] A. L. Fitzpatrick and K.-W. Huang, *Universal Lowest-Twist in CFTs from Holography*, *JHEP* **08** (2019) 138 [1903.05306].

[136] A. L. Fitzpatrick, K.-W. Huang and D. Li, *Probing Universalities in d¿2 CFTs: from Black Holes to Shockwaves*, 1907.10810.

[137] M. Kulaxizi, G. S. Ng and A. Parnachev, *Subleading Eikonal, AdS/CFT and Double Stress Tensors*, 1907.00867.

[138] K.-W. Huang, *Stress-tensor commutators in conformal field theories near the lightcone*, *Physical Review D* **100** (2019) 061701.

[139] A. L. Fitzpatrick and J. Kaplan, *Analyticity and the Holographic S-Matrix*, *JHEP* **10** (2012) 127 [1111.6972].

[140] C. Cardona, S. Guha, S. K. Kanumilli and K. Sen, *Resummation at finite conformal spin*, *JHEP* **01** (2019) 077 [1811.00213].

[141] A. L. Fitzpatrick, J. Kaplan and M. T. Walters, *Virasoro Conformal Blocks and Thermality from Classical Background Fields*, *JHEP* **11** (2015) 200 [1501.05315].

[142] A. L. Fitzpatrick and J. Kaplan, *Conformal Blocks Beyond the Semi-Classical Limit*, *JHEP* **05** (2016) 075 [1512.03052].

[143] A. L. Fitzpatrick and J. Kaplan, *A Quantum Correction To Chaos*, *JHEP* **05** (2016) 070 [1601.06164].

[144] T. Anous and J. Sonner, *Phases of scrambling in eigenstates*, *SciPost Phys.* **7** (2019) 003 [1903.03143].

[145] F. M. Haehl, R. Loganayagam, P. Narayan and M. Rangamani, *Classification of out-of-time-order correlators*, *SciPost Phys.* **6** (2019) 001 [1701.02820].

[146] F. M. Haehl and M. Rozali, *Fine Grained Chaos in AdS_2 Gravity*, *Phys. Rev. Lett.* **120** (2018) 121601 [1712.04963].

[147] H. Casini, M. Huerta and R. C. Myers, *Towards a derivation of holographic entanglement entropy*, *JHEP* **05** (2011) 036 [1102.0440].

[148] M. Mezei and G. Sarosi, *Chaos in the butterfly cone*, 1908.03574.

[149] E. Perlmutter, *Bounding the Space of Holographic CFTs with Chaos*, *JHEP* **10** (2016) 069 [1602.08272].

[150] Y. Ahn, V. Jahnke, H.-S. Jeong and K.-Y. Kim, *Scrambling in Hyperbolic Black Holes*, 1907.08030.

[151] S. Grozdanov, K. Schalm and V. Scopelliti, *Black hole scrambling from hydrodynamics*, *Phys. Rev. Lett.* **120** (2018) 231601 [1710.00921].

[152] M. Blake, R. A. Davison, S. Grozdanov and H. Liu, *Many-body chaos and energy dynamics in holography*, *JHEP* **10** (2018) 035 [1809.01169].

[153] S. Grozdanov, *On the connection between hydrodynamics and quantum chaos in holographic theories with stringy corrections*, *JHEP* **01** (2019) 048 [1811.09641].

[154] S. Grozdanov, P. K. Kovtun, A. O. Starinets and P. Tadic, *The complex life of hydrodynamic modes*, 1904.12862.

[155] M. Blake, R. A. Davison and D. Vegh, *Horizon constraints on holographic Green's functions*, 1904.12883.

[156] M. S. Costa, V. Goncalves and J. Penedones, *Spinning AdS Propagators*, *JHEP* **09** (2014) 064 [1404.5625].

[157] T. Faulkner, R. G. Leigh and O. Parrikar, *Shape Dependence of Entanglement Entropy in Conformal Field Theories*, *JHEP* **04** (2016) 088 [1511.05179].

[158] S. Ohya, *Intertwining operator in thermal CFT_d*, *Int. J. Mod. Phys.* **A32** (2017) 1750006 [1611.00763].

[159] S. Das, B. Ezhuthachan and A. Kundu, *Real time dynamics from low point correlators in 2d BCFT*, *Journal of High Energy Physics* **2019** (2019) 141.

[160] R. F. Penna and C. Zukowski, *Kinematic space and the orbit method*, *JHEP* **07** (2019) 045 [1812.02176].

[161] N. Callebaut, *The gravitational dynamics of kinematic space*, *JHEP* **02** (2019) 153 [1808.10431].

[162] N. Callebaut and H. Verlinde, *Entanglement Dynamics in 2D CFT with Boundary: Entropic origin of JT gravity and Schwarzian QM*, *JHEP* **05** (2019) 045 [1808.05583].

[163] P. Kraus, A. Sivaramakrishnan and R. Snively, *Late time Wilson lines*, *JHEP* **04** (2019) 026 [1810.01439].

[164] Y. Kusuki and M. Miyaji, *Entanglement Entropy, OTOC and Bootstrap in 2D CFTs from Regge and Light Cone Limits of Multi-point Conformal Block*, 1905.02191.

[165] V. Rosenhaus, *Multipoint Conformal Blocks in the Comb Channel*, *JHEP* **02** (2019) 142 [1810.03244].

[166] T. Anous, F. Haehl and E. Perlmutter, *work in progress*, .

[167] M. Van Raamsdonk and C. Waddell, *Finding $AdS^5 \times S^5$ in 2+1 dimensional SCFT physics*, 2109.04479.

[168] A. Almheiri, R. Mahajan, J. Maldacena and Y. Zhao, *The page curve of hawking radiation from semiclassical geometry*, *Journal of High Energy Physics* **2020** (2020) .

[169] A. Almheiri, T. Hartman, J. Maldacena, E. Shaghoulian and A. Tajdini, *Replica wormholes and the entropy of hawking radiation*, *Journal of High Energy Physics* **2020** (2020) .

[170] G. Penington, S. H. Shenker, D. Stanford and Z. Yang, *Replica wormholes and the black hole interior*, 2020.

[171] M. Rozali, J. Sully, M. Van Raamsdonk, C. Waddell and D. Wakeham, *Information radiation in bcft models of black holes*, *Journal of High Energy Physics* **2020** (2020) .

[172] H. Geng and A. Karch, *Massive islands*, *Journal of High Energy Physics* **2020** (2020) .

[173] H. Geng, A. Karch, C. Perez-Pardavila, S. Raju, L. Randall, M. Riojas et al., *Information transfer with a gravitating bath*, 2021.

[174] H. Geng, A. Karch, C. Perez-Pardavila, S. Raju, L. Randall, M. Riojas et al., *Inconsistency of islands in theories with long-range gravity*, 2021.

[175] H. Z. Chen, R. C. Myers, D. Neuenfeld, I. A. Reyes and J. Sandor, *Quantum extremal islands made easy, part i: Entanglement on the brane*, 2020.

[176] H. Z. Chen, R. C. Myers, D. Neuenfeld, I. A. Reyes and J. Sandor, *Quantum extremal islands made easy, part ii: Black holes on the brane*, 2020.

[177] D. Neuenfeld, *The dictionary for double holography and graviton masses in d dimensions*, 2021.

[178] D. Neuenfeld, *Double holography as a model for black hole complementarity*, 2021.

[179] D. Harlow and D. Jafferis, *The Factorization Problem in Jackiw-Teitelboim Gravity*, *JHEP* **02** (2020) 177 [1804.01081].

[180] P. Gao, D. L. Jafferis and D. K. Kolchmeyer, *An effective matrix model for dynamical end of the world branes in Jackiw-Teitelboim gravity*, 2104.01184.

[181] I. Heemskerk, J. Penedones, J. Polchinski and J. Sully, *Holography from Conformal Field Theory*, *Journal of High Energy Physics* **2009** (2009) 079 [0907.0151].

[182] J. Penedones, *Writing CFT correlation functions as AdS scattering amplitudes*, *Journal of High Energy Physics* **2011** (2011) 25 [1011.1485].

[183] Z. Komargodski and A. Zhiboedov, *Convexity and Liberation at Large Spin*, *Journal of High Energy Physics* **2013** (2013) 140 [1212.4103].

[184] S. El-Showk and K. Papadodimas, *Emergent Spacetime and Holographic CFTs*, *JHEP* **10** (2012) 106 [1101.4163].

[185] A. L. Fitzpatrick, J. Kaplan, D. Poland and D. Simmons-Duffin, *The Analytic Bootstrap and AdS Superhorizon Locality*, *Journal of High Energy Physics* **2013** (2013) 4 [1212.3616].

[186] N. Afkhami-Jeddi, T. Hartman, S. Kundu and A. Tajdini, *Einstein gravity 3-point functions from conformal field theory*, *JHEP* **12** (2017) 049 [1610.09378].

[187] M. Kulaxizi, A. Parnachev and A. Zhiboedov, *Bulk Phase Shift, CFT Regge Limit and Einstein Gravity*, *JHEP* **06** (2018) 121 [1705.02934].

[188] D. Meltzer and E. Perlmutter, *Beyond $a = c$: gravitational couplings to matter and the stress tensor OPE*, *JHEP* **07** (2018) 157 [1712.04861].

[189] M. S. Costa, T. Hansen and J. a. Penedones, *Bounds for OPE coefficients on the Regge trajectory*, *JHEP* **10** (2017) 197 [1707.07689].

[190] X. O. Camanho, J. D. Edelstein, J. Maldacena and A. Zhiboedov, *Causality Constraints on Corrections to the Graviton Three-Point Coupling*, *JHEP* **02** (2016) 020 [1407.5597].

[191] A. Belin, D. M. Hofman and G. Mathys, *Einstein gravity from ANEC correlators*, *JHEP* **08** (2019) 032 [1904.05892].

[192] M. Kologlu, P. Kravchuk, D. Simmons-Duffin and A. Zhiboedov, *Shocks, Superconvergence, and a Stringy Equivalence Principle*, *JHEP* **11** (2020) 096 [1904.05905].

[193] S. Caron-Huot, D. Mazac, L. Rastelli and D. Simmons-Duffin, *AdS Bulk Locality from Sharp CFT Bounds*, 2106.10274.

[194] J. L. Cardy, *Conformal invariance and surface critical behavior*, *Nuclear Physics B* **240** (1984) 514.

[195] D. M. McAvity and H. Osborn, *Conformal Field Theories Near a Boundary in General Dimensions*, *Nuclear Physics B* **455** (1995) 522 [cond-mat/9505127].

[196] P. Liendo, L. Rastelli and B. C. van Rees, *The Bootstrap Program for Boundary CFT_d*, *Journal of High Energy Physics* **2013** (2013) [1210.4258].

[197] J. Maldacena, D. Simmons-Duffin and A. Zhiboedov, *Looking for a bulk point*, *arXiv:1509.03612 [hep-th]* (2015) [1509.03612].

[198] M. Dodelson and H. Ooguri, *Singularities of thermal correlators at strong coupling*, *Phys. Rev. D* **103** (2021) 066018 [2010.09734].

[199] N. Engelhardt and G. T. Horowitz, *Towards a Reconstruction of General Bulk Metrics*, 1605.01070.

[200] N. Engelhardt, *Into the Bulk: A Covariant Approach*, *Physical Review D* **95** (2017) 066005 [1610.08516].

[201] S. Hernández-Cuenca and G. T. Horowitz, *Bulk reconstruction of metrics with a compact space asymptotically*, *JHEP* **08** (2020) 108 [2003.08409].

[202] D. Mazáč, L. Rastelli and X. Zhou, *An Analytic Approach to BCFT$_d$*, *arXiv:1812.09314 [hep-th]* (2018) [1812.09314].

[203] D. Pappadopulo, S. Rychkov, J. Espin and R. Rattazzi, *OPE Convergence in Conformal Field Theory*, *Phys. Rev. D* **86** (2012) 105043 [1208.6449].

[204] M. Hogervorst and S. Rychkov, *Radial Coordinates for Conformal Blocks*, *Phys. Rev. D* **87** (2013) 106004 [1303.1111].

[205] M. Fujita, T. Takayanagi and E. Tonni, *Aspects of AdS/BCFT*, *Journal of High Energy Physics* **2011** (2011) [1108.5152].

[206] T. Takayanagi, *Holographic dual of a boundary conformal field theory*, *Physical review letters* **107** (2011) 101602.

[207] A. Karch and L. Randall, *Locally localized gravity*, *JHEP* **05** (2001) 008 [hep-th/0011156].

[208] A. Karch and L. Randall, *Open and closed string interpretation of SUSY CFT's on branes with boundaries*, *JHEP* **06** (2001) 063 [hep-th/0105132].

[209] M. Chiodaroli, E. D'Hoker and M. Gutperle, *Simple Holographic Duals to Boundary CFTs*, *JHEP* **02** (2012) 005 [1111.6912].

[210] M. Chiodaroli, E. D'Hoker and M. Gutperle, *Holographic duals of Boundary CFTs*, *JHEP* **07** (2012) 177 [1205.5303].

[211] L. Berdichevsky and B.-e. Dahan, *Local gravitational solutions dual to M2-branes intersecting and/or ending on M5-branes*, *JHEP* **08** (2013) 061 [1304.4389].

[212] C. Bachas, E. D'Hoker, J. Estes and D. Krym, *M-theory Solutions Invariant under $D(2,1;\gamma) \oplus D(2,1;\gamma)$*, *Fortsch. Phys.* **62** (2014) 207 [1312.5477].

[213] E. D'Hoker, J. Estes and M. Gutperle, *Exact half-BPS Type IIB interface solutions. I. Local solution and supersymmetric Janus*, *JHEP* **06** (2007) 021 [0705.0022].

[214] E. D'Hoker, J. Estes and M. Gutperle, *Exact half-BPS Type IIB interface solutions. II. Flux solutions and multi-Janus*, *JHEP* **06** (2007) 022 [0705.0024].

[215] O. Aharony, L. Berdichevsky, M. Berkooz and I. Shamir, *Near-horizon solutions for D3-branes ending on 5-branes*, *Phys. Rev.* **D84** (2011) 126003 [1106.1870].

[216] D. Gaiotto and E. Witten, *Supersymmetric Boundary Conditions in N=4 Super Yang-Mills Theory*, *J. Statist. Phys.* **135** (2009) 789 [0804.2902].

[217] D. Gaiotto and E. Witten, *S-Duality of Boundary Conditions In N=4 Super Yang-Mills Theory*, *Adv. Theor. Math. Phys.* **13** (2009) 721 [0807.3720].

[218] O. Aharony, O. DeWolfe, D. Z. Freedman and A. Karch, *Defect Conformal Field Theory and Locally Localized Gravity*, *Journal of High Energy Physics* **2003** (2003) 030 [hep-th/0303249].

[219] J. Penedones, *TASI lectures on AdS/CFT*, 1608.04948.

[220] M. Lemos, P. Liendo, M. Meineri and S. Sarkar, *Universality at large transverse spin in defect CFT*, *Journal of High Energy Physics* **2018** (2018) 91 [1712.08185].

[221] C. Bachas and J. Estes, *Spin-2 spectrum of defect theories*, *JHEP* **06** (2011) 005 [1103.2800].

[222] M. Chiodaroli, M. Gutperle and L.-Y. Hung, *Boundary entropy of supersymmetric Janus solutions*, *JHEP* **09** (2010) 082 [1005.4433].

[223] M. Chiodaroli, J. Estes and Y. Korovin, *Holographic two-point functions for Janus interfaces in the D1/D5 CFT*, *JHEP* **04** (2017) 145 [1612.08916].

[224] J. L. F. Barbon and J. M. Magan, *Chaotic Fast Scrambling At Black Holes*, *Phys. Rev. D* **84** (2011) 106012 [1105.2581].

[225] H. Ooguri and C. Vafa, *Non-supersymmetric AdS and the Swampland*, *Adv. Theor. Math. Phys.* **21** (2017) 1787 [1610.01533].

[226] J. Sully, M. V. Raamsdonk and D. Wakeham, *BCFT entanglement entropy at large central charge and the black hole interior*, *JHEP* **03** (2021) 167 [2004.13088].

[227] R. Szmytkowski and S. Bielski, *An orthogonality relation for the whittaker functions of the second kind of imaginary order*, *Integral Transforms and Special Functions* **21** (2010) 739 [https://doi.org/10.1080/10652461003643412].

[228] I. S. Gradshteyn and I. M. Ryzhik, *Table of integrals, series, and products*. Elsevier/Academic Press, Amsterdam, seventh ed., 2007.

[229] D. A. Hejhal and B. N. Rackner, *On the topography of Maass waveforms for* $\mathrm{PSL}(2, \mathbf{Z})$, *Experimental Mathematics* **1** (1992) 275 .

[230] O. Bohigas and M.-J. Giannoni, *Chaotic motion and random matrix theories*, in *Mathematical and Computational Methods in Nuclear Physics*, J. S. Dehesa, J. M. G. Gomez and A. Polls, eds., Lecture Notes in Physics, (Berlin, Heidelberg), pp. 1–99, Springer, 1984, DOI.

[231] Y. Motohashi, *Spectral Theory of the Riemann Zeta-Function*, Cambridge Tracts in Mathematics. Cambridge University Press, 1997, 10.1017/CBO9780511983399.

[232] G. Shimura, *On the holomorphy of certain dirichlet series*, *Proceedings of the London Mathematical Society* **s3-31** (1975) 79 [https://londmathsoc.onlinelibrary.wiley.com/doi/pdf/10.1112/plms/s3-31.1.79].

[233] A. Sankaranarayanan, *Fundamental properties of symmetric square L-functions I*, *Illinois J. Math.* **46** (2002) 23.

[234] J. Hoffstein and P. Lockhart, *Coefficients of Maass Forms and the Siegel Zero*, *Annals of Mathematics* **140** (1994) 161.

[235] J. Newton and J. A. Thorne, *Symmetric power functoriality for holomorphic modular forms*, *Publications mathématiques de l'IHÉS* **134** (2021) [1912.11261].

[236] V. Blomer and A. Corbett, *A symplectic restriction problem*, *Math.Ann.* **382** (2019) 1323–1424 [1912.07496].

[237] V. Blomer, É. Fouvry, E. Kowalski, P. Michel, D. Milićević and W. Sawin, *The second moment theory of families of L-functions*, Dec., 2019. 10.48550/arXiv.1804.01450.

[238] A. Zamolodchikov, *Conformal symmetry in two-dimensional space: Recursion representation of conformal block*, *Theoretical and Mathematical Physics* **73** (1987) 1088.

Appendix A

Appendices for chapter 2

A.1 Notation and conventions

In this appendix we collect some definitions and conventions used in chapters 2 and 3.

We use the following inner product for square-integrable functions on the fundamental domain $\mathcal{F} \equiv \mathbb{H}/SL(2,\mathbb{Z})$:

$$(f,g) = \int_{\mathcal{F}} \frac{dxdy}{y^2}\, f(x+iy)\,\overline{g(x+iy)}\,. \tag{A.1.1}$$

We consider the spectral decomposition of the Laplacian on the fundamental domain $\mathcal{F} = \{\tau = x+iy\,,\ y>0\}/SL(2,\mathbb{Z})$, which admits continuous and discrete solutions:

$$\Delta_{\mathcal{F}} E_s(\tau) = s(1-s)E_s(\tau)\,, \qquad \Delta_{\mathcal{F}} \nu_{n,\pm}(\tau) = \left(\frac{1}{4} + (R_n^{\pm})^2\right)\nu_{n,\pm}(\tau)\,, \tag{A.1.2}$$

where the Eisenstein series and Maass cusp forms have the following Fourier decomposition:

$$\begin{aligned} E_s(\tau = x+iy) &= \left[y^s + \frac{\Lambda(1-s)}{\Lambda(s)}\, y^{1-s}\right] \\ &\quad + \sum_{m\geq 1} \cos(2\pi m x)\, \frac{4\,\sigma_{2s-1}(m)}{m^{s-\frac{1}{2}}\Lambda\left(s\right)}\, \sqrt{y} K_{s-\frac{1}{2}}(2\pi m y)\,, \\ \nu_{n,\pm}(\tau = x+iy) &= \sum_{m\geq 1} \begin{Bmatrix} \cos(2\pi m x) \\ \sin(2\pi m x) \end{Bmatrix} a_m^{(n,\pm)}\, \sqrt{y} K_{iR_n^{\pm}}(2\pi m y)\,. \end{aligned} \tag{A.1.3}$$

The continuous eigenvalues are $s \equiv \frac{1}{2} + i\alpha$ with $\alpha \in \mathbb{R}$, while $R_n^{\pm} > 0$ are discrete randomly distributed real numbers. We work with unnormalized cusp forms, satisfying $a_1^{(n,\pm)} = 1$. We also define normalized Fourier coefficients for the Eisenstein series,

$$a_m^{(\alpha)} = 2m^{-i\alpha}\sigma_{2i\alpha}(m)\,.$$

For any normalizable modular invariant function $f \in L^2(\mathcal{F})$, we have the Roelke-Selberg spectral decomposition:

$$f(\tau) = \frac{1}{4\pi}\int_{-\infty}^{\infty} d\alpha\,\big(f,\, E_{\frac{1}{2}+i\alpha}\big)\, E_{\frac{1}{2}+i\alpha}(\tau) + \sum_{\pm}\sum_{n\geq 0} \frac{(f,\,\nu_{n,\pm})}{\|\nu_{n,\pm}\|^2}\,\nu_{n,\pm}(\tau)\,. \quad \text{(A.1.4)}$$

The unfolding trick allows one to reduce the inner product with Eisenstein series to an integral over their spin 0 part:

$$(f, E_{\frac{1}{2}+i\alpha}) = \int_{\mathcal{F}} \frac{dxdy}{y^2}\, f(x+iy) E_{\frac{1}{2}-i\alpha}(x-iy) = \int_0^{\infty} dy\, y^{-\frac{3}{2}-i\alpha}\, f^{m=0}(y) \tag{A.1.5}$$

where $f^{m=0}(y) \equiv \int_{-\frac{1}{2}}^{\frac{1}{2}} dx\, f(x+iy)$ is the spin 0 component of f.

We frequently use modified Bessel functions. These can be written as

$$K_{i\alpha}(2\pi m y) = \frac{1}{2}\int_{-\infty}^{\infty} d\xi\, e^{-2\pi m y \cosh\xi}\, \cos(\alpha\xi) \tag{A.1.6}$$

and they satisfy the following orthogonality relation, found in [227]:

$$\int_0^{\infty} \frac{dy}{y}\, K_{i\alpha}(2\pi m y) K_{i\alpha'}(2\pi m y) = \frac{\pi^2}{2\alpha \sinh(\pi\alpha)}\, \big[\delta(\alpha-\alpha') + \delta(\alpha+\alpha')\big]\,, \tag{A.1.7}$$

as well as the identities [228]

$$\begin{gathered} \tfrac{1}{\pi}\int_{-\infty}^{\infty} d\alpha\, \alpha\, \tanh(\pi\alpha)\, K_{i\alpha}(2\pi m_1 y_1) K_{i\alpha}(2\pi m_2 y_2) = \tfrac{\sqrt{m_1 y_1\, m_2 y_2}}{m_1 y_1 + m_2 y_2}\, e^{-2\pi(m_1 y_1 + m_2 y_2)}\,, \\ \int_0^{\infty} \tfrac{dy_1}{\sqrt{y_1}}\, \tfrac{e^{-2\pi m_1 y_1}}{y_1+y_2}\, K_{i\alpha}(2\pi m_1 y_1) = \tfrac{\pi\, e^{2\pi m_1 y_2}}{\sqrt{y_2}\, \cosh(\pi\alpha)}\, K_{i\alpha}(2\pi m_1 y_2)\,. \end{gathered} \tag{A.1.8}$$

A.2 Change of bases and the Maass cusp forms

For completeness, we show here the equivalent of the expressions given in section 2.2.2 for the discrete part of the spectrum. The discrete part of the partition function in ξ variables is

$$\begin{aligned} \widetilde{Z}^m_{\text{P,disc.}}(y) &= \sum_n z_n\, a_m^{(n)}\, \sqrt{y} K_{iR_n}(2\pi m y) \\ &= \frac{\sqrt{y}}{2\pi}\int d\xi\, \mathcal{Z}^m_{\text{P,disc.}}(\xi)\, e^{-2\pi m y \cosh\xi} \end{aligned} \tag{A.2.1}$$

where

$$\mathcal{Z}^m_{\mathrm{P,disc.}}(\xi) \equiv \pi \sum_n \cos(R_n\xi)\, a_m^{(n)}\; z_n\,. \tag{A.2.2}$$

Inverting this, the z_n are given by

$$\sum_n a_m^{(n)}\, z_n\, [\delta(R-R_n)+\delta(R+R_n)] = \frac{1}{\pi^2}\int d\xi\; \cos(R\xi)\, \mathcal{Z}^m_{\mathrm{P,disc.}}(\xi) \tag{A.2.3}$$

This expression is more complicated to work with than the analogous one for Eisenstein series. It is natural to conjecture that we can still express the discrete spin m partition function (in ξ-space) through the spin m' partition function via a particular kernel:

$$\mathcal{Z}^m_{\mathrm{P,disc.}}(\xi) \stackrel{?}{=} \int_{-\infty}^{\infty} d\xi'\, \mathcal{K}^{m,m'}_{\mathrm{disc.}}(\xi,\xi')\, \mathcal{Z}^{m'}_{\mathrm{P,disc.}}(\xi') \tag{A.2.4}$$

However, the precise form of the kernel $\mathcal{K}^{m,m'}$ is not simple and requires regularization and a numerical construction. In any case, it will depend on the eigenvalues R_n and the Fourier coefficients $a_m^{(n)}$ in a nonlocal way and it will require the Fourier coefficients to be non-degenerate and non-vanishing; this is a well-known unproven conjecture, but it is most likely true [229].

We also note that the kernels $\mathcal{K}^{m,m'}$ (for both the continuous and discrete parts) have some nice properties: since $\frac{1}{2}a_m^{(\alpha)}$ and $a_m^{(n)}$ are eigenvalues of Hecke operators (defined explicitly in appendix B.1), they satisfy:

$$\left(\frac{1}{2}a_m^{(\alpha)}\right)\left(\frac{1}{2}a_{m'}^{(\alpha)}\right) = \sum_{\substack{\ell|(m,m')\\ \ell>0}} \left(\frac{1}{2}a^{(\alpha)}_{\frac{mm'}{\ell^2}}\right)\,,\; a_m^{(n)}a_{m'}^{(n)} = \sum_{\substack{\ell|(m,m')\\ \ell>0}} a^{(n)}_{\frac{mm'}{\ell^2}} \tag{A.2.5}$$

In particular, the coefficients 'multiply' for prime spins:

$$\sigma_{2i\alpha}(p)\,\sigma_{2i\alpha}(p') = \sigma_{2i\alpha}(pp') \qquad \text{for } p,p' \text{ prime.} \tag{A.2.6}$$

Hence, the only independent data about the kernels consists of $\frac{\sigma_{2i\alpha}(m)}{m^{i\alpha}}$ and $a_m^{(n)}$ for prime m. For any other values of m, these coefficients are determined as linear combinations of those for prime m.

A.3 Numerical data

In this appendix we collect some numerical results, complementing the discussion in sections 2.3.3 and 2.3.3.

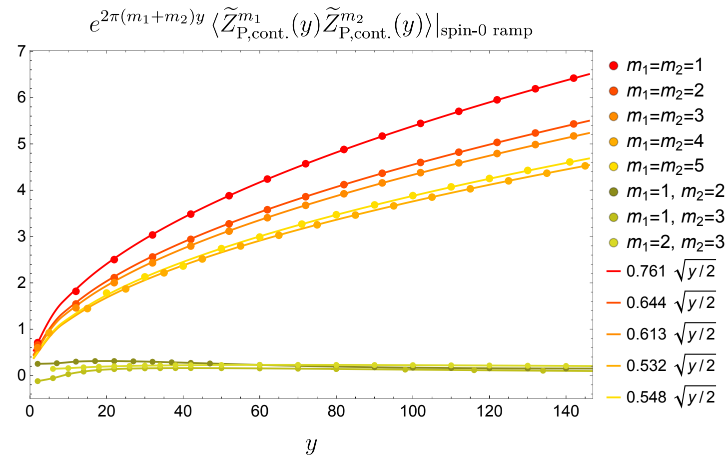

Figure A.1: The result of numerical evaluation of (2.3.17): the contribution to the spin (m_1, m_2) spectral form factor that originates from a spin 0 ramp through symmetries. We plot as a function of $y_1 = y_2 \equiv y$. The plot confirms that this does *not* take the form of a ramp, but is rather a subleading correction to it, (2.3.20). Universal eigenvalue repulsion in the spin 0 sector hence doesn't imply the same in any other spin sector through symmetries (despite spectral determinacy in the exact partition function).

Figures A.1 and A.2 show the result (2.3.20) for different cross sections of the (y_1, y_2)-plane. For example, we show this behavior and the numerical data points for $y_1 = y_2 \equiv y$ in figure A.1. The case of unequal spins yields curves, which are consistent with contributions that are strongly suppressed compared to the equal spin spectral correlators, hence supporting the proportionality to $\delta_{m_1 m_2}$. Similarly, figure A.2 shows the same analysis for $y_1 = 20$ as a function of $y_2 \equiv y$. It is analogous to figure A.1, but shows a different section of the (y_1, y_2)-plane. We have also analyzed other cross sections of the (y_1, y_2)-plane in a similar manner, in order to ascertain the functional form of (2.3.20).

Similarly, in figure A.3 we show the result of numerically evaluating (2.3.24), again as a function of $y_1 = y_2 \equiv y$; other cross sections of the (y_1, y_2) plane can be checked similarly. We performed the evaluation by assuming a saddle point approximation, i.e., approximating the exponent in (2.3.24) by its second order expansion in small ξ_i. The plot confirms the result (2.3.25): we find a functional form that is actually consistent with a ramp, but an overall coefficient that is not. This information is thus not sufficient to conclude random matrix universality at spin (m_1, m_2).

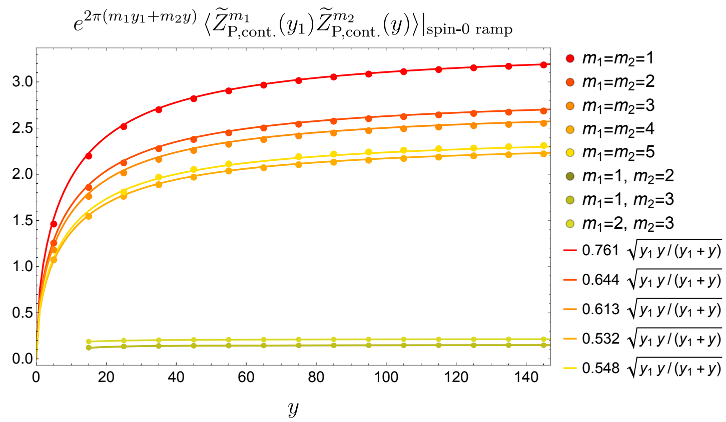

Figure A.2: The result of numerical evaluation of (2.3.17), c.f., figure A.1. In this plot we fix $y_1 = 20$ and plot as a function of $y_2 \equiv y$. Again, the result is well fitted by (2.3.20).

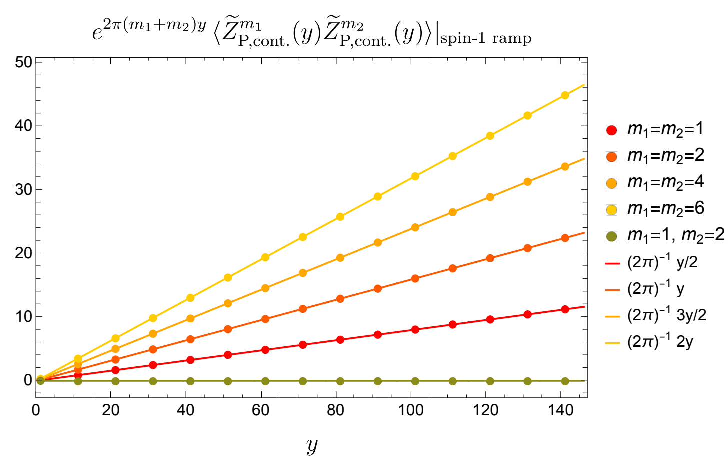

Figure A.3: The result of numerical evaluation of (2.3.24), i.e., the imprint of a ramp at spin 1 onto the spin (m_1, m_2) spectrum, together with a linear fit (solid lines). The y-scaling is linear (as expected for a ramp), but the coefficient doesn't match the random matrix expectation for any $m_1 = m_2 > 1$.

A.4 Details on the S-transform by saddle point

Here we provide details on the saddle point calculation of section 2.4.2, and also discuss subleading corrections.

A.4.1 Saddle point evaluation

Consider the Fourier transforms (2.4.12) and focus for clarity on the first set of variables $(P_1', \bar{P}_1')$. The Fourier transform in only these variables is given by

$$\begin{aligned}
&\langle \rho_{\mathrm{P}}(P_1, \bar{P}_1) \rho_{\mathrm{P}}(P_2', \bar{P}_2') \rangle \\
&\quad \approx 2 \int dP_1' d\bar{P}_1' \, e^{-4\pi i (P_1' P_1 + \bar{P}_1' \bar{P}_1)} \sum_{m_i \in \mathbb{Z}} F^{m_1, m_2}(P_1', \bar{P}_1', P_2', \bar{P}_2') \\
&\qquad\qquad\qquad\qquad\qquad\qquad \delta(P_1'^2 - \bar{P}_1'^2 - m_1) \delta(P_2'^2 - \bar{P}_2'^2 - m_2) \\
&\quad = 4 \sum_{m_i \in \mathbb{Z}} \int d\lambda_1 \, e^{4\pi i m_1 \lambda_1} \Bigg(\int dP_1' d\bar{P}_1' \, e^{-4\pi i (P_1' P_1 + \bar{P}_1' \bar{P}_1 + \lambda_1 (P_1'^2 - \bar{P}_1'^2))} \\
&\qquad\qquad\qquad\qquad F^{m_1, m_2}(P_1', \bar{P}_1', P_2', \bar{P}_2') \Bigg) \delta(P_2'^2 - \bar{P}_2'^2 - m_2)
\end{aligned} \tag{A.4.1}$$

where we exponentiated the delta-function.[100] We now consider $P_i^2, \bar{P}_i^2 \gg 1$ and find the saddle point of the oscillatory exponential (the function F^{m_1, m_2} is slowly varying, hence amenable to saddle point analysis; as pointed out in footnote 42, we assume that the singularity as $\omega \to 0$ is regulated in a more complete description). The saddle points are $(P_{1*}', \bar{P}_{1*}') = \left(-\frac{P_1}{2\lambda_1}, \frac{\bar{P}_1}{2\lambda_1}\right)$. The result is

$$\begin{aligned}
&\langle \rho_{\mathrm{P}}(P_1, \bar{P}_1) \rho_{\mathrm{P}}(P_2', \bar{P}_2') \rangle \\
&\quad \approx \sum_{m_i \in \mathbb{Z}} \int \frac{d\lambda_1}{|\lambda_1|} \, e^{4\pi i \left(m_1 \lambda_1 + \frac{P_1^2 - \bar{P}_1^2}{4\lambda_1} \right)} F^{m_1, m_2} \left(-\frac{P_1}{2\lambda_1}, \frac{\bar{P}_1}{2\lambda_1}, P_2', \bar{P}_2' \right) \\
&\qquad\qquad \times \delta(P_2'^2 - \bar{P}_2'^2 - m_2) \qquad (P_1^2, \bar{P}_1^2 \gg 1)
\end{aligned} \tag{A.4.2}$$

We can now evaluate the integral over λ_1 by another saddle point approximation. The large parameter is $\sqrt{m_1(P_1^2 - \bar{P}_1^2)} \equiv \sqrt{m_1 \mathfrak{m}_1}$, and the saddle

[100] In the case $m_i' = 0$, one can simply use the Dirac delta functions without exponentiating them. This will end up being subleading in our large parameters.

points are $\lambda_{1*} = \pm\frac{1}{2}\sqrt{\frac{\mathfrak{m}_1}{m_1}}$; this is real when $m_1, \mathfrak{m}_1$ have the same sign, and imaginary if they have opposite sign. In the latter case, one can show that the integral decays exponentially, and thus can be neglected.

After doing the integrals over $P_2', \bar{P}_2'$ the same way, we find:

$$\begin{aligned}\langle\rho_{\mathrm{P}}(E_1,\mathfrak{m}_1)\rho_{\mathrm{P}}(E_2,\mathfrak{m}_2)\rangle&\\ \approx 2\sum_{\substack{m_i\in\mathbb{Z}:\\ m_i\mathfrak{m}_i>0}} F^{m_1,m_2}&\left(P_1\sqrt{\frac{m_1}{\mathfrak{m}_1}},\bar{P}_1\sqrt{\frac{m_1}{\mathfrak{m}_1}},P_2\sqrt{\frac{m_2}{\mathfrak{m}_2}},\bar{P}_2\sqrt{\frac{m_2}{\mathfrak{m}_2}}\right)|\mathfrak{m}_1\mathfrak{m}_2m_1m_2|^{-1/4}\\ &\times\cos\left(4\pi\sqrt{m_1\mathfrak{m}_1}+\frac{\pi}{4}\right)\cos\left(4\pi\sqrt{m_2\mathfrak{m}_2}+\frac{\pi}{4}\right)\quad(P_i^2,\bar{P}_i^2,|\mathfrak{m}_i|\gg1)\,.\end{aligned}\tag{A.4.3}$$

Assuming for cleaner notation $\mathfrak{m}_i > 0$, we obtain (2.4.13).

A.4.2 Corrections

Because the P_i', $\bar{P}_i'$, and λ_i saddle points depend on different large parameters, there is a possibility that subleading terms in one saddle point calculation (for example, the $\bar{P}_i$ saddle point) can actually dominate in another saddle point analysis (for example, the λ_i saddle point). We will show that this is not the case, thus providing a consistency check. We assume throughout that $P_i \gg \bar{P}_i$.

First, we consider the subleading terms for the P_1', $\bar{P}_1'$, P_2', $\bar{P}_2'$ saddle points. We use the method of steepest descent to put the integrals in a form amenable to subleading analysis. Focusing on the P_1', $\bar{P}_1'$ integrals for clarity, we first do a change of variables $P_1' \to \frac{P_1}{2\lambda_1}P_1'$, $\bar{P}_1' \to \frac{\bar{P}_1}{2\lambda_1}\bar{P}_1'$ which turns (A.4.1) into

$$\begin{aligned}\langle\rho_{\mathrm{P}}(P_1,\bar{P}_1)\rho_{\mathrm{P}}(P_2',\bar{P}_2')\rangle &= \sum_{m_i\in\mathbb{Z}}\int d\lambda_1\, e^{4\pi i m_1\lambda_1}\,\delta(P_2'^2-\bar{P}_2'^2-m_2)\\ &\times\int dP_1'd\bar{P}_1'\,\frac{P_1\bar{P}_1}{\lambda_1^2}\,e^{2\pi\frac{P_1^2}{|\lambda_1|}\left(-i\,\mathrm{sgn}(\lambda_1)(P_1'+\frac{1}{2}P_1'^2)\right)+2\pi\frac{\bar{P}_1^2}{|\lambda_1|}\left(-i\,\mathrm{sgn}(\lambda_1)(\bar{P}_1'-\frac{1}{2}\bar{P}_1'^2)\right)}\\ &\times F^{m_1,m_2}\left(\frac{P_1}{2\lambda}P_1',\frac{\bar{P}_1}{2\lambda}\bar{P}_1',P_2',\bar{P}_2'\right)\end{aligned}\tag{A.4.4}$$

Our large, positive parameters are $2\pi\frac{P_1^2}{|\lambda_1|}$, $2\pi\frac{\bar{P}_1^2}{|\lambda_1|}$. We rotate our integration contours so that the exponent has constant imaginary part, passes through the saddle point, and is exponentially decaying. The contours that achieve this are parametrized as

$$P_1'(u_1) = u_1 - i\,\mathrm{sgn}(\lambda_1)(u_1+1)\,,\quad \bar{P}_1'(\bar{u}_1) = \bar{u}_1 + i\,\mathrm{sgn}(\lambda_1)(\bar{u}_1-1)\,,\tag{A.4.5}$$

which gives

$$\langle \rho_{\mathrm{P}}(P_1, \bar{P}_1)\rho_{\mathrm{P}}(P_2', \bar{P}_2')\rangle = \sum_{m_i \in \mathbb{Z}} \int d\lambda_1 \, e^{4\pi i\left(m_1\lambda_1 + \frac{P_1^2 - \bar{P}_1^2}{4\lambda_1}\right)} \frac{2P_1\bar{P}_1}{\lambda_1^2} \, \delta(P_2'^2 - \bar{P}_2'^2 - m_2)$$
$$\times \int d^2u_1 \, e^{-2\pi \frac{P_1^2}{|\lambda_1|}(u_1+1)^2 - 2\pi \frac{\bar{P}_1^2}{|\lambda_1|}(\bar{u}_1-1)^2}$$
$$\times F^{m_1,m_2}\left(\frac{P_1}{2\lambda_1}\left(u_1 - i\,\mathrm{sgn}(\lambda_1)(u_1+1)\right), \frac{\bar{P}_1}{2\lambda_1}\left(\bar{u}_1 + i\,\mathrm{sgn}(\lambda_1)(\bar{u}_1-1)\right), P_2', \bar{P}_2'\right) \tag{A.4.6}$$

The corrections to the leading result all come from the Taylor series of $F^{m_1,m_2}(\cdots)$ at $u_1 = -1$, $\bar{u}_1 = 1$. We apply the same procedure to P_2', $\bar{P}_2'$ and get the general form of the corrections to the leading saddle:

$$\begin{aligned} \text{corrections} \propto \; & \frac{\lambda_1^{n_1+\bar{n}_1}\lambda_2^{n_2+\bar{n}_2}}{P_1^{2n_1}\bar{P}_1^{2\bar{n}_1}P_2^{2n_2}\bar{P}_2^{2\bar{n}_2}} \partial_{u_1}^{2n_1}\partial_{\bar{u}_1}^{2\bar{n}_1}\partial_{u_2}^{2n_2}\partial_{\bar{u}_2}^{2\bar{n}_2} \\ & \times F^{m_1,m_2}\Bigg(\frac{P_1}{2\lambda_1}\left(u_1 - i(u_1+1)\right), \frac{\bar{P}_1}{2\lambda_1}\left(\bar{u}_1 + i(\bar{u}_1-1)\right), \\ & \qquad \frac{P_2}{2\lambda_2}\left(u_2 - i(u_2+1)\right), \frac{\bar{P}_2}{2\lambda_2}\left(\bar{u}_2 + i(\bar{u}_2-1)\right)\Bigg) \end{aligned} \tag{A.4.7}$$

where we have factored out the universal part of the corrections and chosen $\lambda_i > 0$ for convenience. The potential issue is now clear; the prefactor contains positive powers of λ_i, whose saddle point is proportional to $\sqrt{\mathfrak{m}_i} \approx P_i$, and the function contains non-trivial dependence on λ_i. However, explicitly checking this issue using (2.4.9) reveals that these corrections are indeed subleading with respect to our large parameters.

Additionally, our saddle point parameter for the $\bar{P}_i'$ integral, $2\pi\frac{\bar{P}_i}{2|\lambda|} \approx \pi\frac{\bar{P}_i^2}{P_i}$, is not guaranteed to be large for all possible regimes of $P_i^2 \gg \bar{P}_i^2 \gg 1$. While at first this suggests a more rigorous scaling is required, explicit analysis of the corrections reveals that any possible relative scaling of P_i^2, $\bar{P}_i^2$ still leads to a subleading correction.

Knowing now that keeping just the leading term is consistent, we analyze the subleading corrections to the λ_i saddle point. The exact form of these corrections is significantly more complicated, as the exponent in the integral is not Gaussian. However, we can still analyze how these corrections will depend on our large parameters. We perform a change of variables $\lambda_i \to \frac{1}{2}\sqrt{\frac{\mathfrak{m}_i}{m_i}}\,\lambda_i$, and have

$$
\begin{aligned}
&\langle \rho_{\rm P}(P_1,\bar{P}_1)\rho_{\rm P}(P_2,\bar{P}_2)\rangle \\
&\quad \approx \sum_{m_i\in\mathbb{Z}} \int \frac{d\lambda_1}{|\lambda_1|}\frac{d\lambda_2}{|\lambda_2|}\, e^{2\pi\sqrt{\mathfrak{m}_1 m_1}i\left(\lambda_1+\frac{1}{\lambda_1}\right)+2\pi\sqrt{\mathfrak{m}_2 m_2}i\left(\lambda_2+\frac{1}{\lambda_2}\right)} \\
&\quad \times F^{m_1,m_2}\left(-P_1\sqrt{\frac{m_1}{\mathfrak{m}_1}}\,\lambda_1^{-1},\bar{P}_1\sqrt{\frac{m_1}{\mathfrak{m}_1}}\,\lambda_1^{-1},-P_2\sqrt{\frac{m_2}{\mathfrak{m}_2}}\,\lambda_2^{-1},\bar{P}_2\sqrt{\frac{m_2}{\mathfrak{m}_2}}\,\lambda_2^{-1})\right)
\end{aligned} \tag{A.4.8}
$$

The large parameters are $2\pi\sqrt{m_i\mathfrak{m}_i}$, and the saddle points are at $\lambda_i = \pm 1$. However the steepest descent contour $\lambda_1(t) = \lambda_2(t) \equiv \lambda(t)$ is quite complicated. Additionally, subleading terms do not come just from a Taylor expansion of $F^{m_1,m_2}(\cdots)$, but also from expanding the exponent $\phi(t) = i\left(\lambda(t_i)+\frac{1}{\lambda(t_i)}\right)$ beyond quadratic order. Thankfully, all the dependence on the large parameters comes only from (i) powers of $\sqrt{m_i\mathfrak{m}_i}$, and (ii) the dependence of the function F^{m_1,m_2} on the large parameters, which is insensitive to the details of the steepest descent contours. Thus, the corrections are of the general form

$$
\begin{aligned}
&\text{corrections} \propto\ (m_1\mathfrak{m}_1)^{-n_1/2}(m_2\mathfrak{m}_2)^{-n_2/2}\,\partial_{t_1}^{c_1}\partial_{t_2}^{c_2} \\
&\times F^{m_1,m_2}\left(-P_1\sqrt{\frac{m_1}{\mathfrak{m}_1}}\lambda(t_1)^{-1},\bar{P}_1\sqrt{\frac{m_1}{\mathfrak{m}_1}}\lambda(t_1)^{-1},-P_2\sqrt{\frac{m_2}{\mathfrak{m}_2}}\lambda(t_2)^{-1},\bar{P}_2\sqrt{\frac{m_2}{\mathfrak{m}_2}}\lambda(t_2)^{-1}\right)
\end{aligned} \tag{A.4.9}
$$

with $c_i \le 2n_i$. Here, the lower order derivative terms come from terms where the exponential is expanded.[101] Explicitly checking using (2.4.9), we see that all corrections are indeed subleading with respect to all our large parameters, and they do not depend on the specifics of the relative scaling of P_i^2, $\bar{P}_i^2$.

We also briefly mention the comment after (2.4.13). Strictly speaking, for $\mathfrak{m}_i$ large but fixed, because we sum over all spins there will eventually be a regime where $\sqrt{\frac{m_i}{\mathfrak{m}_i}}$ is not small. We assume that these asymptotic contributions are negligible; however this does require us to assume we can exchange the limits $\mathfrak{m}_i \to \infty$ and $M \to \infty$. That we get a sensible result in the decompactification limit suggests this is a reasonable assumption; addressing this in detail with more care would require an analysis of the full modular invariant density of states, which is beyond the scope of this chapter.

[101]For a standard one-dimensional Laplace integral, $\int dx\, e^{a\phi(x)}f(x)$, there are higer order terms such as $\frac{1}{a}\frac{f'(c)\phi'''(c)}{2\phi''(c)^2}$.

Appendix B

Appendices for chapter 3

B.1 Statistics of Maass cusp forms: arithmetic chaos

We review some statistical facts about the Maass cusp forms, along with clarifying aspects that (to our knowledge) do not appear in the literature. Some of this information can also be found in the main text, repeated here for convenience. We use the first 5832 even and 6282 odd cusp forms for all numerics (this corresponds to $R_n^{\pm} < 400$) [98].

The eigenvalues of cusp forms are distributed according to the *Weyl law* [100, 101]:

$$\begin{aligned} \mu_+(R) \approx \bar{\mu}_+(R) &= \frac{1}{12}\,R - \frac{3}{2\pi}\,\log R + \frac{\log\left(\pi^4/2\right)}{4\pi} + \mathcal{O}\left(\frac{\log R}{R^2}\right)\,, \\ \mu_-(R) \approx \bar{\mu}_-(R) &= \frac{1}{12}\,R - \frac{1}{2\pi}\,\log R - \frac{\log 8}{4\pi} + \mathcal{O}\left(\frac{\log R}{R^2}\right)\,. \end{aligned} \tag{B.1.1}$$

We illustrate this in figure B.1.

The Fourier coefficients $\{a_p^{(n,\pm)}\}$ for fixed prime spin p and ordered by increasing corresponding eigenvalue $R_n^{\pm}$ are equidistributed according to the distributions [100, 102]

$$\mu_p(x) = \begin{cases} \frac{(p+1)\sqrt{4-x^2}}{2\pi\left(\left(p^{1/2}+p^{-1/2}\right)^2-x^2\right)} & \text{if } |x|<2 \\ 0 & \text{otherwise} \end{cases} \tag{B.1.2}$$

which approaches the Wigner semi-circle $\frac{1}{2\pi}\sqrt{4-x^2}$ as $m \to \infty$. Equidistribution means that averages over all cusp forms for a given spin can be replaced with averages over the distribution, i.e.

$$\lim_{n_0\to\infty} \sum_{n=1}^{n_0} f\left(a_m^{(n,\pm)}\right) = \int dx\,\mu_m(x) f(x). \tag{B.1.3}$$

This is illustrated in figure B.2.

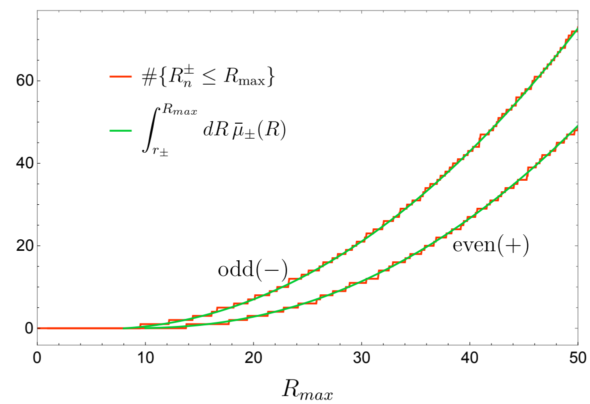

Figure B.1: Comparison of the exact counting function of discrete eigenvalues of the Laplacian with the Weyl law approximation as given in (B.1.1).

We now investigate the nearest-neighbour level spacing, both for the eigenvalues $R_n^\pm$ and for the Fourier coefficients $a_m^{(n,\pm)}$. This provides a more numerically tractable way of analyzing the correlations than the density of states two-point function. After "unfolding" the spectrum,[102] we calculate the distribution of the difference between nearest-neighbour levels:

$$P_{R_n^\pm}(s) \equiv \#\{x_n :\ x_{n+1} - x_n = s\}\,. \tag{B.1.4}$$

An integrable spectrum is distributed according to Poissonian statistics, $P_P(s) = e^{-s}$, which means level *attraction*: $P_P(s) \to 1$ as $s \to 0$. Chaotic spectra, on the other hand, are distributed according to the ensemble with appropriate symmetries, e.g., the Gaussian orthogonal ensemble with $P_{\rm GOE}(s) = \frac{1}{2}\pi s e^{-\pi s^2/4}$, which exhibits level *repulsion*: $P_{\rm GOE}(s) \to 0$ as $s \to 0$.

The eigenvalues of the cusp forms are known to obey Poissonian statistics [93], and we find that the Fourier coefficients for prime spin obey the same, shown in figure B.3; hence, both the eigenvalues and Fourier coefficients are distributed *randomly but not chaotically*. Effectively, for any given spin m, the Fourier coefficients for different n are independent random variables.

We can equivalently characterize the distributions (B.1.2) through their moments. For the distributions of prime spin Fourier coefficients, (B.1.2),

[102] Unfolding the spectrum corresponds to replacing each member $R_n^\pm \to x_n^\pm = \langle N^\pm(R_n^\pm)\rangle$. This yields $\langle N^\pm(R^\pm)\rangle = \int_{-\infty}^{R^\pm} dR'^\pm\, \overline{\mu}_\pm(R'^\pm) = \int_{-\infty}^{x^\pm} dx'^\pm = x^\pm$, i.e., the spectrum has constant unit density in x variables [230].

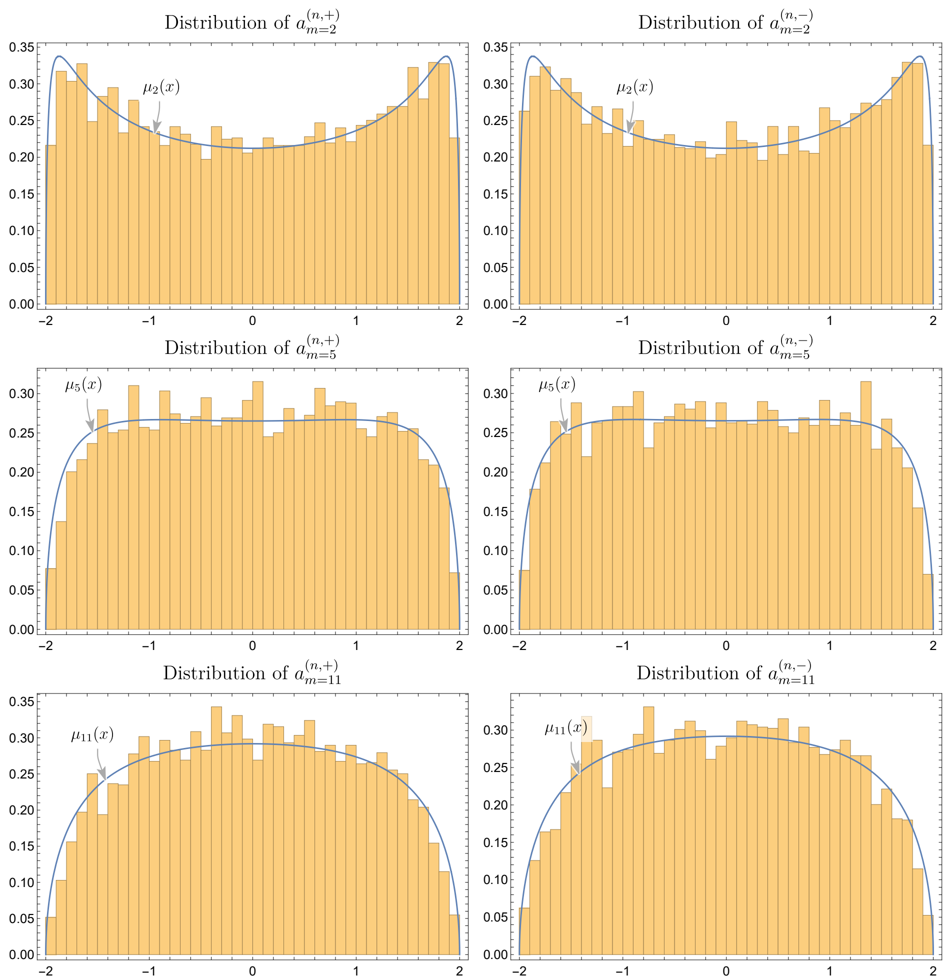

Figure B.2: The distribution of the first 5832 even and 6282 odd Fourier coefficients for prime spins, compared to the distribution they are equidistributed with respect to.

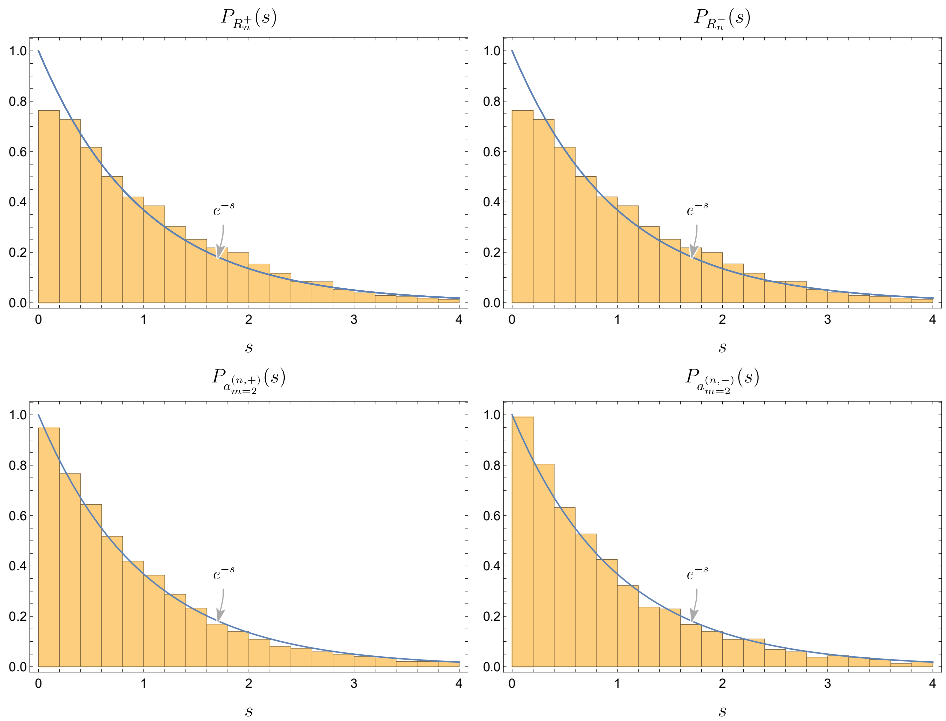

Figure B.3: The distribution of the nearest neighbor spacing of the first 5832 even and 6282 odd eigenvalues and spin 2 Fourier coefficients, compared to the Poissonian expectation. Note that the statistics for all other prime spins is similar.

the odd moments are zero and the even moments are:[103]

$$\boxed{p \text{ prime:} \qquad \overline{\left(a_p^{(n,\pm)}\right)^{2k}} = \frac{p}{p+1}\,\frac{(2k)!}{k!(k+1)!}\;{}_2F_1\left(1,\, k+\tfrac{1}{2},\, k+2,\, \tfrac{4p}{(p+1)^2}\right).} \tag{B.1.5}$$

For example:

$$\overline{\left(a_p^{(n,\pm)}\right)^2} = \frac{p+1}{p}\,, \qquad \overline{\left(a_p^{(n,\pm)}\right)^4} = \frac{(p+1)(2p+1)}{p^2}\,. \tag{B.1.6}$$

These distributions for Fourier coefficients are specifically for prime spins. All Fourier coefficients for non-prime (composite) spins are fully determined in terms of these by Hecke relations because Maas cusp forms are eigenfunctions of Hecke operators:

$$T_m \nu_{n,\pm}(\tau) = a_m^{(n,\pm)}\,\nu_{n,\pm}(\tau) \quad \text{where} \quad T_m f(\tau) = \frac{1}{\sqrt{m}} \sum_{\substack{a,b,d:\\ ad=m\\ 0\leq b\leq d-1}} f\left(\frac{a\tau+b}{d}\right). \tag{B.1.7}$$

This implies immediately:

$$\boxed{a_m^{(n,\pm)} a_{m'}^{(n,\pm)} = \sum_{\substack{\ell|(m,m')\\ \ell>0}} a_{\frac{mm'}{\ell^2}}^{(n,\pm)}\,.} \tag{B.1.8}$$

For example, if p, p' are prime we get the important multiplicative relation: $a_p^{(n,\pm)} a_{p'}^{(n,\pm)} = a_{pp'}^{(n,\pm)} + \delta_{pp'}$ (see Lemma 1 for more relations of this type).

The Hecke relations allow us to construct the non-prime Fourier coefficients from the prime ones. This in turn implies that the variances ('normalization factors' $\mathcal{N}_m^{\pm}$) of the distributions of Fourier coefficients for non-prime spins follow from higher moments of the prime distributions. We give a few examples:

$$\begin{aligned}
a_4^{(n,\pm)} &= \left(a_2^{(n,\pm)}\right)^2 - 1 &\Rightarrow\quad& \mathcal{N}_4^{\pm} \equiv \overline{\left(a_4^{(n,\pm)}\right)^2} = \overline{\left(a_2^{(n,\pm)}\right)^4} - 2\,\overline{\left(a_2^{(n,\pm)}\right)^2} + 1\\
a_6^{(n,\pm)} &= a_2^{(n,\pm)} a_3^{(n,\pm)} &\Rightarrow\quad& \mathcal{N}_6^{\pm} \equiv \overline{\left(a_6^{(n,\pm)}\right)^2} = \overline{\left(a_2^{(n,\pm)}\right)^2}\;\overline{\left(a_3^{(n,\pm)}\right)^2}\\
a_8^{(n,\pm)} &= \left(a_2^{(n,\pm)}\right)^3 - 2\,a_2^{(n,\pm)} &\Rightarrow\quad& \mathcal{N}_8^{\pm} \equiv \overline{\left(a_8^{(n,\pm)}\right)^2} = \overline{\left(a_2^{(n,\pm)}\right)^6}\\
&&& \qquad - 4\,\overline{\left(a_2^{(n,\pm)}\right)^4} + 4\,\overline{\left(a_2^{(n,\pm)}\right)^2}
\end{aligned} \tag{B.1.9}$$

[103] This formula can be easily derived by computing arbitrary moments of (B.1.2) and realizing that they correspond to an integral representation of the hypergeometric function.

spin m	$\overline{\left(a_m^{(n,\pm)}\right)}$	$\overline{\left(a_m^{(n,\pm)}\right)^2}$	$\overline{\left(a_m^{(n,\pm)}\right)^3}$	$\overline{\left(a_m^{(n,\pm)}\right)^4}$	$\overline{\left(a_m^{(n,\pm)}\right)^5}$
2	0	$\frac{3}{2} = 1.5$	0	$\frac{15}{4} = 3.75$	0
3	0	$\frac{4}{3} = 1.33..$	0	$\frac{28}{9} = 3.11..$	0
4	$\frac{1}{2} = 0.5$	$\frac{7}{4} = 1.75$	$\frac{25}{8} = 3.16..$	$\frac{127}{16} = 7.94..$	$\frac{601}{32} = 18.78..$
5	0	$\frac{6}{5} = 1.2$	0	$\frac{66}{25} = 2.64$	0
6	0	2	0	$\frac{35}{3} = 11.67..$	0
7	0	$\frac{8}{7} = 1.14..$	0	$\frac{120}{49} = 2.45..$	0
8	0	$\frac{15}{8} = 1.88..$	0	$\frac{831}{64} = 12.98..$	0
9	$\frac{1}{3} = 0.33..$	$\frac{13}{9} = 1.44..$	$\frac{61}{27} = 2.26..$	$\frac{469}{81} = 5.79..$	$\frac{3181}{243} = 13.09..$

Table B.1: Exact values of the moments of the distributions of Fourier coefficients. For prime m, these follow from (B.1.5). For composite m, they are constructed from prime moments using Hecke relations.

We give exact analytical and numerical values for some of these moments in tables B.1 and B.2. The composite spins $m = 4$ and $m = 8$ are special cases of a general result, see Lemma 4. The numerical values for the second moments are within a few percent of the theoretical values. This error increases for higher moments due to the limited number of cusp forms available numerically. The numerical results for odd forms are consistently slightly better because we have more of them available.

More generally, computing just the variances $\mathcal{N}_m^{\pm}$ for *all* non-prime m requires knowledge of *all* moments of the distributions of prime coefficients. Since the distributions are bounded, their moments determine the distributions fully. In other words, knowledge of *all* variances $\mathcal{N}_m^{\pm}$ is equivalent to complete knowledge of all the prime distributions (B.1.2). We show the variance of the Fourier coefficients for a large number of spins in figure B.4.

B.2 Hecke relations, cusp form norms, and L-functions

In this appendix we provide some mathematical details relating to the norms of cusp forms and their relation to objects in analytic number theory. In order to be pedagogical, we provide step-by-step proofs of some important statements. Most of the general definitions and results can be found in the literature, see, for example, [231–234].

spin m	$\overline{\left(a_m^{(n,\pm)}\right)}$	$\overline{\left(a_m^{(n,\pm)}\right)^2}$	$\overline{\left(a_m^{(n,\pm)}\right)^3}$	$\overline{\left(a_m^{(n,\pm)}\right)^4}$	$\overline{\left(a_m^{(n,\pm)}\right)^5}$
2	0.01..(+) −0.01..(−)	1.46..(+) 1.47..(−)	0.02..(+) −0.02..(−)	3.56..(+) 3.62..(−)	0.09..(+) −0.08..(−)
3	0.01..(+) −0.01..(−)	1.27..(+) 1.30..(−)	0.03..(+) −0.03..(−)	2.87..(+) 2.95..(−)	0.10..(+) −0.09..(−)
4	0.46..(+) 0.47..(−)	1.65..(+) 1.68..(−)	2.82..(+) 2.91..(−)	7.10..(+) 7.31..(−)	16.42..(+) 16.97..(−)
5	0.01..(+) −0.01..(−)	1.13..(+) 1.16..(−)	0.03..(+) −0.03..(−)	2.38..(+) 2.45..(−)	0.10..(+) −0.09..(−)
6	0.01..(+) −0.01..(−)	1.84..(+) 1.89..(−)	0.11..(+) −0.10..(−)	9.99..(+) 10.37..(−)	1.39..(+) −1.21..(−)
7	0.01..(+) −0.01..(−)	1.07..(+) 1.09..(−)	0.03..(+) −0.03..(−)	2.19..(+) 2.25..(−)	0.10..(+) −0.09..(−)
8	0.01..(+) −0.01..(−)	1.72..(+) 1.76..(−)	0.11..(+) −0.11..(−)	10.86..(+) 11.28..(−)	1.19..(+) −1.19..(−)
9	0.27..(+) 0.30..(−)	1.32..(+) 1.36..(−)	1.90..(+) 2.00..(−)	4.85..(+) 5.08..(−)	10.52..(+) 11.10..(−)

Table B.2: Numerical values of the moments of the distributions of Fourier coefficients, computed using the Fourier coefficients for cusp forms with eigenvalue $R_n^\pm < 400$ (separately for even and odd parity).

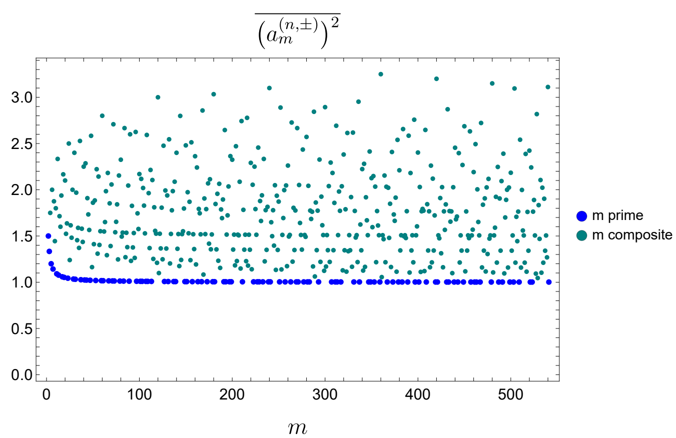

Figure B.4: Exact variance of the Fourier coefficients as a function of m, up to the 100th prime. The prime coefficients have variance $1 + \frac{1}{m}$, while the composite primes have much more complicated behaviour (which is determined by the Hecke relations and higher moments of the distribution of prime Fourier coefficients); in this range, all variances are $\mathcal{O}(1)$, but as m grows, the maximum possible value grows as well.

B.2.1 Hecke relations and L-functions

We first note some useful relations between Fourier coefficients of prime power spins.

Lemma 1. *Let $p, p_1, \dots p_r$ be distinct primes. Then:*

$$\begin{aligned}
(i) \quad & a^{(n,\pm)}_{p_1^{k_1}\cdots p_r^{k_r}} = a^{(n,\pm)}_{p_1^{k_1}} \cdots a^{(n,\pm)}_{p_r^{k_r}} \\
(ii) \quad & a^{(n,\pm)}_{p^k} = a^{(n,\pm)}_{p^{k-1}}\, a^{(n,\pm)}_{p} - (1-\delta_{k,1})\, a^{(n,\pm)}_{p^{k-2}} \\
(iii) \quad & a^{(n,\pm)}_{p^k} = \frac{1}{2^k} \sum_{\ell=0}^{\lfloor k/2 \rfloor} \binom{k+1}{2\ell+1} \sum_{r=0}^{\ell} \binom{\ell}{r} (-4)^r \left(a^{(n,\pm)}_p\right)^{k-2r} \\
(iv) \quad & \left(a^{(n,\pm)}_{p^k}\right)^2 = \frac{1}{2^{2k+1}} \sum_{\ell=0}^{k} \left[\binom{2k+2}{2\ell+2} + (-1)^\ell \binom{k+1}{\ell+1}\right] \\
& \qquad\qquad \times \sum_{r=0}^{\ell} \binom{\ell}{r} (-4)^r \left(a^{(n,\pm)}_p\right)^{2(k-r)}
\end{aligned} \tag{B.2.1}$$

Proof: (i) and (ii) follow immediately from the Hecke algebra (B.1.8). (iii) follows by viewing (ii) as a recursion relation and solving it in terms of $a^{(n,\pm)}_p$. (iv) follows from squaring and simplifying (iii). $\square$

Let us define the following Hecke L-functions for any of the cusp forms, defined by its Fourier coefficients:

$$L^{(n,\pm)}(s) \equiv \sum_{m \geq 1} \frac{a^{(n,\pm)}_m}{m^s} \qquad (\mathrm{Re}(s) > 1)\,. \tag{B.2.2}$$

These L-functions are absolutely convergent in an s-half plane and they admit an analytic continuation to an entire function on the whole complex plane (see, e.g., [233]).

Lemma 2. *The L-function* (B.2.2) *admits an Euler product representation:*

$$L^{(n,\pm)}(s) = \prod_{p \text{ prime}} \frac{1}{1 - a^{(n,\pm)}_p\, p^{-s} + p^{-2s}}\,. \tag{B.2.3}$$

Proof: Note that, as a consequence of the Hecke relations, we have

$$\left[1 - a^{(n,\pm)}_p\, p^{-s} + p^{-2s}\right] \sum_{k \geq 0} a^{(n,\pm)}_{p^k}\, p^{-ks} = 1\,. \tag{B.2.4}$$

The Euler product can then be written as a sum using Lemma 1(i):

$$\prod_{p\text{ prime}} \frac{1}{1-a_p^{(n,\pm)}\,p^{-s}+p^{-2s}} = \prod_{p\text{ prime}} \left(\sum_{k\geq 0} a_{p^k}^{(n,\pm)}\,p^{-ks}\right) = \sum_{m\geq 1} \frac{a_m^{(n,\pm)}}{m^s}\,. \quad \square \tag{B.2.5}$$

To make contact with the cusp form norms, we now consider the 'symmetric square L-function', defined as[104]

$$L_{\nu\times\nu}^{(n,\pm)}(s) \equiv \zeta(2s)\sum_{m\geq 1}\frac{a_{m^2}^{(n,\pm)}}{m^s} \qquad (\mathrm{Re}(s)>1)\,. \tag{B.2.8}$$

Lemma 3. *The symmetric square L-function admits an Euler product representation*:

$$L_{\nu\times\nu}^{(n,\pm)}(s) = \prod_{p\text{ prime}} \frac{1}{1-\left(a_p^{(n,\pm)}\right)^2\left(p^{-s}-p^{-2s}\right)+\left(p^{-s}-p^{-2s}-p^{-3s}\right)} \tag{B.2.9}$$

Proof: The proof is the same as for Lemma 2, but starting from the observation that the following product simplifies:

$$\left[1-\left(a_p^{(n,\pm)}\right)^2\left(p^{-s}-p^{-2s}\right)+\left(p^{-s}-p^{-2s}-p^{-3s}\right)\right]\sum_{k\geq 0} a_{p^{2k}}^{(n,\pm)}\,p^{-ks} = 1-p^{-2s}\,, \tag{B.2.10}$$

and recalling that $\prod_p (1-p^{-2s})^{-1} = \zeta(2s)$. $\quad\square$

[104]More generally, for $\alpha_p, \beta_p \in \mathbb{C}$ satisfying

$$1-a_p^{(n,\pm)}\,p^{-s}+p^{-2s} = \left(1-\alpha_p p^{-s}\right)\left(1-\beta_p p^{-s}\right)\,, \tag{B.2.6}$$

i.e., $\alpha_p+\beta_p = a_p^{(n,\pm)}$ and $\alpha_p\beta_p = 1$, the Ramanujan-Petersson conjecture asserts $|\alpha_p| = |\beta_p| = 1$. The symmetric ℓ-th power L-function is then an automorphic function [235], defined as

$$L_{\nu^\ell}^{(n,\pm)}(s) = \prod_{p\text{ prime}}\prod_{k=0}^{\ell}\frac{1}{\left(1-\alpha_p^{\ell-2k}p^{-s}\right)}\,. \tag{B.2.7}$$

The symmetric square L-function is the special case $\ell = 2$. We suspect that ℓ-th power L-functions play a role in the computation of higher moments of the CFT partition function.

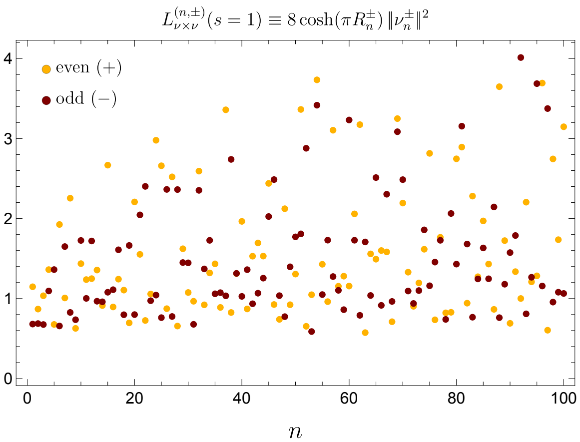

Figure B.5: Plot of the even and odd cusp form norms, rescaled by $8\cosh(\pi R^{\pm}_n)$. The norms themselves decay exponentially: $\|\nu^+_1\|^2 \approx 4.54 \times 10^{-20}, \ldots, \|\nu^+_{100}\|^2 \approx 1.42 \times 10^{-90}$ and $\|\nu^-_1\|^2 \approx 1.67 \times 10^{-14}, \ldots, \|\nu^-_{100}\|^2 \approx 2.86 \times 10^{-79}$. This is equivalently computable through the symmetric square L-function.

Theorem 1. *The norms of the cusp forms satisfy:*

$$\|\nu_{n,\pm}\|^2 \equiv (\nu_{n,\pm}, \nu_{n,\pm}) = \frac{1}{8\cosh\left(\pi R^{\pm}_n\right)}\, L^{(n,\pm)}_{\nu\times\nu}(1)\,. \tag{B.2.11}$$

Proof: (See, e.g., references [236, 237].) We compute the norm using the Rankin-Selberg trick, i.e., note that a constant expression can be computed as the residue at $s = 1$ with an Eisenstein series, which in turn allows for unfolding of the fundamental domain:

$$
\begin{aligned}
\|\nu_{n,\pm}\|^2 &= \frac{\pi}{3}\,\mathrm{Res}_{s=1}\big(|\nu_{n,\pm}(\,\cdot\,)|^2,\, E_s(\,\cdot\,)\big)\\
&= \frac{\pi}{3}\,\mathrm{Res}_{s=1}\int_{\mathcal{F}}\frac{dxdy}{y^2}\,|\nu_{n,\pm}(x+iy)|^2\,E_s(x+iy)\\
&= \frac{\pi}{3}\,\mathrm{Res}_{s=1}\int_0^\infty dy\,y^{s-2}\,\left(\int_{-\frac{1}{2}}^{\frac{1}{2}}dx\,|\nu_{n,\pm}(x+iy)|^2\right)\\
&= \frac{\pi}{6}\,\mathrm{Res}_{s=1}\sum_{m\geq 1}\big(a_m^{(n,\pm)}\big)^2\int_0^\infty dy\,y^{s-1}\,\big(K_{iR_n^\pm}(2\pi m y)\big)^2 \qquad\qquad \text{(B.2.12)}\\
&= \frac{\pi}{6}\,\mathrm{Res}_{s=1}\sum_{m\geq 1}\big(a_m^{(n,\pm)}\big)^2\,\frac{\Gamma\left(\frac{s}{2}+iR_n^\pm\right)\Gamma\left(\frac{s}{2}-iR_n^\pm\right)\Gamma\left(\frac{s}{2}\right)^2}{8(\pi m)^s\Gamma(s)}\\
&= \frac{\pi^2}{48\cosh\big(\pi R_n^\pm\big)}\,\mathrm{Res}_{s=1}\sum_{m\geq 1}\frac{\big(a_m^{(n,\pm)}\big)^2}{m^s}\,.
\end{aligned}
$$

To evaluate the residue, we note that the sum in the last line is related to a Rankin-Selberg zeta function and has an Euler product formula ([233], Lemma 3.1 with $k=1$),

$$
\zeta(2s)\sum_{m\geq 1}\frac{\big(a_m^{(n,\pm)}\big)^2}{m^s} = \zeta^2(s)\prod_{p\text{ prime}}\frac{1}{1+2p^{-s}-\big(a_p^{(n,\pm)}\big)^2p^{-s}+p^{-2s}}\,. \qquad \text{(B.2.13)}
$$

This function is known to have a simple pole at $s=1$. Then,

$$
\begin{aligned}
\zeta(2s)\sum_{m\geq 1}\frac{\big(a_m^{(n,\pm)}\big)^2}{m^s} &= \prod_{p\text{ prime}}\frac{1}{(1-p^{-s})^2\left(1+2p^{-s}-\big(a_p^{(n,\pm)}\big)^2p^{-s}+p^{-2s}\right)}\\
&= \prod_{p\text{ prime}}\frac{1}{(1-p^{-s})\left(1-\big(a_p^{(n,\pm)}\big)^2\big(p^{-s}-p^{-2s}\big)+(p^{-s}-p^{-2s}-p^{-3s})\right)}\\
&= \zeta(s)L_{\nu\times\nu}^{(n,\pm)}(s)\,.
\end{aligned}
\qquad \text{(B.2.14)}
$$

Taking the residue at $s=1$ of both sides and using $\mathrm{Res}_{s=1}\zeta(s)=1$ yields

$$
\|\nu_{n,\pm}\|^2 = \frac{\pi^2}{48\cosh\big(\pi R_n^\pm\big)}\sum_{m\geq 1}\frac{a_{m^2}^{(n,\pm)}}{m} = \frac{1}{8\cosh\big(\pi R_n^\pm\big)}\,L_{\nu\times\nu}^{(n,\pm)}(1)\,. \qquad \square \qquad \text{(B.2.15)}
$$

B.2.2 Statistical averages and moments of L-functions

Having reviewed some basic facts about the cusp form norms and the distribution of their Fourier coefficients, we can now state some of the crucial properties that hold after statistical averaging over n. Let us first state the following useful

Lemma 4. *Let $k \in \mathbb{N}$ and p be prime. Then the average over n yields the following results:*

$$\begin{aligned}
&(i) && \overline{\big(a_{p^k}^{(n,\pm)}\big)^2} = \sum_{\ell=0}^{k} p^{-\ell} = \frac{p-p^{-k}}{p-1} \\
&(ii) && \overline{\big(a_{p^{k+1}}^{(n,\pm)} a_{p^{k-1}}^{(n,\pm)}\big)} = \sum_{\ell=1}^{k} p^{-\ell} = \frac{1-p^{-k}}{p-1} \\
&(iv) && \overline{\big(a_{p^k}^{(n,\pm)}\big)^2 \big(a_{p}^{(n,\pm)}\big)^2} = \frac{2(p+1)-p^{-k}(p+2+p^{-1})}{p-1} \\
&(iii) && \overline{\big(a_{p}^{(n,\pm)}\big)^{2(k+1)}} = \frac{(p+1)^2}{p}\, \overline{\big(a_{p}^{(n,\pm)}\big)^{2k}} - (p+1)\, \frac{(2k)!}{k!(k+1)!}
\end{aligned} \tag{B.2.16}$$

Proof: To prove (i), we start with Lemma 1(iv) and evaluate its average using the moments of the distributions for prime Fourier coefficients (B.1.5):

$$\begin{aligned}
\overline{\big(a_{p^k}^{(n,\pm)}\big)^2} &= \frac{p}{2^{2k+1}(p+1)} \sum_{\ell=0}^{k} \sum_{r=0}^{\ell} \left[\binom{2k+2}{2\ell+2} + (-1)^\ell \binom{k+1}{\ell+1} \right] \\
&\times \binom{\ell}{r} (-4)^r \frac{(2(k-r))!}{(k-r)!(k-r+1)!}\, {}_2F_1\left(1, k-r+\frac{1}{2}, k-r+2, \frac{4p}{(p+1)^2}\right) \\
&= \frac{p}{2^{2k+1}(p+1)} \sum_{\ell=0}^{k} \sum_{r=0}^{\ell} \left[\binom{2k+2}{2\ell+2} + (-1)^\ell \binom{k+1}{\ell+1} \right] \binom{\ell}{r} (-4)^r \\
&\times \frac{(2(k-r))!}{(k-r)!(k-r+1)!} \sum_{q=0}^{\infty} \frac{\Gamma\left(k-r+\frac{1}{2}+q\right) \Gamma(k-r+2)}{\Gamma\left(k-r+\frac{1}{2}\right) \Gamma(k-r+2+q)} \left(\frac{4p}{(p+1)^2} \right)^q \\
&= \frac{p}{p+1} \sum_{q=0}^{\infty} \sum_{\ell=0}^{k} \left[\binom{2k+2}{2\ell+2} + (-1)^\ell \binom{k+1}{\ell+1} \right] \\
&\times \frac{(-1)^{k+q}\, \Gamma\left(\ell+\frac{3}{2}\right)}{\Gamma\left(\ell-k-q+\frac{1}{2}\right) \Gamma(k+q+2)} \left(\frac{4p}{(p+1)^2} \right)^q \\
&\;\;\vdots
\end{aligned}$$

$$\begin{aligned}\overline{\left(a_{p^k}^{(n,\pm)}\right)^2} &= \frac{p}{p+1}\sum_{q=0}^{\infty}\frac{(2q)!}{2^{2q}}\left[\frac{1}{(q!)^2} - \frac{\Theta(q-k)}{(q+k+1)!(q-k-1)!}\right]\left(\frac{4p}{(p+1)^2}\right)^q \\ &= \frac{p}{p+1}\left[\frac{p+1}{p-1} - \frac{p+1}{p^{k+1}(p-1)}\right] = \frac{p-p^{-k}}{p-1}\,,\end{aligned} \tag{B.2.17}$$

where $\Theta(n) = 1$ if $n > 0$ and vanishes otherwise. The second result, (ii), can be proven in a similar fashion, using Lemma 1(ii) to simplify. To prove (iii), we use Lemma 1(ii) to calculate as follows:

$$\begin{aligned}\overline{\left(a_{p^k}^{(n,\pm)}\right)^2\left(a_p^{(n,\pm)}\right)^2} &= \overline{\left(a_{p^{k+1}}^{(n,\pm)} + (1-\delta_{k,0})\,a_{p^{k-1}}^{(n,\pm)}\right)^2} \\ &= \sum_{\ell=0}^{k+1} p^{-\ell} + (1-\delta_{k,0})\left[\sum_{\ell=0}^{k-1} p^{-\ell} + 2\sum_{\ell=1}^{k} p^{-\ell}\right] \\ &= \frac{2(p+1) - p^{-k}(p+2+p^{-1})}{p-1}\,.\end{aligned} \tag{B.2.18}$$

Finally, to prove (iv), we use (B.1.5) and the series representation of the hypergeometric function:

$$\begin{aligned}\overline{\left(a_p^{(n,\pm)}\right)^{2(k+1)}} &= \frac{p}{p+1}\frac{(2k+2)!}{(k+1)!(k+2)!}\sum_{q=0}^{\infty}\frac{\Gamma\left(k+\frac{3}{2}+q\right)\Gamma(k+3)}{\Gamma\left(k+\frac{3}{2}\right)\Gamma(k+3+q)}\left(\frac{4p}{(p+1)^2}\right)^q \\ &= \frac{4p}{p+1}\frac{(2k)!}{k!(k+1)!}\sum_{q=1}^{\infty}\frac{\Gamma\left(k+\frac{1}{2}+q\right)\Gamma(k+2)}{\Gamma\left(k+\frac{1}{2}\right)\Gamma(k+2+q)}\left(\frac{4p}{(p+1)^2}\right)^{q-1} \\ &= \frac{(p+1)^2}{p}\left[\overline{\left(a_p^{(n,\pm)}\right)^{2k}} - \frac{p}{p+1}\,\frac{(2k)!}{k!(k+1)!}\right]. \qquad \square\end{aligned} \tag{B.2.19}$$

Corollary: *For any $k \in \mathbb{N}$ and p prime,*

$$\overline{\left(a_{p^k}^{(n,\pm)}\right)^2\left[1 - \left(a_p^{(n,\pm)}\right)^2\left(p^{-1}-p^{-2}\right) + \left(p^{-1}-p^{-2}-p^{-3}\right)\right]} = 1 - p^{-2}\,. \tag{B.2.20}$$

Proof: Follows immediately from Lemma 4(i) and (iii). $\square$

Finally, the central property needed in our analysis of the gravity amplitude concerns the interplay of the moments of distributions of Fourier coefficients and the cusp form norms:

Theorem 2. *Let $m \geq 1$ be any integer spin. Then the statistical averaging over different cusp forms indexed by n yields:*

$$\overline{\left(a_m^{(n,\pm)}\right)^2 \left(8\cosh\left(\pi R_n^{\pm}\right)\|\nu_{n,\pm}\|^2\right)^{-1}} = \overline{\left(a_m^{(n,\pm)}\right)^2 \left(L_{\nu\times\nu}^{(n,\pm)}(1)\right)^{-1}} = \frac{6}{\pi^2}\,. \tag{B.2.21}$$

Proof: The first equality follows from Theorem 1. To prove the second equality, write the L-function in terms of its Euler product:

$$\begin{aligned}&\overline{\left(a_m^{(n,\pm)}\right)^2 \left(L_{\nu\times\nu}^{(n,\pm)}(1)\right)^{-1}}\\ &\quad= \overline{\left(a_m^{(n,\pm)}\right)^2 \prod_{p\text{ prime}} \left[1-\left(a_p^{(n,\pm)}\right)^2\left(p^{-1}-p^{-2}\right)+\left(p^{-1}-p^{-2}-p^{-3}\right)\right]}\\ &\quad= \prod_{p\text{ prime}}\left(1-p^{-2}\right) = \frac{1}{\zeta(2)} = \frac{6}{\pi^2}\,,\end{aligned} \tag{B.2.22}$$

where we applied the Corollary of Lemma 4 factor by factor after decomposing $a_m^{(n,\pm)}$ into factors of Fourier coefficients of prime powers (Lemma 1(i)):

$$m = p_1^{k_1}\cdots p_r^{k_r} \qquad \Rightarrow \qquad \left(a_m^{(n,\pm)}\right)^2 = \left(a_{p_1^{k_1}}^{(n,\pm)}\right)^2 \cdots \left(a_{p_r^{k_r}}^{(n,\pm)}\right)^2 . \qquad \square \tag{B.2.23}$$

B.2.3 Derivation of the arithmetic kernel $f^{(n,\pm)}$

In the main text we verified that the arithmetic kernel (3.3.23) has the required properties to produce a ramp in all spin sectors. We also outlined how to derive it, but provide more details here. The derivation essentially also shows that it is unique, up to modifications, which are invisible to our averaging condition (3.3.21).

Construction of $f^{(n,\pm)}$: The goal is to find a function $f^{(n,\pm)}$ which satisfies (3.3.21). Since the Fourier coefficients have multiplicativity properties determined by Hecke relations, it is convenient to begin by decomposing $a_m^{(n,\pm)}$ into coefficients with prime-power index:

$$m = p_1^{k_1}\cdots p_r^{k_r} \qquad \Rightarrow \qquad a_{p_1^{k_1}\cdots p_r^{k_r}}^{(n,\pm)} = a_{p_1^{k_1}}^{(n,\pm)}\cdots a_{p_r^{k_r}}^{(n,\pm)} \tag{B.2.24}$$

where p_i are distinct primes. Let us therefore first find a function $f_p^{(n,\pm)}$ which is fine tuned to Fourier coefficients with prime-power index p^k such that:

$$\overline{\big(a_{p^k}^{(n,\pm)}\big)^2 f_p^{(n,\pm)}} = 1 \quad \text{for all } k \geq 0\,. \tag{B.2.25}$$

It is important to note that $a_{p^k}^{(n,\pm)}$ is fully determined by powers of $a_p^{(n,\pm)}$, see Lemma 1(iv). In order for a condition such as (B.2.25) to hold, the function $f_p^{(n,\pm)}$ must balance different moments of the distribution of $a_p^{(n,\pm)}$. This is captured by an ansatz of the following form:

$$f_p^{(n,\pm)} = \sum_{r\geq 0} c_{p,r} \left(a_p^{(n,\pm)}\right)^{2r}. \tag{B.2.26}$$

We only need even powers of the Fourier coefficients because any odd powers will have vanishing expectation value. We also do not need any Fourier coefficients with spin other than p because these are distributed independent of $a_p^{(n,\pm)}$, so they can be absorbed into $c_{p,r}$ as far as the averaged (B.2.25) is concerned. The condition (B.2.25) then amounts to an infinite number of constraints on $c_{p,r}$. For example:

$$\begin{aligned}
k=0: &\qquad 1 \stackrel{!}{=} \overline{f_p^{(n,\pm)}} = \sum_{r\geq 0} c_{p,r} \overline{\big(a_p^{(n,\pm)}\big)^{2r}} \\
k=1: &\qquad 1 \stackrel{!}{=} \overline{\big(a_p^{(n,\pm)}\big)^2 f_p^{(n,\pm)}} = \sum_{r\geq 0} c_{p,r} \overline{\big(a_p^{(n,\pm)}\big)^{2r+2}} \\
k=2: &\qquad 1 \stackrel{!}{=} \overline{\big(a_{p^2}^{(n,\pm)}\big)^2 f_p^{(n,\pm)}} = \overline{\Big(\big(a_p^{(n,\pm)}\big)^2 - 1\Big)^2 f_p^{(n,\pm)}} \\
&\qquad\quad = -1 + \sum_{r\geq 0} c_{p,r} \overline{\big(a_p^{(n,\pm)}\big)^{2r+4}} \\
k=3: &\qquad 1 \stackrel{!}{=} \overline{\big(a_{p^3}^{(n,\pm)}\big)^2 f_p^{(n,\pm)}} = \overline{\Big(\big(a_p^{(n,\pm)}\big)^3 - 2a_p^{(n,\pm)}\Big)^2 f_p^{(n,\pm)}} \\
&\qquad\quad = -4 + \sum_{r\geq 0} c_{p,r} \overline{\big(a_p^{(n,\pm)}\big)^{2r+6}}
\end{aligned} \tag{B.2.27}$$

and so on. Iterating this process, one finds for general k:

$$\sum_{r\geq 0} c_{p,r} \overline{\big(a_p^{(n,\pm)}\big)^{2(k+r)}} = \frac{(2k)!}{k!(k+1)!}\,, \tag{B.2.28}$$

where the r.h.s. is the k-th Catalan number. Using a general recursion relation of the moments of Fourier coefficients (Lemma 4(iv)), we can write the r.h.s. as follows:

$$\sum_{r\geq 0} c_{p,r}\,\overline{\left(a_p^{(n,\pm)}\right)^{2(k+r)}} = \frac{p+1}{p}\,\overline{\left(a_p^{(n,\pm)}\right)^{2k}} - \frac{1}{p+1}\,\overline{\left(a_p^{(n,\pm)}\right)^{2k+2}}\,. \tag{B.2.29}$$

It is now obvious to see that a simple solution exists for all k:

$$c_{p,0} = \frac{p+1}{p}\,, \qquad c_{p,1} = -\frac{1}{p+1}\,, \qquad c_{p,r>1} = 0\,. \tag{B.2.30}$$

To see that this is the *only* solution, note that the equations (B.2.28) form a linear system. Therefore, the existence of any other solution $c'_{p,r}$ would mean that there exist coefficients $\tilde{c}_{p,r} \equiv c_{p,r} - c'_{p,r}$ such that

$$\sum_{r\geq 0} \tilde{c}_{p,r}\,\overline{\left(a_p^{(n,\pm)}\right)^{2(k+r)}} = 0 \tag{B.2.31}$$

for all k. This can be written as an infinite list of equations labelled by k, which we call

$$\mathcal{E}_{p,k} \equiv \sum_{r\geq k} \tilde{c}_{p,r-k}\,\overline{\left(a_p^{(n,\pm)}\right)^{2r}} = 0\,. \tag{B.2.32}$$

This can be thought of as an (infinite dimensional) triangular matrix acting on the vector of moments of Fourier coefficients. If $\tilde{c}_{p,0} \neq 0$, we can form a linear combination which cancels all terms but one:

$$0 = \mathcal{E}_{p,0} - \frac{\tilde{c}_{p,1}}{\tilde{c}_{p,0}}\,\mathcal{E}_{p,1} - \left(\frac{\tilde{c}_{p,2}}{\tilde{c}_{p,0}} - \frac{\tilde{c}_{p,1}^2}{\tilde{c}_{p,0}^2}\right)\mathcal{E}_{p,2} - \ldots = \tilde{c}_{p,0}\,. \tag{B.2.33}$$

This contradicts the assumption, so we must have $\tilde{c}_{p,0} = 0$. Next, if $\tilde{c}_{p,1} \neq 0$ we could form a similar linear combination

$$0 = \mathcal{E}_{p,0} - \frac{\tilde{c}_{p,2}}{\tilde{c}_{p,1}}\,\mathcal{E}_{p,1} - \left(\frac{\tilde{c}_{p,3}}{\tilde{c}_{p,1}} - \frac{\tilde{c}_{p,2}^2}{\tilde{c}_{p,1}^2}\right)\mathcal{E}_{p,2} - \ldots = \tilde{c}_{p,1}\,\overline{\left(a_p^{(n,\pm)}\right)^2}\,, \tag{B.2.34}$$

which is again contradictory and thus implies $\tilde{c}_{p,1} = 0$. Continuing this way, we must have $\tilde{c}_{p,k} = 0$ for all k. Therefore, there does not exist any solution different from $c_{p,k}$.

To summarize, we have shown that

$$f_p^{(n,\pm)} = \frac{p+1}{p} - \frac{1}{p+1}\left(a_p^{(n,\pm)}\right)^2 \tag{B.2.35}$$

solves (B.2.25) and is unique as far as our ansatz is concerned.[105] This function will give a ramp in all spin sectors of the form $m = p^k$. From the multiplicative property of the Fourier coefficients, (B.2.24), it is then clear how to construct the function that will yield a linear ramp for all spins $m = p_1^{k_1} \cdots p_r^{k_r}$; indeed, we simply construct it as

$$\begin{aligned} f^{(n,\pm)} &= \prod_{p \text{ prime}} \left[\frac{p+1}{p} - \frac{1}{p+1} \left(a_p^{(n,\pm)}\right)^2 \right] \\ &= \prod_{p \text{ prime}} \left(1 - p^{-2}\right)^{-1} \times \left[1 - \left(a_p^{(n,\pm)}\right)^2 \left(p^{-1} - p^{-2}\right) + \left(p^{-1} - p^{-2} - p^{-3}\right) \right] \\ &= \frac{\pi^2}{6} \frac{1}{L_{\nu\times\nu}^{(n,\pm)}(1)} , \end{aligned} \tag{B.2.36}$$

where we used $\zeta(2) = \prod_{p \text{ prime}} (1 - p^{-2})^{-1} = \frac{\pi^2}{6}$ and we used the symmetric square L-function associated with the cusp form $\nu_{n,\pm}$, see Lemma 3. It is a meromorphic function in s with a potential pole at $s = 1$ [232] (in our case there is no pole, so we can simply evaluate at $s = 1$).[106] This completes our derivation of the arithmetic kernel $f^{(n,\pm)}$.

B.2.4 L-function for Eisenstein series

It is natural to define the following continuous family of L-functions for the Eisenstein series $E_{\frac{1}{2}+i\alpha}(x, y)$ in terms of their Fourier coefficients (c.f., (3.2.6)):[107]

$$L_E^{(\alpha)}(s) \equiv \frac{1}{2} \sum_{m\geq 1} \frac{a_m^{(\alpha)}}{m^s} , \qquad a_m^{(\alpha)} = \frac{2\sigma_{2i\alpha}(m)}{m^{i\alpha}} \qquad (\mathrm{Re}(s) > 1) . \tag{B.2.37}$$

Lemma 5. The meromorphic continuation of the Eisenstein series L-function is

$$L_E^{(\alpha)}(s) = \zeta(s + i\alpha)\zeta(s - i\alpha) . \tag{B.2.38}$$

[105] There are ways to modify $f_p^{(n,\pm)}$ that are invisible to the statistical averaging. For example, one can add odd powers of $a_p^{(n,\pm)}$ with arbitrary coefficients, as these will vanish in the evaluation of (3.3.21). See main text for more comments.

[106] Note that there would be a pole at $s = 1$ if there was some prime Fourier coefficient with $a_p^{(n,\pm)} = \pm 2$. It is unproven but widely believed to be true that such a Fourier coefficient does not exist (Ramanijan-Petersson conjecture) [102].

[107] The factor $\frac{1}{2}$ is unconventional, but will make the following discussion more convenient.

Proof: We expand the zeta-functions formally in the domain where they converge:

$$\begin{aligned}\zeta(s+i\alpha)\zeta(s-i\alpha) &= \sum_{n_1\geq 1}\sum_{n_2\geq 1}\frac{1}{n_1^{s+i\alpha}n_2^{s-i\alpha}} = \sum_{m\geq 1}\sum_{\substack{n_1,n_2:\\ n_1n_2=m}}\frac{1}{n_1^{s+i\alpha}n_2^{s-i\alpha}}\\ &= \sum_{m\geq 1}\frac{1}{m^{s+i\alpha}}\,\sigma_{2i\alpha}(m) = L_E^{(\alpha)}(s) \qquad \square\end{aligned} \tag{B.2.39}$$

Note in particular:

$$L_E^{(2\alpha)}(s=1) = \cosh(\pi\alpha)\Lambda(i\alpha)\Lambda(-i\alpha)\,, \qquad \Lambda(s) = \pi^{-s}\Gamma(s)\zeta(2s)\,, \tag{B.2.40}$$

which is similar to the symmetric square L-function for cusp forms evaluated at $s=1$. See [103] for more details on this connection.

B.3 Independence of chaos in different spin sectors and the plateau

In this appendix we show that the existence of a ramp (or plateau) in a given spin sector is generically not sufficient to conclude the existence of a ramp (or plateau) in another spin sector. We showed this for the ramp in the Eisenstein series in chapter 2; here we repeat the analysis for the cusp forms and the plateau. We make some preliminary remarks on how the plateau can appear in the cusp forms.

B.3.1 Signatures of a spin m ramp at spin (m_1, m_2): Maass cusp forms

Similar to the analysis of section 2.3.2, let us assume that the spin m spectrum of Maass cusp forms contains a linear ramp. As discussed in the main text, the statistical averaging over cusp form data, which is automatic in the large y_i limit, means that there are different choices of correlations which would all yield a linear ramp in some given spin sector. Ultimately, we found (3.4.1) by demanding a ramp with the correct slope in *every* spin sector. That is, we demanded that the imprint of any spin sector is the same on any other spin sector. In this appendix we analyze the consequences of working with less fine-tuned spectral correlations that are engineered to only describe RMT statistics in a fixed spin sector. In particular, consider the most naive ansatz, obtained by taking (3.3.9) and simply dividing out the Fourier coefficients:

$$\left\langle z_{n_1,\pm}\, z_{n_2,\pm}\right\rangle_{\text{spin } m \text{ ramp naive'}} \approx \frac{1}{a_m^{(n_1,\pm)} a_m^{(n_2,\pm)}}\, \frac{2R_{n_1}^{\pm}\tanh\!\big(\pi R_{n_1}^{\pm}\big)}{\pi^2\, \bar{\mu}_{\pm}(R_{n_1}^{\pm})}\, \delta_{n_1 n_2}\,. \tag{B.3.1}$$

Such a correlation implies that the spin (m_1, m_2) sector must contain the following term:

$$\begin{aligned}\big\langle \widetilde{Z}^{m_1}_{\mathrm{P,disc.},\pm}(y_1)\widetilde{Z}^{m_2}_{\mathrm{P,disc.},\pm}(y_2)\big\rangle &\supset_m \sum_{n_1,n_2} \langle z_{n_1,\pm}\, z_{n_2,\pm}\rangle_{\text{spin } m \text{ ramp naive'}}\, a_{m_1}^{(n_1,\pm)} a_{m_2}^{(n_2,\pm)} \\ &\quad\times \sqrt{y_1} K_{iR_{n_1}^{\pm}}(2\pi m_1 y_1)\sqrt{y_2}K_{iR_{n_2}^{\pm}}(2\pi m_2 y_2) \\ &\approx \sum_n \frac{2R_n^{\pm}\tanh(\pi R_n^{\pm})}{\pi^2 \bar{\mu}_{\pm}(R_n^{\pm})}\, \frac{a_{m_1}^{(n,\pm)} a_{m_2}^{(n,\pm)}}{\big(a_m^{(n,\pm)}\big)^2}\, \sqrt{y_1}K_{iR_n^{\pm}}(2\pi m_1 y_1)\sqrt{y_2}K_{iR_n^{\pm}}(2\pi m_2 y_2)\,.\end{aligned} \tag{B.3.2}$$

This can be evaluated numerically, which yields similar results as in the case of Eisenstein series discussed in section 2.3.2:

$$\big\langle \widetilde{Z}^{m_1}_{\mathrm{P,disc.},\pm}(y_1)\widetilde{Z}^{m_2}_{\mathrm{P,disc.},\pm}(y_2)\big\rangle \supset_m \eta^{\pm}_{m,m_1} \times \delta_{m_1 m_2}\, \frac{1}{\pi}\, \frac{y_1 y_2}{y_1+y_2}\, e^{-2\pi m_1 (y_1+y_2)} \qquad (y_i \gg 1)\,, \tag{B.3.3}$$

where the spin-dependent coefficient $\eta^{\pm}_{m,m_1}$ is generally different from 1. This is illustrated in figure B.6. From the curves in that figure, we find the following numerical fit:

$$\text{num. fit:} \quad \begin{cases} \eta^{+}_{1,1} = 1\,, \quad \eta^{+}_{1,2} = 1.44..\,, \quad \eta^{+}_{1,3} = 1.25..\,, \quad \eta^{+}_{1,4} = 1.61..\,, \quad \dots \\ \eta^{-}_{1,1} = 1\,, \quad \eta^{-}_{1,2} = 1.46..\,, \quad \eta^{-}_{1,3} = 1.28..\,, \quad \eta^{-}_{1,4} = 1.65..\,, \quad \dots \end{cases} \tag{B.3.4}$$

This matches within $\sim 10\%$ with the theoretical expectation based on statistical averaging, namely $\eta^{\pm}_{m,m_1} = \mathcal{N}^{\pm}_{m_1}/\mathcal{N}^{\pm}_{m}$, which follows after replacing squares of Fourier coefficients by their variances in (B.3.2):[108]

$$\text{theoretical values:} \qquad \eta^{\pm}_{1,1} = 1\,, \quad \eta^{\pm}_{1,2} = \frac{3}{2}\,, \quad \eta^{\pm}_{1,3} = \frac{4}{3}\,, \quad \eta^{\pm}_{1,4} = \frac{7}{4}\,, \quad \dots \tag{B.3.5}$$

[108]Computing $\mathcal{N}^{\pm}_{m_1}/\mathcal{N}^{\pm}_{m}$ using the finite number of cusp forms available to us, i.e., using (3.3.17), yields agreement within $\sim 2\%$. This shows that a still much larger number of cusp forms is required in order to get very close to the theoretical values for $\eta^{\pm}_{m,m_1}$.

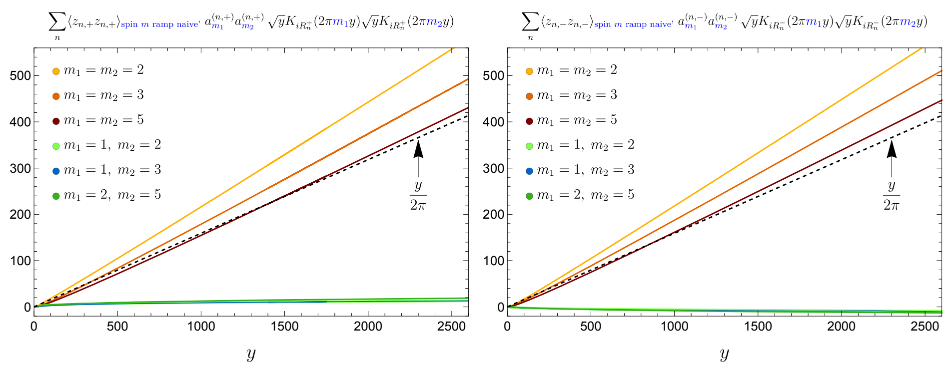

Figure B.6: Numerical evaluation of (B.3.2): we show the imprint of a ramp in the spin $m = 1$ sector onto the spin (m_1, m_2) sector of the spectral form factor, assuming the naive form of correlations (B.3.1) which is not engineered to have information about any other spin sector. While the asymptotic contribution has the correct linear y-dependence (for $m_1 = m_2$), it does not have the correct slope to account for all the information encoded in a ramp.

The fact that the prefactor $\eta^{\pm}_{m,m_1}$ in (B.3.3) is not 1 means that the ramp at spin (m_1, m_2) is not fully encoded in the ramp at spin m. Random matrix universality in one spin sector therefore does not imply random matrix universality in a different spin sector – as is consistent with general expectations in the theory of quantum chaos. Instead, one must fine-tune the approximation (B.3.1) in a way that is informed by cusp form data in all other spin sectors. This is achieved by the arithmetic kernel $f^{(n,\pm)}$ discussed in the main text.

B.3.2 Independence of the plateaus

Here we discuss the numerical imprint of a plateau in one spin sector onto other sectors. We begin with the imprint of a spin 0 plateau onto the spin

(m_1, m_2) sector:

$$\begin{aligned}\left\langle \widetilde{Z}^{m_1}_{\mathrm{P,cont.}}(y_1)\widetilde{Z}^{m_2}_{\mathrm{P,cont.}}(y_2)\right\rangle &\supset^{\mathrm{plateau}}_{m=0} \frac{\sqrt{y_1y_2}}{4\pi^2}\iint d\alpha_1 d\alpha_2 \left\langle z_{\frac{1}{2}+i\alpha_1} z_{\frac{1}{2}+i\alpha_2}\right\rangle_{\text{spin 0 plateau}} \\ &\quad\times \frac{a^{(\alpha_1)}_{m_1}a^{(\alpha_2)}_{m_2}}{\Lambda(-i\alpha_1)\Lambda(-i\alpha_2)} K_{i\alpha_1}(2\pi m_1 y_1)K_{i\alpha_2}(2\pi m_2 y_2) \\ &= \frac{\sqrt{y_1y_2}}{\pi^2}\int d\alpha\, 2i\pi^2 \frac{1}{\sinh(\pi\alpha)}\frac{\sigma_{2i\alpha}(m_1)\sigma_{-2i\alpha-2}(m_2)}{m_1^{i\alpha}m_2^{-i\alpha-1}\Lambda(-i\alpha)\Lambda(i\alpha+1)} \\ &\quad\times K_{i\alpha}(2\pi m_1 y_1)K_{-i\alpha-1}(2\pi m_2 y_2)\end{aligned} \tag{B.3.6}$$

The result, as shown in figure B.7, is

$$\left\langle \widetilde{Z}^{m_1}_{\mathrm{P,cont.}}(y_1)\widetilde{Z}^{m_2}_{\mathrm{P,cont.}}(y_2)\right\rangle \supset^{\mathrm{plateau}}_{m=0} \lambda^{(\mathrm{p})}_m \langle \rho^m_D(E_m)\rangle e^{-2\pi|m|(y_1+y_2)} \qquad (y_i \gg 1)\,, \tag{B.3.7}$$

where the spin m coefficient $\lambda^{(\mathrm{p})}_m$ is a small, $\mathcal{O}(e^{-2\pi m})$ coefficient:

$$\begin{aligned}&\lambda^{(\mathrm{p})}_1 \approx 6.04\times 10^{-3}\,, \quad \lambda^{(\mathrm{p})}_2 \approx 1.51\times 10^{-5} \\ &\lambda^{(\mathrm{p})}_3 \approx 3.49\times 10^{-8}\,, \quad \lambda^{(\mathrm{p})}_5 \approx 1.38\times 10^{-13}\,,\ \ldots\end{aligned} \tag{B.3.8}$$

Thus the spin 0 plateau produces a small constant in the spin m sector. Since the plateau also goes to a constant for $y_i \gg 1$, $y_1/y_2 =$ fixed, this represents a subleading correction to the true spin m plateau. This is a similar situation to the imprint of the spin 0 ramp; however, here we find that it is subleading due to the *coefficient*, rather than the *functional form*.

The imprint of a spin 1 plateau, through a similar calculation, is as follows (see figure B.8):

$$\left\langle \widetilde{Z}^{m_1}_{\mathrm{P,cont.}}(y_1)\widetilde{Z}^{m_2}_{\mathrm{P,cont.}}(y_2)\right\rangle \supset^{\mathrm{plateau}}_{m=1} \mu^{(\mathrm{p})}_m \sqrt{\tfrac{y_1+y_2}{2}}\langle \rho^m_D(E_m)\rangle \tfrac{\sqrt{y_1y_2}}{y_1+y_2} e^{-2\pi|m|(y_1+y_2)} \qquad (y_i \gg 1) \tag{B.3.9}$$

where

$$\mu^{(\mathrm{p})}_2 \approx 8.13..\times 10^{-3}\,, \quad \mu^{(\mathrm{p})}_3 \approx 1.97..\times 10^{-5}\,, \quad \mu^{(\mathrm{p})}_5 \approx 7.78..\times 10^{-11}\,,\ \ldots \tag{B.3.10}$$

We obtain a function that dominates over the plateau at large y_i. This is a similar situation to the ramp, where the imprint of the spin 1 ramp dominated over the true spin m ramp; however, here we find that it dominates due to the *functional form*, rather than the *coefficient*. It would obviously be interesting to study the implications of this further.

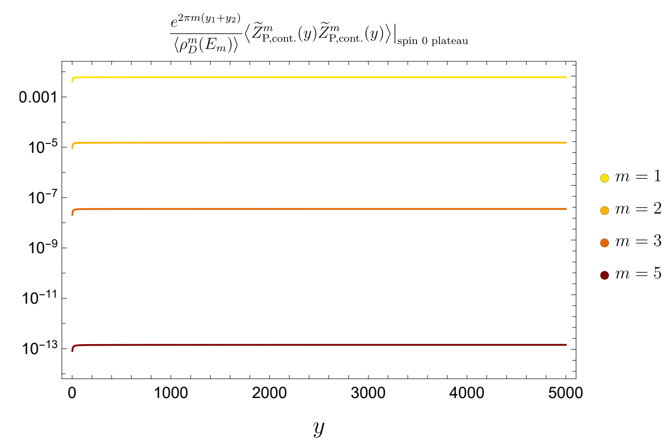

Figure B.7: Plot of the imprint of the spin 0 plateau on other spin sectors (note the log scaling of the y-axis). In order to get a result that is c-independent and compare with the true spin m plateau (3.5.4), we normalize the imprint by $\langle \rho_D(E_m)\rangle e^{-2\pi m(y_1+y_2)}$; at large c, $\langle \rho_D(E_0)\rangle/\langle \rho_D(E_m)\rangle \approx \frac{1}{2}e^{-2\pi m}$. With this normalization, the true spin m plateau becomes equal to $1/2$ for $y_1 = y_2$. The results shown therefore amount to a small constant $\sim \mathcal{O}(e^{-2\pi m})$.

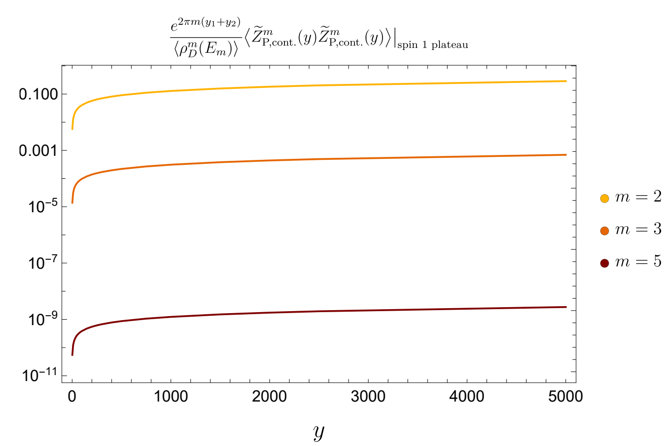

Figure B.8: Plot of the imprint of the spin 1 plateau on other spin sectors for $y_1 = y_2 = y$. We again normalize by $\langle \rho_D(E_m)\rangle e^{-2\pi m(y_1+y_2)}$; at large c, $\langle \rho_D(E_1)\rangle/\langle \rho_D(E_m)\rangle \approx e^{-2\pi(m-1)}$. The result is a function that grows like $\sqrt{y}$; creating a similar plot for a fixed y_2 yields the functional form in (B.3.9).

B.3.3 Comments on the plateau and the cusp forms

When trying to find an expression for the spectral decomposition of the plateau into the cusp forms, we can apply the logic of section 3.3, i.e., use arithmetic chaos and the continuous approximation. Using (3.5.7), this would immediately give:

$$\begin{aligned}\langle z^{m_1}_{n_1,\pm} z^{m_1}_{n_2,\pm}\rangle_{\text{spin } m \text{ plateau}} \overset{?}{\approx} -\frac{4m}{\pi\bar{\mu}(R^{\pm}_{n_1})\bar{\mu}(R^{\pm}_{n_2})}\langle \rho^m_D(E_m)\rangle \\ \times \mathcal{D}\left(\frac{1}{\left(R^{\pm}_{n_1}-R^{\pm}_{n_2}\right)^2}+\frac{1}{\left(R^{\pm}_{n_1}+R^{\pm}_{n_2}\right)^2}\right)\delta_{m_1 m_2}\,.\end{aligned} \tag{B.3.11}$$

These correlations should then produce a plateau in the spectral form factor. Unfortunately, (B.3.11) is not as well suited for numerical analysis as the ramp. The reason is that the factor $(R^{\pm}_{n_1} \pm R^{\pm}_{n_2})^{-2}$ decays for large $R^{\pm}_n$, meaning that the integrand is peaked at small values of $R^{\pm}_n$. This is in contrast to the ramp, where we instead had the factor $R^{\pm}_{n_1}\tanh\left(\pi R^{\pm}_{n_1}\right)$ which leads to an integrand peaked at large values of $R^{\pm}_n$.

However we do expect that as y_i and $R^{\pm}_{n_i}$ increase, the continuous approximation (B.3.11) becomes better. The reason is that in the continuous approximation, the region of $R^{\pm}_{n_i}$ where the integrand has support increases as $y_i \to \infty$. Thus, even though the correlations are peaked at small R_{n_i}, (B.3.11) should reproduce the plateau at sufficiently large y_i. We do not have access to enough cusp form data to demonstrate this, and we leave (B.3.11) as a conjecture.

Appendix C

Appendices for chapter 4

C.1 Conventions and useful formulae

Conventions in $d = 2$. For reference, we collect some of our conventions for calculations in two-dimensional CFTs. On the Euclidean plane $x^\mu = (x^0, x^1)$, we define $z = x^0 + ix^1$ and $\bar{z} = z^*$. After mapping to the cylinder via $z = e^{-iu}$, we similarly write $u = \tau + i\sigma$. These conventions yield:

$$\begin{aligned}
\text{metric:} \qquad & ds^2 = dz\, d\bar{z} = (dx^0)^2 + (dx^1)^2 \\
& \quad\;\; = e^{i(\bar{u}-u)}\, du\, d\bar{u} = e^{2\sigma} \left(d\tau^2 + d\sigma^2\right) , \\
\text{derivatives:} \qquad & \partial_u \equiv \frac{1}{2}(\partial_\tau - i\partial_\sigma) \, , \quad \bar{\partial}_{\bar{u}} \equiv \frac{1}{2}(\partial_\tau + i\partial_\sigma) \, , \\
\text{integral measure:} \qquad & \int d^2 z \equiv \frac{i}{2} \int dz d\bar{z} = \int d^2 x \, , \qquad \int d^2 u \equiv \int d\tau d\sigma \, .
\end{aligned} \tag{C.1.1}$$

We define the holomorphic stress tensor on the plane as $T \equiv -2\pi T_{zz}$, and similarly $\overline{T} \equiv -2\pi T_{\bar{z}\bar{z}}$.

Conventions in $d \geq 2$. In higher dimensions, we often use the symmetric-traceless projector and the inversion tensor:

$$\mathbb{P}^{\mu\nu}_{\;\rho\sigma} \equiv \frac{1}{2}\left(\delta^\mu_\rho \delta^\nu_\sigma + \delta^\nu_\rho \delta^\mu_\sigma\right) - \frac{1}{d}\,\eta_{\rho\sigma}\eta^{\mu\nu} \, , \qquad I^{\mu\nu}(x) \equiv \eta^{\mu\nu} - 2\,\frac{x^\mu x^\nu}{x^2} \, . \tag{C.1.2}$$

The inversion tensor satisfies the following useful relations:

$$\frac{1}{x^2}\, I^\mu_\nu(x) = \partial_\nu \left(\frac{x^\mu}{x^2}\right) = \partial_\nu \partial^\mu \log|x| \, , \qquad \partial_\mu I^\rho_\nu = -\frac{2}{x^2}\left[I^\rho_\mu\, x_\nu + x^\rho\, \eta_{\mu\nu}\right] \, . \tag{C.1.3}$$

Conventions for embedding space. A general point in embedding space $\mathbb{R}^{1,d+1}$ is denoted as X^A, where $A = (I, II, \mu) = (I, II, 0, m)$. The metric is $\eta_{AB} = \mathrm{diag}(-1, 1, \ldots, 1)$. Let us consider points P^A that lie on the (upper) projective null cone characterized by $P \cdot P = 0$ and $P^I > 0$. The CFT spacetime consists of points on the null cone subject to the projective identification $P^A \equiv \lambda P^A$. A point P^A in the CFT can be represented in different useful ways. We mainly use the following representations:

$$\begin{aligned}
&\text{Poincaré section:} \qquad && P^A_{\text{P}} = \left(\frac{1+x^2}{2}\,,\ \frac{1-x^2}{2}\,,\ x^\mu\right) \qquad x^\mu \in \mathbb{R}^d \\
&\text{Rindler section:} \qquad && P^A_{\text{R}} = \left(\frac{1+\rho^2+x_\perp^2}{2}\,,\ \frac{1-\rho^2-x_\perp^2}{2}\,,\ \rho\,\sin\tau\,,\ \rho\,\cos\tau\,,\ x_\perp^i\right), \\
&\text{Hyperbolic space:} \qquad && P^A_{\text{H}} = \frac{1}{\rho}\,P^A_{\text{R}}\,, \qquad \rho > 0\,,\ x_\perp^i \in \mathbb{R}^{d-1}\,.
\end{aligned} \tag{C.1.4}$$

The Poincaré section is appropriate for studying zero-temperature CFTs on d-dimensional Minkowski spacetime (or simply Euclidean $\mathbb{R}^d$ as above). For instance, in Poincaré coordinates we have $(-2P_1 \cdot P_2) = (x_1 - x_2)^2$.

On the other hand, the Rindler coordinates correspond to studying CFTs which look thermal with respect to Rindler time τ. The temperature is fixed as $T = 2\pi$. The hyperbolic section is conformal to Rindler space, and the conformal factor can simply be read off from the third line of (C.1.4). In the hyperbolic (or Rindler) section it is useful to parametrize the hyperbolic space $\mathbb{H}^{d-1}$ by itself (without the time direction) in terms of

$$Y^A = \left(\frac{1+\rho^2+x_\perp^2}{2\rho},\ \frac{1-\rho^2-x_\perp^2}{2\rho},\ 0,\ 0,\ \frac{x_\perp^i}{\rho}\right)\,. \tag{C.1.5}$$

The $SO(d-2,1)$ invariant geodesic distance in $\mathbb{H}^{d-1}$ is

$$\mathbf{d}(1,2) = \cosh^{-1}(-Y_1 \cdot Y_2) = \cosh^{-1}\left[\frac{\rho_1^2+\rho_2^2+x_{\perp 12}^2}{2\,\rho_1\rho_2}\right]\,. \tag{C.1.6}$$

We sometimes change to a radial hyperbolic coordinate, $\rho = e^\sigma$.

Conformal integrals. We frequently write integrals over all of Euclidean spacetime. These are typically determined by conformal symmetry, and evaluating them in practice is most conveniently done in embedding space, see e.g. [119] for examples, some of which we review now. Embedding space integrals in higher dimensions should be understood as follows:

$$\int d^dP\ f(P) \equiv \int_{P^I>0} \frac{d^{d+2}P}{\text{Vol GL}(1,\mathbb{R})^+}\,\delta(P^2)\,f(P)\,. \tag{C.1.7}$$

where division by the volume of the gauge group of planar boosts associated with identification of points under rescaling ($P^A \equiv \lambda P^A$) renders the result finite. For example, in the coordinates introduced above, these definitions reduce to:

$$\int d^dP\, f(P) \equiv \int d^dx\, f(P_{\text{P}}) \equiv \int_0^{2\pi} d\tau \int_0^{\infty} \frac{d\rho}{\rho^{d-1}} \int d^{d-2}x_{\perp}\, \Omega(P_{\text{H}})^{-\Delta} f(P_{\text{H}})\,, \tag{C.1.8}$$

where Δ is the conformal weight of $f(P)$.

An important example of an embedding space integral, that can be used to check various normalizations in this chapter, is the following:

$$\iint \frac{d^dP_1\, d^dP_2}{(-2X_1\cdot P_1)^{\Delta}(-2X_2\cdot P_2)^{d-\Delta}(-2P_1\cdot P_2)^{\Delta}} = \frac{\pi^d\Gamma(\Delta-\frac{d}{2})\Gamma(\frac{d}{2}-\Delta)}{\Gamma(\Delta)\Gamma(d-\Delta)}\frac{1}{(-2X_1\cdot X_2)^{\Delta}}\,, \tag{C.1.9}$$

and similarly for conformal integrals involving spinning propagators, where the normalization on the right hand side gets replaced by $\pi^d(k_{\Delta,\ell}\, k_{d-\Delta,\ell})^{-1}$, c.f., (4.2.6).

Shadows and projectors. We can use (C.1.9) to check various normalizations in §4.2. As a first application, we determine the normalization of two-point functions of shadow operators in terms of the normalization of their physical partners. Define the two-point function of scalar operators $\mathcal{O}$ as $\langle\mathcal{O}(P_1)\mathcal{O}(P_2)\rangle = \frac{C_{\mathcal{O}}}{(-2P_1\cdot P_2)^{\Delta}} = \frac{C_{\mathcal{O}}}{(x_1-x_2)^{2\Delta}}$. Using the definition of the shadow operator (4.2.12), it follows immediately from (C.1.9) that

$$\langle\widetilde{\mathcal{O}}(P_1)\widetilde{\mathcal{O}}(P_2)\rangle = \frac{C_{\widetilde{\mathcal{O}}}}{(-2P_1\cdot P_2)^{\Delta}} \qquad \text{with} \qquad C_{\widetilde{\mathcal{O}}} = C_{\mathcal{O}}\,\frac{k_{\Delta,0}}{k_{d-\Delta,0}}\,, \tag{C.1.10}$$

and similarly for spinning operators.

Let us check more features of the definition of the shadow operator, (4.2.12). In order to show that $\widetilde{\widetilde{\mathcal{O}}} = \mathcal{O}$, one can, for example, verify that $\langle\widetilde{\widetilde{\mathcal{O}}}(x)\mathcal{O}(y)\rangle = \langle\mathcal{O}(x)\mathcal{O}(y)\rangle$ using (C.1.9). In general we define the projectors onto the conformal family associated with an operator $\mathcal{O}$ and its shadow as:

$$\begin{aligned} |\mathcal{O}| &\equiv \frac{1}{C_{\mathcal{O}}}\frac{k_{d-\Delta,\ell}}{\pi^{d/2}}\int d^d\xi\; \mathcal{O}^{\mu\cdots}(\xi)|0\rangle\langle 0|\widetilde{\mathcal{O}}_{\mu\cdots}(\xi)\,,\\ |\widetilde{\mathcal{O}}| &\equiv \frac{1}{C_{\widetilde{\mathcal{O}}}}\frac{k_{\Delta,\ell}}{\pi^{d/2}}\int d^d\xi\; \widetilde{\mathcal{O}}^{\mu\cdots}(\xi)|0\rangle\langle 0|\mathcal{O}_{\mu\cdots}(\xi) \end{aligned} \tag{C.1.11}$$

where $C_{\widetilde{\mathcal{O}}} \equiv C_{\mathcal{O}}\,\frac{k_{\Delta,\ell}}{k_{d-\Delta,\ell}}$ as above. This ensures that $|\mathcal{O}| = |\widetilde{\mathcal{O}}|$ as is obvious from the definition (4.2.12). One can furthermore check that $|\mathcal{O}|$ leaves correlators involving the operator $\mathcal{O}$ invariant. For instance, one easily checks that $\langle \mathcal{O}(x)|\mathcal{O}|\mathcal{O}(y)\rangle = \langle \mathcal{O}(x)\mathcal{O}(y)\rangle$, which is again a direct consequence of the integral (C.1.9). Similarly, the fact that $|\mathcal{O}|^2 = |\mathcal{O}|$ is another simple application of (C.1.9). For more general statements, see [119].

C.2 Exponentiation of the light-light Virasoro block

As a simple illustrative example of the reparametrization mode formalism, we briefly review the exponentiation of the light-light conformal block in $d = 2$ as presented in [115]. In the "light-light" regime we take the external holomorphic operators V and W to have dimensions $h_V = h_W \equiv h \sim \sqrt{c}$. The leading reparametrization mode exchanges in this regime correspond to diagrams of order $(h^2/c)^n \sim \mathcal{O}(1)$. These diagrams are the ladder diagrams of the following form:

$$\mathcal{V}_0\big|_{\mathcal{O}(1)} \quad = \quad 1 \quad +$$

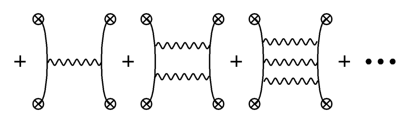

where $\mathcal{V}_0$ denotes the normalized *Virasoro identity block*. The wavy lines indicate exchanges of reparametrization modes between two pairs of external operators. At leading order in large c, we get

$$\begin{aligned}
\mathcal{V}_0\big|_{\mathcal{O}(1)} &= \sum_{n\geq 0} \left\langle \mathcal{B}^{(n)}_{\epsilon,h}(z_1,z_2)\, \mathcal{B}^{(n)}_{\epsilon,h}(z_3,z_4)\right\rangle\Big|_{\mathcal{O}\left((\frac{h^2}{c})^n\right)} + \mathcal{O}\left(c^{-1}\right) \\
&= \sum_{n\geq 0} \frac{1}{n!}\left(\frac{2h^2}{c} z^2\, {}_2F_1(2,2,4,z)\right) + \mathcal{O}\left(c^{-1}\right) \qquad\qquad (\text{C.2.1}) \\
&= \exp\left(\frac{2h^2}{c} z^2\, {}_2F_1(2,2,4,z)\right) + \mathcal{O}\left(c^{-1}\right)\,,
\end{aligned}$$

where we used (4.3.19) to replace $\mathcal{B}^{(n)}_{\epsilon,h} \to \frac{1}{n!}\left(\mathcal{B}^{(1)}_{\epsilon,h}\right)^n$ and included an additional factor of $n!$ to account for permutations of contractions. This is simply the exponentiated version of the physical block in (4.4.7).

C.3 Details on calculations in section 4.5.2

In this appendix we collect some details on calculations outlined in the main text.

C.3.1 Derivation of $\mathcal{G}_{00,00}(P_1, P_2)$

In order to prove (4.5.14), we first note that the general two-point function (4.5.11) can be written as

$$\begin{aligned}\mathcal{G}_{\mu\nu,\rho\sigma}(P_1, P_2) =& \frac{8C_T}{(-2P_1 \cdot P_2)^{d+2}} \mathbb{P}^{AB}_{\mu\nu}(P_1)\, \mathbb{P}^{CD}_{\rho\sigma}(P_2) \\ & \Big[\left((P_1 \cdot P_2)\eta_{BC} - P_{1,C}P_{2,B}\right) \left((P_1 \cdot P_2)\eta_{AD} - P_{1,D}P_{2,A}\right) \Big]\end{aligned} \tag{C.3.1}$$

To compute the time-time component of this, we note that the time-time component of the projectors takes the simple form[109]

$$\mathbb{P}^{AB}_{\tau\tau}(P) = m^A m^B - \frac{1}{d}\eta^{AB}\,, \quad \text{where} \;\; m^A \equiv m^A(\tau) = (0, 0, \cos\tau, -\sin\tau, \vec{0}). \tag{C.3.2}$$

Using this, we can write out the terms in (C.3.1) explicitly. The terms simplify upon using the following identities:

$$\begin{aligned} \eta_{AB}\, m^A m^B &= 1\,, \qquad & \eta_{AB}\, m_1^A m_2^B &= \cos(\tau_1 - \tau_2)\,, \\ \eta_{AB}\, m^A P^B &= 0\,, \qquad & \eta_{AB}\, m_1^A P_2^B &= -\sin(\tau_1 - \tau_2)\,. \end{aligned} \tag{C.3.3}$$

Finally, writing all $\sin^2(\tau_1 - \tau_2) = 1 - \cos^2(\tau_1 - \tau_2)$, one finds

$$\begin{aligned}\mathcal{G}_{00,00}(P_1, P_2) = \frac{8C_T}{(-2P_1 \cdot P_2)^{d+2}} \bigg\{ & 1 + \frac{2(d-1)}{d} \cos(\tau_1 - \tau_2)\,(Y_1 \cdot Y_2) \\ & - \frac{1}{d}\left(\cos^2(\tau_1 - \tau_2) + (Y_1 \cdot Y_2)^2\right) + \cos^2(\tau_1 - \tau_2)\,(Y_1 \cdot Y_2)^2 \bigg\}\,.\end{aligned} \tag{C.3.4}$$

Clearly, all the appearances of $\cos(\tau_1 - \tau_2)$ and $Y_1 \cdot Y_2$ can be obtained by differentiating the auxiliary quantity $\mathcal{G}^{a,b}_{\Delta}(P_1, P_2)$ with respect to a and b. The result then takes the form (4.5.14).

C.3.2 Derivation of $\mathcal{G}^{a,b}_{\Delta}(\omega_E, k)$

We provide here some details on the Fourier transform leading to (4.5.18). Essentially, the calculation is the same as a Euclidean version of Appendix A.2

[109] This can be expressed more covariantly by noting that $m^A(\tau) = \Omega^A{}_B(P^B - Y^B)$, where the rotation matrix $\Omega_{AB} = \delta^{II}_A \delta^0_B - \delta^0_A \delta^{II}_B$.

of [158] with the additional replacement of Bessel functions $I_{\omega_E}(u) \to I_{\omega_E}(au)$ and $K_{ik}(u) \to b^{-(d-2)/2} K_{ik}(bu)$ to take the propagator off-shell. We now recall some of the essential steps.

We start with the following identity that follows from orthonormality and completeness of the basis functions $f_{\omega_E,k,p_\perp}(P)$:

$$
\begin{aligned}
\mathcal{G}^{a,b}_\Delta(\omega_E,k)\, f_{\omega_E,k,p_\perp}(P) &= \int dP'\, \mathcal{G}^{a,b}_\Delta(P,P')\, f_{\omega_E,k,p_\perp}(P') \\
&= \left(\frac{4k\,\sinh(\pi k)}{\pi}\right)^{1/2} \int_0^{2\pi} d\tau' \int_0^\infty \frac{d\rho'}{\rho'^{d-1}} \int d^{d-2}x'_\perp \\
&\quad \times \frac{\rho'^{\frac{d-2}{2}}\, K_{ik}(|p_\perp|\,\rho')\, e^{i(\omega_E\tau' + p_\perp\cdot x'_\perp)}}{\left[-2a\,\cos(\tau-\tau') + b\,\frac{\rho^2+\rho'^2+|x_\perp - x'_\perp|^2}{\rho\rho'}\right]^\Delta} \\
&= \left(\frac{4k\,\sinh(\pi k)}{\pi}\right)^{1/2} \frac{1}{2^\Delta\Gamma(\Delta)}\, e^{i(\omega_E\tau + p_\perp\cdot x_\perp)} \int_0^{2\pi} d\tau' \int_0^\infty dz\, z^{\Delta-1} e^{i\omega_E\tau' + az\,\cos\tau} \\
&\quad \times \int_0^\infty d\rho'\, \rho'^{-d/2}\, K_{ik}(|p_\perp|\,\rho')\, e^{-\frac{bz}{2\rho\rho'}(\rho^2+\rho'^2) - \frac{\rho\rho'}{2bz}p_\perp^2} \left(\frac{2\pi\rho\rho'}{bz}\right)^{(d-2)/2}
\end{aligned}
\tag{C.3.5}
$$

where we introduced the Schwinger parameter z to exponentiate the denominator of the two-point function in the last step. We now use the following identities:

$$
\begin{aligned}
\int_0^{2\pi} d\tau'\, e^{i\omega_E\tau' + az\,\cos\tau'} &= 2\pi\, I_{\omega_E}(az)\,, \\
\int_0^\infty \frac{d\rho'}{\rho'}\, K_{ik}(|p_\perp|\,\rho')\, e^{-\frac{bz}{2\rho\rho'}(\rho^2+\rho'^2) - \frac{\rho\rho'}{2bz}p_\perp^2} &= 2\, K_{ik}(bz) K_{ik}(|p_\perp|\,\rho)\,.
\end{aligned}
\tag{C.3.6}
$$

Inserting these in (C.3.5) yields a prefactor that is precisely $f_{\omega_E,k,p_\perp}(P)$. We can thus strip this factor off of (C.3.5) and write:

$$
\begin{aligned}
\mathcal{G}^{a,b}_\Delta(\omega_E,k) &= \frac{(2\pi)^{d/2}}{2^{\Delta-1}\Gamma(\Delta)}\, b^{-\frac{d-2}{2}} \int_0^\infty dz\, z^{\Delta-\frac{d}{2}}\, I_{\omega_E}(az)\, K_{ik}(bz) \\
&= \frac{\pi^{d/2}}{\Gamma(\Delta)} \frac{a^{\omega_E}}{b^{\omega_E+\Delta}} \frac{|\Gamma(\alpha)|^2}{\Gamma(\omega_E+1)}\, {}_2F_1\left(\alpha,\alpha^*,\omega_E+1;\frac{a^2}{b^2}\right)_{\text{reg.}}
\end{aligned}
\tag{C.3.7}
$$

where $\alpha \equiv \frac{1}{2}\left(\Delta - \frac{d-2}{2} + ik + \omega_E\right)$. The last integral is strictly valid only when $\mathrm{Re}(\alpha) > 0$ and $a < b$.[110] Especially when we take the limit $a,b \to 1$, we need to regularize the expression and extract the finite piece. We achieve

[110] See, for example, section 6.576 on page 684 of [228].

this as follows. When computing (4.5.19), we first take derivatives with respect to a and b as instructed by (4.5.14). We then replace any instances of hypergeometric functions according to

$$ {}_2F_1\left(\alpha,\alpha^*,\omega_E+1;\frac{a^2}{b^2}\right) \to \frac{\Gamma(\omega_E+1)\Gamma(\omega_E+1-\alpha-\alpha^*)}{\Gamma(\omega_E+1-\alpha)\Gamma(\omega_E+1-\alpha^*)} \tag{C.3.8} $$

It is now well-defined to set $a=b=1$ in the resulting expression.

C.3.3 Dimensional regularization for even dimensions

In this section we describe how to perform the dimensional regularization of (4.5.19) in the case of even dimensions. We set $d=2m-\varepsilon$ and wish to extract the finite term as $\varepsilon\to 0$.

For the divergent Γ-function, we have $\Gamma(-\frac{d}{2}) \to \frac{(-1)^m}{m!}\left(\frac{2}{\varepsilon}+\psi(m+1)+\mathcal{O}(\varepsilon)\right)$. A similar expansion of the other d-dependent terms yields the following result for the $\mathcal{O}(\varepsilon^0)$ term:

$$ \begin{aligned} &\mathcal{G}_{00,00}(\omega_E,k)_{\text{finite}} \\ &\quad= \frac{2C_T\,(-1)^{m-1}\pi^m(m-1)}{4^m(2m+1)m!(2m-1)!}\left(\prod_{j=1}^{m-2}\left((m+\omega_E-1-2j)^2+k^2\right)\right) \\ &\qquad\times\left(k^2+m^2\right)\left(k^2+(m-1)^2\right)\left\{\psi\left(\frac{\omega_E+ik+m-1}{2}\right)\right. \\ &\qquad\left.+\psi\left(\frac{\omega_E-ik+m-1}{2}\right)+\psi\left(\frac{\omega_E+ik-m+3}{2}\right)+\psi\left(\frac{\omega_E-ik-m+3}{2}\right)\right\} \end{aligned} \tag{C.3.9} $$

where $\psi(z)$ is the digamma function. In writing this, we have dropped various contact terms (i.e., terms involving only polynomials in ω_E and k, but no singular functions such as $\psi(...)$).

Appendix D

Appendices for chapter 5

D.1 Bulk Canonical Commutators

In section 5.2.2 we showed that a bulk scalar operator ϕ can be expressed as

$$\phi(\vec{y}, u, r) = \sum_n c_n \bar{\psi}_n(r) \hat{\phi}_n(\vec{y}, u) \,, \tag{D.1.1}$$

where the $\hat{\phi}_n(\vec{y}, u)$ are codimension-1 fields of asymptotic dimension (5.3.9), and $\bar{\psi}_n(r)$ are the normalizable mode functions (normalized with leading unit coefficient near the asymptotically-AdS boundary). That analysis was insufficient to determine the overall constants c_n.

To determine the c_n we require that the operators ϕ and $\hat{\phi}_n$ satisfy the equal time canonical commutation relations

$$[\phi(t, \vec{v}_1, u_1, r_1), \pi(t, \vec{v}_2, u_2, r_2)] = i\delta^{d+1}(\vec{v}_1 - \vec{v}_2, u_1 - u_2, r_1 - r_2), \tag{D.1.2}$$

$$[\phi_n(t, \vec{v}_1, u_1), \pi_m(t, \vec{v}_2, u_2)] = i\delta^{d}(\vec{v}_1 - \vec{v}_2, u_1 - u_2)\delta_{m,n}, \tag{D.1.3}$$

where $\vec{y} = (t, \vec{v})$ and where $\pi \equiv -\sqrt{-g} g^{tt} \partial_t \phi$ and $\pi_n \equiv -\sqrt{-\tilde{g}} \tilde{g}^{tt} \partial_t \phi_n$ are the canonically conjugate fields to ϕ and π_n, with $\tilde{g}$ the induced metric on the AdS$_d$ slices of fixed r. This gives

$$\int_{r_0}^{\infty} dr \cosh^{d-2}(r) \psi_n(r) \psi_m(r) = \frac{1}{c_n^2} \delta_{nm}, \tag{D.1.4}$$

which we can evaluate to obtain c_n.

D.2 Asymptotically AdS Toy Model and the Reflected Singularity

In this appendix, we will provide some details for the calculation involving a free scalar field propagating on an asymptotically locally AdS background that was mentioned in section 5.6.1. Recall that our goal is to provide evidence in a concrete example that different KK modes will give rise to the same reflected singularity when the bulk geometry has finite causal depth. As pointed out earlier, it is sufficient to demonstrate that the asymptotic frequency spacing $\Delta\omega$ for each mode in this model is equal to π; we approach this problem numerically.

Recall that the background geometry is

$$ds^2 = \frac{L^2}{z^2}\left(dz^2 - dt^2 + z^2 f(z)^2 d\theta^2\right) , \qquad f(z) = \frac{1-z^2}{2} , \qquad \theta \in (0, 2\pi) . \tag{D.2.1}$$

The massive scalar wave equation $\Box\phi = M^2\phi$ on this background yields

$$\partial_z^2\phi - \frac{2z}{1-z^2}\partial_z\phi = \left(\partial_t^2 - \frac{4}{z^2(1-z^2)^2}\partial_\theta^2 + \frac{M^2L^2}{z^2}\right)\phi . \tag{D.2.2}$$

Separating variables by writing

$$\phi(z,t,\theta) = e^{im\theta}e^{i\omega t}\phi_{m,\omega}(z) , \tag{D.2.3}$$

the $\phi_{m,\omega}(z)$ must satisfy

$$\partial_z^2\phi - \frac{2z}{1-z^2}\partial_z\phi = \left(-\omega^2 + \frac{4m^2}{z^2(1-z^2)^2} + \frac{M^2L^2}{z^2}\right)\phi . \tag{D.2.4}$$

This equation has general solution

$$\begin{aligned}\phi(x) =& c_1(z^2-1)^m x^{\frac{1}{2}+\frac{\sqrt{1+4M^2L^2+16m^2}}{2}} \\ &\times H\left(0, \frac{\sqrt{1+4M^2L^2+16m^2}}{2}, 2m, \frac{\omega^2}{4}, \frac{8m^2-\omega^2+1}{4}, z^2\right) \\ &+ c_2(z^2-1)^m x^{\frac{1}{2}-\frac{\sqrt{1+4M^2L^2+16m^2}}{2}} \\ &\times H\left(0, -\frac{\sqrt{1+4M^2L^2+16m^2}}{2}, 2m, \frac{\omega^2}{4}, \frac{8m^2-\omega^2+1}{4}, z^2\right) ,\end{aligned} \tag{D.2.5}$$

where $H(\cdot)$ is a confluent Heun function, and c_1, c_2 are undetermined constants. The Heun function is analytic at the point where its last argument vanishes (the asymptotic boundary $z=0$), where it takes value $H(\ldots,0)=1$, and is singular for generic m,ω when its last argument is unity (the "IR wall" $z=1$). For $M^2>0$, we see that the first function is the normalizable solution at $z=0$; for negative M above the Breitenlohner-Freedman bound

$$-1 \le M^2L^2 < 0 , \tag{D.2.6}$$

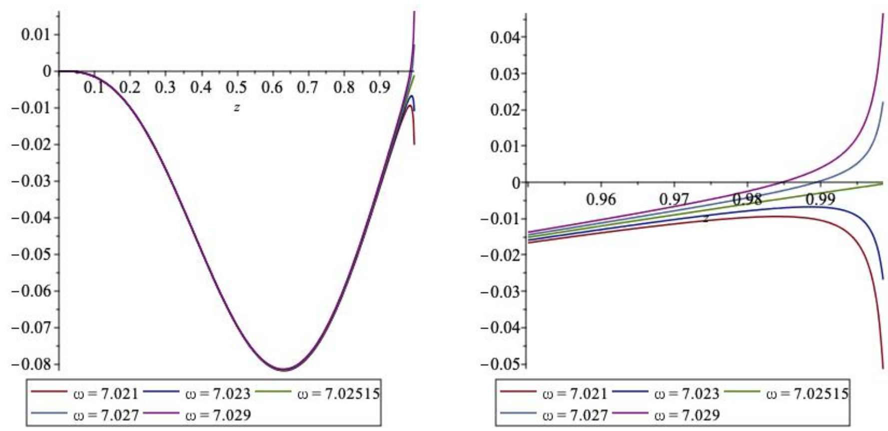

Figure D.1: Illustration of procedure for determining allowed frequencies ω. We plot solutions $\phi_{m,\omega}(x)$ with $m = 1$ consistent with normalizability at $z = 0$, for various values of ω. We have chosen $ML = 1$ for concreteness. The figure on the left shows the full range of z, while the figure on right shows a close-up in the vicinity of $z = 1$.

we also have an alternate quantization as usual.

With the general solution to the equation of motion in hand, we will proceed to fix various values of m, and numerically determine the values of ω consistent with regularity at $z = 1$. The appropriate boundary condition to impose is

$$\phi_{m,\omega}(z) \overset{z\to 1}{\sim} (1-z)^m \,, \tag{D.2.7}$$

since otherwise the θ-dependence will generate a singularity at $z = 1$. When computing the allowed frequencies numerically, we simply look for roots of $\phi_{m,\omega}(z = 1)$ as a function of ω. In particular, we do not manually impose the correct power law $(1 - z)^m$ in the vicinity of $z = 1$, but rather we merely require that $\phi_{m,\omega}(z = 1)$ vanishes. For $m \neq 0$ and generic ω, $\phi_{m,\omega}(z)$ actually has a singularity at $z = 1$; the desired values of ω occur when $\phi_{m,\omega}$ transitions between becoming large and positive and becoming large and negative in the vicinity of this singularity. This procedure is illustrated in Figure D.1.

Applying this procedure for various values of m, we indeed find that the spacing of allowed frequencies ω quickly converges to $\Delta\omega = \pi$, precisely as required to produce the singularity at $\Delta t = 2$; see Figure 5.9 of section 5.6.1. We note that this convergence appears to become slower with increasing m, though there is no reason to expect that the convergence would break down at any finite m.

D.3 BCFT Singularities in 2D

Consider insertions z_i on the (Euclidean) upper-half plane, with distances z_{ij} and $z_{i\bar{j}}$ defined as usual. We will be interested in the correlator $\langle \mathcal{O}(z_1)\mathcal{O}(z_2)\rangle$ and its Lorentzian continuation.

D.3.1 OPE expansion

The OPE expansion of our BCFT two-point correlator is just a sum over holomorphic Virasoro conformal blocks. In the bulk CFT channel $\xi \to 0$, we have

$$\mathcal{F}(\eta) := \langle \mathcal{O}(z_1)\mathcal{O}(z_2)\rangle = \sum_h C_{\mathcal{O}\mathcal{O}h} A_h \mathcal{V}_h(1-\eta), \tag{D.3.1}$$

where $C_{\mathcal{O}\mathcal{O}h}$ are bulk CFT OPE coefficients, A_h is the one-point function associated with the primary h, and $\xi = (1-\eta)/\eta$. In the boundary channel $\eta \to 0$ ($\xi \to \infty$), we have

$$\mathcal{F}(\eta) = \sum_{\hat{h}} |B_{\mathcal{O}\hat{h}}|^2 \mathcal{V}_{\hat{h}}(\eta), \tag{D.3.2}$$

where $B_{\mathcal{O}h}$ is a boundary OPE coefficient. It is possible to expand Virasoro blocks as [238]

$$\mathcal{V}_h(\eta) = (16q)^{h-(c-1)/24}[\eta(1-\eta)]^{(c-1)/24-2h}\theta_3(q)^{(c-1)/2-16h}H(h,q), \tag{D.3.3}$$

where $H(h,q)$ is a power series in q which can be determined recursively, θ_3 is a Jacobi theta function, and q is the elliptic nome defined by

$$q = e^{i\pi\tau(\eta)}, \quad \tau = i\frac{K(1-\eta)}{K(\eta)}, \quad K(\eta) = \frac{1}{2}\int_0^1 \frac{dt}{\sqrt{t(1-t)(1-\eta t)}}. \tag{D.3.4}$$

This can be inverted to give $\eta = [\theta_2(q)/\theta_3(q)]^4$.

D.3.2 The pillow geometry

The parameter τ appearing in q is the modulus of a torus which covers the Riemann sphere twice. We will proceed with this construction, using Cardy's doubling trick to suppose we have a whole plane to play around with. We will pick a torus T^2 which branches at $0, \eta, 1, \infty$, a Riemann surface described by the following equation:

$$y^2 = x(x-\eta)(x-1), \tag{D.3.5}$$

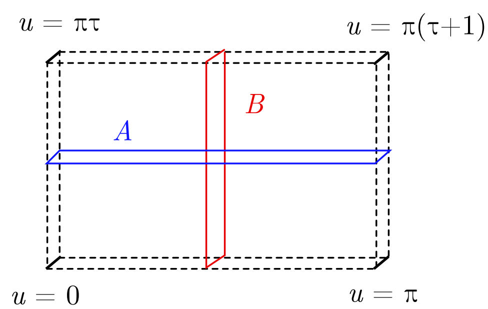

Figure D.2: The $\mathbb{Z}_2$ quotient of the torus leads to a double-cover of the sphere which is flat except for conical defects at the corners, with uniformizing coordinates u as indicated. The A and B cycles of the torus can be associated with bulk and boundary OPE channels in the (B)CFT, with insertions at the corners.

where $x, y \in \hat{\mathbb{C}}$ are points on the Riemann sphere. This is the Weierstrass cubic associated with the lattice $\Lambda = \langle 1, \tau \rangle$ which quotients the complex plane to give the torus. This provides a double cover of the sphere since the defining equation is invariant under $y \mapsto -y$, and the fixed points of this map are precisely the branch points. The pillow has the topology of a sphere, and is flat, except for conical defects at these branch points, as depicted in Fig. D.2.

The fundamental domain of the torus is oblique for general τ, but we can transform it into a rectangle using a *uniformizing* coordinate u defined by

$$du = \frac{L}{\theta_3(q)^2} \frac{dx}{y}. \tag{D.3.6}$$

This has width $2\pi L$, as one can check by performing the x integral. The $\mathbb{Z}_2$ action $y \mapsto -y$ becomes $u \mapsto -u$. In the u coordinates, the defects have coordinates

$$u(x = 0) = 0, \quad u(x = \eta) = \pi, \quad u(x = 1) = \pi(\tau + 1), \quad u(x = \infty) = \pi\tau. \tag{D.3.7}$$

We can cut the pillow in half in two ways: the horizontal A cycle and the vertical B cycle, which separate the corners into pairs, also shown in D.2.

D.3.3 Evaluating the correlator

We now consider how to implement this in the BCFT. In the BCFT, $\eta = z_{12}z_{34}/z_{13}z_{24}$. Thus, our insertions and their mirror images have the following identification on the pillow in u coordinates:

$$z_1 \mapsto 0, \quad z_{\bar{1}} \mapsto u = \pi, \quad z_2 = \pi\tau, \quad z_{\bar{2}} = \pi(\tau+1). \tag{D.3.8}$$

Thus, the boundary lies on the B cycle, and we should quantize on the A cycle. If we normalize this cycle to have length 2π (or π in the halved geometry), then the relevant Hamiltonian is just the dilatation operator in radial quantization (now on a half-cylinder), $H = L_0 - c/24$.

We evolve upwards by $\pi\tau$, i.e., with Euclidean time evolution operator

$$e^{i\pi\tau(L_0 - c/24)} = q^{L_0 - c/24}. \tag{D.3.9}$$

The change to u coordinates is a Weyl rescaling, leading to an anomalous contribution to the correlator. Performing this change and regularizing as in [197], we obtain

$$\mathcal{F}(\eta) = \Lambda(\eta) g(q) \tag{D.3.10}$$

$$g(q) = \langle \mathcal{O}(u=0)\mathcal{O}(u=\pi\tau)\rangle_{\text{pillow}} \tag{D.3.11}$$

$$\Lambda(\eta) = \theta_3(q)^{c/2-16h}[\eta(1-\eta)]^{c/24-2h}. \tag{D.3.12}$$

We can think of the pillow two-point function $g(q)$ as an expectation value

$$g(q) = \langle\psi|q^{L_0-c/24}|\psi\rangle, \quad |\psi\rangle = \mathcal{O}(0)|0\rangle, \tag{D.3.13}$$

where due to our choice of quantization, $\langle\psi| = \langle 0|\mathcal{O}(\pi\tau)$. To be clear, here $|0\rangle$ is the vacuum state on the half-cylinder. In the boundary channel, factoring out the Λ prefactor also gives

$$g(q) = \sum_{\hat{h}} |B_{\mathcal{O}\hat{h}}|^2 \tilde{\mathcal{V}}_{\hat{h}}(q), \quad \tilde{\mathcal{V}}_{\hat{h}}(q) = \Lambda(\eta)^{-1}\mathcal{V}_{\hat{h}}(\eta). \tag{D.3.14}$$

We can split the block into descendants:

$$\tilde{\mathcal{V}}_{\hat{h}}(q) = \sum_{n\geq 0} a_n q^{n+\hat{h}-c/24}. \tag{D.3.15}$$

In a unitary BCFT, the $a_n \geq 0$, since otherwise we can construct a linear combination of descendants with negative norm.

The bulk channel is naturally interpreted as quantizing on the B cycle:

$$g(q) = \langle\psi'|\bar{q}^{L_0-c/24}|B\rangle, \tag{D.3.16}$$

where $|\psi'\rangle = \mathcal{O}(\pi\tau)\mathcal{O}(0)|0\rangle$, $|0\rangle$ now the vacuum state for the full cylinder, and $\bar{q} = e^{-\pi i/\tau}$ is the S-transformed modular parameter. Performing the bulk OPE expansion of our two operators, we end up with precisely the sum of bulk Virasoro primaries weighted by OPE coefficients and one-point functions given above.

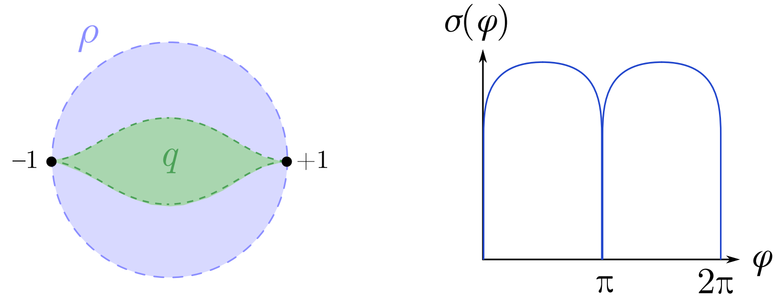

Figure D.3: *Left.* Relation between the radial ρ variable and the nome q. *Right.* The real part of $-\log q$ as a function of Lorentzian cross-ratio.

D.3.4 Seeking Lorentzian singularities

Mapping the unit disk $|\rho| \leq 1$ to the q variable leads a region sitting inside the unit disk of q, and hitting the boundary at $q = \pm 1$, which corresponds to $\rho = \pm 1$, and hence $\eta = 1, -\infty$, or $\xi = 0, -\infty$ in our preferred cross-ratio. Note that $g(q)$ is finite inside the unit disk, since it is given by an expansion in powers of q with positive, bounded coefficients. We depict this in Fig. D.3 (left) below.

We would like to use the behaviour of $g(q)$ to deduce that the only Lorentzian singularities are the light-cone singularities. Let us define

$$\log q \left[\xi = -\cos^2\left(\frac{\phi}{2}\right)\right] = -\sigma(\phi) + i\theta(\phi), \tag{D.3.17}$$

where ϕ is the argument of ρ. We plot the values of $\sigma(\theta) = -\log|q|$ in Fig. D.3 (right). It is positive except when $\phi \in \pi\mathbb{Z}$. Recall that $\rho = re^{i\phi} = e^{\tau + i\phi}$ in radial quantization, so that when we continue to the Lorentzian cylinder, $\tau = it$, the analytically continued nome becomes $q = e^{-\sigma(\phi+t)+i\theta(\phi+t)}$. The Cauchy-Schwarz inequality then gives

$$|g(q)| \leq \langle\psi||q|^{L_0 - c/24}|\psi\rangle = g(e^{-\sigma(\phi-t)}). \tag{D.3.18}$$

This is the Euclidean pillow correlator again, which is finite except when $q = 1$, i.e., $\sigma = 0$, or $\phi + t \in \pi\mathbb{Z}$. These are precisely the light-cone singularities. We have thus proved that the only singularities in a 2D BCFT are the expected Euclidean and lightcone singularities, as advertised.

D.4 Bulk Causality in Top-Down Model

In this appendix, we will endeavour to give further background information about causal features of the top-down construction mentioned in section 5.6.2, namely the AdS_2-cap solution of Chiodaroli, D'Hoker, and Gutperle. The metric functions for this solution are given by

$$\begin{aligned} f_1^4 &= \frac{2\kappa^2}{\mu_0^2}\frac{\mu_0^2\mathrm{Im}\,(w)^2+\kappa^2|1-w^2|^2}{|w|^4} \\ f_2^4 &= \frac{2\kappa^2\mu_0^2\mathrm{Im}\,(w)^4}{|w|^4\left(\mu_0^2\mathrm{Im}\,(w)^2+\kappa^2|1-w^2|^2\right)} \\ \rho^4 &= \frac{\mu_0^2}{8\kappa^2}\frac{\mu_0^2\mathrm{Im}\,(w)^2+\kappa^2|1-w^2|^2}{|w|^4|1-w^2|^4}\,, \end{aligned} \tag{D.4.1}$$

where $\kappa > 0$ and μ are two real parameters. We will sometimes denote $a \equiv \frac{2\kappa}{\mu_0}$ for convenience. The asymptotically $\mathrm{AdS}_3 \times S^3$ region is located at $w = 0$, whereas the AdS-cap singularities are located at $w = \pm 1$.

Let (u, t) be the Poincaré coordinates of the AdS_2 factor and (θ, ϕ) be the angular coordinates of the S^2 factor, so that

$$ds^2_{\mathrm{AdS}_2} = \frac{du^2 - dt^2}{u^2}\,, \qquad ds^2_{S^2} = d\theta^2 + \sin^2\theta d\phi^2\,. \tag{D.4.2}$$

It is straightforward to demonstrate that, in the limit that we approach the asymptotic boundary, the AdS_2 coordinates (u, t) agree with the BCFT coordinates $(x_\perp, \hat{t})$ (arising in Fefferman-Graham gauge) up to a constant factor

$$u\big|_\partial = -x_\perp/a\,, \qquad t\big|_\partial = \hat{t}/a\,. \tag{D.4.3}$$

In particular, these factors will drop out of a calculation of the BCFT cross-ratio, so we can calculate the cross-ratio directly using the (u, t) parameters.

We would like to shoot in geodesics from the asymptotic boundary of the $\mathrm{AdS}_3 \times S^3$ region, provided initial data consistent with the null constraint

$$0 = \frac{f_1^2}{u^2}\left(\dot{u}^2 - \dot{t}^2\right) + f_2^2\left(\dot{\theta}^2 + \sin^2\theta\dot{\phi}^2\right) + \rho^2\left(\dot{x}^2 + \dot{y}^2\right)\,, \tag{D.4.4}$$

and solve the geodesic equation to determine the intersection of the bulk light cone with the asymptotic boundary.

Before proceeding to determine the null geodesics, we may choose to multiply the metric functions by some fixed conformal factor, since this will not affect the bulk light cone structure; we therefore choose for convenience to multiply the metric by f_1^{-2}, to obtain

$$d\tilde{s}^2 = ds^2_{\mathrm{AdS}_2} + \frac{f_2^2}{f_1^2} ds^2_{S^2} + \frac{\rho^2}{f_1^2} dw d\bar{w} \,. \tag{D.4.5}$$

Our choice is motivated by the fact that ρ^2/f_1^2 is a simple function of the complex coordinates $(w, \bar{w})$, namely

$$\frac{\rho^2}{f_1^2} = \frac{1}{a^2} \frac{1}{|1-w^2|^2} \,. \tag{D.4.6}$$

With this choice, and taking fixed $\theta = \frac{\pi}{2}$ without loss of generality, we find the components of the geodesic equation decouple pairwise, giving

$$\begin{aligned}
\ddot{x} &= \frac{4y(x^2+y^2+1)}{((x-1)^2+y^2)\,((x+1)^2+y^2)} \dot{x}\dot{y} + \frac{2x(x^2+y^2-1)}{((x-1)^2+y^2)\,((x+1)^2+y^2)} \left(\dot{x}^2 - \dot{y}^2\right) \\
&\quad - 8xy^2\dot{\phi}^2 \left(\frac{\left(x^2+y^2-1\right)\left((x+1)^2+y^2\right)\left((x-1)^2+y^2\right)}{\left((1-x^2)^2+y^4+2\left(x^2+1+\frac{\mu_0^2}{2\kappa^2}\right)y^2\right)^2} \right) , \\
\ddot{y} &= \frac{4x(x^2+y^2-1)}{((x-1)^2+y^2)\,((x+1)^2+y^2)} \dot{x}\dot{y} - \frac{2y(x^2+y^2+1)}{((x-1)^2+y^2)\,((x+1)^2+y^2)} \left(\dot{x}^2 - \dot{y}^2\right) \\
&\quad + 4y\dot{\phi}^2 \left(\frac{\left(\left(x^2-1\right)^2 - y^4\right)\left((x+1)^2+y^2\right)\left((x-1)^2+y^2\right)}{\left((1-x^2)^2+y^4+2\left(x^2+1+\frac{\mu_0^2}{2\kappa^2}\right)y^2\right)^2} \right) \\
\frac{\ddot{\phi}}{\dot{\phi}} &= \left(\frac{4x^2\left(x^2+y^2-1\right)}{(1-x^2)^2+y^4+2\left(x^2+1+\frac{\mu_0^2}{2\kappa^2}\right)y^2} \right) \frac{\dot{x}}{x} \\
&\quad - \left(\frac{2\left(\left(x^2-1\right)^2 - y^4\right)}{(1-x^2)^2+y^4+2\left(x^2+1+\frac{\mu_0^2}{2\kappa^2}\right)y^2} \right) \frac{\dot{y}}{y} \,,
\end{aligned} \tag{D.4.7}$$

and

$$\ddot{u} = \frac{1}{u}\left(\dot{u}^2 + \dot{t}^2\right) \,, \quad \ddot{t} = \frac{2}{u}\dot{u}\dot{t} \,, \tag{D.4.8}$$

while the null condition is still as above (with $\dot{\theta} = 0$).

D.4.1 Short Light-Crossing Time with Fine-Tuned Initial Conditions

Before considering more general initial data, we will consider the case $\dot{x}(0) = 0$; it is straightforward to see that $x(s) = 0$ for the entire trajectory in this case, so that the equations simplify to

$$\begin{aligned}
\frac{\ddot{y}}{y} &= \frac{2\dot{y}^2}{(1+y^2)} + 4\dot{\phi}^2 \left(\frac{\left(1-y^4\right)\left(1+y^2\right)^2}{\left(1+\left(1+\frac{\mu_0^2}{2\kappa^2}\right)y^2+y^4\right)^2} \right) \\
\frac{\ddot{\phi}}{\dot{\phi}} &= -\left(\frac{2\left(1-y^4\right)}{1+\left(1+\frac{\mu_0^2}{2\kappa^2}\right)y^2+y^4} \right) \frac{\dot{y}}{y} \,.
\end{aligned} \tag{D.4.9}$$

We can integrate out the ϕ equation, which gives

$$\begin{aligned}
\ln\Big(\dot{\phi}(s)/\dot{\phi}(s_0)\Big) &= -\int_{s_0}^{s} ds' \left(\frac{2\left(1-y(s')^4\right)}{1+\left(1+\frac{\mu_0^2}{2\kappa^2}\right)y(s')^2+y(s')^4} \right) \frac{\dot{y}(s')}{y(s')} \\
&= \left[\ln\left(\frac{y(s)^4+\left(1+\frac{\mu_0^2}{2\kappa^2}\right)y(s)^2+1}{y(s)^2} \right) \right]_{s_0}^{s} ,
\end{aligned} \tag{D.4.10}$$

that is,

$$\dot{\phi}(s) = c \cdot \frac{y(s)^4+\left(1+\frac{\mu_0^2}{2\kappa^2}\right)y(s)^2+1}{y(s)^2} \,, \qquad c \equiv \frac{\dot{\phi}_0 y_0^2}{y_0^4+\left(1+\frac{\mu_0^2}{2\kappa^2}\right)y_0^2+1} \,, \tag{D.4.11}$$

where the subscript zero denotes evaluation at a reference value $s = s_0$. The y equation then gives

$$\frac{\ddot{y}}{y} - \frac{2\dot{y}^2}{(1+y^2)} = \frac{4c^2}{y^4}(1-y^4)(1+y^2)^2 \,, \tag{D.4.12}$$

where $y(s_0) = y_0$ and $\dot{\phi}(s_0) = \dot{\phi}_0$. Note that the parameters μ_0, κ have dropped out of this expression.

For any choice of initial conditions for this ODE, the trajectory diverges to $y = \infty$ in some finite affine parameter. The point ∞ on Σ is a regular point of the smooth 6D geometry; in particular, making coordinate transformation

$$v = \frac{1}{w} \,, \qquad \bar{v} = \frac{1}{\bar{w}} \,, \tag{D.4.13}$$

and letting

$$v = re^{i\varphi} \,, \qquad \bar{v} = re^{-i\varphi} \,, \tag{D.4.14}$$

we have for small r

$$ds^2 \approx \frac{\mu_0}{\sqrt{8}}\left(\frac{dr^2}{r^2}+\frac{a^2}{u^2}\left(du^2-dt^2\right)\right)+\frac{\mu_0}{\sqrt{8}}\left(d\varphi^2+4r^2\sin^2\varphi\left(d\theta^2+\sin^2\theta d\phi^2\right)\right). \tag{D.4.15}$$

Evidently, this point is at an infinite proper distance from any other point in the geometry that we might choose, but is reached by our null geodesic in finite affine parameter; the metric in the vicinity of this point is conformal to

$$ds^2 = \left(dr^2+r^2d\varphi^2\right)+O(r^2)\,, \tag{D.4.16}$$

so our geodesic will "turn around" at this point.

For concreteness, we can consider the case $\dot\phi(0)=0$; the corresponding geodesic leaves and returns to the asymptotic boundary $y=0$ in affine parameter $s=\frac{\pi}{\dot y(0)}$. Indeed, the ODE determining the trajectory on the Riemann surface Σ

$$\ddot y = \frac{2y}{(y^2+1)}\dot y^2\,, \qquad y(0)=0\,,\ \dot y(0)=y_1\,, \tag{D.4.17}$$

has solution

$$y(s)=\begin{cases}\tan(y_1 s) & 0<s<\frac{\pi}{2y_1}\\ \tan\left(\pi-y_1 s\right) & \frac{\pi}{2y_1}<s<\frac{\pi}{y_1}\end{cases}. \tag{D.4.18}$$

In particular, we see that the geodesic returns to the asymptotic boundary in affine parameter $s=\frac{\pi}{y_1}$. Without loss of generality, we take $y_1=1$ in the following, which is simply a choice of normalization for the affine parameter.

We can now turn to the coordinates (u,t). The general solution to the differential equations for these parameters is

$$\begin{aligned} u(s) &= u(s_0)\sec\left(\frac{(s-s_0)}{a}\right)\\ t(s) &= u(s_0)\tan\left(\frac{(s-s_0)}{a}\right)+u(s_0)\tan\left(\frac{s_0}{a}\right)\,. \end{aligned} \tag{D.4.19}$$

The only way that this trajectory couples to the trajectory on Σ is that the latter determines the total affine parameter S elapsed along the trajectory. Thus, in particular, we may calculate the cross-ratio for the initial and final coordinates on the geodesic, finding

$$\xi = \frac{-\left(t(S)-t(0)\right)^2+\left(u(S)-u(0)\right)^2}{4u(0)u(S)} = \frac{1}{2}\left(\cos\left(S/a\right)-1\right)\,. \tag{D.4.20}$$

In terms of the "radial coordinate" cross-ratio ρ defined by

$$\xi = \frac{(1-\rho)^2}{4\rho} \, , \tag{D.4.21}$$

we have

$$\rho = \cos{(S/a)} \pm i \sin{(S/a)} = e^{\pm \frac{iS}{a}} \, , \tag{D.4.22}$$

where for example $S = \pi$ for the case $\dot{\phi}(0) = 0$. Consequently, if we expect this cross-ratio to describe the locus of a Lorentzian singularity of a BCFT two-point function, then we might expect that such singularity can be attributed to the contribution of a particular tower of boundary operators with dimensions exhibiting an asymptotic spacing which is an integer multiple of $2a$.

D.4.2 Geodesics for General Initial Conditions

More general solutions to the geodesic equations (D.4.7), (D.4.8) and the null constraint, without the assumption $x(s) = 0$, may also be studied numerically. Doing so, we appear to find that null geodesics with initial momentum in the x-direction quite generically approach the AdS-caps. In Figure D.4, we plot the distance of various geodesics from the curvature singularity as a function of affine parameter for various initial conditions, restricting momentarily to the case with no momentum on the S^2. This is consistent with the conclusion of our perturbative argument in the main text; indeed, the perturbative assumption made there appears to hold in general, with an example of this fact illustrated in Figure D.5.

We can attempt to extend this analysis to the case with momentum on the S^2. However, we cannot actually send in geodesics from the asymptotic boundary with momentum on the S^2; the system of ODEs is singular at $x = y = 0$, and the angular momentum on S^2 diverges there in general. Instead, we choose a point near the the origin of Σ and send a geodesic in from this point with initial momentum on the S^2, with the hopes that this will capture the relevant behaviour. Doing so, we again find that the AdS-caps act as attractors; see Figure D.6 for an example.

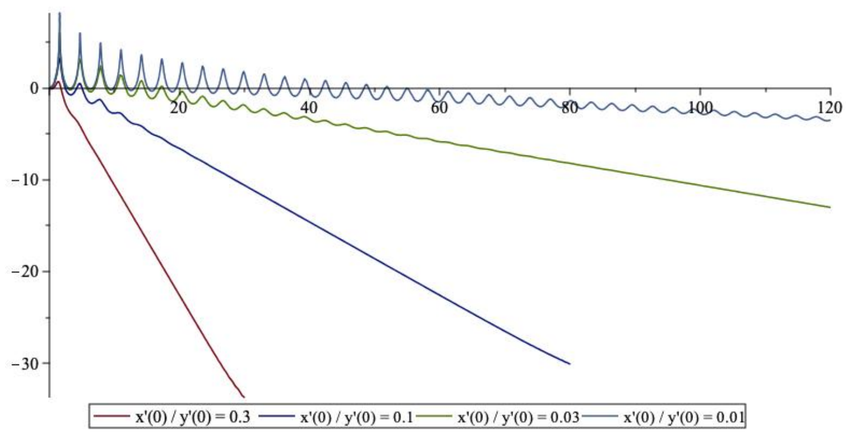

Figure D.4: Logarithmic distance to the AdS-cap $\ln\left((x(s)-1)^2+y(s)^2\right)$ versus affine parameter s for geodesics with various initial conditions on the internal space Σ. Here we have chosen $\mu_0=\kappa=1$ for concreteness.

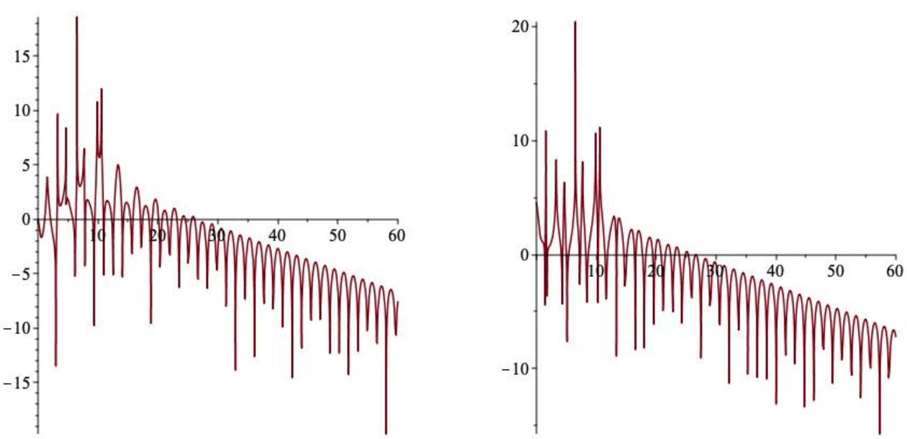

Figure D.5: Plots of $\ln\left(\frac{\dot{\epsilon}_x^2/\epsilon}{\dot{\epsilon}^2/\epsilon^2}\right)$ (left) and $\ln\left(\frac{\dot{\epsilon}_y^2/\epsilon}{\dot{\epsilon}^2/\epsilon^2}\right)$ (right) versus affine parameter for a geodesic with initial condition $\dot{x}(0)/\dot{y}(0)=0.3$; these quantities are required to be small for ingoing geodesics to approach the cap exponentially in the affine parameter. Here we have chosen $\mu_0=\kappa=1$ for concreteness.

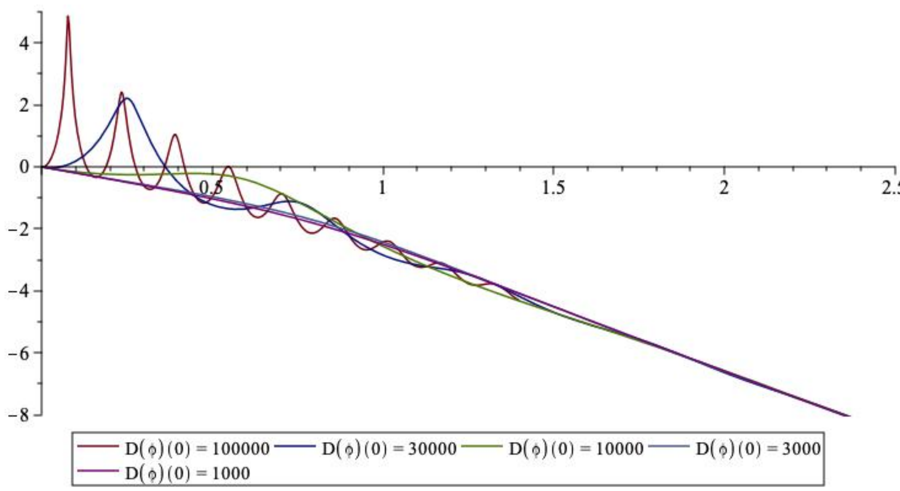

Figure D.6: Logarithmic distance to the AdS-cap $\ln\left((x(s)-1)^2+y(s)^2\right)$ versus affine parameter s for geodesics with various initial conditions on the S^2. We take $x=y=10^{-4}$ as the origin for these geodesics, with initial condition $\dot{x}(0)=\dot{y}(0)=1$. Here we have chosen $\mu_0=\kappa=1$ for concreteness.